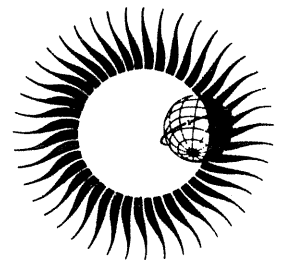


WORLD DATA CENTER A for Solar-Terrestrial Physics



EXPERIENCE WITH PROPOSED IMPROVEMENTS
OF THE INTERNATIONAL REFERENCE IONOSPHERE (IRI)



MAY 1984

WORLD DATA CENTER A
National Academy of Sciences
2101 Constitution Avenue, NW
Washington, D.C. 20418 USA

World Data Center A consists of the Coordination Office
and the following eight Subcenters:

COORDINATION OFFICE
World Data Center A
National Academy of Sciences
2101 Constitution Avenue, NW
Washington, D.C. 20418 USA
Telephone: (202) 334-3359

GLACIOLOGY (Snow and Ice)
World Data Center A: Glaciology
(Snow and Ice)
Cooperative Inst. for Research in
Environmental Sciences
University of Colorado
Boulder, Colorado 80309 USA
Telephone: (303) 492-5171

MARINE GEOLOGY AND GEOPHYSICS
(Gravity, Magnetics, Bathymetry,
Seismic Profiles, Marine Sediment,
and Rock Analyses):

World Data Center A for Marine
Geology and Geophysics
NOAA, E/GC3
325 Broadway
Boulder, Colorado 80303 USA
Telephone: (303) 497-6487

METEOROLOGY (and Nuclear Radiation)
World Data Center A: Meteorology
National Climatic Data Center
NOAA, E/CC
Federal Building
Asheville, North Carolina 28801 USA
Telephone: (704) 259-0682

OCEANOGRAPHY
World Data Center A: Oceanography
National Oceanographic Data Center
NOAA, E/OC
2001 Wisconsin Avenue, NW
Page Bldg. 1, Rm. 414
Washington, D.C. 20235 USA
Telephone: (202) 634-7510

ROCKETS AND SATELLITES
World Data Center A: Rockets and
Satellites
Goddard Space Flight Center
Code 601
Greenbelt, Maryland 20771 USA
Telephone: (301) 344-6695

ROTATION OF THE EARTH
World Data Center A: Rotation
of the Earth
U.S. Naval Observatory
Washington, D.C. 20390 USA
Telephone: (202) 254-4547

SOLAR-TERRESTRIAL PHYSICS (Solar and
Interplanetary Phenomena, Ionospheric
Phenomena, Flare-Associated Events,
Geomagnetic Variations, Aurora,
Cosmic Rays, Airglow):

World Data Center A
for Solar-Terrestrial Physics
NOAA, E/GC2
325 Broadway
Boulder, Colorado 80303 USA
Telephone: (303) 497-6323

SOLID-EARTH GEOPHYSICS (Seismology,
Tsunamis, Gravimetry, Earth Tides,
Recent Movements of the Earth's
Crust, Magnetic Measurements,
Paleomagnetism and Archeomagnetism,
Volcanology, Geothermics):

World Data Center A
for Solid-Earth Geophysics
NOAA, E/GC1
325 Broadway
Boulder, Colorado 80303 USA
Telephone: (303) 497-6521

World Data Centers conduct international exchange of geophysical observations in accordance with the principles set forth by the International Council of Scientific Unions. WDC-A is established in the United States under the auspices of the National Academy of Sciences. Communications regarding data interchange matters in general and World Data Center A as a whole should be addressed to World Data Center A, Coordination Office (see address above). Inquiries and communications concerning data in specific disciplines should be addressed to the appropriate subcenter listed above.

WORLD DATA CENTER A for Solar-Terrestrial Physics



REPORT UAG-90

EXPERIENCE WITH PROPOSED IMPROVEMENTS OF THE INTERNATIONAL REFERENCE IONOSPHERE (IRI)

Contributed papers, mainly from the URSI-COSPAR workshop held in Budapest in 1980

Edited by

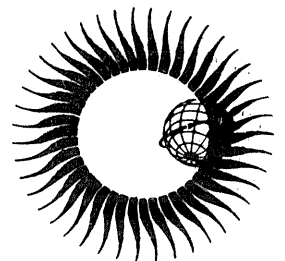
K. Rawer

University, Freiburg, F.R. Germany

and

C.M. Minnis

Former Secretary General of URSI, Brussels, Belgium



May 1984

U.S. Department of Commerce
National Oceanic and Atmospheric Administration
National Environmental Satellite, Data, and Information Service
National Geophysical Data Center
Boulder, Colorado

PUBLISHER'S NOTE

Some comments are necessary on the discrepancy between the date of the symposium at which the papers in this volume were presented (June 1980 at Budapest) and the publication date of this report (May 1984).

At about the time of the symposium I agreed it would be appropriate to issue the papers in the data report series (UAG) of the WDC-A for STP. These data and discussions would obviously enhance the usefulness of the IRI and the associated data in the WDCs. The editors agreed to provide us with camera-ready copy of the text and did so within a reasonable time. They did ask us to cope with preparing the figures for publication but provided captions and much detailed planning information along with the drawings received from the authors.

The ensuing delays in completing the publication are a great personal embarrassment to me, which, I am afraid, spreads over to the WDC and its staff. There were a number of staff changes and changes in responsibilities, and other pressures and events which affected priorities. But the sum of the delays was and is inexcusable.

Another effect of the above circumstances was that we have not been able to give here the degree of publisher's attention that has been applied to most of the other volumes in this series. We have done almost no typographical corrections in the text. We have compromised on the figures being legible rather than clear or composed or elegant. There probably remain many unintentional clumsinesses of language by authors not experienced with English. But we think information is transferred.

It was only in the first part of 1983 that a draft of the full publication was completed and nine copies were sent to the COSPAR IRI Working Group meeting at Bulgaria. A copy of the final draft was also sent to the 1984 COSPAR meeting at Graz.

Thus, the lateness of this publication is in no way attributable to the editors or authors, and we offer them our profound apologies. We agree that most of the material included here continues to have importance and relevance to modeling the ionosphere, and will continue to be a valuable complement to the IRI tables and computer tapes which are in remarkably high demand from the data centers.

I should acknowledge the leading role in completing this publication of R. O. Conkright, head of the Ionosphere Branch of the National and World Data Centers. He should receive any credit which may remain to us, for without his perseverance and labor after I undertook personal responsibility for the project, we never would have completed it. C. T. Shanks, as usual, has done yeoman work in trying to rehabilitate the diagrams.

My apologies to the authors, the editors and the community for the lateness and the publication quality.

A. H. Shapley
Former Director, NGSDC
May 1984

DESCRIPTION OF WORLD DATA CENTERS

World Data Centers conduct international exchange of geophysical observations in accordance with the principles set forth by the International Council of Scientific Unions (ICSU). They were established in 1957 by the International Geophysical Year Committee (CSAGI) as part of the fundamental international planning for the IGY program to collect data from the numerous and widespread IGY observational programs and to make such data readily accessible to interested scientists and scholars for an indefinite period of time. WDC-A was established in the U.S.A.; WDC-B, in the U.S.S.R.; and WDC-C, in Western Europe, Australia, and Japan. This new system for exchanging geophysical data was found to be very effective, and the operations of the World Data Centers were extended by ICSU on a continuing basis to other international programs; the WDC's were under the supervision of the Comité International de Geophysique (CIG) for the period 1960 to 1967 and are now supervised by the ICSU Panel on World Data Centres.

The current plans for continued international exchange of geophysical data through the World Data Centers are set forth in the *Fourth Consolidated Guide to International Data Exchange through the World Data Centres*, issued by the ICSU Panel on World Data Centres. These plans are broadly similar to those adopted under ICSU auspices for the IGY and subsequent international programs.

Functions and Responsibilities of WDC's

The World Data Centers collect data and publications for the following disciplines: Glaciology; Meteorology; Oceanography; Rockets and Satellites; Solar-Terrestrial Physics disciplines (Solar and Interplanetary Phenomena, Ionospheric Phenomena, Flare Associated Events, Geomagnetic Phenomena, Aurora, Cosmic Rays, Airglow); Solid-Earth Geophysics disciplines (Seismology, Tsunamis, Marine Geology and Geophysics, Gravimetry, Earth Tides, Recent Movements of the Earth's Crust, Rotation of the Earth, Magnetic Measurements, Paleomagnetism and Archeomagnetism, Volcanology, Geothermics). In planning for the various scientific programs, decisions on data exchange were made by the scientific community through the international scientific unions and committees. In each discipline the specialists themselves determined the nature and form of data exchange, based on their needs as research workers. Thus the type and amount of data in the WDC's differ from discipline to discipline.

The objects of establishing several World Data Centers for collecting observational data were: (1) to insure against loss of data by the catastrophic destruction of a single center, (2) to meet the geographical convenience of, and provide easy communication for, workers in different parts of the world. Each WDC is responsible for: (1) endeavoring to collect a complete set of data in the field or discipline for which it is responsible, (2) safe-keeping of the incoming data, (3) correct copying and reproduction of data, maintaining adequate standards of clarity and durability, (4) supplying copies to other WDC's of data not received directly, (5) preparation of catalogs of all data in its charge, and (6) making data in the WDC's available to the scientific community. The WDC's conduct their operation at no expense to ICSU or to the ICSU family of unions and committees.

World Data Center A

World Data Center A, for which the National Academy of Sciences through the Geophysics Research Board and its Committee on Data Interchange and Data Centers has over-all responsibility, consists of the WDC-A Coordination Office and seven subcenters at scientific institutions in various parts of the United States. The GRB periodically reviews the activities of WDC-A and has conducted several studies on the effectiveness of the WDC system. As a result of these reviews and studies some of the subcenters of WDC-A have been relocated so that they could more effectively serve the scientific community. The addresses of the WDC-A subcenters and Coordination Office are given inside the front cover.

The data received by WDC-A have been made available to the scientific community in various ways: (1) reports containing data and results of experiments have been compiled, published, and widely distributed; (2) synoptic type data on cards, microfilm, or tables are available for use at the subcenters and for loan to scientists; (3) copies of data and reports are provided upon request.

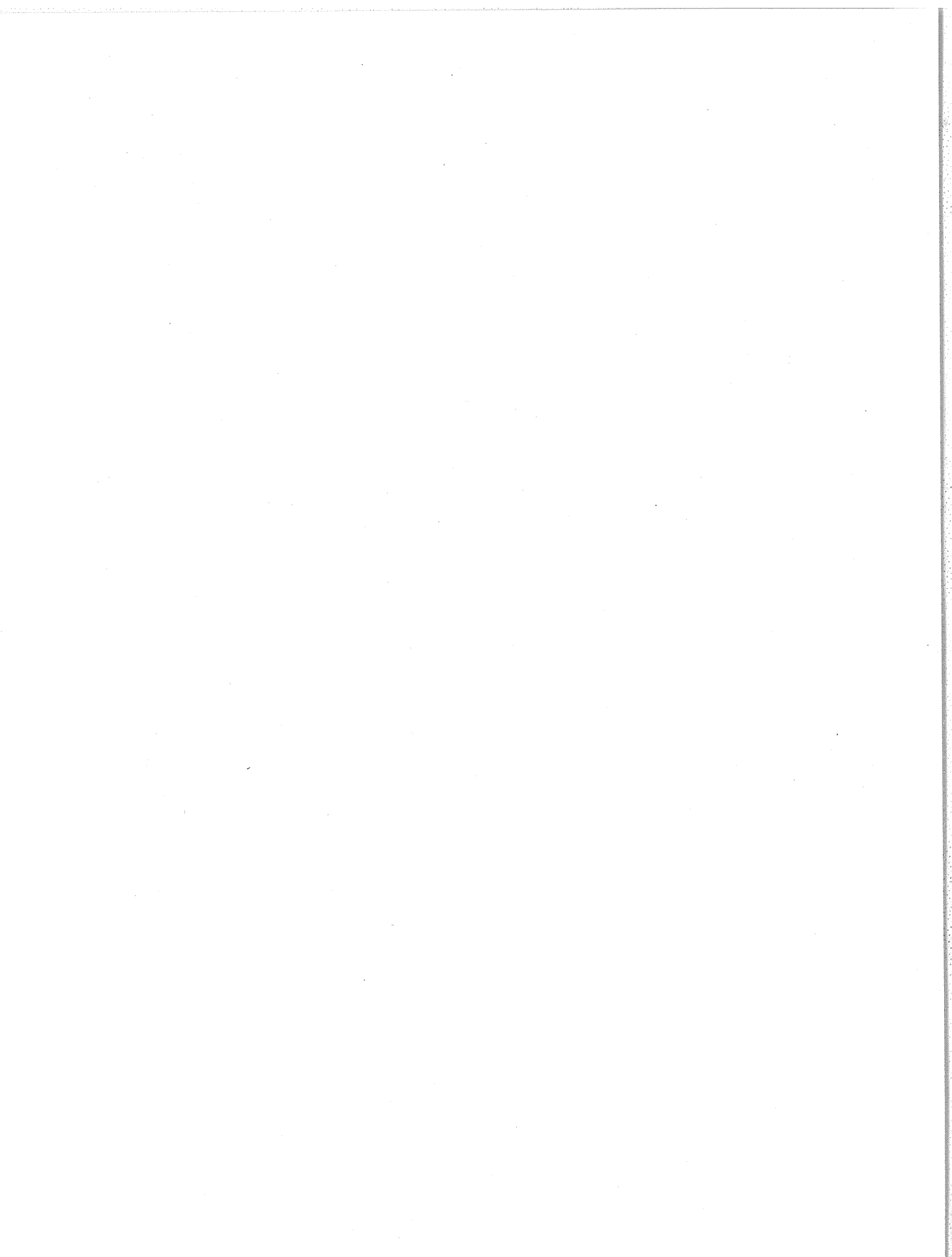


TABLE OF CONTENTS

1	<u>Electron Density Profile</u>	
1.1	<u>D- and E- Region</u>	
1.1.1	D- and Lower E- Region Electron Density Profiles Compared with LF and MF Absorption Data W. Singer, J. Taubenheim, J. Bremer	1
1.1.2	D- and Lower E- Region Electron Density Profiles Compared with LF and VLF Reflection Data Y.V. Ramanamurty	9
1.1.3	Comparison of Ionospheric Electron Density Models Using Data from a Mid-Latitude Absorption Path M. Friedrich, K.M. Torkar	19
1.2	<u>Bottomside F-Region</u>	
1.2.1	Critical Comparison of IRI with Information Obtained from Bottomside Ionograms T.L. Gulyaeva	22
1.2.2	Comparison of IRI with Measurement of N(h) Profiles in the Bottomside Ionosphere V.M. Sinel'nikov, G.P. L'vova, T.L. Gulyaeva, S.V. Pakhomov, A.P. Glotov	31
1.2.3	Comparison of IRI with Electron Density Profiles Obtained below 200 km By Different Methods Yu.K. Chasovitin, A.D. Danilov, S.M. Demykin, T.L. Gulyaeva, V.I. Ivanov, V.G. Khriukin, A.A. Nikitin, L.L. Sukhacheva, V.B. Shushkova, S.P. Tikhomirov	38
1.2.4	Comparison of IRI-78 with IZMIRAN'S Equinoctial Models T.L. Gulyaeva, A.G. Israetel, T.Yu. Leshchinskaya, T.N. Soboleva, E.E. Tzedilina	50
1.2.5	Bottomside Electron Density Profile Measurement by Rocket Borne Probes over the Equator S.P. Gupta	53
1.3	<u>Topside</u>	
1.3.1	Rocket and Satellite Measurements Compared with the IRI-79 Electron Density Profiles E. Neske, S. Ramakrishnan, C. Rebstock	57
1.3.2	Comparison between Plasma Densities Measured with the AEROS-B and S3-1 Satellites and the IRI model C.R. Philbrick, P. Lammerzahn, E. Neske, A. Dumbs	62

1.3.3	Comparison of Theoretical Electron Density profiles at the Magnetic Equator with IRI Model and Incoherent Scatter data T.Yu. Leshchinskaya, A.V. Mikhailov	68
1.3.4	Intercomparison of Various Measurements of Thermal Plasma Densities at and near the Plasmapause D.V. Williams, M.J. Rycroft, A.J. Smith, V.V. Bezrukikh, K.I. Gringauz, N.C. Maynard, M.J. Morgan, T.W. Thomas (This paper was withdrawn by the authors)	71
1.3.5	Comparison with IRI of Electron Density and Temperature at the Magnetic Equator G.F. Deminova, L.A. Yudovich	75
1.4	<u>Variability</u>	
1.4.1	Variability of the Equatorial F-Region K. Bibl	78
1.4.2	Construction of Electron Density Profiles for the Flare-Disturbed Ionosphere with Data from Doppler Measurements I.N. Odintsova, V.D. Novikov	86
2	<u>Plasma Temperatures</u>	
2.1	<u>Electron Temperature</u>	
2.1.1	Comparisons of ISIS and AE Satellite Measurements of Electron Temperature with the International Reference Ionosphere L.H. Brace, R.F. Theis	89
2.1.2	Proposal of Improvement of the Electron Temperature Model in IRI K. Hirao	95
2.1.3	Verification of the International Reference Ionosphere on Electron Temperature Profiles Obtained by Various Methods below 200 km Yu.K. Chasavitin, N.M. Klyueva	100
2.1.4	Electron Temperature Modelling in the F-Region and Topside of the Ionosphere: A Proposal for Improving the IRI K.K. Mahajan, V.K. Pandey	107
2.1.5	Estimation of a Model Electron Temperature Distribution based on Absorption Measurement K.B. Serafimov	113
2.2	<u>Ion and Electron Temperatures</u>	
2.2.1	The Atmospheric Explorer C Ionospheric Temperatures: Dependence and Representation D. Bilitza	114

2.2.2	Comparison of the Ion Density and Temperature Data Obtained by the RPA on OGO-6 and the IRI Model Ts.P. Dachev, N.S. Trendafilov, D.G. Goshev	123
2.2.3	Comparison of the IRI with Ion Temperature and Ion Density as Measured during Very Quiet Geomagnetic Conditions on board the Geophysical Rocket "Vertical-6" P. Bencze, K. Kovacs, I. Apa'thy, I. Szemerey, V. Afonin, V. Bezrukih, N. Shutte	126
2.2.4	Observation of Ne, Te and Ti by Incoherent Scatter Technique during a Period of Low Solar Activity V.I. Taran, E.V. Rogozhkin, D.A. Dzyubanov	129
2.3	<u>Variability</u>	
2.3.1	Studies of the Topside Ionosphere Using the Satellite "Interkosmos-19" Part I - The Ionospheric Satellite "Interkosmos-19" M.M. Gogoshev, A. Kiraga, Z. Klos, K. Kubat Yu.V. Kushnerevsky, V.V. Migulin, K.B. Serafimov, P. Triska, M.D. Fligel, J. Similauer	134
	Part II - First Results of a Statistical Evaluation of Electron Temperature Measurements on Board the Inter- kosmos-19 Satellite J. Smilauer, V.V. Afonin	135
2.3.2	Extremely High F-Region Electron Temperatures During the Present Maximum of Solar Cycle No. 21 (extended abstract) M. Gogoshev, G. Moraitis, Ts. Gogosheva, B. Komitov B. Taneva-Mendava, T. Markova, I. Mendov, Ts. Pashova, K. Kunev, S. Spasov	138
3	<u>Ionospheric Structure</u>	
3.1	<u>Ionic Composition</u>	
3.1.1	Ion Composition in the D- and Lower E-Regions with Particular Emphasis on Cluster Ions E. Kopp	140
3.1.2	A Proposed Improvement of IRI Using the O ⁺ - H ⁺ Transition Level I. Kutiev, K. Serafimov, M. Karadimov, K. Heelis	150
3.1.3	Comparison of IRI with Vertical Profiles for Ion and Electron Density and Electron Temperature Deduced on Board Vertical Rockets K. Serafimov, I. Kutiev, L. Bankov, N. Bankov, Ts. Dachev, B. Kirov, D. Teodosiev	155
3.1.4	Empirical F-Regions Model Development Based on S3-1 Satellite Measurement C.R. Philbrick	159
3.1.5	Temperature Control of Cluster Ion Concentration Maria Dymek	167

3.2	<u>Planetary Distribution</u>	
3.2.1	Proposal for "Mapping" the Spectral Components of foF2 A.K. Paul	171
3.2.2	Comparison of the IRI Model and the Real Planetary Distribution of F2-Ionospheric Layer Charged Particles Based on Satellite Measurement Data I.B. Balev, A.A. Goldin, E.G. Greenwald, V.A. Pavlenko, A.I. Savin, V.L. Talrose	178
3.2.3	Upper Atmosphere Dynamics and the International Reference Ionosphere E.S. Kazimirovsky	185
3.3	<u>Present and Future IRI</u>	
3.3.1	Limitations of the IRI-78 Models S. Ramakrishnsn, D. Bilitza, H. Thiemann	192
3.3.2	Summary and Conclusions Concerning IRI K. Rawer	198
4	<u>References</u>	200
5	<u>Index of Authors</u>	232

CHAPTER 1. ELECTRON DENSITY PROFILE

Section 1.1 D- and E-Region

1.1.1 D- and Lower E-Region Electron Density Profiles Compared with LF and MF Absorption Data

W. Singer, J. Taubenheim, J. Bremer

Akademie der Wissenschaften der DDR, Zentralinstitut für solar-terrestrische Physik (Heinrich-Hertz-Inst.)
1199 Berlin-Adlershof, German Democratic Republic

Abstract: Data on day-time and night-time radio wave absorption (at oblique and vertical incidence) in the frequency range 50 to 2614 kHz, obtained in long-term observational programmes in Central Europe, are compared with the corresponding absorption values calculated from electron density profiles of the International Reference Ionosphere (IRI-1979), for the geographic latitude 54°N. Full-wave and phase-integral methods were used, the necessary collision frequency data being deduced from the CIRA 1972 neutral pressure profiles. The observed seasonal variation of the noon absorption values at lower solar activity ($R = 10$) is generally well reproduced by the corresponding IRI-profiles. Discrepancies between calculated and observed absorption values, however, were found for the diurnal and the solar-cycle variation.

1, Introduction

A comparison of the D- and E-region electron density profiles of the 1977 provisional version of the International Reference Ionosphere ("IRI-77") /Rawer 1977/ with experimental radio propagation data from a mid-latitude observational programme has been published by us earlier /Singer et al., 1980/. The present paper reports on the analogous comparison carried out with the "official" IRI-1978 model /Rawer et al., 1978a/ in its corrected version of August 1979 /Rawer, personal communication/. The latter will here be referred to as "IRI-79".

Our experimental radio wave absorption data, observed at latitudes around 54°N in central Europe, in the frequency range from 50 kHz to 2614 kHz at oblique or vertical incidence (cf. Table I), cover a time interval of about two decades including a sunspot maximum (1969/70) and two sunspot minima (1964/65 and 1976). Thus the main objective of our comparison is to test the absolute absorption values as predicted from the IRI models, as well as their diurnal variation in different seasons, and their change between conditions of low and moderately enhanced solar activity (corresponding to Zürich sunspot numbers $R = 10$ and $R = 100$, respectively).

2, Important features of the IRI-78 and IRI-79 models

The IRI-78 and IRI-79 models are more suitable than the earlier IRI-77 for comparisons with observed radio propagation data, since they give a full representation of the (diurnal) electron density variation with solar zenith angle, χ , instead of noon and midnight only as in IRI-77. Shape and amplitude of the diurnal variation of the D-layer electron density parameter, NMD, depending on solar activity differ remarkably between IRI-1978 and its corrected version IRI-79, as shown in Figure 1. In IRI-79, the solar-cycle variation

is considerably reduced as compared with IRI-1978. Another characteristic feature of the solar zenith angle variation of NMD in both models can also be seen in Figure 1; this is the rather artificial assumption that all diurnal curves of NMD have to merge at higher solar zenith angles ($\chi \geq 60^\circ$) into a constant night-time level.

With IRI-77, the comparison of mid-latitude observational data had to be made with model values for 45° latitude only, which could give rise to considerable errors in prediction, particularly in winter. The IRI-1978 and IRI-79 models now permit calculation for the proper latitudes of the reflection points of the real propagation paths.

3. Method of comparison

For the observed frequencies, propagation paths and parameters as listed in Table I, theoretical absorption values were calculated from the IRI-79 electron density profiles for 54°N latitude in the following way (see also Singer et al., 1980).

Table I

Theoretical calculation of absorption values

Input data: Collision frequency, ν_m (h) = $7.5 \cdot 10^5$ p/Nm⁻² (p from CIRA 72, 55°N , month).
 Observing frequency, f.
 Electron density, N_e (h) after IRI ($\varphi = 54^\circ\text{N}$; χ , month, R = 10 and 100),
 Geomagnetic field, B , at reflection point.

Oblique incidence

Vertical incidence

Full-wave method

Phase-integral method

L_{\perp} or L (penetrating mode)

L_o (ordinary mode)

Experimental data

f/kHz	(A 3 method)			(A 1 method)	
	d/km	$\varphi/^\circ\text{N}$		f/kHz	$\varphi/^\circ\text{N}$
50	190	50.7	Freiburg	1725	48.1
128.5	188	53.7		2050	
185	182	53.5		2440	
245	178	54.9	De Bilt	2300	52.1
529	83	53.8			
2614	395	53.5			

With oblique incidence at low and medium frequencies, the complex reflection (conversion) coefficient, R_{\perp} , was computed by the method of full-wave solutions, and from this the absorption value (in dB)

$$L_{\perp} = -20 \log |R_{\perp}|$$

was determined. For vertical incidence in the medium frequency range, theoretical absorption values were calculated by the phase integral method. In both cases, the geomagnetic field at the reflection point was taken into account, and the (mono-energetic) collision frequency was assumed to be proportional to neutral air pressure,

$$\nu_m(h) / \text{s}^{-1} = 7.5 \cdot 10^5 p / \text{Nm}^{-2}$$

where the pressure, p, was taken from the CIRA 1972 models for 55°N latitude and for the corresponding month.

The experimental data for radio wave absorption at oblique inci-

dence (A3 method) are provided by an extensive long-term observational programme in the German Democratic Republic. The measured quantity in the LF and MF ranges is the conversion coefficient R_{Xp} determined immediately from the ratio of sky-wave to ground-wave field strengths, so that instrumental (sensitivity) drifts are eliminated. HF absorption data at vertical incidence are taken from observational measurements made at Freiburg (FRG) and De Bilt (NL) following the internationally standardized procedures (A1 method).

4, Results of comparison

4,1 Summer day

D- and lower E-region electron density profiles from IRI-79 for summer (June) at 54° N latitude are shown in Figure 2 for solar zenith angles 31° , 60° and 80° . In Figure 3 and Figure 4, theoretical absorption values calculated on the basis of these model electron density profiles are represented by triangular symbols, whereas the experimentally observed absorption values and their diurnal variation are shown by curves.

Inspection of Figures 3 and 4 shows that, under conditions of low solar activity (thin curves, open triangles), the observed diurnal variation of oblique-incidence absorption between noon and $\chi = 60^{\circ}$ is generally well reproduced by the IRI model, except for some slight systematic differences in absolute magnitude on higher frequencies. The agreement between model and observation in the trend of the diurnal variation continues to be satisfactory up to $\chi = 80^{\circ}$ for higher frequencies. At lower frequencies, however, the calculated $\chi = 80^{\circ}$ absorption values are always slightly too large, probably in consequence of the artificial assumption about NMD remaining at the constant night level for $\chi \geq 60^{\circ}$.

The diurnal variation of observed absorption at vertical incidence is not well reproduced by the IRI model. This might be due to the fact that there is a rather large contribution of deviative absorption on the frequencies used, which introduces strong changes in resulting total absorption, even with minor changes in the shape of the electron density profile.

The outstanding problem showing up in Figures 3 and 4 is the fact that the variation between low and high solar activity appears to be much too large in the IRI-79 model as compared with the experimental data, at noon and at $\chi = 60^{\circ}$. On the other hand, at $\chi = 80^{\circ}$, a slight difference between low and high solar activity values is predicted by the IRI model for higher frequencies only. This is easily understood because the IRI-79 model assumes the existence of a solar activity dependence for the E-region, but not for the constant NMD night-time level valid at large zenith angles.

This discrepancy between model and observed solar-cycle variations in LF and MF absorption has already been found in our earlier work /Singer et al., 1980/ with the IRI-77 model. It has been reduced, but not removed, by the new IRI-79 model.

4,2 Equinox day

The behaviour of theoretical and experimental absorption values for April and September is essentially similar to that described above for summer. On lower frequencies, the calculated daytime values are generally higher than the observed ones. Also for equinox months, the amplitude of the solar-cycle variation is significantly larger in the IRI model than in the experimental data.

4,3 winter_day

Figure 5 shows profiles of electron density at 54°N latitude for solar zenith angles $\chi = 77^\circ$ (near noon) and 85° in winter (December). The full and dash-dotted curves represent the IRI-79 model, and the dashed curves are profiles derived from observed radio propagation data by a trial-and-error procedure /Bremer and Singer, 1977/. The latter curves show that, for an optimum interpretation of observed absorption data, a more complicated profile structure than that of IRI is needed.

When calculating absorption for winter at 54°N from the IRI model, we are restricted all the day to that range of solar zenith angles where the model no longer assumes any diurnal variation of the model parameter NMD (see Figure 1), but only a variation of the height parameter HMD. Nevertheless, comparison with experimental data presented in Figure 6 shows that the IRI model leads to a diurnal variation of absorption, the amplitude of which is in fair agreement with the observed one.

Large discrepancies, however, arise between model and observation in the absolute magnitude of radio wave absorption. At low frequencies (influenced mainly by the D-region part of the profile) the calculated absorption values are generally too large, whereas at higher frequencies the converse is true. This means that at least the D-region part of the IRI model electron density profiles is inadequate for describing the real winter behaviour. This is confirmed by the dissimilarity of the profiles in Figure 5 also.

The solar-cycle variation, which is clearly present in the experimental absorption data on 128.5 to 529 kHz, is not reproduced by the IRI model, because the observation frequencies do not penetrate sufficiently high into the E-region.

4,4 Night

The results of a comparison between observed and calculated IRI-model absorption during summer night are presented in Table II. The experimental absorption data are determined as average values over the time interval where $\chi \geq 100^\circ$. The theoretical values are therefore calculated for a corresponding time interval.

Table II

Comparison of observed night-time values of LF absorption with values calculated from the International Reference Ionosphere (IRI-79), for Summer (June)

Frequency (kHz)	Low solar activity (R = 10)		High solar activity (R=100)	
	L_{min} (obs.) (dB)	L_{min} (calc.) (dB)	L_{min} (obs.) (dB)	L_{min} (calc.) (dB)
50	14.0	15.5	no obs.	15.4
128.5	15.6	18.0	20.2	17.6
185	23.0	24.5	29.0	24.2
245	14.9	18.1	19.2	17.4

The agreement between observed and calculated absorption at night is quite satisfactory, the differences being not larger than 10 or 20

percent for low and high solar activity respectively. The character of the solar-cycle variation in the IRI model, however, is different from that observed, because IRI does not assume a solar-cycle variation in the night-time D-region, but only in the E-region. Thus, the height gradient of the IRI model electron density at the lower edge of the E-region at night becomes steeper with increasing solar activity, resulting in a decrease in the absorption loss of waves reflected there. Conversely, the observed data show an increase in night-time absorption with growing solar activity, which indicates that the night-time D-region ionisation also undergoes a solar-cycle variation. This solar-cycle variation is positively correlated with sunspot number, which means that the dominant night-time ionisation source for the D-region cannot be galactic cosmic rays (which should exhibit a negative correlation with sunspot number), but rather of solar origin (e.g., scattered Lyman-alpha and/or energetic particles).

The comparison between model and observed night-time absorption for equinox and winter leads to essentially the same results as for summer.

5. Conclusions

Our comparison of absorption values calculated from the most recent IRI-79 model with observed mid-latitude absorption data shows that, for the purposes of reference standards and practical applications, the IRI-model allows satisfactory prediction of radio wave absorption and its diurnal variation under conditions of low solar activity for all seasons except winter. There remain still the following shortcomings of the present IRI model of the D- and lower E-regions:

(1) The artificial assumption in the IRI, namely that the D-region parameter NMD at higher solar zenith angles merges into the constant, solar-cycle-independent night-time value, leads to deviations in the diurnal variation in the summer and equinox seasons, and is not realistic for winter at medium latitudes.

(2) The assumption made in IRI-79, namely that the constant night-time NMD value is independent of solar activity, leads wrongly to the prediction of an absence of solar-cycle variation at high solar zenith angle in winter, and to an erroneous negative solar-cycle variation of night-time absorption, in contradiction to the observational results.

(3) The most important discrepancy between the IRI model and our observational data is found in the solar-cycle variation of the D-region part of the daytime IRI electron density profiles, which leads to the amplitudes of the solar-cycle variation of absorption being considerably larger than the observed variation (by 10 to 30 dB in summer).

Discussion remark:

A.D. Danilov mentioned the recent determinations of collision frequencies from USSR rocket data made by Danilkin. K. Rawer pointed to the apparent discrepancy with available rocket measurements of the electron density profile which is still unresolved.

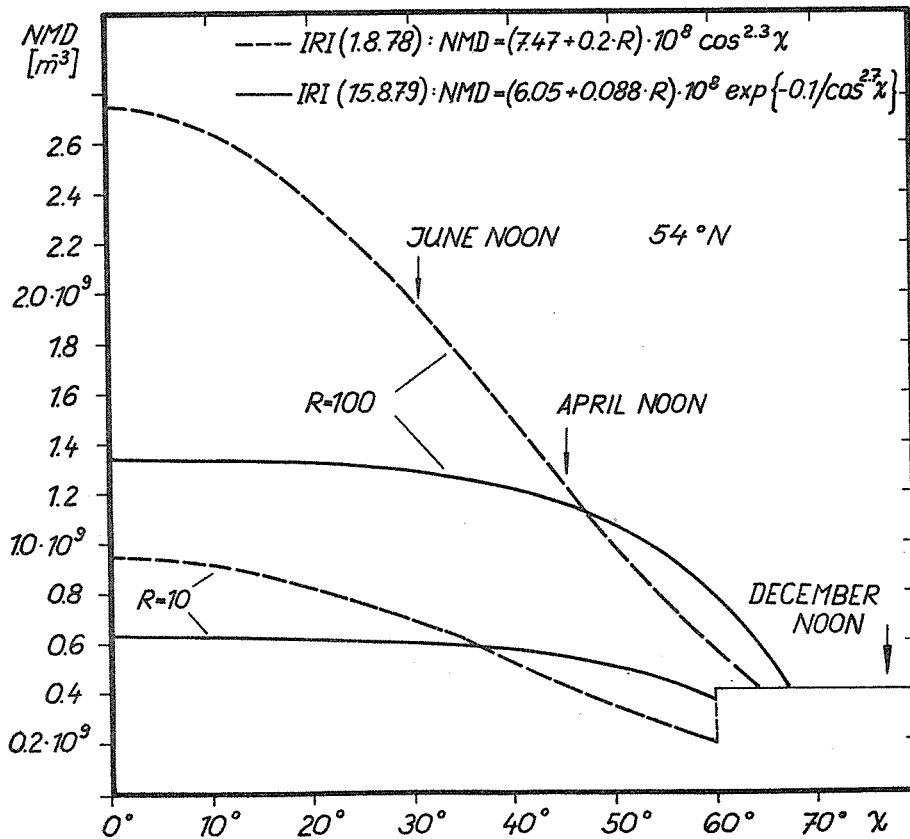


Fig. 1 D-Region parameter NMD as a function of solar zenith angle, χ , from the IRI versions of 1978 (dashed) and 1979 (full curve).

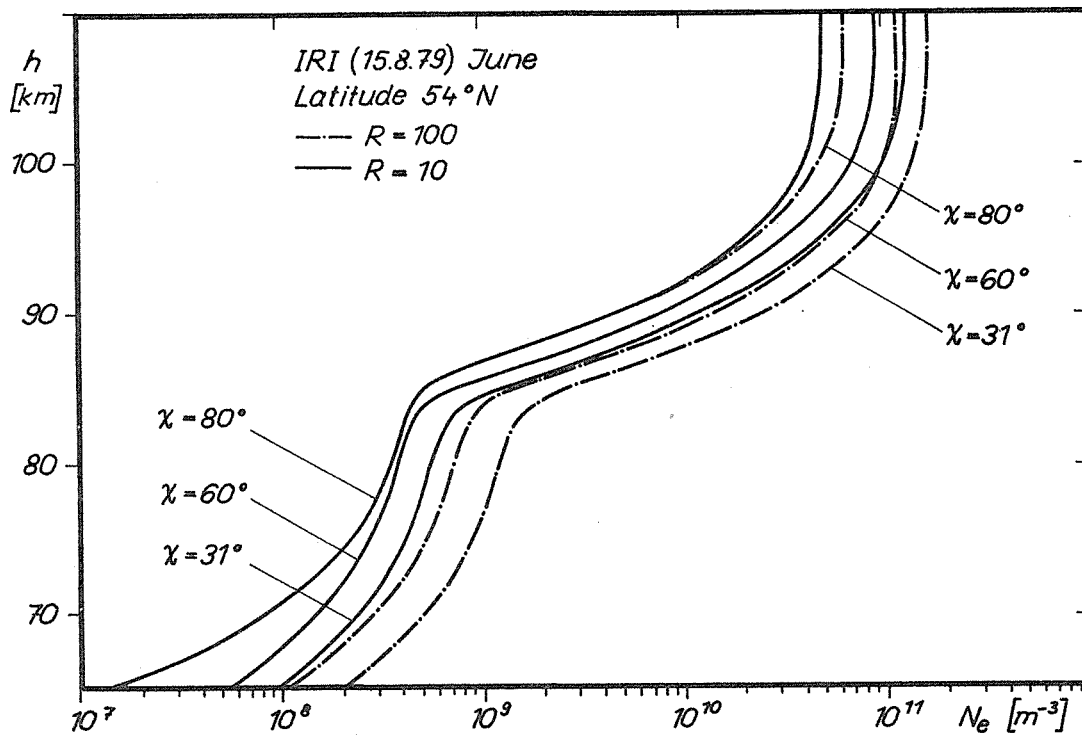


Fig. 2 Electron density profiles for summer (June) at $54^\circ N$ after IRI-79

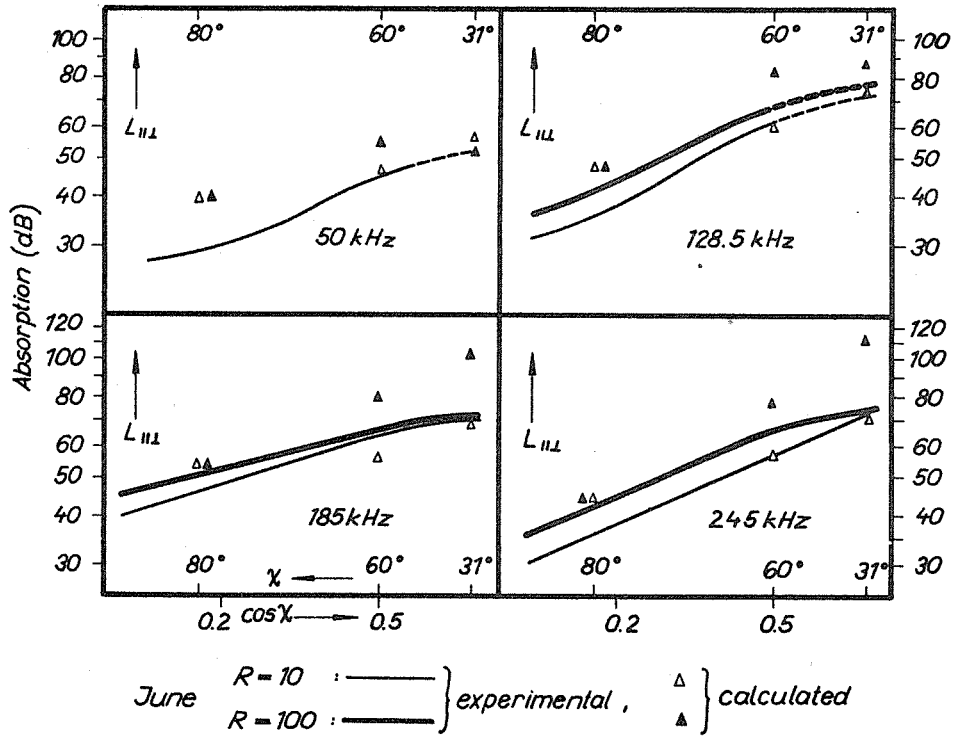


Fig. 3 Calculated (symbols) and observed (curves) radio wave absorption on LF, in dependence on the cosine of solar zenith angle, for summer.

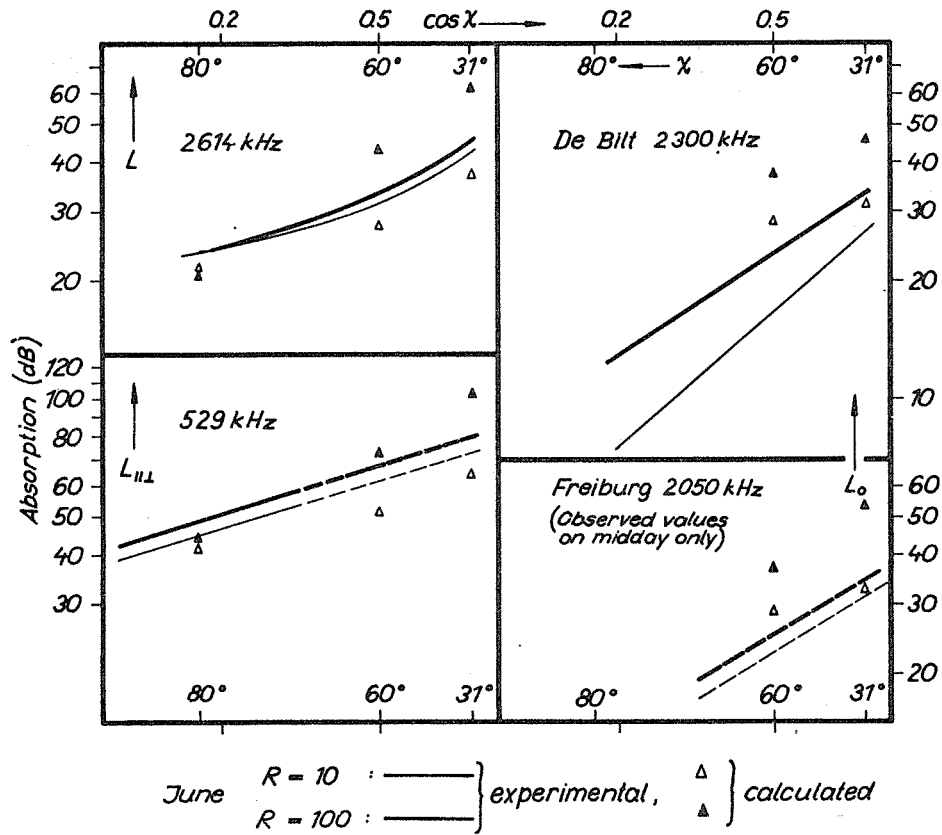


Fig. 4 Same as in Fig. 3, for MF and HF.

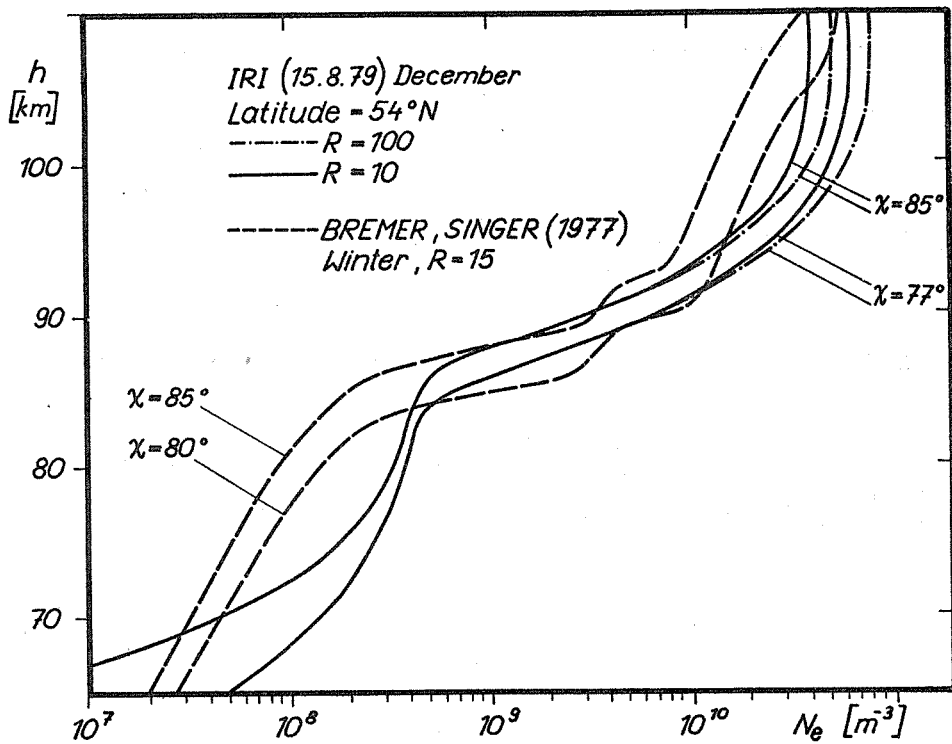


Fig. 5 Electron density profiles for winter (December) at 54°N after IRI-79 (full and dash-dotted curves, and after BREMER and SINGER (1977) (dashed curves)

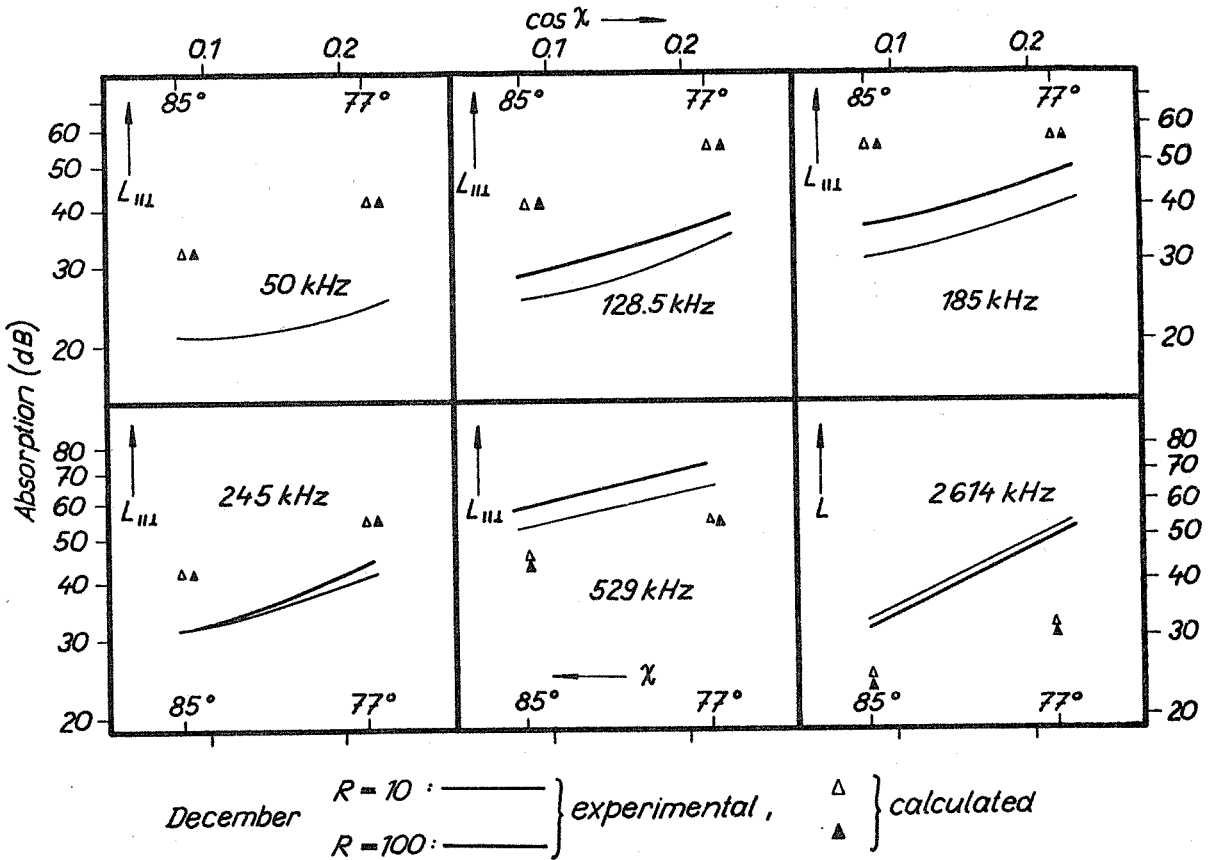


Fig. 6 Radio wave absorption for winter calculated after IRI-79 (symbols), and observed values (curves), in dependence on the cosine of solar zenith angle

1.1.2 D- and Lower E-Region Electron Density Profiles Compared
with LF and VLF Reflection Data

Y.V. Ramanamurty

Radio Science Division, National Physical Laboratory
Hillside Road, New Delhi-110012, India

Abstract: The reported best fit models from VLF and LF reflection data are compared amongst themselves, and with rocket profiles, in order to see whether the profiles obtained through the inversion process are similar to each other, and whether they agree with the direct measurements. The comparison shows (for both day and night conditions) that there are considerable differences amongst the profiles obtained by inversion on the one hand, and those given by direct measurements by rockets on the other hand. It was felt that there were considerable uncertainties associated with profile inversion, and that it should not be applied to averaged data. There still remains, however, the reverse possibility: to postulate a profile and to calculate its reflection characteristics. Model calculations show that the expected differences, which enable one to distinguish between various profiles, show up in the polarization. In future, one should have more accurate MF/LF/VLF measurements, giving due consideration to polarization, and one should devise a combination of experiments in which it may be possible to measure all the four conventional reflection coefficients, in order to decide on the merits of the various postulated models through comparison of calculated and measured coefficients.

1, Introduction

With given reflection data at various frequencies and distances, one may look for an electron density profile which fits well with the data. The question then is whether one gets a clear-cut realistic profile. For comparison, one might use rocket measured profiles and try to identify the propagation effects in conjunction with the height dependent features of electron density. Rocket profiles of electron density measured on the same day near noon at Thumba /Alkin et al., 1972/ are shown in Figure 1. Apart from some fine structure, a characteristic step at about 80 km can be seen, a feature which is also proposed in the International Reference Ionosphere (IRI) Models compiled by Rawer et al. /1978a/.

Rocket measurements of electron density at night for the solar zenith angles χ of 98° , 108° and 152° due to Kane /1972/, Mechtly and Smith /1968/ and Irakash et al. /1970/, respectively, are shown in Figure 2. There is wide divergence in the shape of the profiles.

So we come to the following questions:

(i) Through the inversion process of MF/LF/VLF data do we obtain profiles similar to each other? Do we find the same characteristic features in all of these?

(ii) Do these profiles agree with the direct measurements?

The present paper deals with these questions and tries to describe the current status in this regard.

2, D- and Lower E-Region Electron Density Profiles

Rocket launches with instrumentation for local electron density measurement were made at various places around the world. Different attempts were made to synthesize these profiles so as to reach a global model. About 700 published D-region profiles were made computer-accessible by McNamara /1978/, and 242 of these profiles were reported to pass through 90 km. The shape and gradient of electron density distribution are of importance in characterising the profiles, and for comparison with VLF and LF reflection data. Mechtly and Bilitza /1974/ were the first to classify the then available rocket profiles into different types. They clearly identified two types of D-region profiles: those with a steep gradient of electron density above an inflexion point, and those which resemble a sloping letter S. Certain daytime profiles show a nearly monotonic increase of electron density with height. There are also profiles with a distinct C layer, and some without it. The presence of this layer is known to have a significant influence on the propagation of VLF radio waves to long distances.

A proper and convenient representation of electron density for different geophysical conditions is very important also from the application point of view. Booker /1977/ favours an analytical form of representation of electron density with one appropriate analytical function maintaining continuity, so that no significant errors occur when certain types of numerical technique are used for the calculation of wave propagation characteristics. A representation in the form of a computer program is described by Rawer et al., /1978a/. The electron density at a particular height in the D-region is, in general, dependent on solar zenith angle, season, sunspot number and latitude, probably in decreasing order of importance as indicated by the results of McNamara /1978/ and Mitra and Somayajulu /1979/. It is also known that the degree of dependence of D-region electron density on the solar zenith angle varies with height. Since, in the observed profiles, variability (a part of which could be due to the dynamics of the middle atmosphere) is evident, simple averages may not show clearly the individual influences of solar zenith angle, season, sunspot activity and latitude. Shape and gradient of electron density are of importance particularly when considering the twilight periods and when interpreting solar flare effects at LF/VLF. There is also the need to look for physical/empirical relationships showing the various factors which influence the electron density at a particular height, so that various types of VLF/LF data collected under different geophysical conditions may be compared with the profiles.

3, LF and VLF Reflection Data

For the purpose of profile inversion, it is desirable to include only short path (less than 500 km) observations. The assumption of a plane stratified ionosphere is justified for such paths and full-wave theory can immediately be used as the connecting link between the reflection data and the ionospheric profile. The resulting profile can then be assumed to represent the electron distribution over a particular location for the corresponding geophysical conditions. Certain problems appear when the long path VLF/LF observations are used for profile inversion; these will be discussed in a subsequent section. Most of the published LF and VLF reflection data have already been discussed by several investigators in terms of the best-fit electron density profiles, as shown in Figures 3 and 4 for day and night conditions respectively.

In Figure 3, curve 1 shows the best-fit profile obtained by Deeks /1966/ at noon ($\chi \approx 50^\circ$) for mid-latitude, March, low solar activity conditions; it shows a prominent C layer. The profile shown as curve

2 represents the best-fit profile obtained by Bain and Harrison /1972/ at noon ($\chi \approx 30^\circ$) for mid-latitude, Summer (June), high solar activity conditions; it also shows a C-layer. However, Foley et al. /1977/ found that the VLF Omega ground interference data at low latitudes are more consistent with a profile similar to the one obtained by Beeks, but without a C-layer below 70 km. Their representation of the profile below 70 km for low latitudes, at noon ($\chi \approx 20^\circ$) in August for low solar activity conditions is shown as curve 3. Bremer and Singer /1977/ used a large set of VLF/LF/MF reflection/propagation data (for the latitude range $35^\circ \dots 55^\circ$ N) to deduce a set of average profiles for different geophysical conditions. A typical profile derived by them for $\chi \approx 60^\circ$, low solar activity, mid-latitude summer conditions is shown as curve 4. The most recent equatorial profile for high solar activity conditions has been derived by Behroozi-Toosi and Booker /1980/ and is based on ELF propagation evaluation; it is shown as curve 5. The profile marked 6, discussed by Bain and May /1967/, has been obtained by Krasnushkin and Kolesnikov /1962/. Neither this profile, nor the revised set of profiles obtained by Krasnushkin and Knyazewa /1970/ for various geophysical conditions at mid-latitudes, show a distinct C-layer. The curve marked 7 was obtained by Shellman /1973/ and is based on near vertical incidence VLF sounder data referring to noon-time, mid-latitude, March, high solar activity conditions. This profile also shows a prominent C-layer; however, the peak is at a somewhat higher level during this month. In the L-region profile obtained by Shellman /1970/ for October, the peak of the C-layer is about 5 km lower. It is also interesting to note that his results indicate the filling up of the valley above the C-layer peak after the commencement of a solar flare. A typical exponential daytime profile /Wait and Spies, 1964/, a model which has been extensively used by several investigators for the interpretation of long path VLF observations, is shown as curve 8 in Figure 3.

Some typical best-fit night-time profiles are shown in Figure 4. The profile obtained by Beeks /1966/ for low solar activity, March, mid-latitude conditions is shown as curve 1, and that obtained by Thomas and Harrison /1972/ for high solar activity, Summer, mid-latitude conditions as curve 2. The profile obtained by Behroozi-Toosi and Booker /1980/ for representative equatorial low solar activity conditions is shown as curve 3; it was based on ELF propagation considerations. The profile obtained by Cairo et al. /1974/ for moderate to high solar activity conditions at mid-latitudes in summer is shown as curve 4. Curve 5 was obtained by the same authors for moderate to high solar activity conditions at mid-latitudes. The profile marked 6 was an earlier typical International Reference Ionosphere model suggested by Rawer et al. /1977/ for low latitude (18° N), June, midnight, low solar activity conditions.

4. Comparison of Profiles

It can be seen that, during day-time, the step at about 80 km exists in most but not all of the profiles. There is evidence for the existence of a C-layer around 70 km in a few cases, and this is important for VLF reflection phenomena. Moreover, there are profiles which have many layer-like structures as well as some which are nearly flat. This is true also for the more recent profiles: curves 3, 4 and 5 in Figure 3. One must therefore conclude that there is no definite evidence to show that the reported best-fit profiles agree with each other or with the direct rocket measurements. Some of the direct measurements, such as those shown in Figure 1, and the rocket LF propagation measurements discussed by Hall /1973/, provide evidence for the existence of a clear C-layer, but show little similarity to those obtained from profile inversion. The two questions posed in the Introduction must therefore be answered in the negative.

The situation for night conditions (Figures 2 and 4) is much worse. The best-fit night-time profiles drawn in Figure 4 show a sharp gradient near 88 km, but considerable differences exist in the shape and

and absolute values at all heights. The position of the gradient and the shape of the profile below 90 km are very important features both for modelling purposes and for VLF/LF reflection phenomena. Average electron density profiles based on rocket measurements /Maeda, 1969/ reveal some systematic time variations during night-time near the peak (100...105 km) of the E-layer. However, as can be seen from Figure 2, the individual profiles show large variability as a function of height for night-time conditions. It is thus seen that for both day and night conditions, there are considerable differences between the profiles obtained by inversion on the one hand and by direct measurements by rockets on the other hand.

It is, therefore, important to know whether the reflection characteristic depends sensitively on certain parameters like the frequency or the angle of incidence. In spite of the limits of error associated with the measurements of Shellman /1973/, it is quite clear from the frequency dependence (Figure 5) that a selective minimum occurs, and hence conclusions based on measurements at a few frequencies only are not good enough. Moreover, averaged field-strength values are likely to smear out typical effects associated with the very nature of the reflection process. As shown in Figure 7, a strong variation of the reflection coefficient is found for large angles of incidence, and hence such angles must be avoided in D-region modelling considerations through inversion procedures.

It is therefore evident that considerable uncertainties are associated with profile inversion and, in consequence, it should not be applied to averaged data. There still remains, however, the reverse possibility, namely to postulate a profile and to calculate its reflection characteristics.

5, Model Calculations

The four conventional reflection coefficients ${}_{\perp}R_{\parallel}$, ${}_{\parallel}R_{\perp}$, ${}_{\perp}R_{\perp}$, ${}_{\parallel}R_{\parallel}$ discussed by Budden /1962/ provide a connecting link between the measured parameters and those computed from models, while the reflection coefficients R_{\parallel} and R_{\perp} for the penetrating and non-penetrating modes discussed by Pitteway /1965/ give an insight into the transmission properties of the assumed profiles. Conservation of energy requires /Figgott et al., 1965/ that:

$$R_{\parallel}^2 + R_{\perp}^2 = |{}_{\perp}R_{\perp}|^2 + |{}_{\perp}R_{\parallel}|^2 + |{}_{\parallel}R_{\parallel}|^2 + |{}_{\parallel}R_{\perp}|^2 \leq 2 \quad (1)$$

At short distances (less than about 500 km) one or two of the conventional reflection coefficients are usually obtained from the measurements as indicated in Table 1.

Table 1

Connecting Parameters

short distance (500 km)

${}_{\parallel}R_{\parallel}$	${}_{\parallel}R_{\perp}$
${}_{\perp}R_{\perp}$	${}_{\perp}R_{\parallel}$

long path

Ray Theory

$$R_m = \begin{bmatrix} {}_{\parallel}R_{\parallel} & {}_{\parallel}R_{\perp} \\ {}_{\perp}R_{\parallel} & {}_{\perp}R_{\perp} \end{bmatrix} \begin{bmatrix} R_{g\parallel} & 0 \\ 0 & R_{g\perp} \end{bmatrix}$$

Mode Theory

$$\Delta\alpha_i \approx \Delta\alpha_i(\phi) + \Delta\alpha_i(\chi) + \Delta\alpha_i(LAT) + \Delta\alpha_i(R)$$

$$\alpha_i = -20 \log_{10} (R(\text{model}))$$

Attenuation: total = ground attenuation + ionospheric atten. α_i

In order to interpret the long path VLF and LF fieldstrength and relative phase measurements, either from ray or from mode theory considerations, an adequate number of hops (m) or modes should be considered. For such situations, all the four conventional reflection coefficients are involved, and in multihop ray theory considerations, also the ground reflection coefficients /wait, 1961/. The interpretation based on waveguide mode theory is usually carried out /wait, 1967/ using an effective attenuation decrement α_i due to the ionosphere. Any change in the electrical properties of the ground or the ionosphere influences the effective attenuation rate. The change in ionospheric attenuation, $\Delta\alpha_i$, can be regarded as the sum of the individual contributions depending on longitude (ϕ), solar zenith angle (χ), latitude (Lat) and sunspot number (R) as shown in Table 1.

It is difficult, on long propagation paths, to evaluate the individual reflection coefficients from total fieldstrength measurements alone. It is equally difficult to calculate an effective reflection coefficient R(model) from profiles in view of the strong dependence of the reflection coefficients on angle of incidence at large angles of incidence, and because of the fact that an integrated effect along the whole propagation path is involved. For some typical models, the magnitudes of the computed reflection coefficients obtained with the full-wave computer program due to Scarabuci /1969/ are shown in Table 2.

Table 2

Description of the Model

Model No.

1. Daytime model due to Earrington and Thrane (Figure 6) /1962/.
2. Daytime model due to Pain and Harrison (Figure 3, curve 2) /1972/.
3. Night-time exponential model discussed by Figgott et al., /1965/ with $H_o = 3.42$ km, $h_o = 80$ km.
4. Night-time exponential model discussed by same authors with $H_o = 1.71$ km, $h_o = 60$ km.
5. Night-time eralier IRI model suggested by Rawer et al., (curve 6, Figure 4) /1977/.

Model No.	i	f (kHz)	ϕ	I	R_p	R_n	$\perp R_{\perp}$	$\perp R_{\parallel}$	$\parallel R_{\perp}$	$\parallel R_{\parallel}$
1.	83°	16	111°	68°	0.66	0.67	0.63	0.02	0.05	0.66
2.	33°	16	111°	68°	0.11	0.31	0.24	0.11	0.11	0.17
3.	30°	16	111°	68°	0.07	0.77				
4.	30°	16	111°	68°	0.18	0.34				
5.	83°	16	111°	68°	0.69	0.76	0.44	0.23	0.25	0.70
6.	83°	22.3	132°	14°	0.62	0.35	0.43	0.12	0.32	0.16

The daytime model (Figure 6) due to Barrington and Thrane /1962/ is designated as Model 1 and its reflection properties have already been discussed by Piggott et al. /1965/. This model has a characteristic step similar to the one found in rocket profiles, but at a lower height. The daytime model (Figure 3, curve 2) due to Bain and Harrison /1972/ is designated as Model 2. For the night-time, the properties of an exponential model of the form

$$N = N_0 \cdot \exp \left\{ -(h-h_0) / H \right\} \quad (2)$$

were already discussed by Piggott et al. /1965/. In Table 2, Model 3 represents the exponential height distribution with $H_0 = 3.42$ km and $h_0 = 80$ km, while Model 4 stands for the distribution with $H_0 = 9.71$ km and $h_0 = 60$ km. The earlier night-time IRI profile (Figure 4, curve 6) suggested by Rawer et al. /1977/ is designated as Model 5.

The reflection coefficients were computed for the two frequencies 16 and 22.3 kHz for the IRI model with the same (real) angle of incidence (θ) and with specific values of azimuth (ϕ) and dip (I) as shown in Table 2. (The profile below 85 km was extended by the author as indicated by the dashed line extending curve 6 in Figure 4.) The results of calculations for Model 1 are in agreement with those presented by Piggott et al. /1965/ and provide a reference for comparison with subsequent calculations. The reflection coefficients obtained from Model 2 are also in reasonable agreement with those obtained by Bain and Harrison /1972/. The values of R_p and R_n obtained by Piggott et al. /1965/ for the night-time exponential models for the two sets of h_0 and H_0 are also shown in Table 2.

The results of the calculations discussed by Piggott et al. /1965/ showed that R_p was very small for all angles of incidence near 10° and was less than R_n for all angles of incidence. The ratio R_p/R_n approached unity for large angles of incidence. The calculated frequency dependence of R_p (for a fixed angle of incidence of 25°) for the night profile (Model 3) showed a strong minimum near 14 kHz, and R_p was always less than R_n for frequencies less than about 100 kHz. It had also been noted that R_n increased by about 8% and R_p by 40% when the scale height (H_0) was halved, while keeping the electron density at 80 km constant.

The results of calculations for the earlier night-time IRI model (Model 4) indicate large values of R_p comparable with the value for the daytime profile (Model 1), and in fact R_p exceeded R_n at 22.3 kHz. There is a large difference between the calculated magnitudes of " R_n " for the night-model for the two frequencies, which differ by only 6.3 kHz, while it is nearly the same at 16 kHz for both day and night conditions. Differences which might make it possible to distinguish between various profiles appear only in the polarization. The rather large values of R_p at 16 and 22.3 kHz, coupled with the fact that the conservation of energy requirement (Equation (1)) is not satisfactorily fulfilled, suggests however that the calculation should be repeated using a different shape (gradient) in the earlier IRI profile, especially at heights below 85 km. Unfortunately, detailed polarization measurements are almost inexistent. In future, it would be desirable to have simultaneous accurate measurements of the conventional reflection coefficients so as to make it possible to decide between the various models proposed.

Concluding remarks :

A proper and convenient representation of electron density for different geophysical conditions is very important both from research and application points of view. As far as the D- and E-regions are considered the IRI /Rawer et al., 1978a/ considers (at a particular height) four parameters, the solar zenith angle, season, sunspot number and latitude in decreasing order of importance. This is also

shown by the results of McNamara /1978/ and Mitra and Somayajulu /1979/. It is also known that the degree of dependence of D-region electron density varies with height; this might be due to the dynamics of the middle atmosphere. Anyway, since variability in the observed D-region profiles is evident, the influence of these factors has to be carefully formulated. The shape and gradient of electron density are of importance, particularly when considering the twilight periods and while interpreting solar flare effects at VLF/LF. While the IRI procedures for the D- and E-region modelling adopt the peak/inflexion point electron densities, the height of the peak and of the inflexion point, the profile should be given as an analytic function of height once it is established based on IRI procedures. At frequencies below 300 kHz such representation is needed when computing full wave reflection coefficients to avoid errors when certain numerical operations are performed on these profiles. This was pointed out by Booker /1977/ and was subsequently emphasized by Gulyaeva /1980/ who has also suggested a FORTRAN Subroutine to incorporate this aspect in the IRI /1978/ program. Besides this aspect it is also easier to feed the profile to other computer programs like VLF/LF fieldstrength and phase calculation programs which require a lot of computer memory.

Summary

It would be desirable to have more accurate MF/LF/VLF measurements, giving due consideration to polarization, and to devise a combination of experiments in which it may be possible to measure all four conventional reflection coefficients, in order to facilitate a decision between the various postulated models by comparison of calculated and measured coefficients.

Acknowledgement

The author is indebted to Prof. Karl Rauer for presenting the invited paper at the twenty-third COSPAR Conference at Budapest and for many valuable suggestions for preparing this revised text. Part of the work was done while the author was with him as Fellow of the Alexander von Humboldt Foundation at Institut für physikalische Weltraumforschung, Freiburg, F.R.Germany.

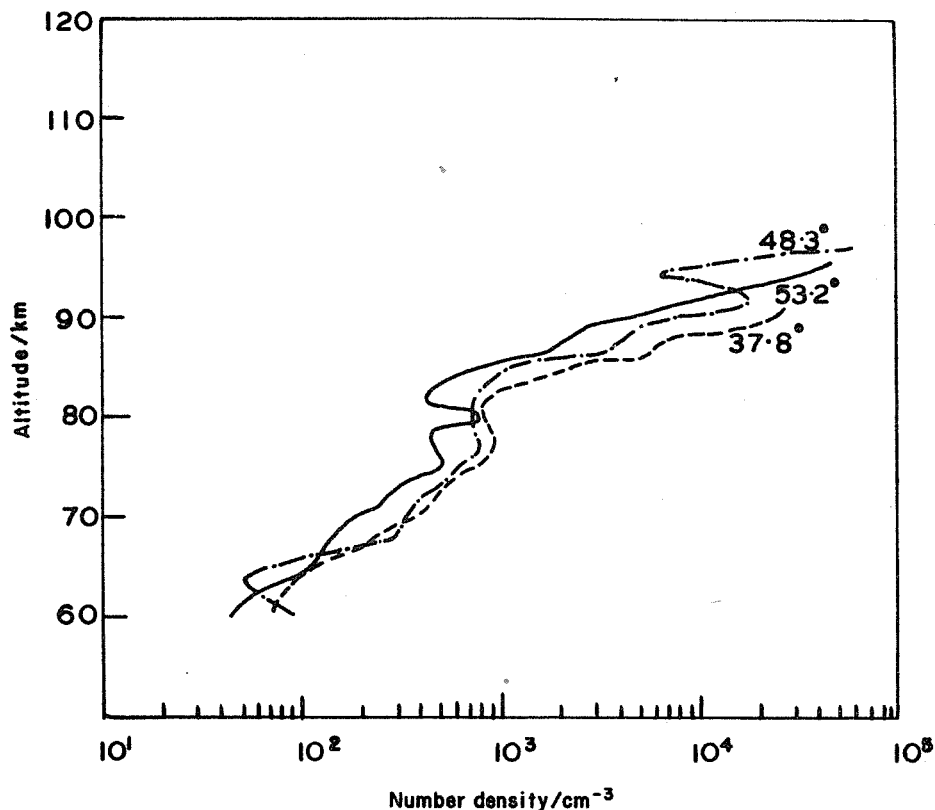


Fig. 1 Daytime electron density profiles obtained on 19 March 1970 with different solar zenith angles (parameter) at Thumba by a propagation experiment between ground and rocket. [Aikin et al., 1972]

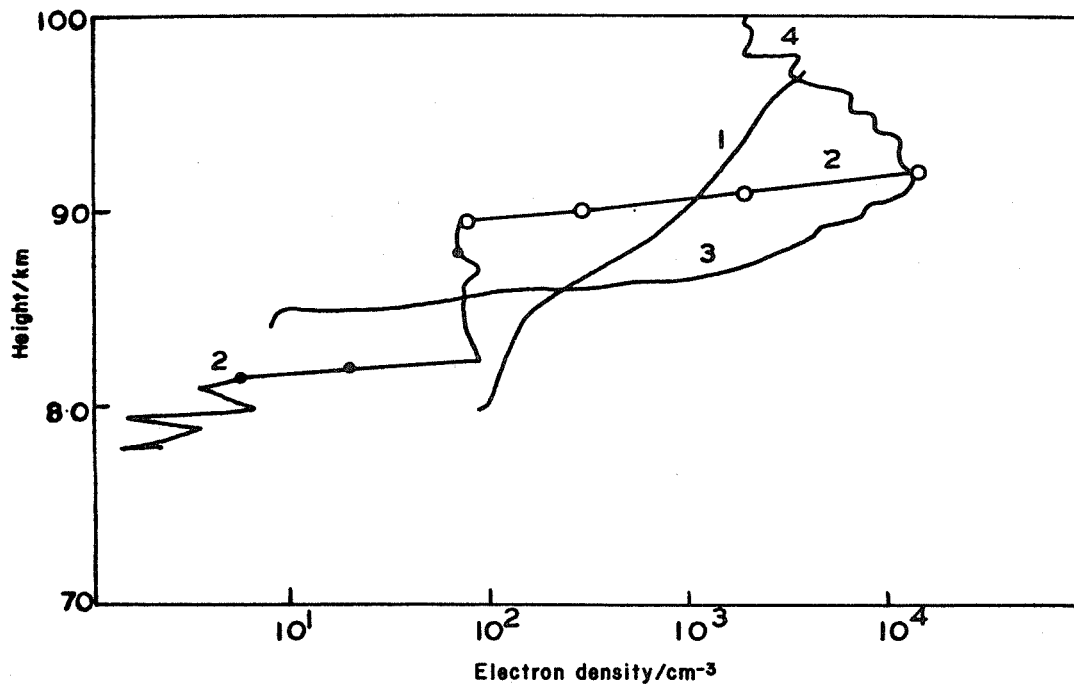


Fig. 2 Nighttime electron density profiles obtained at different times at Thumba: (1) $\chi=98^\circ$ [Kane, 1972]; (2) $\chi=108^\circ$ (circles: propagation, dots: Langmuir probe) [Mechtly and Smith, 1968]; (3) $\chi=152^\circ$ [Satya Prakash et al., 1970].

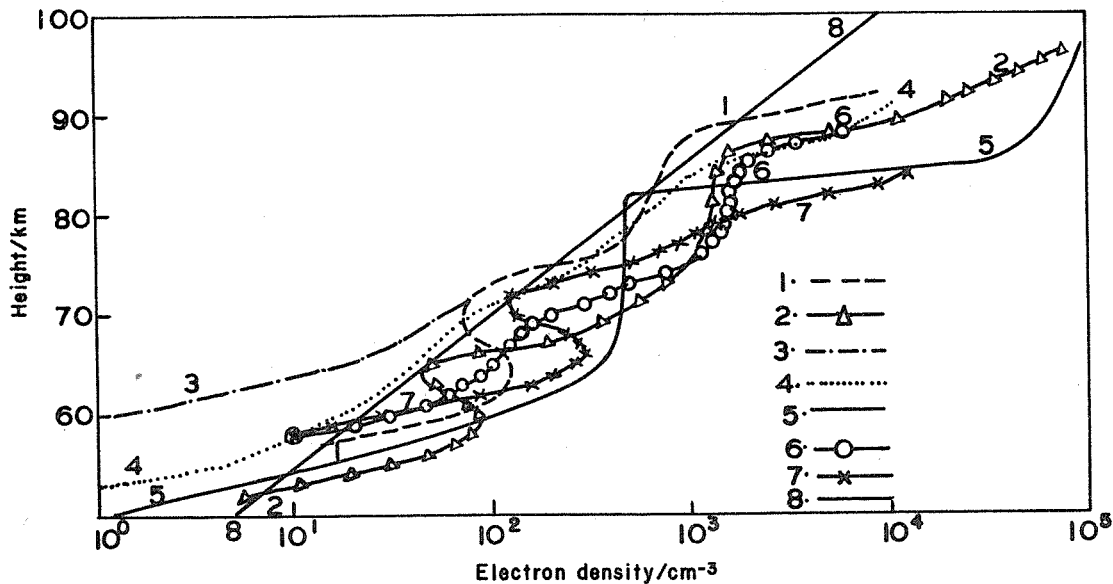


Fig. 3 Some typical daytime best-fit profiles of electron density reported from ELF, VLF, LF data: (1) Noon-time (χ 50°), mid-latitude, March, low solar activity [Deeks, 1966]; (2) Noon-time (χ 30°), mid-latitude, summer (June), high solar activity [Bain and Harrison, 1972]; (3) χ 20°, low latitude, August, low solar activity [Foley et al., 1977]; (4) χ =60°, mid-latitude, summer, low solar activity [Bremer and Singer, 1977]; (5) χ =0°, low latitude, high solar activity [Behroozi-Toosi and Booker, 1980]; (6) Noon-time, mid-latitude, summer, high solar activity [Krasnushkin and Kolesnikov, 1962]; (7) Noon-time, mid-latitude, March, high solar activity [Shellman, 1973]; (8) Noon-time, exponential profile with a typical slope [Wait and Spies, 1964].

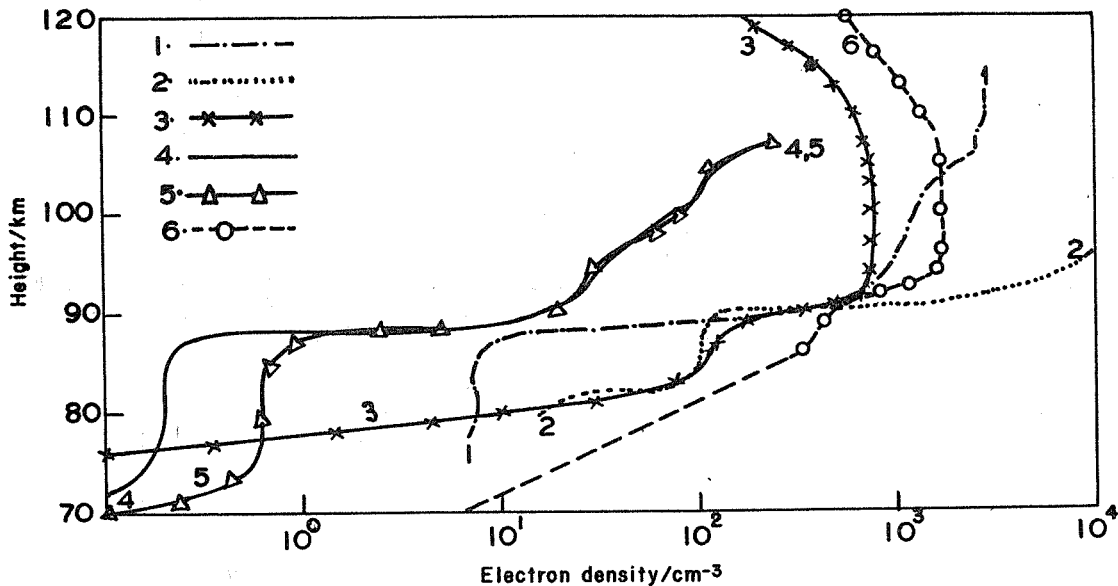


Fig. 4 Some typical nighttime best-fit profiles of electron density reported from ELF, VLF, LF data: (1) night, mid-latitude, March, low solar activity [Deeks, 1966]; (2) Night, mid-latitude, summer, high solar activity [Thomas and Harrison, 1970]; (3) Night, low-latitude, average, low solar activity [Behroozi-Toosi and Booker, 1980]; (4) Night, mid-latitude, summer, moderate/high solar activity [Cairo et al., 1974]; (5) Night, mid-latitude, winter, moderate/high solar activity [Cairo et al., 1974]; (6) Mid-night, low latitude, June, low solar activity [Rawer et al., 1977].

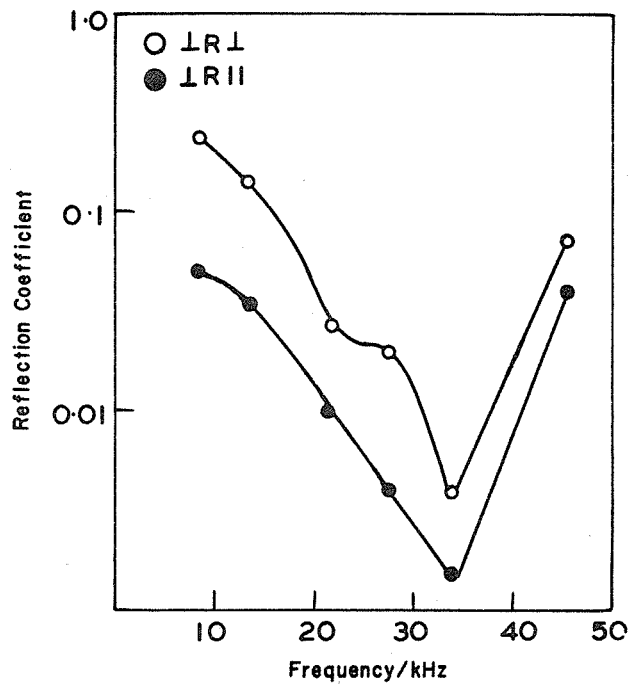


Fig. 5 Frequency dependence of LRI and LRII at near vertical incidence reported as by Shellman [1973]. Arizona 23 Mar 1971, 03LT.

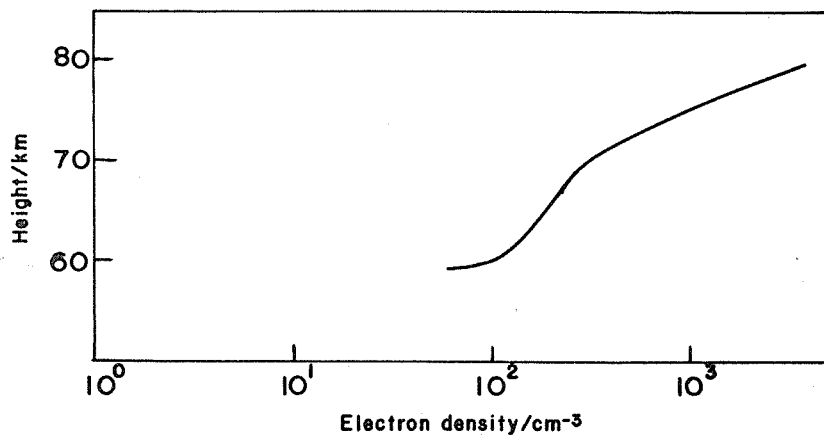


Fig. 6 Model electron density distribution due to Barrington and Thrane [1962]. VLF/LF reflection properties were discussed by Piggott et al. [1965].

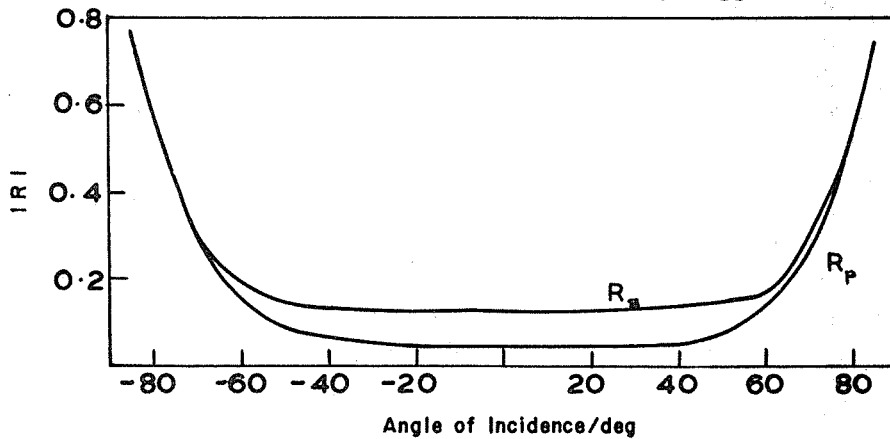


Fig. 7 Dependence of the reflection coefficients R_p and R_n for the penetrating and non-penetrating modes on angle of incidence calculated for Model 1 (Fig. 6).

1.1.3 Comparison of Ionospheric Electron Lensity Models Using Data from a Mid-Latitude Absorption Path

M. Friedrich¹, K.M. Torkar²

¹Dept. of Communications and Wave Propagation,

²Space Res. Inst. of the Austrian Academy of Sciences,
Technical University, Graz, Austria

Abstract: Ionospheric radio wave absorption is computed for different solar zenith angles and seasons using IRI and an ion-chemical model. When compared with measurements, it appears that IRI can only insufficiently reproduce the sudden increase of absorption at sunrise, whereas the ion-chemical model suffers from a deficiency in the electron density in the lower E-region.

Between October 1974 and June 1976, an A3 absorption path was in operation between Coburg (FRG) and Graz (Austria). The frequency used was 2.83 MHz and the distance was 502 km. The CW transmissions were interrupted during one out of every five minutes to allow a check of the background noise to be made /Torkar et al., 1978/. The highest signal in each 5-min interval was recorded and filed with the solar zenith angle χ at the mid-point of the path (48.7°N, 13.2°E).

In Figure 1 the absorption (vs. an assumed reference via a nocturnal E_s) is plotted for $\chi = 40 \pm 10^\circ$ to $140 \pm 10^\circ$. One can clearly see the higher absorption in winter at the same solar zenith angles (winter anomaly). The absorption h was also computed theoretically, using IRI /Rawer et al., 1978a/ for the path's mid-point with solar activity $R = 20$ for each month in a ray tracing programme for a spherical Earth /Torkar, 1977/. The 'most probable transport collision frequency' ν was determined from the pressure p of the recent atmospheric model by Cole and Kantor /1978/ interpolated for the correct latitude, multiplying p by a proportionality factor K which was chosen as $5.8 \cdot 10^5 \text{ m}^2\text{N}^{-1}\text{s}^{-1}$ after Smith et al. /1978/. These authors determined K from observations where ν and p were measured simultaneously. Proportionality of both can be assumed according to the laboratory measurements by Phelps and Pack /1959/. It is important to note that ν was used by Sen and Wyller /1960/ in their formulation of the refractive index as used in the present ray tracing calculations. (In the classical dispersion formulas, however, the 'averaged transport collision frequency' is used.)

One clearly sees in Figure 1 seasonal variation of the simulated absorption. In winter, however, its variations do not agree with those of the mean day-time absorption. This is to be expected since electron density profiles of days including typical winter anomaly 'events' were deliberately excluded in the construction of IRI. The rather large variations at night are not due only to the scarcity of usable data, but more likely to be a consequence of the changing reflection conditions rather than of absorption. At large zenith angles the simulated absorption is in reasonable agreement with the observations; however, for large absorption (L greater 30 dB at $\chi < 60^\circ$) the measured data tend to be somewhat lower than the simulation. Now the measured mean values are probably slightly biased towards 'moderate' absorption due to saturation (at night) or to the occurrence of signals below the equipment's threshold (at noon). Nevertheless, it must be concluded that the model electron densities are too high since the above value of K (relating ν to p) is perhaps the lowest in the literature. From a recent compilation of laboratory measurements by Aggarwal et al. /1979/ one should expect $6.34 \cdot 10^5 \text{ m}^2\text{N}^{-1}\text{s}^{-1}$ for D-region temperatures. Other experimental

values are nearer to $8.0 \cdot 10^5 \text{ m}^2 \text{N}^{-1} \text{ s}^{-1}$ /e.g., Thrane, 1968/. (The even higher value of $9.9 \cdot 10^5$ reported by Bennett et al. /1972/ is probably due to the determination of the pressure p.) The old CIK /1972/ atmospheric model would give about 30% less pressure, and therefore a smaller collision frequency in the L-region. However, as pointed out by Cole /1979/, the much higher number of measurements strongly supports the choice of the present atmospheric model /Cole and Kantor, 1978/.

It was also attempted to build an ion chemical model using physical and chemical considerations rather than statistics. The complete description is given elsewhere /Torkar and Friedrich, 1980/, and here only the main features will be indicated. In a steady state model, the production processes include scattered light, cosmic rays, direct solar UV and X-rays and the neutral atmosphere taken from the Cole and Kantor /1978/ model. As for the (variable) minor species, the density of atomic oxygen O was basically taken from the model computation by Thomas and Fowman /1972/, but the NO density came from the measurement of Tohmatsu and Iwagami /1975/. This low latitude measurement on the average provided the best agreement with the observations. The frequently used NO densities of Meira /1971/ are now widely considered to give values which are too large.

As a next step the absorption as a function of solar zenith angle was calculated using IKI and the ion chemical model. Figure 2 shows the comparison with the measurement (mean over a month) for January and July. Two features can be deduced:

- a) Similarly to Figure 1 one realises that, for small zenith angles in summer, both simulated absorptions are too high. If in winter they are too low, this is because as observed absorption we took a simple mean over all data for the months of January 1975 and 1976 and thus included days of pronounced winter anomaly. For the compilation of IKI such cases were deliberately omitted.
- b) Sunrise occurs some 10^0 earlier in the absorption when using IKI. Qualitatively, the ion chemical model reproduces the sunrise conditions in a more realistic manner.

The results using the ion chemical model can be brought into gross agreement by varying the NO densities with season (i.e., higher in winter, lower in summer) as predicted from model calculations, e.g. by Shimazaki and Laird /1972/.

The steeper variation at sunrise must be expected from the variation of the electron densities vs. the solar zenith angle which is different in the two models. Figure 3 shows IKI for geographic and geomagnetic latitude 45^0 , equinox and $R = 50$ from 0 to 12 LT together with the result of the present ion chemical model for the same conditions. One can clearly see the much steeper increase at sunrise occurring in two steps (Photodetachment and subsequent direct solar ionization). During the day there is a notable deficiency at 90 and 100 km of the modelled electron density as compared with IKI which, because of the larger number of measurements, is probably reliable at these heights. This problem has been encountered by other authors /e.g., Golshan and Sechrist, 1975/ and seems to be due to uncertainties in the ion production by soft and medium X-rays. It should be mentioned here, that other and more sophisticated models /e.g., Ogawa and Shimazaki, 1975/ similarly show a sudden increase of the electron density at sunrise.

Discussion remarks:

The author admitted that below 90 km he had changed the CIR model adapting it to the Cole and Kantor chemical model which gives higher temperature. Also the coefficient of proportionality was chosen somewhat lower than the most recent laboratory measurements (5.8 instead of 6.4) while earlier determinations ended up with higher values up to 9.9.

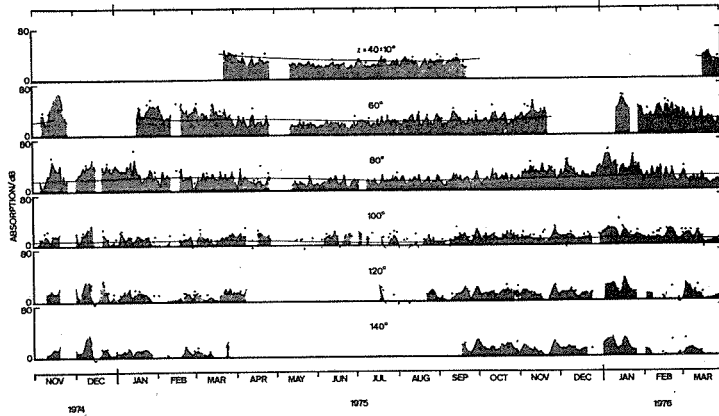


Fig. 1

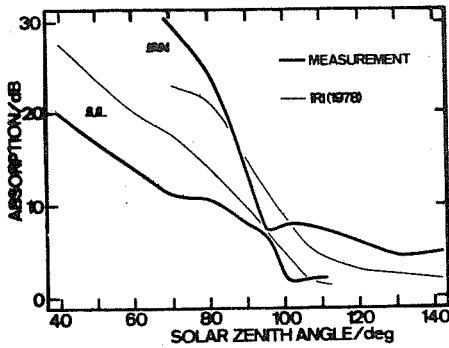


Fig. 2

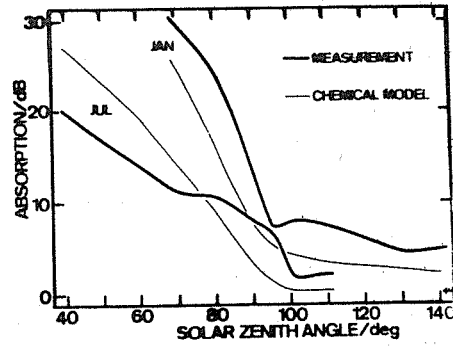


Fig. 3

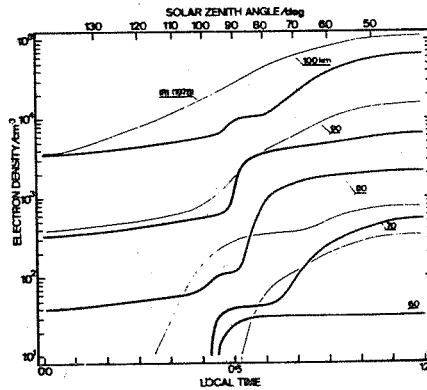


Fig. 4

- Fig. 1 Observed absorption at constant solar zenith angles obtained by A3-measurements over the distance Coburg-Graz, and simulated with IRI (1978).
- Fig. 2 Measured and simulated absorption vs. solar zenith angle.
- Fig. 3 Measured absorption vs. zenith angle and result of theoretical computations using the ion-chemical model.
- Fig. 4 Diurnal variation of electron density after IRI (1978) and from the ion-chemical model (equinox).

Section 1.2 Bottomside F-Region

1.2.1 Critical Comparison of IRI with Information Obtained from Bottomside Ionograms

T.L. Gulyaeva

Institute of Terrestrial Magnetism, Ionosphere and
Radio Wave Propagation, USSR Academy of Sciences, (IZMIRAN)
142092, Troitsk, Moscow Region, USSR

Abstract: The results of comparing the IRI electron density profile with one $N(h)$ distribution obtained from the analysis of ionograms are presented for the quiet and disturbed mid-latitude ionosphere at high solar activity. The valley depth and valley width for the interlayer E-F and F1-F2 regions were evaluated by calculating the $N(h)$ profiles from the bottomside ionograms. The IRI and N profiles were adjusted at the peaks of the E- and F2-layers, the comparisons being made at the intermediate heights. It has been found that the E-F valley depth obtained by $N(h)$ analysis agrees well with that of IRI. The E-F valley width of IRI is about half as much as that of NH . The largest disagreement between the IRI and the ionogram profiles occurs above the valley at the transition from the intermediate region to the F layer subpeak section, where there are discrepancies of up to 100 km in height and of a factor of two in electron density during an ionospheric storm, especially with the F1 layer present. Corrections to IRI using the vertical-incidence sounding data are proposed.

1, Introduction

During many years, data from vertical-incidence soundings have been used for developing ionospheric models. They formed also an essential part of the data base in IRI /Rawer et al., 1978a/: the most representative empirical model of the ionosphere nowadays. These data, with all the well-known difficulties of their inversion into electron density profiles, cover a wide range of heights through the bottomside and topside ionosphere, but never provide a world-wide description of the complete $N(h)$ profile such as, say, the IRI profiles at heights from 70 to 1000 km. But IRI as a summary model offers an approximation to the real ionosphere within the limits of the data base used.

To re-establish more accurately the real state of the ionosphere, it appears to be reasonable to use the system of IRI combined with a system for analysis of the vertical-incidence sounding data. The fundamentals of IRI offer favourable grounds for such a coupling. Thus, an outstanding feature of IRI is the profiles description given in a form reduced to the F2-layer peak plasma density and its height. Consequently, having these peak values as determined from the vertical-incidence sounding data for individual days, makes it possible to adjust the IRI profile to these measured values.

On the other hand, the E-region IRI profile does not depend on the F2-layer peak values, since it is determined by the solar zenith angle, geographic coordinates and solar activity. At the same time the E-layer $N(h)$ profile can be obtained by ionogram inversion within certain error limits /Wright et al., 1975/, but only for day-time conditions, the E-layer not being observed by ionosondes at night. To make up for the insufficient information, it has been decided to take over the E-region data from IRI for $N(h)$ analysis of ionograms. Input of the HME is sufficient by day to be fitted by the E-layer real heights when calculated from ionogram. At night, and in other cases when an E-layer trace is not observed by vertical-incidence sounding, a section of the E-layer elec-

trondensity profile from IRI is used as input data for the system of ionogram analysis, together with the F-layer virtual heights.

Thus, the IRI profiles and ionogram electron density profiles coincide at the two nodal points - the E-layer peak and F-layer peak. Given this link, it is essential to check how the shape of the remainder of IRI profile agrees with the real observational data. The results of such a comparison are presented below.

2, Determination of the Valley Depth and Valley Width from Ionograms

The valley, or decrease of electron density between the ionospheric layers, has long been a problem in the analysis of bottomside ionograms. Recent studies have verified the feasibility of determining two main parameters of the unseen ionisation - the valley depth and valley width - from actual ionograms /Gulyaeva, 1979, 1980/.

When comparing the model electron density profiles with the corresponding numerical $h'(f)$ curves, three constituents of the virtual height have been separated: the subpeak delay due to the underlying regions, that produced by the valley, and the contribution of the ionosphere above the valley. These components and their sum, a curve of the virtual heights h' in the F-layer (the ordinaty mode), are shown in Figure 1 for three model profiles /Herbert, 1967, Tables 3, 5, 7/: (a) an example of the monotonic profile with no valley, but only a ledge of $N(h)$ between the E- and F-layers; (b) the case with a deep valley, where the percentage depth relative to h'_{mE} is about 44%; (c) the model with a shallow valley where the percentage depth is 6%.

One can see from Figure 1 that the subpeak delay due to the E-region, I_E , when sounding the F-layer, is greatest at frequencies just above f_{oE} , decreasing rapidly towards f_{oF} to the value of h'_{mE} . Hence, the shape of the E-layer profile is not essential for the inversion of the F-layer virtual heights, but a knowledge of the two peak parameters, h'_{mE} and h'_{mF} , is very important.

Taking the contribution of the interlayer region, I_V , to the F-layer delay-times, one can see from Figure 1 that, with increasing radio frequency from f_{oE} towards f_{oF} , it decreases asymptotically approaching the value of the valley width, W . This results obviously from the expression for the valley componenz of the integral of the retardation if it is presented using the law of the mean as has been done by Koutiev /1972/ and Denisenko and Sotsky /1978/:

$$I_V(f_k, f_v, W) = \int_{h_{mE}}^{h_{mE}+W} \mu'(f_k, f_v) dh = \mu'(f_k, f_v^*) \cdot W \quad (1)$$

Since, by definition, the group refractive index $\mu' > 1$ for any mean plasma frequency f_v^* in the valley: $f_v < f_v^* < f_{oE}$, it follows from Equation (1) that the contribution of the interlayer region to the virtual heights h'_{mF} is greater than the actual width at all frequencies of the F-layer:

$$I_V > W \quad (2)$$

Lastly, the contribution of the F-region, I_F , to the F-layer virtual heights is given in Figure 1; it grows from zero at the base of the layer to become dominant at the higher frequencies as compared with other constituents of the integral of retardation, h'_{mF} .

Any inversion method permits the determination of the real heights for the E- and F-regions; thus the delay due to both regions can be

calculated from these at any frequency f_k . When this is done, the E- and F-region delays may be subtracted from the observed virtual heights $h'F$ to yield the integral of the group retardation due to the valley region:

$$I_V(f_k, f_v, W) = h'(f_k) - I_E(f_k) - I_F(f_k) \quad (3)$$

The most accurate methods of calculating the $N(h)$ profile enable one to determine the valley width W /Faul, 1966; Gulyaeva, 1972; Koutiev, 1972; Lobb and Titheridge, 1977/. Using this value of W and calculating I_V by Equation (3), then from Equation (1) we get the mean value of the group refractive index in the valley:

$$\mu'(f_k, f_v^*) = I_V / W \quad (4)$$

($f_0E < f_k < f_0F$)

A corresponding mean value f_v^* for the plasma frequency in the valley can then be found from the formulae for the group refractive index /Shinn and Whale, 1952/.

The use of the above reverse procedure with numerical ionograms has shown that, with any actual shape of the $N(h)$ distribution in the valley, it can be assumed that:

$$f_v^* = 1/2 \cdot (f_v + f_0E) \quad (5)$$

This assumption was tested empirically elsewhere and proved to be valid for F-layer frequencies appreciably higher than the critical frequency f_0E , thus permitting the value of the minimum valley frequency f_v to be determined from these within an error about 10% /Gulyaeva, 1979/.

Figure 2 illustrates the results of the application of the above procedure to the O and X echoes for the three cases shown in Figure 1. The horizontal lines indicate the exact valley depth in the parent profiles: (a) $f_v = f_0E$, there is no valley; (b) $f_v = 3.0$ MHz with $f_0E = 4.0$ MHz, a deep valley; (c) $f_v = 3.873$ MHz with $f_0E = 4.0$ MHz, a shallow valley. The calculated minimum valley frequency, f_v , is given by the letters O and X for the correct valley width W fitted by the $N(h)$ profile; curves O_1 and X_1 show the variation of f_v obtained when the valley was ignored in the $N(h)$ analysis (monotonic assumption) which yielded underestimated F-layer real heights in cases (b) and (c); O_2 and X_2 refer to the valley width W overestimated by 20 km as compared with the initial model.

One can see from Figure 2 that the O and X values of f_v differ from each other for the different fixed widths, W , within the range of possible solutions of $N(h)$. They coincide, or are close to each other, for the value of W corresponding to the exact F-region profile consistent with the numerical $h'(f)$ curve /Herbert, 1967/. Therefore, the coincidence of the O and X values of the calculated valley frequency f_v , together with the best approach to the correct valley width W , can serve as a criterion for finding the required $N(h)$ profile /Gulyaeva, 1979/. This criterion was used in the present paper, when calculating the $N(h)$ profiles from experimental ionograms, for determining the valley depth and valley width in the E-F- and F1-F2 regions of the ionosphere.

When the X echoes could not be observed in the F-layer, empirical expressions /Gulyaeva, 1980/ have been used to determine the width of the interlayer E-F valley through a direct estimate of a real height at the frequency corresponding to the minimum in $h'F$. At night, the calculation of the F-region profile was carried out first from the ionogram data with an initial correction for the unseen ionisation. Then the E-region profile from IRI was combined with these F-layer ionogram results for the

determination of the E-F valley depth using Equations 3 to 5 above. The results of these calculations are discussed below.

3. Comparison of Parameters of N(h) Profile from Ionograms with IRI

Some 100 ionograms for April, 1979 were chosen to calculate the N(h) profiles. This month was characterized by interesting solar and geophysical conditions. The monthly average sunspot number, $R = 103$, was about 30 units less than that predicted, while in March and May, 1979 the number was close to the predicted values (135). Early in April and late in the month, two strong negative ionospheric storms were observed, and a moderate positive disturbance occurred during several days in the middle of the month. Ionograms for the quiet, moderately disturbed and the most disturbed conditions were selected for comparison with IRI.

Monthly average IRI profiles were calculated using the median values of f_oF2 and $M(3000)F2$ from the monthly tables of ionospheric data for Moscow in April, 1979, to yield the required initial peak values of $HMF2$ and $HMF2$ /Eilitz et al., 1978/. The evolution of the IRI profile with different assumptions for the peak values is shown in Figure 3 in which curve 1 is the monthly average profile of plasma frequency, $f_H(h)$, at 2130 LT derived from the median values of f_oF2 and $M(3000)F2$ as above. The IRI programme provides also an option of fitting the average profile to the F-region peak values given by Chiu /1975/. This version of the calculation has been illustrated by the curve 2 in Figure 3.

When comparing IRI with rocket observations of the E-region N(h) profile /Sinel'nikov et al., 1980/, it was found when fitting IRI to individual days, the date is required in addition to month and hour as input for IRI. This parameter is preferable, as input, to the solar zenith angle XMI , as proposed in corrections to IRI-78 /Rawcr, 1979/, because the input of the date specifies not only XMI , but also the Sun's declination, sunrise and sunset, and consequently all other parameters of IRI depending upon these. The section of the IRI profile below the base of the F-region, HMF , corrected by the input of the data observed, is shown in Figure 3 (curves 2, 3, 4). All the results of calculations with IRI, as presented below have been obtained with the program modified by input of the data observed.

The profiles in Figure 3 represent the moment of the maximum phase of the ionospheric storm with a decrease of f_oF2 of more than by 50% as compared with the running median value. Specification of f_oF2 from the ionogram taken at 2130 LT for the day of April 25, 1979, still keeping $HMF2$ as described by Chiu /1975/, changes considerably the required N(h) profile: curve 3 in Figure 3. An additional correction of $HMF2$, using $M(3000)F2$ from the ionogram, yields the N(h) profile of curve 4. Thus Figure 3 illustrates how the use of only two parameters, estimated directly from the routine ionograms, enables the IRI electron density profile to be greatly improved, by more than by 6 times in the values of M_e for the case considered.

In Figure 4 three N(h) profiles are given for April 21, 1979, at different solar zenith angles for quiet conditions (0915 LT) and at the start of an ionospheric storm (1800 and 2230 LT). At the top of Figure 4 the corresponding ionograms are shown, two of these show the E-layer o-ray echoes and all three ionograms show both O and X traces in the F-region (the x-ray trace at 0915 LT has been typically observed only at frequencies appreciably higher than f_oE).

Electron density profiles obtained from the ionograms will be denoted by NI and are shown as full lines in Figure 4: the IRI profiles are shown as dotted lines. An appreciable deviation of N(h) from IRI is seen for the E-region. It is caused by the limitations of O-only analysis in the E-layer /Wright et al., 1975/. The N(h) results for the F-region are obtained by our procedure /Gulyaeva, 1979/ using complementary IRI E-layer profile, at 2230, for the evaluation of the valley

depth. The valley width W from ionograms is about twice as great as the distance HER from IRI, the ionogram valley depth and that of IRI being much closer. A rather marked difference is observed at the height of HZ where an intermediate region (a concave curve above the valley) joins on to a quasi-parabolic F-layer subpeak section. This is particularly evident in 0915 LT and will be illustrated further in a number of other cases.

The five profiles in Figure 5 refer to those rare cases for April when the E, F1 and F2 were all observed. They occurred in two of the disturbed days - D5 and D4 - for the month considered, and at low zenith angles ($XHI \leq 60^\circ$). Note the close agreement of f_oE and f_oF1 given by IRI with the values observed on the ionograms. The E-layer ionogram and the IRI results are different, but the peak height HME is the same for both; it was taken over from IRI when computing $N(h)$ from ionograms. An appreciable difference was obtained for the E-F valley width and valley depth; these values from ionograms are greater by a factor two or more than those of IRI. Yet the largest discrepancies between the $N(h)$ and IRI profiles were obtained in the point of HZ (greater than 100 km in height and more than 2 or 3 times in electron densities). Consequently the F1-layer peak height of IRI is much greater than $HMF1$ from $N(h)$ (light vertical lines in Figure 5). It should be noted that the F1-F2 valley size, as obtained from ionograms, is up to 50 km wide, although all the valleys for the region are shallow, while no valley for the F1-F2 transition is specified in IRI but rather a ledge of $N(h)$ between the F1 and F2 layers.

Considering that the IRI and the ionogram profiles have been adjusted at the two peaks for the E and F2 regions as above, the conclusion drawn concerning the discrepancies between the two profiles at the level of HZ and the peak of the F1 layer is independent of the method of ionogram inversion. Indeed, if the $N(h)$ analysis were carried out ignoring the E-F and F1-F2 valleys, the real heights of the base of the F1 and F2 layers, as obtained from ionograms, would decrease by 20 to 50 km, and $HMF2$ would decrease by 10 to 15 km. This would yield the values of HZ and $HMF1$ in IRI by 10 to 15 km lower but the difference between the IRI and $N(h)$ shown in Figure 5 would remain.

Examples of reasonable consistency of IRI and $N(h)$ profiles in the F-layer above the E-F valley are given in Figure 6. They were chosen for the quiet day of April 11, 1979 (Q3K) tending to a moderate positive ionospheric disturbance, one case (0730 LT) being for the maximum increase of Δf_oF2 (by more than by 50%). The increased values of the critical frequencies in all the cases considered resulted in an increased slope, dN/dh , in the intermediate region above the E-F valley, and a rather flexible transition to the subpeak F2 layer section. The E-F valley width of IRI is close to that of N , while the valley depth in two of the four cases considered differs by more than 30% at 0130, and by 25% at 1815 LT.

Note that at 0130 and 2000 LT the E-layer was not observed in the ionogram; only night-time F-layer echoes were registered. That is why they were combined with the E-layer data from IRI for evaluating the valley depth, these being modified so that the value of f_oE in each case was close to that in ionogram (dashes in the E-layer at the curves 0130 and 2000). The electron density distribution in the interlayer regions and near the critical frequencies, where it is not observed by the ionosonde, has been extrapolated either to the minimum valley frequency f_v calculated by the formulae Equations 3 to 5, or to the values of f_oF2 . Those extrapolated sections are shown by the dashed curves in Figures 4, 5 and 6.

4, Discussion

The diurnal variation of the main parameters of the $N(h)$ profile for April, 1979 is shown in Figures 7 and 8. The full curves show the monthly-average IRI results using median values of f_oF2 and $M(3000)F2$ from the monthly tables of ionospheric data. Also shown are the variations of the critical frequencies and the peak heights for the E, F1 and F2 layers, the plasma frequency f_{NHZ} , and the height HZ of the junction of the intermediate region above the valley with the subpeak F2 (or F1) section, as well as the minimum valley frequency f_{NM} and the difference in height between the E- and F-regions, HBR . Individual values of f_oF2 and h_mF2 , as chosen from the ionogram analysis, are shown by an appropriate sign: quiet conditions - circles, negative ionospheric disturbances - minus, and positive disturbances - plus. The comparison made in the present paper refers to those individual values of f_oF2 and h_mF2 .

In Figure 9 we have plotted the results against solar zenith angle; these show the differences in height, ΔHZ (= IRI minus $N(h)$), and the ratio, NH/NZ , of the values of electron density at the level of HZ as obtained from ionograms relative to those of IRI.

The height HZ given by IRI agrees best with that from the ionograms at the morning and evening hours. The difference rises to 50 km at noon for quiet conditions (b), and moderate positive disturbances (c). On the whole, the differences in HZ are minimal for these two cases. However, during negative disturbances (a), departures of HZ of up to 50 km by night and over 100 km by day occur with the occurrence of the F1 layer (sign \downarrow in Figure 9a).

From the changes in the IRI profile during the disturbances considered, including its distortion at the height of HZ , it would appear to be reasonable to modify the IRI description so that its analytical functions involve a dependence on an ionospheric disturbance parameter. This could be, say, the deviation of the critical frequencies f_oF2 from the median values as predicted or as observed daily, or some other parameter.

The difference in electron density between IRI and $N(h)$, at the base of the subpeak F-layer section, is similar to that in height but opposite in sign; the values of NZ given by IRI are less than the corresponding values of $N(h)$ (Figure 9, bottom). With regard to the position of the inflexion point in the F-layer, corresponding to the maximum of the vertical electron density gradient /Anufrieva et al, 1980/, a shift of the junction between the intermediate region and the subsequent F-layer section towards the inflexion point at the F-region may be recommended. The latter may be derived from the empirical data of $N(h)$. Usually the plasma frequency at the inflexion point remains less than about 1 MHz below the critical frequency f_oF2 . For a more flexible fitting of $N(h)$ in the intermediate region, the proper descriptive function should be replaced by a function giving a more pronounced concave curvature such as the "positive" parabola /Gulyaeva, 1974/ or Booker's proposed unique analytical function /1977/.

Figure 10 shows the ratio of HBR/W of the E-F valley width given by IRI relative to that given by ionogram, and the difference in the percentage depth for the valley: $NDEL = NDEL(IRI) - NDEL(NH)$. As a rule, the valley width HBR of IRI is about half as much as W of $N(h)$; this is true for all the cases considered (Figure 10 a, b, c, upper part). Hence, without changing the complete electron density profile of IRI at other heights, the increase of HBR by about 2 times can be recommended for the middle latitudes at high solar activity ($R = 100$).

The good consistency (within 20%) of the E-F valley depth given by IRI and $N(h)$ analysis is illustrated in the lower part of Figure 10. By

day the difference is slightly more; the valley depth from IRI is about 30% less than that obtained from ionograms. Since the valley width given by ionograms is about twice as that given by IRI, the difference in the valley depth is quite explicable; the relation between the width and depth as obtained from ionograms is discussed in detail elsewhere /Gulyaeva, 1979/.

5, Conclusions

1. The feasibility of determining the interlayer valley depth for the E-F and F1-F2 regions of the ionosphere is demonstrated by the calculations of N(h) profiles from the experimental ionograms using the reverse procedure /Gulyaeva, 1979/. The agreement obtained between the minimum electron density for the valley region given by IRI and by NH data provides evidence confirming that the evaluation of this parameter from the vertical-incidence ionograms should be continued.

2. The comparison made has shown that the E-F valley thickness as provided by IRI is about half as much as that given by ionogram analysis for the mid-latitude ionosphere at high solar activity.

3. The greatest disagreement between the N(h) profile given by IRI and ionograms has been found at the level of transition from the intermediate region above the valley to the subsequent F-layer section; this is most pronounced by day and with the appearance of the F1 layer during an ionospheric storm.

4. The above differences indicate those aspects should IRI be developing as every viable system. They do not in the least belittle the value of IRI which has manifested itself by its flexibility, the modular system approach, the solar and geophysical conditions which are taken into account, and the possibility of adapting the system to real conditions of observation.

6, Acknowledgement

The author would like to express her sincere gratitude to K. Rower for giving her the opportunity to present this paper at the COSPAR meeting.

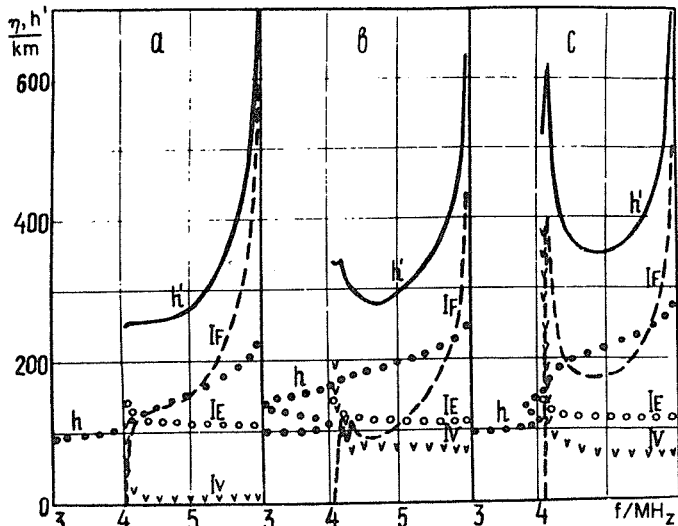


Fig. 1

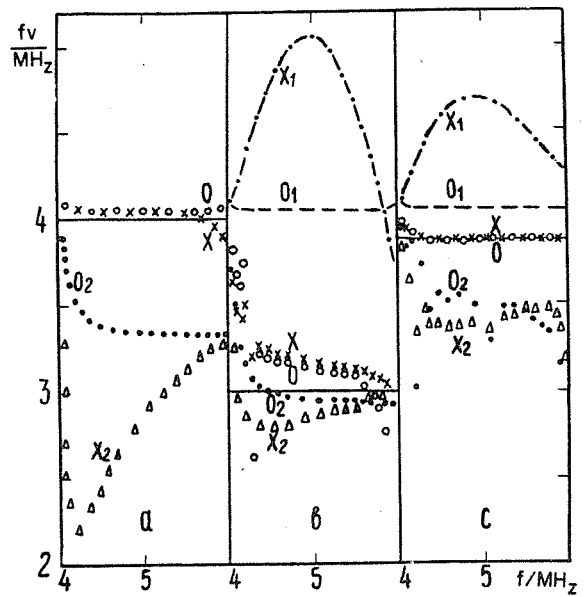


Fig. 2

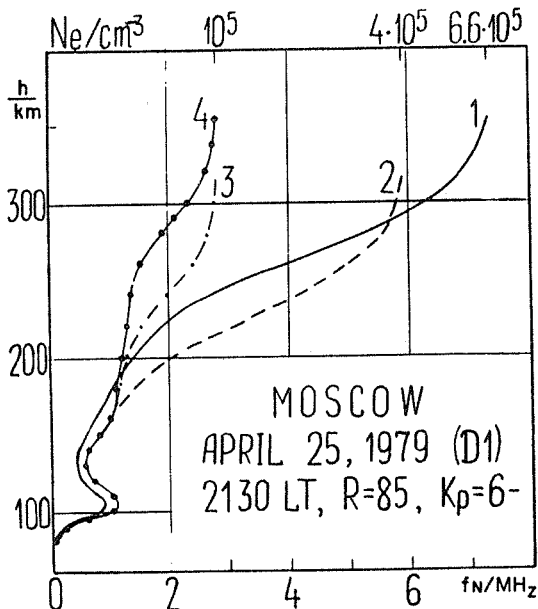


Fig. 3

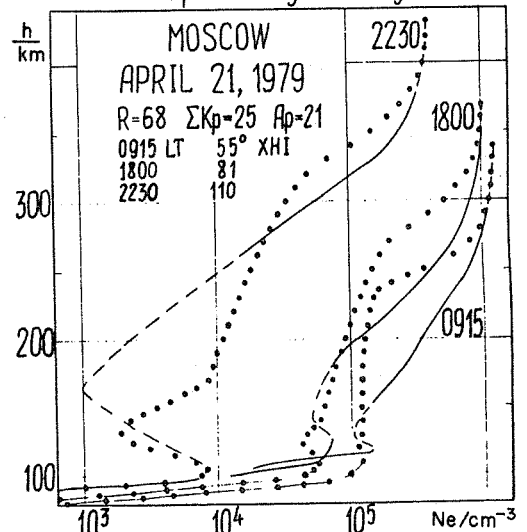
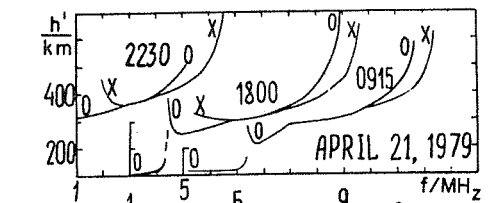


Fig. 4

- Fig. 1 Division of the vertical height $h'F$ into three constituents: delay from ionisation below the E-layer peak (I_E), valley ionisation (I_V), and the F-layer ionisation above the valley (I_F).
- Fig. 2 Variation of the minimum valley frequency f_v calculated from the O and X echoes in the F-layer for different valley widths: correct (O,X), too low due to monotonic assumption (O_1, X_1), and increased by 20 km as compared with correct width (O_2, X_2).
- Fig. 3 Correction of monthly-average IRI profile (1,2) using the F2-layer peak values for individual day from ionogram (3,4).
- Fig. 4 Comparison of IRI electron density profile (dotted line) with NH results (full line) calculated from the ionograms given at the top of the Figure.

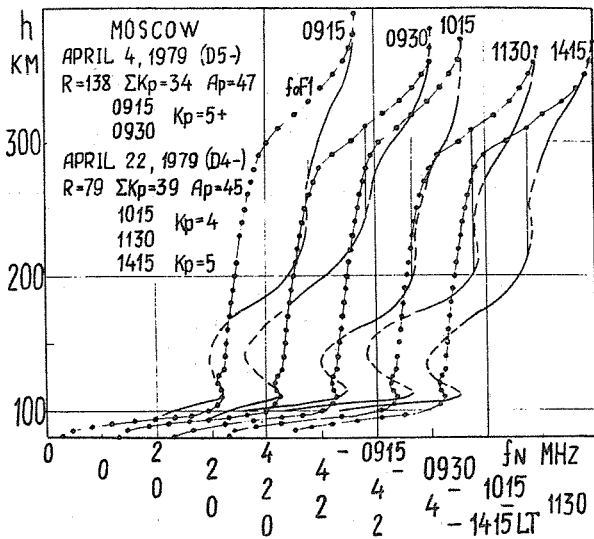


Fig. 5

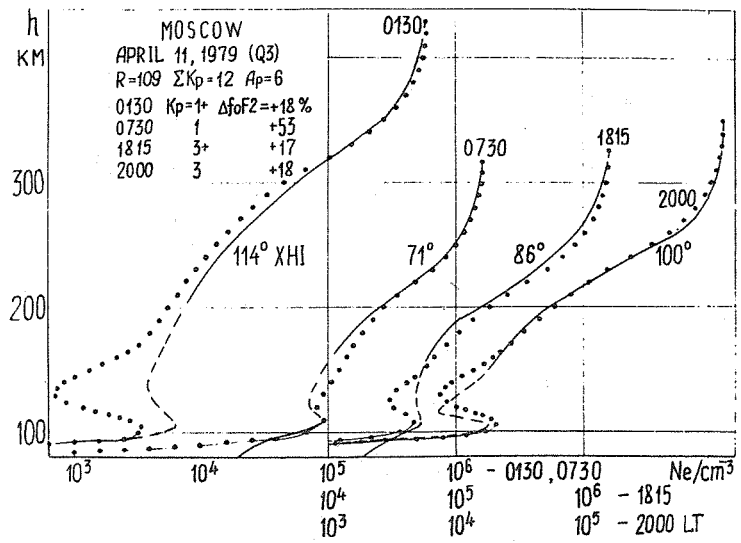
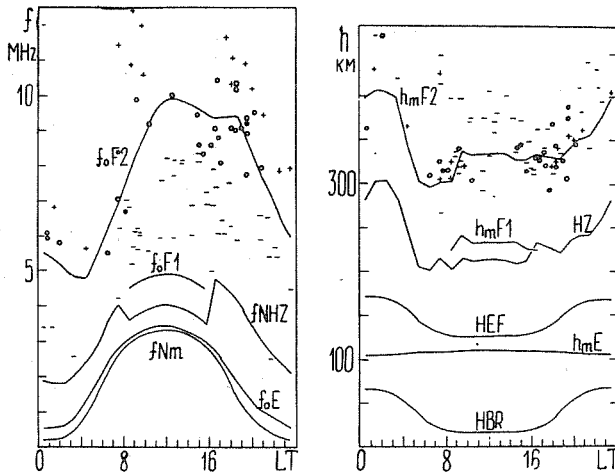


Fig. 6



Figs. 7 & 8

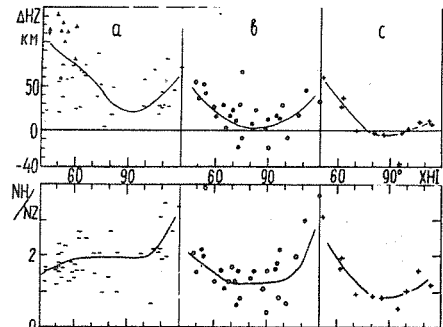


Fig. 9

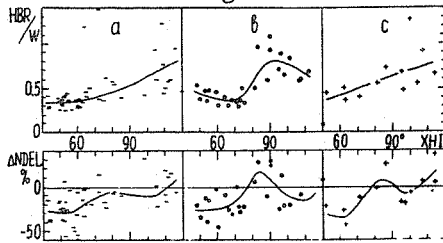


Fig. 10

- Fig. 5 The largest disagreement between the IRI and NH profile is observed above the valley with the appearance of the F1 layer during an ionosphere storm.
- Fig. 6 Examples of a good consistency of the IRI and NH results in the F region above the valley with increased values of critical frequency foF2 (positive disturbance in the ionosphere on a magnetically quiet day).
- Figs. 7 & 8 Diurnal variation of the main parameters of the N(h) profile (Moscow, April 1979). Individual values of foF2 and hmF2 are indicated by o, -, and + for quiet conditions, negative and positive disturbances, respectively.
- Fig. 9 Differences in height and electron density, as given by IRI and NH, at the transition between the intermediate region above the valley and the F-layer sub-peak section: a) during negative disturbances; b) during quiet conditions; c) during moderate positive disturbances.
- Fig. 10 Relations between the E-F valley width and valley depth given by IRI and by ionograms results.

1.2.2 Comparison of IRI with Measurements of N(h) Profiles in the Bottomside Ionosphere

V.M. Sinel'nikov, G.F. L'vova, T.L. Gulyaeva¹
S.V. Pakhomov, A.P. Glotov²

¹Institute of Terrestrial Magnetism, Ionosphere and Radio Wave Propagation, USSR Academy of Sciences, (IZMIRAN), 142092, Troitsk, Moscow Region, USSR

²Central Aerological Observatory, Moscow, USSR

Abstract: The possibility of measuring the electron density profile in the height interval of 70 to 110 km with a two-frequency coherent transmitter in a "small" geophysical rocket of type M-100 has been investigated.

Presented are the results of measurements made using the phase Doppler method carried out on May, 1979 and February, 1980 at middle latitudes. Good agreement of the profiles measured for the D- and E-regions of the ionosphere with those of IRI has not always been obtained, even when the correct solar and geophysical conditions of the experiments were given for calculations with IRI.

1, Introduction

Several experimental radiophysical methods are available for the study of the vertical distribution of electron density in the lower ionosphere. The measurement of differences of Doppler frequency shifts, and of Faraday rotation of the polarisation plane of coherent radio-waves, with the use of vertical rockets, plays an important rôle among those methods.

This technique was proposed first for rocket exploration of the Earth's ionosphere /Seddon, 1953/. Later, the method was used in satellite experiments of various types /Al'pert, 1976/ and it provided us with information on the topside ionosphere of the Earth, the Solar corona, the Solar wind and the ionospheres of other planets. In particular, exploration of the Earth's ionosphere by the coherent frequencies method has been carried out using "large" geophysical rockets (of apogee from 250 to 1500 km) /Gringauz et al., 1958, 1961, 1970; Birukov et al., 1972/. However, the coherent 3-channel transmitter with frequencies 24,48 and 144 MHz used in these experiments permits the determination of the electron density N(h) profiles only above about 100 km.

An attempt was made to measure the N(h) profile in the D-layer of the ionosphere /Pedyashev and Tuchkov, 1972/ using the coherent emission for appreciably lower frequencies: 3 and 21 MHz. It failed, for the values of N at heights of 50 to 80 km were considerably overestimated (up to 1 to 1.5 orders as an average), and it gave no information on the accuracy of the method or possible equipment errors.

The so called "inverse" radiobeacon experiment, with the ground-based transmitter and the rocket-based receiver, has been widely developed in recent years /Bennet, 1972; Jespersen, 1970; Kane, 1961; Mechtly et al., 1967/. This technique allows the researcher to use rather simple polarisation measurements, by comparison with phase measurements, at frequencies of several MHz and ground transmitters with a power of several KW. However, such an experiment, using the sophisticated receiving and telemetric equipment, seems to be cumbersome and expensive. Hence it appears to be of little value for making regular observations, or for adoption in the numerous rocket launches

envisaged in the complex programs for a study of the lower ionosphere.

In the present paper the possibility of measuring the electron density profile in the height interval 70 to 110 km with a two-frequencies transmitter in a "small" geophysical rocket of type M-100 has been investigated. Attention was given to the simplicity and efficiency of the technique developed.

2, Equipment

2,1 The Rocket Equipment

The two-frequencies coherent transmitter has the following parameters:

1st channel: 10.005 MHz, radiated power 2.0 W
2nd channel: 40.02 MHz, radiated power 0.5 W

An original idea in the rocket-based equipment is that of using the body of the rocket as the transmitting aerial. The leading part and the first stage of the rocket (whose lengths are 1.9 and 2.5 m respectively) are separated by an insulating layer and are used as a short dipole aerial; both channels of the transmitter are connected to the aerial by separating filters. It has been found experimentally that the radiation diagrams in the channels 10 and 40 MHz differ little and there is no sharp minimum except for the natural one along the axis of the rocket. The latter prevents the placing of the reception station near the launch position because, with the quasi-vertical rocket ascent, the relative orientation of the "transmitter-receiver" system is unfavourable.

2,2 Ground Equipment

The ground receiver and recording equipment comprises the two-channel receiver for the coherent frequencies, and analog 3-channel recorder, and the receiving aerials, i.e. crossed half-wave dipoles for each receiving channel. The reception system is of high sensitivity (0.05 V with 50 Hz bandwidth and signal 20 dB above noise) and is a 2-channel receiver with double transformation of frequency and a phase lock loop system. One of the important characteristics of the receiver is the phase stability for large changes (up to 40 dB) of the input signal level. The RMS error of the measurement (due to phase instability of receiver) is about 0.9°.

3, The Flights Experiment

3,1 Rocket Flight

During the launches, a number of important facts concerning the relation of the phase measurements to rocket flight ballistics were discovered. In particular, the absence of any effect of rocket spin (up to 6 to 8 Hz) on measurements of the reduced phase difference, as assumed a priori, was confirmed by the experiment.

The variation of the amplitude of the received signals and the reduced phase difference during the rocket flight are shown in Figure 1. Such pattern, repeated in the most of the launches, enables us to determine those parts of the rocket trajectory where the ballistics do not influence the phase measurements. It was found there were no ballistic limitations for the whole of the ascent part of the trajectory, and for the descent down to 70 km.

3,2 Experimental Procedure

It is well known that direct measurements of the ionospheric Doppler shift for a moving emitter are difficult to make in practice since they yield large errors; these are due first to the insufficient stability of the emitter frequency, and then to the difficulty of separating out the "ionosphere contribution" to the measured frequency shift, since so-called

"optical" Doppler effect is much greater than the effect of the ionosphere plasma. This is why the measurement of the difference of Doppler frequency shifts of two (or more) coherent frequencies is in common use. The general theoretical formulae describing the dependence of the measured reduced phase difference on the ionospheric parameters and the elements of the emitter's orbit are given by Al'pert /1960, 1976/.

The necessary equations for the case of a quasi-vertical emitter orbit (rocket experiment) are given by Sinel'nikov et al., /1980/. The mean value of the electron density, $N_{1,2}$, in the height range of $\Delta h_{1,2}$ is:

$$\overline{N_{1,2}} / \text{cm}^{-3} = \frac{\Delta \phi_{1,2} / ^\circ}{1.8 \cdot 10^{-7} \Delta h_{1,2} / \text{cm}} \cdot \overline{\cos \psi_{1,2}}$$

where $\overline{\cos \psi_{1,2}}$ is the mean value of the zenith angle for the same range. Therefore, it is sufficient to determine experimentally the $\Delta \phi$ values for the consecutive time intervals, as well as the information on the rocket trajectory ($h(t)$ and $\psi(t)$), required for data processing.

The total error of N , as determined by the phase Doppler method for frequencies of 10 and 40 MHz and for maximum plasma frequencies of 2 MHz (corresponding to $N \sim 5 \cdot 10^4 \text{ cm}^{-3}$) is less than 10%.

The sensitivity of the phase measurements at the frequencies chosen is such that $\Delta \psi = 2^\circ$ for passing through a plasma column of 1 km with a mean density of $N \sim 10^2 \text{ cm}^{-3}$. Thus, with our experiments it is possible to measure electron densities as low as 30 to 50 cm^{-3} .

4. Some Results of the N(h)-Profile Determination

Below are given some results of electron density profile determination using the phase Doppler method with the geophysical rockets M-100 and M-100B. Measurements were carried out near Volgograd in two series of three rocket launches in May, 1979, and February, 1980. The following objectives were kept in view:

- to obtain the experimental N(h)-profiles for the D-region and the lower E-region at different solar zenith angles, so as to estimate the effectiveness of the method;
- to measure two N(h)-profiles during every launch, thereby increasing the reliability of the data and allowing the spatial and temporal variability of the lower ionosphere to be estimated;
- to compare the measured N(h)-profiles with data from simultaneous vertical incidence sounding of the ionosphere, and to study the feasibility of measuring the fine structure of the electron density vertical distribution (such as E_s);
- to compare the experimental profiles with those of the model calculation so as to find the most suitable model of N(h) distribution in the lower ionosphere.

The main parameters of the launches are given in Table I :

Rocket Launches

Table I

Launch characteristics	Date of launch					
	16.V.1979	18.V.1979	23.V.1979	27.II.1980	29.II.1980	29.II.1980
1. Local time of measurement	o625 - o630	o515 - o520	o303 - o308	1200 - 1205	o740 - o745	1200 - 1205
2. Solar zenith angle/ ^o	73	84	101	55	80	80
3. Peak altitude / km	108,3	106,8	108,3	111,7	111,5	114,6
4. Magnetic disturbance, ΣKp	17	23	24	23	20	20
5. Solar activity index, R	239	183	139	238	226	226
6. Accompanying measurements	iono-sonde	iono-sonde	iono-sonde	ionosonde, Langmuir probe	ionosonde, Langmuir probe	ionosonde, Langmuir probe

It should be noted that the launches were conducted at different local times in order to observe the dynamics of the ionisation profile in the D-layer and to estimate the effectiveness of the method. Parts of the amplitude-phase analog records for two of the rocket launches are shown in Figure 1.

The following features are specific to the initial information:

- the almost constant signal amplitude, which confirms the good stabilisation of the rocket during the measurements;
- the continuity of the amplitude-phase information during the whole period of measurements;
- the complete symmetry of the phase variation in the ascent and descent parts of the rocket trajectory, which confirms the coincidence of the measured profiles of ionisation;
- since the plasma density turning point "turn" occurs exactly at the peak of the emitter's trajectory, the effect of the ionospheric instability can be neglected, because an appreciable instability would result in a shift of the time of the phase turning point relative to the apogee of the rocket trajectory;
- the electron concentration is proportional to the total phase difference (number of 360° cycles) during flight. For example, the electron density for the launch of 18 May, 1979 is 6 to 10 times greater than for 23 May, 1979 as illustrated in Figure 1.

The electron density profiles for the data obtained in 5 of the 6 experiments listed in Table 1 are shown in Figures 2 and 3. Near the apogee of the rocket trajectory, the N(h)-profiles are terminated at altitudes where the vertical and horizontal components of the rocket velocity become equal to one another and where the trajectory is no longer almost vertical. Good coincidence of the profiles obtained during the ascent and descent parts of the trajectory in the same launch should be noted (even in details; for example, on 18 May, 1979).

The construction of the profiles in considerable detail was possible due to the height spacing at intervals of $h = 1$ km for the first three launches (1979), and the time spacing of $t = 1$ s for the latter three

launches (1980). In addition, a more detailed picture near the peak of the trajectory could be achieved by decreasing the height interval to 100 or 200 m. This is useful in those cases when fine structure in the $N(h)$ profile is observed, such as for the E_S -layer. The E_S -layer was observed in the experiment on 16 May, 1979 and was first noticeable at an altitude of 102.5 km; the most pronounced layer was registered between 104.5 and 106 km. It should be noted that at the nearest vertical incidence sounding station the E_S -layer was recorded at 106 km (see Figure 2).

We have compared the observed rocket $N(h)$ -profiles with the data from vertical incidence soundings. Unfortunately, the ionosonde data at the station placed near the point of launch proved to be of no use owing to the poor quality of the ionograms near the base of the E-layer. This is why we compared our results with vertical incidence data from Rostov-on-Don (about 500 km from the rocket launching station) for the same solar zenith angles. The results of the comparison are given in Figures 2 and 3. A comparison of the rocket profiles with data from vertical soundings shows differences due to the following facts:

- the minimum plasma frequency measured by the ionosonde is about 1 MHz ($N \sim 1.3 \cdot 10^4 \text{cm}^{-3}$);
- the accuracy of the profile in the height interval 95 to 105 km from the ionosonde data appears to be 2 to 5 km, depending on the ionogram quality and the method of inversion of the virtual heights to give the real heights of reflection.

Therefore, another source of information about the $N(h)$ distribution in the D-layer was used, namely, the model calculation. We have chosen the well-known model IRI-78 /Rawer et al., 1978/. The initial data introduced into the model were those of the coordinates of station, date, solar zenith angle or local time /Barclay, 1963/, and a parameter for solar activity.

The model $N(h)$ -profiles are shown in Figures 2 and 3 with a dotted line. Rather good agreement is obtained between the rocket data and the model in a number of cases; for instance, IRI-78 describes properly the main regularities of electron density distribution in the D-layer. The base of the E-layer at middle latitudes is not always described by parabolic approximation.

5, Conclusion

The phase Doppler method of measuring the $N(h)$ -profile in the D- and E-layers of the ionosphere has been developed using geophysical rockets M-100 and M-100E.

The experiments carried out have demonstrated the usefulness of the information and the quality of the height data obtained.

The agreement of the rocket electron density profiles with those from IRI enables us to recommend that the E-layer profile of IRI be used for the correction of the E- and F-region $N(h)$ -profiles calculated from the vertical incidence ionograms.

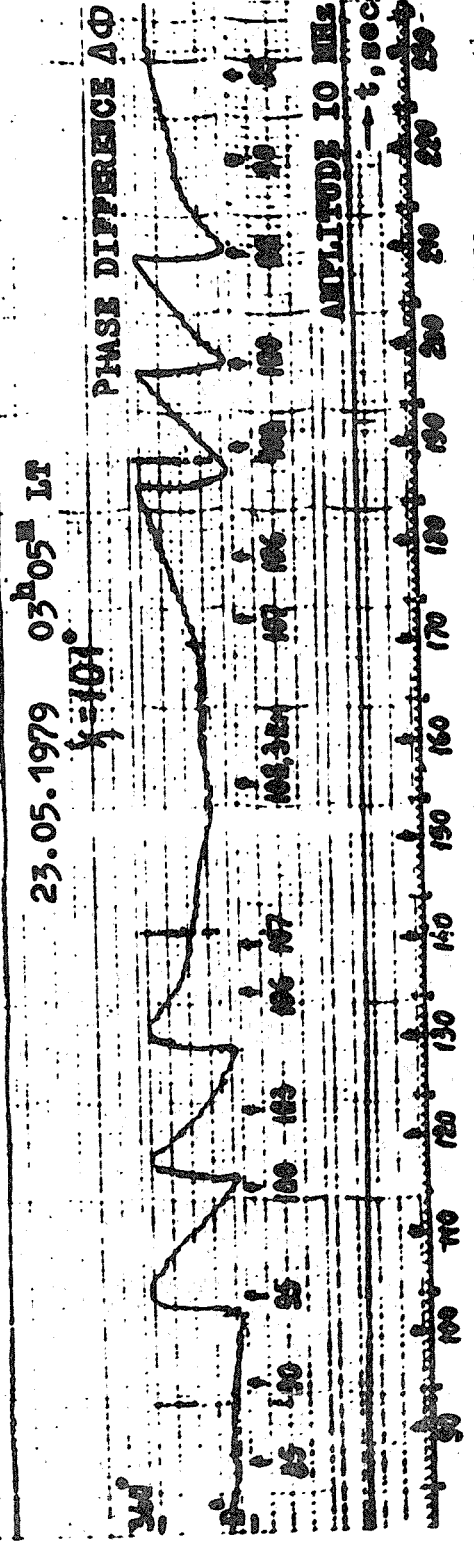
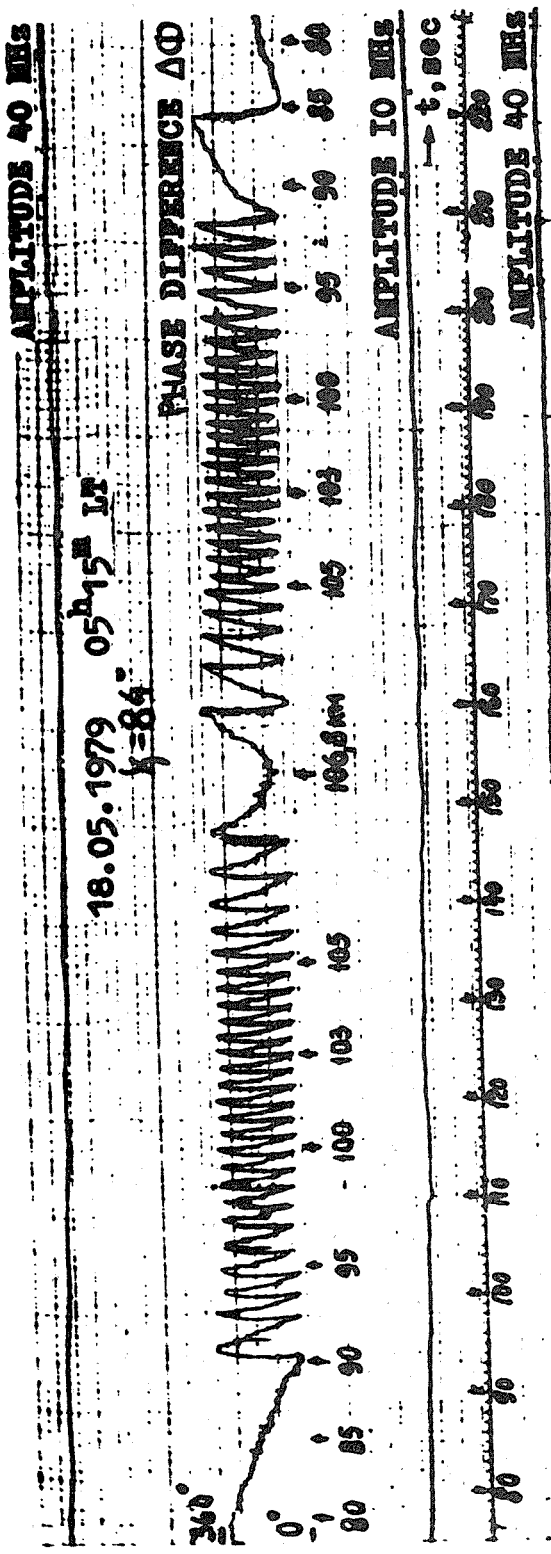


Fig. 1 Variation of the amplitude of the received signals and of the reduced phase difference over the rocket trajectory.

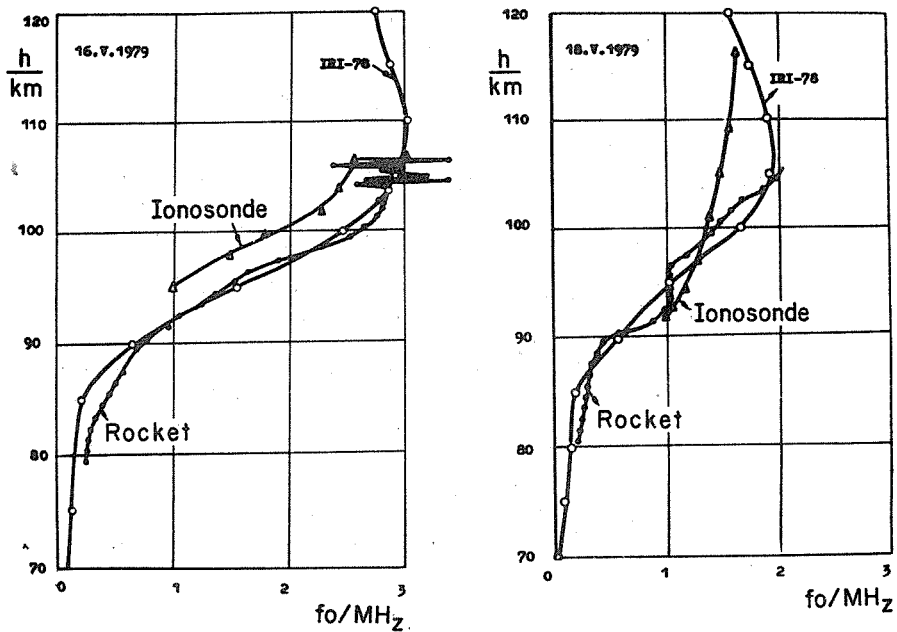


Fig. 2 Two samples of comparisons of the rocket plasma frequency profiles with those from IRI and ionograms in May 1979.

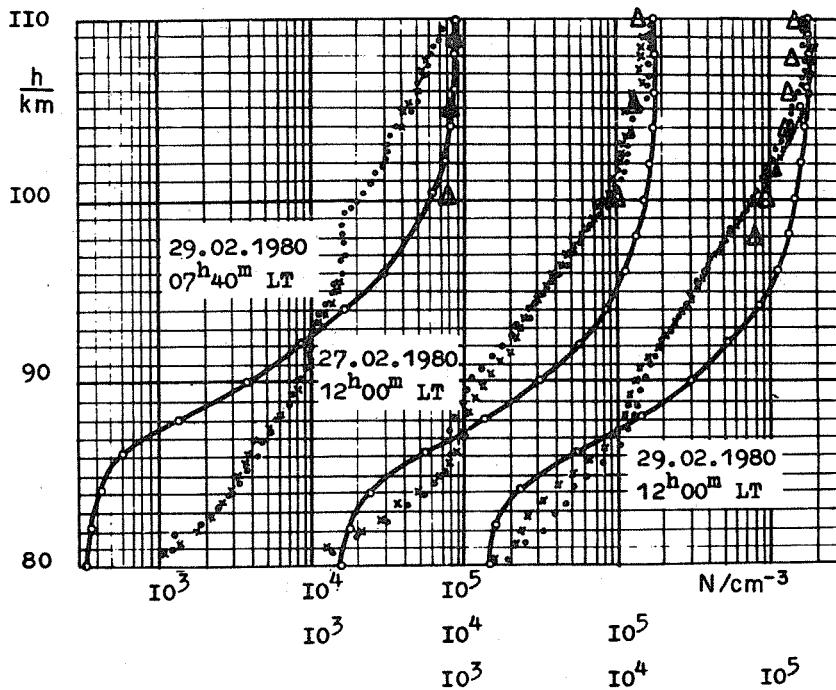


Fig. 3 Differences of the rocket and IRI electron density profiles obtained in the D and lower E regions of the ionosphere in February 1980.

1.2.3 Comparison of IRI with Electron Density Profiles Obtained below 200 km by Different Methods

Yu.K. Chasovitin ¹, A.D. Danilov ¹, S.M. Demykin ²,
T.L. Gulyaeva ³, V.I. Ivanov ², V.G. Khriukin ¹,
A.A. Nikitin ², L.L. Sukhacheva ², V.B. Shushkova ¹,
S.P. Tikhomirov ².

¹ State Committee on Hydrometeorology, Moscow, USSR;

² Physical Department, Leningrad State University, Leningrad;
USSR;

³ Izmiran, Troitsk, Moscow Region, USSR.

Abstract: Electron concentration profiles given by IRI are compared with the results of direct measurements by different methods.

In the range 100 to 200 km a set of direct measurements made on board MR-12 geophysical rockets is used for comparison with IRI. 20 flights made during various geophysical conditions at mid-latitudes (Volgograd) are considered as well as mid-latitude rocket and incoherent scatter measurements available in the literature. Empirical electron concentration models are also compared with IRI. At heights below 100 km measurements made by the partial reflection method from 1972 to 1976 in Leningrad, as well as phase and amplitude measurements of VLF over both short and long paths are used for comparison.

Outside the midlatitude region, the IRI-profiles are compared with the results of rocket measurements at low and high latitudes. The validity of IRI for various conditions is finally discussed.

1, Introduction

In this paper: IRI is tested by comparing it with various experimental data in the difficult modelling altitude interval of 60 to 200 km. Since we know that the reliability of the experimental data differs for the height range 100 to 200 km and for the D-region, we consider these two altitude intervals separately.

For heights from 200 km, the basic experimental data stem from rocket and incoherent scatter measurements, and from empirical models based on such measurements. Vertical sounding data below 200 km are considered separately in paper 1.2.1.

In the D-region, data from partial reflection and cross-modulation measurements were used as well as VLF and LF propagation data. IRI is not supposed to describe disturbed conditions, so only measurements for quiet days were used. At heights above 90 km a few tests could be made with different latitudes, but for the D-region only midlatitude data were at hand. All model profiles were computed by the special algorithm after Chiu /1975/, not with the CCIR-tape.

2, Mid-latitude Profiles above 90 km

About 40 profiles were used (see review papers by Chasovitin and Shushkova /1978/ and by Koriakona and Shushkova /1979/), obtained by probe technique in rocket flights, half of them at Volgograd by Chasovitin and collaborators /Andreeva et al., 1971; Klyueva et al., 1977/. Other profiles are from other launching stations (Wallops, Eglin, Kagoshima) or were obtained by the incoherent scatter method at Millstone Hill and Malvern.

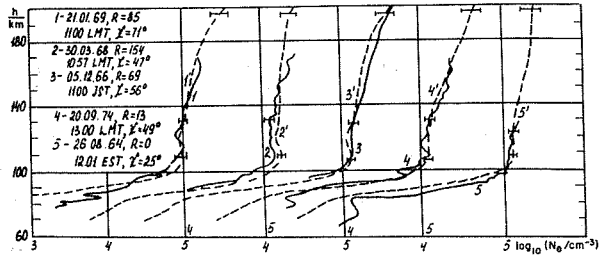


Fig. 1

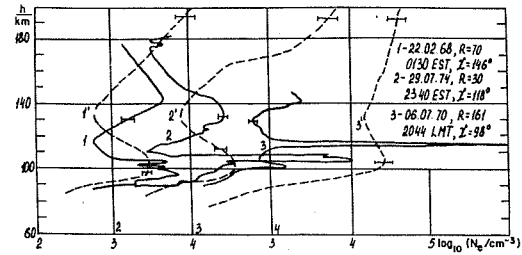


Fig. 2

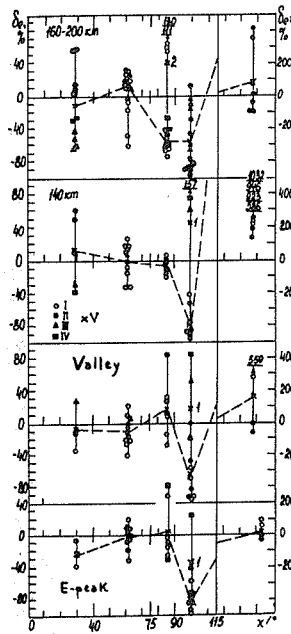


Fig. 3

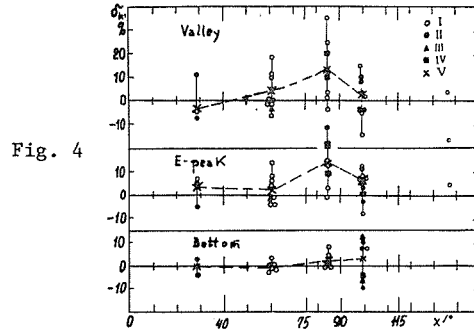


Fig. 4

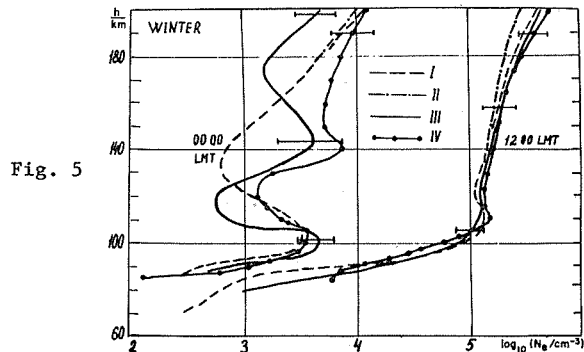


Fig. 5

Fig. 1 Rocket electron density profiles for midlatitudes (1,2,4 - Volgograd, 3 - Kagoshima, 5 - Wallops Is.) and corresponding IRI-profiles (1' - 5'). Sources: Andreeva et al., 1971; Klyueva et al., 1977; Oya and Obayashi, 1968; Bourdeau et al., 1966.

Fig. 2 Rocket density profiles for midlatitudes (1,2 - Wallops Is. [9,10], 3 - Volgograd [11] and corresponding IRI-profiles (1' - 3'). Sources: Smith, 1970, 1977; Chasovitin et al., 1974.

Fig. 3 Relative deviations δ of the experimental density values from the model ones at fixed altitudes, at the valley minimum, and at the E-region peak for various intervals of χ and different stations (I - Volgograd; II - Wallops Is.; III - Kagoshima, Eglin; IV - Millstone Hill, Malvern; V - average values; 1 - winter, 2 - summer).

Fig. 4 Relative deviations of the experimental height values for valley, peak and bottom (the height where $N_e = 5 \cdot 10^3 \text{ cm}^{-3}$ at the bottom of the E-layer from the model values for various intervals of χ and for the stations denoted as in Fig. 3.

Fig. 5 Midlatitude profiles for winter (noon and midnight), different models: I, II - IRI January, $R = 100$, $\Psi = 40^\circ$) for $\lambda = 50^\circ$ and $\lambda = 280^\circ$ respectively; III - Koriakina and Shushkova, 1979; IV - Chasovitin et al., 1979a,b; Zelenova et al., 1976a,b.

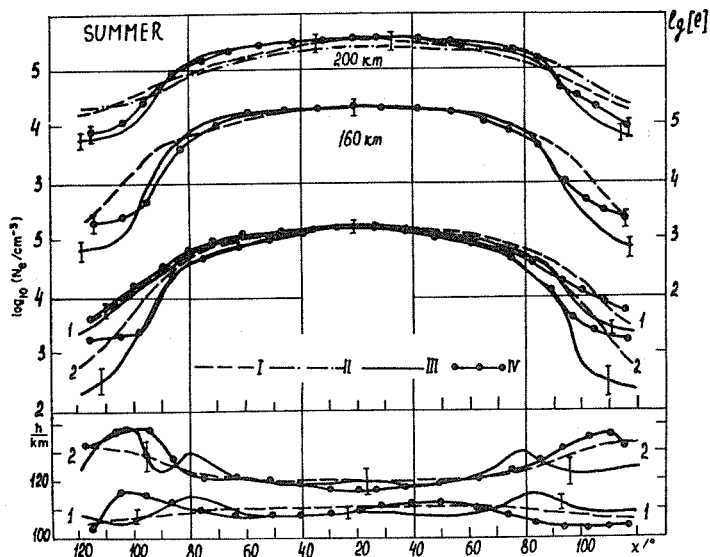


Fig. 6 Solar zenith angle dependence in summer of mid-latitude model density - top of diagram - at fixed altitudes, E-peak (1) and valley (2). Below: same for altitude of peak (2) and valley (2) - bottom of diagram. I, II - IRI, July, $R = 100$, $\Psi = 40^\circ$; $\lambda = 50^\circ$ and 280° respectively; III, IV: same sources as in Figure 5.

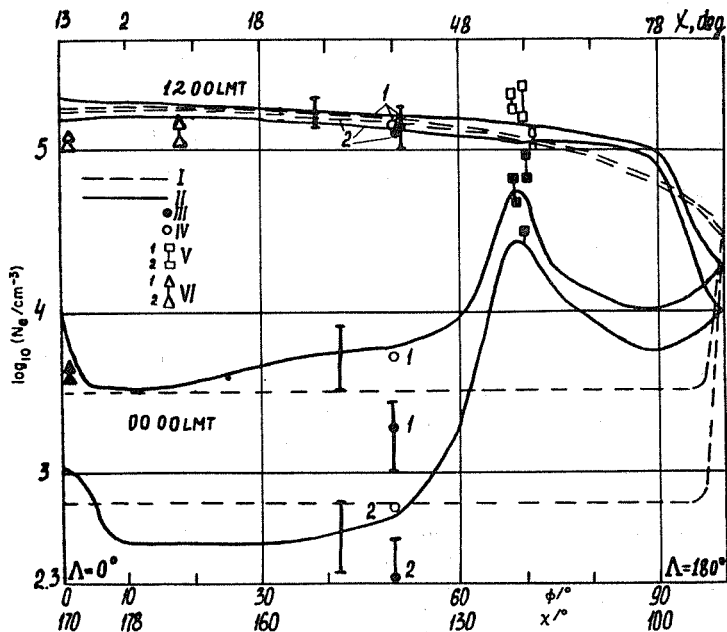


Fig. 7 Latitudinal variation of peak (1) and valley (2) density (see text) for equinox noon (white plots) and midnight (black plots) along geomagnetic meridian zero; from different models (I ... IV) and experimental: I - IRI (September, $R = 100$); II - Kadukhin et al., 1978; III - Chasovitin et al., 1978; Koriakina et al., 1979; IV - Andriyako et al., 1978; V - Experimental data for high latitude (Churchill) [Chasovitin and Shushkova, 1980]; VI - Experimental data for low latitude [Kriukin and Chasovitin, 1976]. (white squares and triangles - noon; black ones - midnight).

Day ($\chi < 75^\circ$): Some typical examples are presented in Figure 1. It is seen that there is generally good agreement between the model and experiments both in the absolute values and in the shape of the vertical profile.

Twilight and night ($\chi > 75^\circ$): For twilight and night conditions the agreement between the model and the experiments is less good. A discrepancy appears both in the absolute values and in the profile shape. Typical examples are given in Figure 2. As appears from this latter, in twilight ($\chi \approx 75$ to 115°) IRI near the E-layer maximum systematically gives higher values than those observed experimentally. One should also pay attention to the fact that the experimental profiles show a second maximum at 120 to 140 km which is absent on the model curves.

An analysis for various χ -intervals is given in Figures 3 and 4. In these, for various altitudes, the variation with χ of the relative error δ is given (index M means model):

$$\delta_e = \frac{N_e - N_{eM}}{N_{eM}} ; \quad \delta_h = \frac{h - h_M}{h_M}$$

Figure 3 illustrates the above mentioned fact that IRI is good in describing the daytime conditions at 90 to 200 km, with an average error of about 20%. In twilight ($\chi = 75$ to 115°), δ_e comes to about minus 33%, and deep in the night ($\chi > 115^\circ$) it rises to 200 to 400% such that the experimental values are several times higher than those of the model.

3. Midlatitudes, Empirical Models

There exist a few empirical models of electron concentration below 200 km, based on the analysis of a great number of such measurements /see, apart from the above cited review papers, Zelenova et al., 1976a,b/.

Figure 5 shows typical daytime (12.00 LT) profiles according to IRI and the empirical models, and confirms the conclusions already drawn above. In the daytime there is reasonable agreement between IRI and the empirical models, but during the nighttime there are essential discrepancies. One of them is (as in Figure 2) the absence of the second maximum which, after Chasovitin et al. has been observed regularly above the E-layer, though with variable heights of "valley" and peak. We feel that this is an essential feature of the nighttime ionosphere which should be taken account of when improving IRI in the future.

Diurnal variations at several altitudes are shown in Figure 6, which shows the discrepancy between IRI and the empirical models at 200 km during the daytime. We believe that this discrepancy is due to some drawback of the Chiu program. At lower altitudes the influence of this uncertainty is small and does not affect the IRI profiles. The same might be true for the differences between eastern and western hemispheres, also appearing on Figure 6.

4. High and Low Latitudes

Figure 7 shows the IRI model and experimental data for various geographic latitudes ϕ . The electron concentration at the E-layer maximum and in the valley between the E- and F-layers was chosen for comparison. One can see from Figure 7 that, during daytime, there is reasonable agreement between IRI, and the experimental data and models up to latitudes of about 60 to 65° , but for higher latitudes an essential difference appears. Similar analysis for other altitudes confirms this conclusion for the whole interval 90 to 200 km.

During night, the agreement with experimental data and models is poor for all latitudes. An especially great difference is observed for the

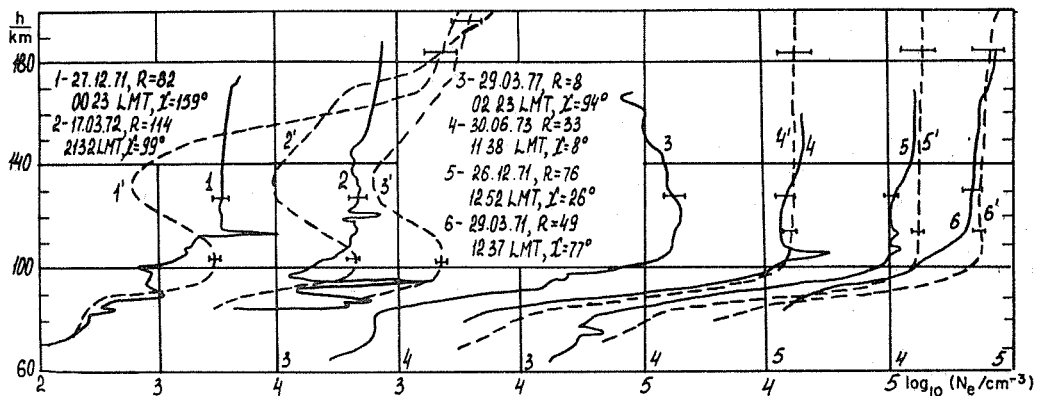


Fig. 8 Rocket profiles for low and high latitudes (1,4,5 - low latitudes; 2,3,6 - Heiss Is.) and corresponding IRI - profiles (1' - 6'). Sources: Kriukin et al., 1976; Chasovitin and Shushkova, 1980; Chasovitin et al., 1976; Klyueva et al., 1973.

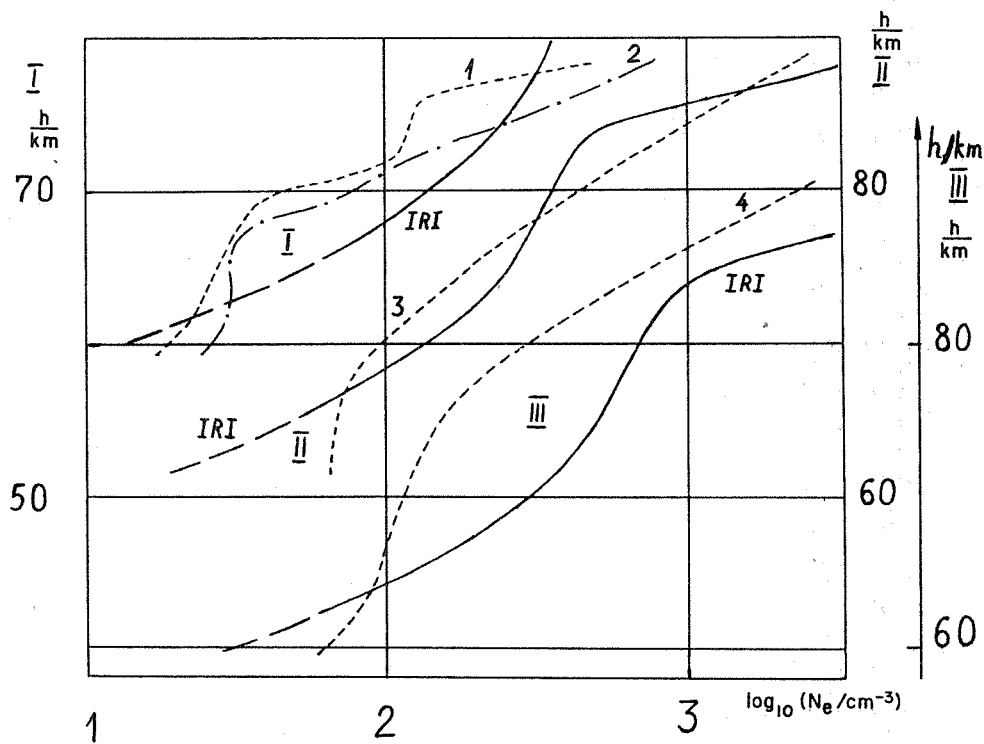


Fig. 9 Experimental and IRI electron density profiles in the D-region for different conditions: 1 and 2: CM method averaged over 11 days (Sept. - Oct., 1972, LT 09 ... 10 and 10 ... 11 respectively; 3: PR method, 12 Nov., 1975, 11 LT; 4: PR method, 24 May 1973, 14 LT; [3 and 4 obtained after averaging over 10 min].

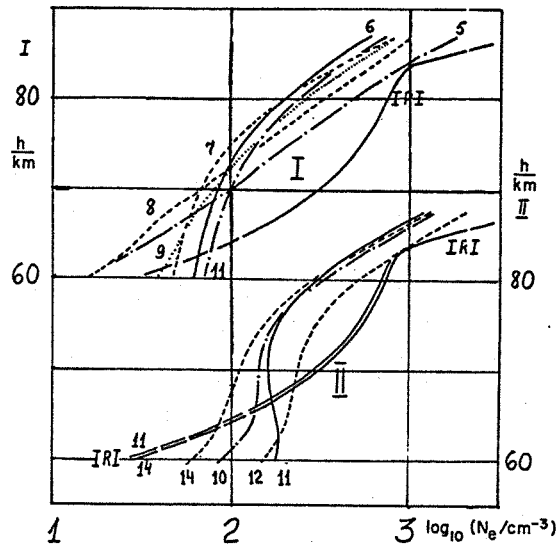


Fig. 10 Experimental and IRI electron density profiles in the D-region for different conditions: I. PR method, June 1973, 11 ... 12 LT. The numbers near the curves give the dates. II. PR method, May 24, 1973. The numbers near the curves give local time. Averaged over 10 min.

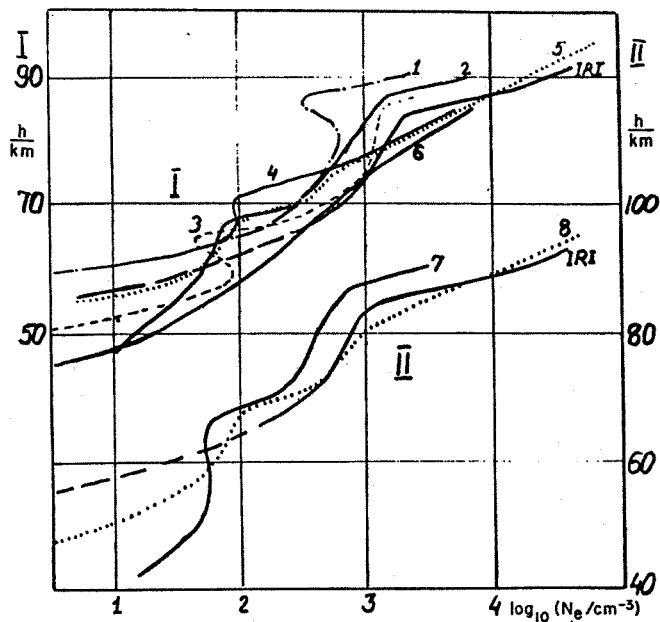


Fig. 11 Comparison of IRI with daytime summer VLF models for solar maximum (I) and minimum (II):
 1. noon, $\psi = 40^\circ$ to 50° [Nertney, 1953];
 2 and 7. noon, $\psi = 45^\circ$ [Azarnin and Orlov, 1976];
 3. noon, $\psi = 50^\circ$ [Bain and Harrison, 1972];
 4. $\psi = 26^\circ$, $\psi = 30^\circ$ [Bjontegaard, 1974];
 5 and 8. noon, $\psi = 50^\circ$ [Krasnushkin and Knyazewa, 1970];
 6. noon, $\psi = 50^\circ$ to 80° [Rinnert, 1973].

region of the auroral oval; this is quite natural because in this region auroral electrons provide an additional source of ionization.

High and low latitudes are considered in Figure 8, with measurements of Chasovitin and Shushkova /1976, 1980/, Klyueva et al., /1973/ and Khriukin and Chasovitin /1976/.

To summarize our findings for the height interval 90 to 200 km, may be put as follows: for daytime quiet conditions, IRI describes the vertical distribution of electron concentration well enough for all latitudes up to geomagnetic latitudes of 60° or 65° . During the night there is an essential disagreement with the majority of the experimental data, even for middle latitudes; at higher latitudes ($\phi > 55^\circ$) IRI can not be used at all for nighttime conditions.

5, D-Region (50 to 90 km)

Reliable measurements of the electron concentration below 90 km are still difficult to obtain. Also the profiles in the D-region are very variable. All this makes the comparison of IRI with experimental data in this height range rather difficult. We compare here with measurements obtained by Cross-Modulation (CM) and by Partial Reflection (PR) techniques, and VLF and LF propagation data.

We must confess that, while recognizing that IRI is supposed to give profiles only down to 65 km in the daytime and down to 80 km during the night, we deliberately changed the program so as to extend the profiles down to 40 to 50 km just to see if such an extrapolation would give reasonable results.

5,1 CM and PR Measurements

These methods have been recognized to yield the most reliable results of all ground-based D-region measurements /Kawer et al., 1974/. We have observations by PR in Leningrad and CM in Moscow, for several periods during 1972 to 1976. About 50 averaged profiles for different periods were analysed.

Typical examples are shown in Figure 9. It is seen that the model values are close to, or coincide with, the experimental ones at 80 to 90 km and around 65 km. But otherwise the profiles are rather different; in particular, at 65 to 80 km the model and the experimental data may differ by a factor of 3 to 5. Below 65 km, extrapolated model profiles give much lower values than that given by CM and PR measurements.

An important feature of the D-region electron concentration behavior is its strong variability. Figure 10 shows IRI profiles and the experimental data obtained by PR-method at different hours of the same day (May 24, 1973) and at the same hour (10 to 11 LT) during six consecutive days. It is evident from Figure 10 that the experimental data show remarkable variations of electron concentration at each altitude, which can not be represented by a model. Below 65 km, the reliability of the PR-method is less good, one should not pay too much attention to this range.

The strong variability in the D-region during similar geophysical conditions apparently shows that D-region behaviour is controlled not only by the usual geophysical factors (solar and geomagnetic activity, solar zenith angle etc.) but also by meteorological factors, connected with thermo-dynamical regime of the stratosphere and mesosphere, atmospheric circulation and so on. Some indication of such a control has been found, first in connection with the winter anomaly, by many authors /see, for example Offermann, 1979; Labitzke et al., 1979; Danilov and Ledomsкая, 1979/. The abovementioned variability of the electron density profiles below 90 km provides additional evidence that such a control exists. If so, in order to give an adequate description of the

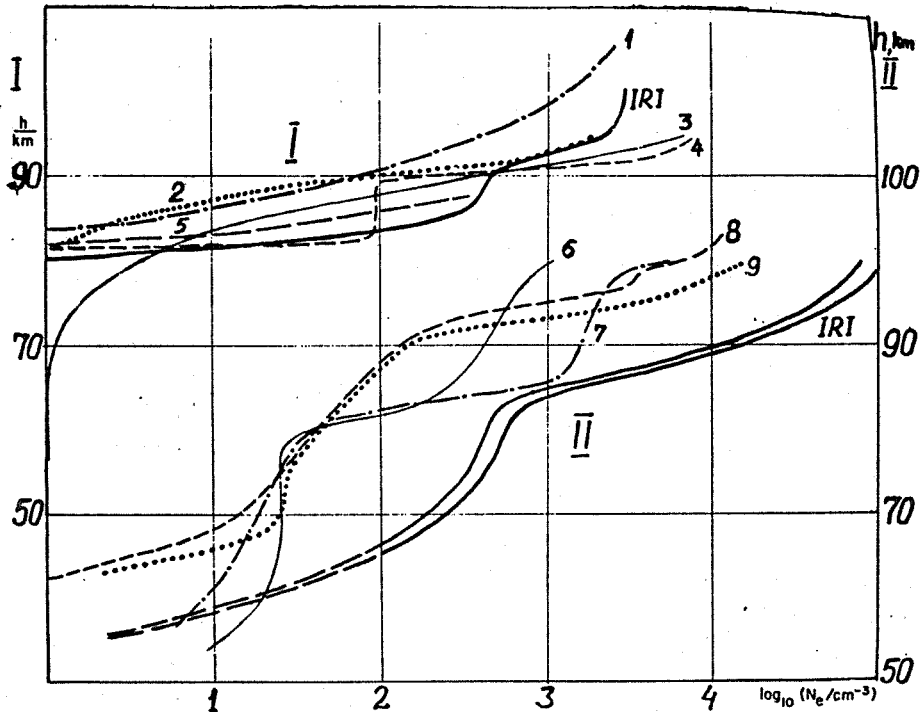


Fig. 12 Comparison of IRI with nighttime (I) and winter day (II) VLF models. Night: 1 - Nertney, 1953; 2 - Krasnushkin et al., 1970; 3 - Rinnert, 1973; 4 - Thomas and Harrison, 1970; 5 - Bjontegaard, 1974: sunset ($\chi = 101^\circ$). Winter day (upper IRI curve: $R = 20$, lower: $R = 150$): 6,7 - noon [Azarnin and Orlov, 1978], solar minimum (6) and maximum (7); 8 - ($R \approx 15$, $\chi = 80^\circ$) Singer, 1976; 9 - (noon) Krasnushkin et al., 1970.

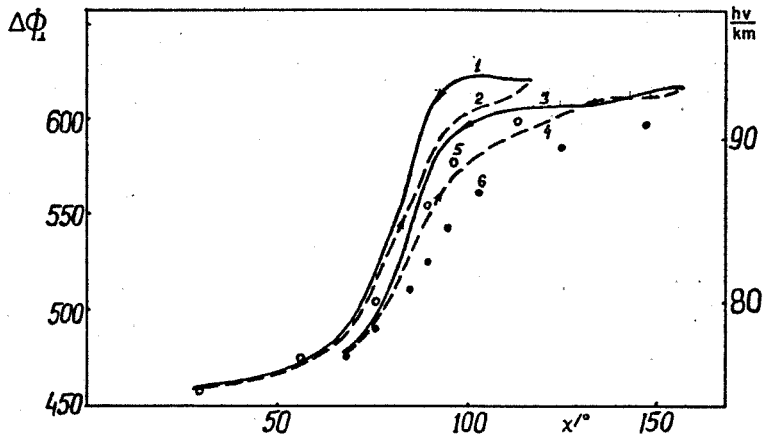


Fig. 13 14.9 kHz short-path observations of the abnormal component phase $\Delta\phi_1$ as compared with IRI computations: 1 - observations, May 1974, after midnight; 2 - same, afternoon; 3 - observations, December 1973, after midnight; 4 - same, afternoon; 5 - IRI, May 1974; 6 - IRI, December 1973.

electron concentration profiles for any given set of conditions, all models, and first of all IRI, should include as input parameters not only the abovementioned geophysical factors, but also some parameter (or parameters) characterizing the meteorological situation in the stratosphere/mesosphere region. The question of what this parameter should be and how it might be determined is beyond the scope of this paper and requires serious investigation.

5.2 Comparison with the VLF and LF Data

Neither the experimental data on VLF and LF propagation, nor the electron concentration profiles obtained by interpreting these data, have been included in the basic data used in constructing IRI /see Rawer (ed.), 1974/. In spite of some defects in E-region models based on low frequency radiowave propagation (VLF-models), it is worth comparing them with IRI, because now it is widely accepted that VLF and, partly, LF propagation parameters in the Earth-ionosphere wave guide are very sensitive to ionospheric conditions below 75 km in daytime and 90 to 92 km in nighttime /Sechrist, 1974; Azarnin and Orlov, 1978/. It is also interesting to compare VLF propagation parameters, computed with the help of IRI, with the real VLF data, especially with those not used earlier while constructing empirical models /Nertncy, 1953; Thomas and Harrison, 1970; Krasnushkin and Knyazeva, 1970; Bain and Harrison, 1972; Bjontegaard, 1974; Kinnert, 1973; Singer, 1976/.

For comparison with IRI, we have chosen the probably most reliable VLF-models, those for noon and midnight conditions, shown in Figures 11 and 12. For summer noon there is satisfactory absolute agreement between the IRI and VLF models above 60 to 65 km. Considering the shape of the profiles, it is worth mentioning that VLF-models give three well pronounced regions, which might be connected with three different sources of ionization. IRI obviously can not show the C-layer below 65 km which, according to VLF models does exist; it is more pronounced during solar minimum than during solar maximum. For winter the systematical difference between IRI and VLF models at noon is typical with IRI values 3 to 10 times higher than those obtained by fitting the VLF-data.

For nighttime conditions, all models show a large vertical gradient in the lower part of the profiles; hence it is more reasonable to compare the altitudes where this gradient appears rather than values at fixed levels. All the VLF-models give close values for the characteristic altitudes, namely about 80 to 85 km. (Kinnert /1973/ gives lower values for the gradient and increased values of density below 80 km, probably because the majority of the paths considered were located at very high latitude).

One can see from Figure 12 that the IRI profile is situated a little below the VLF profiles. Thomas and Harrison /1970/ locate one typical "step" at 82 to 88 km, which is partly reproduced by IRI.

Some results of short path /Kashpar et al., 1978 (p.193), 1979/ and long path /Demykin et al., 1974; Kashpar et al., 1978 (p.189)/ VLF observations were taken for sample comparison with IRI. Numerical methods for the computation of VLF propagation parameters and fields from a given model electron density distribution had been elaborated and programmed by one of the authors /Galyuk and Ivanov, 1978/.

It is necessary to emphasize once again that all VLF computations could only be performed for the "extended" IRI model, in which, at heights below 65 km by day and 80 km at night, the electron densities were calculated by the same formulae as for greater heights.

Midlatitude VLF short-path phase measurements of the abnormal component H_1 relative to ground wave /Kashpar et al., 1979/ are compared in Figure 13 with IRI model calculations. Noon values of the phase $\Delta\phi_1$ and the corresponding virtual reflection heights h_v computed from IRI

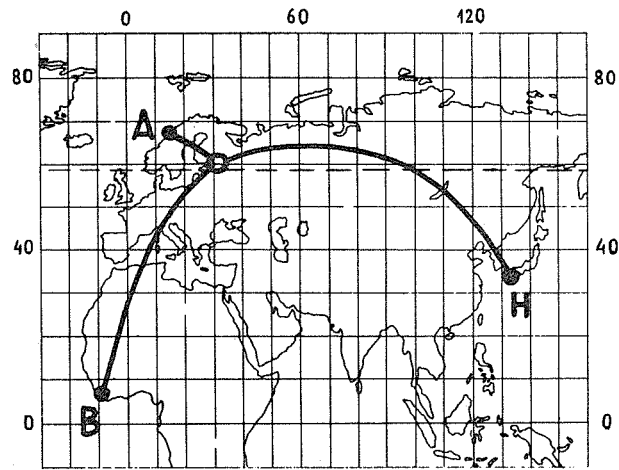


Fig. 14 Propagation path geometry for the OMEGA stations A, B and H monitored in Leningrad at 13.6 kHz from 18 to 22 June 1976. To the north of the dashed line, the maximum value of solar zenith angle was less than 98° at that time.

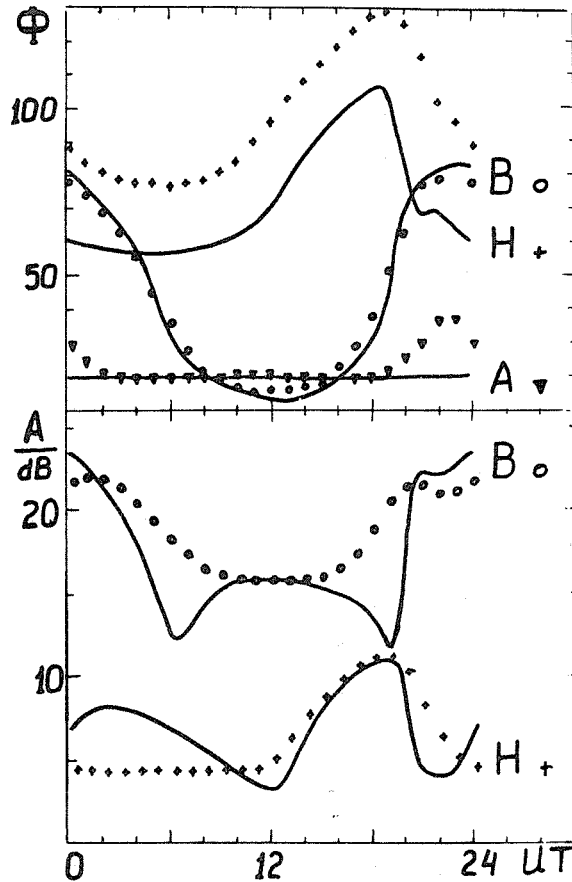


Fig. 15 Comparison of long path VLF observations at 13.6 kHz (solid lines) with IRI model calculations (circles, crosses and triangles) for June 1976. Letters near the curves are standard OMEGA station indicators. The observed and computed noon phase values for station A were fitted together to form a common phase reference for all the other observations and computations. The computed amplitudes were fitted to the observed values at 1200 UT for station B and at 1500 for station H.

are close to their respective experimental values, both for May and for December. At night the computed heights h_v are about 2 km lower than observed, the rms day-to-day variation being about 1 km. The general features of the predicted and observed diurnal variation patterns seem to be similar. However, the IRI apparently fails to reproduce the well-known asymmetry of the diurnal variation which is evident from Figure 13 (for $\chi > 75^\circ$).

Comparison of the observed and calculated amplitudes of the abnormal component H_{\perp} shows that daytime experimental amplitudes at 14.9 kHz are 1.5 to 2 times higher than the computed values. The observed amplitudes at night are either lower than, or are close to, the calculated values.

Figure 14 shows long-path geometry for three VLF OMEGA navigational aid stations monitored in Leningrad at 13.6 kHz during the summer solstice 1976. The latitude at which the midnight solar zenith angle is equal to 98° during this period is shown by the dashed line. It can be seen from Figure 14 that the lower ionosphere above the path for station A (OMEGA Norway) is illuminated all the time, while more than half of the path from station H (Tsushima) to Leningrad is sunlit at any moment. Only the path from Liberia (station B) to Leningrad undergoes day-to-night illumination changes. The different latitudes of these paths make it possible to check IRI not only for moderate but also for sub-auroral latitudes.

Phase measurements relative to a local stable reference were carried out in Leningrad; it was found that the observed phase of station A stayed practically unchanged over the whole 24-hour period. For this reason the noon phase of the signal of station A in Leningrad was taken as a reference in further calculations. In addition to phase measurements, observations of relative signal amplitudes of stations B and H were carried out.

A comparison of the IRI model calculation with experimental results for the period 18 to 22 June 1976 is presented in Figure 15. For the mid-latitude Liberia-Leningrad path, the model reproduces quite well both the absolute VLF phase value and its diurnal variation. For geomagnetic latitudes near 50° N (the Tsushima to Leningrad path) the model systematically gives the effective height of the ionosphere (about 4 to 6 km) higher than observed. Moreover, it is worth noting that IRI predicts an appreciable diurnal phase variation for the Norway to Leningrad path which is not actually seen. Apparently these discrepancies between IRI and VLF observations for the Tsushima to Leningrad and the Norway to Leningrad paths are caused in part by a latitudinal variation not included in the IRI, and they may also be explained by the failure of IRI to describe the twilight conditions prevailing over these two propagation paths.

The latter assumption seems to be supported by the amplitude observations (see Figure 15). Indeed, although the size of the observed diurnal variation of the amplitudes considered is close to its calculated value, on the other hand the model calculations give amplitudes which depart appreciably from the experimental values for large solar zenith angles. Thus, it seems likely that IRI fails to describe the lower D-region electron density variations during the twilight hours.

6. Conclusions

The present comparison of IRI with various sets of experimental data leads to the following conclusions about the validity of IRI in various geophysical conditions.

1. During daytime ($\chi < 75^\circ$) at 90 to 200 km, IRI agrees satisfactorily both with the results of individual rocket measurements and with corresponding empirical models.

2. In twilight and during nighttime, the shape of the model profiles differs from the observations because it does not show a second maximum during the night.

3. Comparison with CM and PR data shows large differences between 65 and 80 km in daytime. Values given can be 3 to 5 times greater than the observed electron concentrations.

4. Models deduced from VLF and LF data for winter daytime conditions lead to the same conclusion: above 65 km, IRI gives greater values of electron density than those found from radiowave propagation data. But for summer daytime conditions, the agreement between IRI and VLF models seems to be quite satisfactory.

5. Measurements by CM and PR methods, and also VLF data, show that the extrapolation of IRI down below 65 km leads to values of the electron concentration which are too low; this contradicts both groups of experimental data. According to the VLF data, the daytime model should show a C-layer with concentrations of the order of 10^8 m^{-3} at 55 to 60 km.

6. Comparison with the VLF models for nighttime conditions shows that IRI correctly represents the high gradient region above 80 km. The altitude of this region according to IRI is, however, 2 to 3 km lower than that given by the VLF data.

7. Direct comparison of the IRI field calculations with the observed VLF fields show that there is reasonable agreement for midlatitude noon and nighttime conditions. However, appreciable discrepancies may be found for the twilight period and, presumably, for latitudes greater than 50° . Evidently the VLF data must be considered when constructing electron density distribution models below 90 km, and especially below 70 km.

Discussion remarks:

The additional maximum between the E- and F-regions should be considered as to be a dynamic phenomena which must not be included into a global model like IRI (K. Serafimov). As for the regular valley above the E-peak its depth is found to be different over both sides of the Atlantic (K. Bibl). The Chiu-model for the electron density peak is quite obviously oversimplified. Replacement by the CCIR-model might have given different results at altitudes near 200 km (K. Rawer).

1.2.4 Comparison of IRI-78 with IZMIRAN's Equinoctial Models

T.L. Gulyaeva, A.G. Israetel, T.Yu. Leshchinskaya,

T.N. Soboleva, E.E. Tzedilina

Institute of Terrestrial Magnetism, Ionosphere and
Radio Wave Propagation, Troitsk, Moscow Region,
142092 USSR

In 1972/73 IZMIRAN established global analytical models of electron density and electron collision frequency in the ionosphere with the aim of investigating long range short wave propagation by means of adiabatic and ray-tracing methods /Gurevich et al., 1972/. The models were constructed for equinoctial conditions of minimum solar activity. The coefficients of EM (equinoctial model) for electron density were determined on the basis of the model profiles for the latitudes 0° , 30° , 50° and 70° for midnight and noon; also determined was the diurnal variation at the latitudes from 50° to 55° /Soboleva, 1972a; 1972b/. The latitudinal dependence of the EM coefficients was revised in 1974 /Tushentsova et al., 1975/ on the basis of new model profiles /Soboleva, 1973/. The profiles are described by functions which are continuous everywhere, including the first derivative. With these models problems like long-range short wave propagation, and round-the-world echo signals in particular, were investigated /Gurevich, Tzedilina, 1979/. At the present time the models are utilized for investigations of oblique incidence ionogram structure for long and round-the-world paths /Tzedilina, 1980/.

The development of the common international ionospheric model /Rawer et al., 1978a/ is rather important both for ionospheric physics studies and for investigations of radio wave propagation. Until now we have not yet combined the computer programs of IRI-78 with our computer programs for calculating radio wave propagation parameters over long range paths using the adiabatic approach. We therefore can not say whether we can utilize the IRI-78 as one component of our rather complicated computer programs. But we have made a first step by comparing IRI-78 with our models which had been widely tested in different investigations and had gained recognition as a reliable average description of the ionosphere.

Since the height profile $N(h)$ in IRI admits introduction of NMF2 and HMF2 from any source, these parameters taken from our analytical equinoctial model for low solar activity /Gurevich et al., 1972; Soboleva 1972 b/, that for minimum solar activity (sunspot number $R = 10$) /Soboleva, 1972 b, Soboleva, 1973/ and for high solar activity ($R = 110$) /Kadukhin and Soboleva, 1972/ were put into IRI-78.

Next, the peak values of electron density (NME) and height (HME) of the E-layer, and also the minimum density in the valley (N_v) and the corresponding height (h_v) were compared for the same values of NMF2 and HMF2. The results of the comparison are shown in Figures 1 to 3.

Figure 1a (on top) shows $K_E = NME_1/NME_2$ viz. the ratio of E-peak density from our analytical models to the corresponding IRI-78 density for day and night and at different latitudes. By day the difference in NME is only 10 to 30%. At night, however, the ratio is as high as 2 to 3 at middle and low latitudes and even 16 in the auroral oval. At the bottom, in Figure 1b, the corresponding variation of the ratio of minimum densities in the valley is shown for different latitudes. Near noon the differences at all latitudes do not exceed 20 to 30%, but for dawn and dusk and, in particular, at night the differences are greater. At middle and low latitudes the ratio can be 2 and, in the auroral oval, near midnight, as high as 70.

In Figure 2 the difference between characteristic heights in the models can be seen. For the E-peak the height difference Z_{NE} is slight: 1 to 3 km at the middle latitudes; at low latitudes it is 4 to 6 km. It should be noted that in the model profiles of Soboleva the values of Z_{NE} are greatest during the dawn/dusk hours (see the upper most curve). As for the valley the height difference ΔZ_V is small at noon, but during dawn/dusk, for all latitudes goes up to 20 to 30 km.

The differences of valley width W at different latitudes at noon and midnight, and for a whole day at latitude 50° , is shown in Figure 3. It is small at middle and low latitudes in the day-time (about 2 to 10 km and 20 km for low and high solar activity respectively). It is much greater at high latitudes at night (about 60 to 80 km).

Summarizing we may state that IRI-78 and the IZMIRAN models agree well by day for all latitudes and for different solar activity. Greater discrepancies occur, however, at night with factors going up to 2 to 4 in density and up to 30 km for the height of the minimum. At high latitude, in the auroral oval, very large differences were found.

The differences in $N(h)$ profile parameters for the night E-region and valley are due firstly to the lack of complete experimental data at different latitudes, and secondly to the fact that the night-time experimental profiles are rather "ridged" and have ledges or peaks in the valley region. Therefore, the mean profiles depend significantly on the technique adopted in the averaging process. Besides, in our model we have given special considerations to the concentration in the auroral region, which does not seem to have been done in IRI-78.

Discussion remarks:

The author confirmed that data had been available referring to the valley in the southern hemisphere as well as at high latitudes.

K. Rower pointed out the IRI valley model is based on incoherent scatter data from mid-latitudes mainly. The difference between IRI and the IZMIRAN model is particularly large at high latitudes by night. It should be kept in mind that in IRI no effort was undertaken until now to cope with the special conditions in the auroral oval.

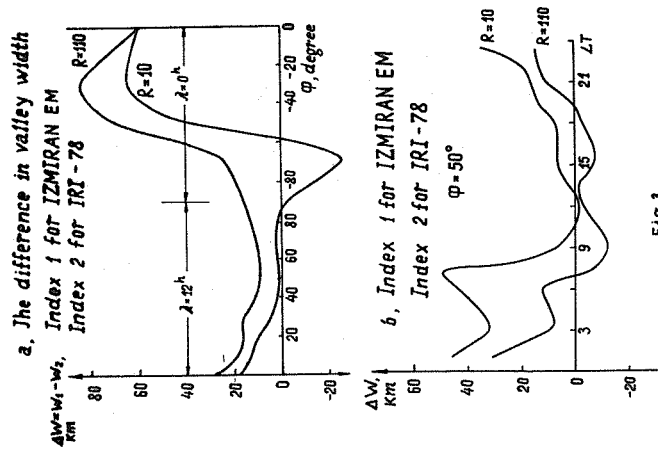


Fig. 3

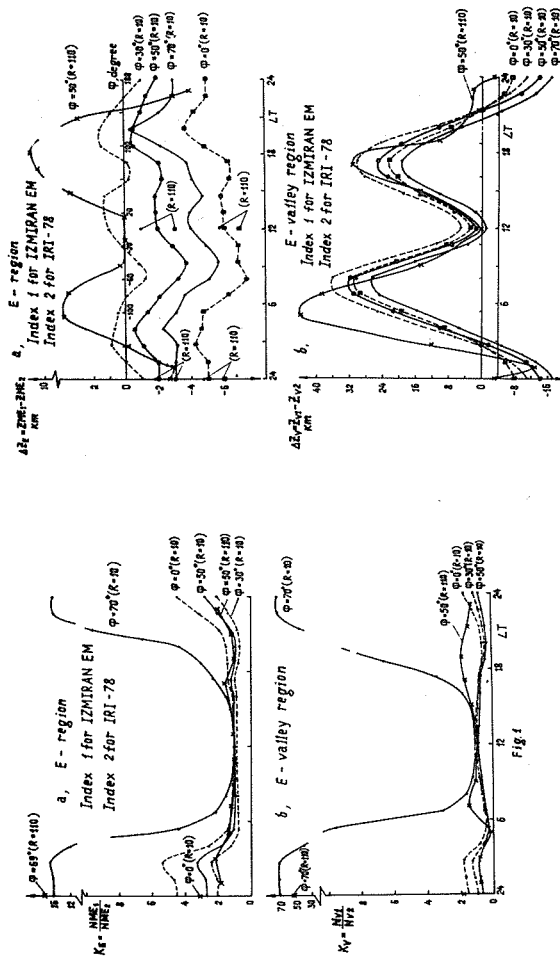


Fig. 2

Fig. 1 Electron density ratio for IZMIRAN and IRI models at E-peak (top) and valley minimum (bottom).

Fig. 2 Height differences between IZMIRAN and IRI models at E-peak (top) and valley minimum (bottom).

Fig. 3 Valley width differences between IZMIRAN and IRI models.

1.2.5 Bottomside Electron Density Profile Measurements by

Rocket Borne Probes over the Equator

S.F. Gupta

Physical Research Laboratory Navrangpura,
Ahmedabad 380009 India

The purpose of this paper is:

a) to present the experimental data obtained from rocket-borne probes over a low-latitude station at Thumba (India), dip = 0.6° S; and

b) to compare these results with the International Reference Ionosphere. The rocket flights were carried out between 1967 and 1978. The D.C. probe technique was used and, since identical sensors and payloads were used in all our flights, we have used a fixed calibration factor to convert D.C. probe current into ambient electron density. This calibration factor was correct to within 10% in altitude region 90 to 180 km, but in the D-region from 60 to 90 km the uncertainty is greater.

Comparison of the profiles in Figures 1 and 2 shows the changes that occurred near sunrise following a 10° decrease in the solarzenith angle. The profile in Figure 3 is very close to a noon profile of Gupta and Irakash /1979/. The density of the layer near 74 km is 10 times that in the profile in Figure 2. Figure 4 shows the noon profile, and the base of the E-layer is less structured than in the afternoon profile (Figure 5). In the evening profile (Figure 6), layers above 140 km can be seen. Although Figures 2 and 6 refer to the same zenith angle, the profiles are very different. The midnight profile in Figure 7 shows a very much layered structure.

These results will be published elsewhere: Gupta /1980/; see also Rees et al., /1976/.

Comparison with International Reference Ionosphere

It is suggested that some of the assumptions made in the IRI by Rawer et al, /1978a/ are not realistic and are not in accord with experimental results. For example:

1. The evening and night time profiles are the same in IRI but, according to our results, they are very much different.
2. The night profile is assumed to be smooth from 90 to 130 km, but it is generally very much structured.
3. At sunrise and at sunset layers are observed in the E-region.
4. 'Holes' have been observed in the F-region over the equator near 250 km, at night. The electron and ion density varies by a factor of 1000 within these 'holes' over a distance of 50 to 100 km. The holes are observed mainly in O^+ ions. It will be essential to include these new results in IRI. Within a year, F-region measurements from the Indian rocket ranges will be available.

Suggestions

It is suggested that the IRI in future should include real measured profiles for low latitudes for noon and midnight, and perhaps also for evening and morning. It is probably not possible to include such profiles of other parameters but at least the electron density profiles in IRI must be realistic.

Acknowledgements: This work was supported by the Department of Space, Govt. of India. The author is thankful to Alexander von Humboldt Foundation, West Germany and to Prof. K. Rawer.

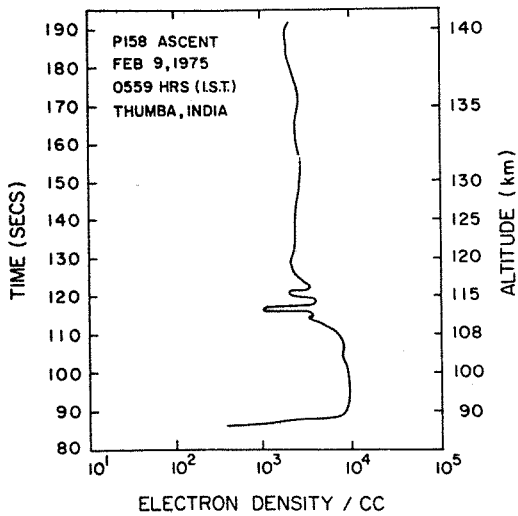


Fig. 1

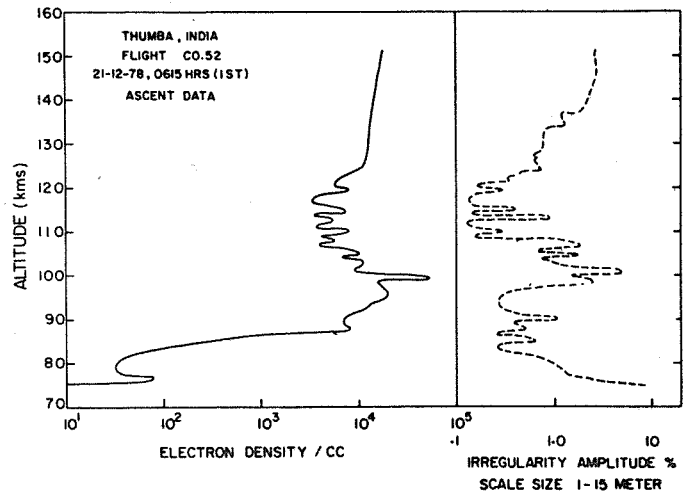


Fig. 2

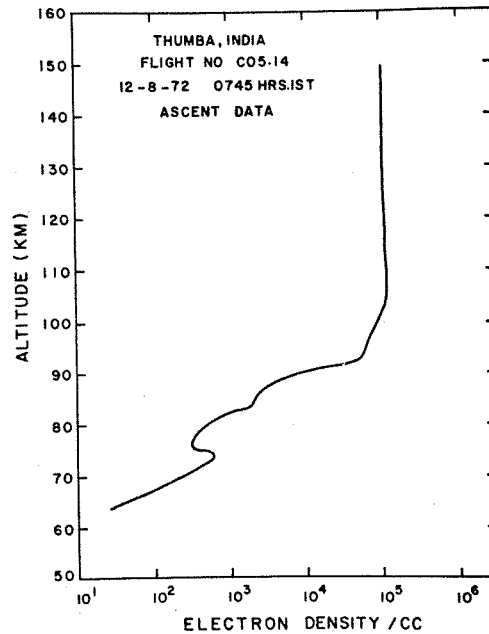


Fig. 3

- Fig. 1 Electron density/height profile obtained by a rocket launched before sunrise ($\chi = 105^\circ$).
- Fig. 2 Electron density/height profile (left) obtained by a rocket launched near sunrise ($\chi = 95^\circ$). The amplitude of the irregularities is indicated at the right.
- Fig. 3 Electron density/height profile obtained by a rocket launched after sunrise ($\chi = 70^\circ$).

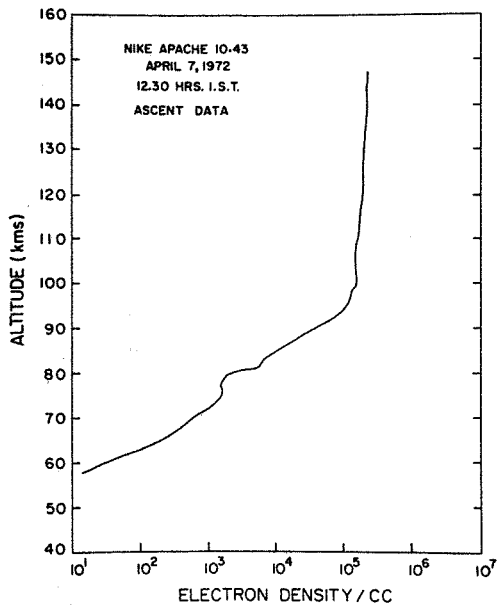


Fig. 4

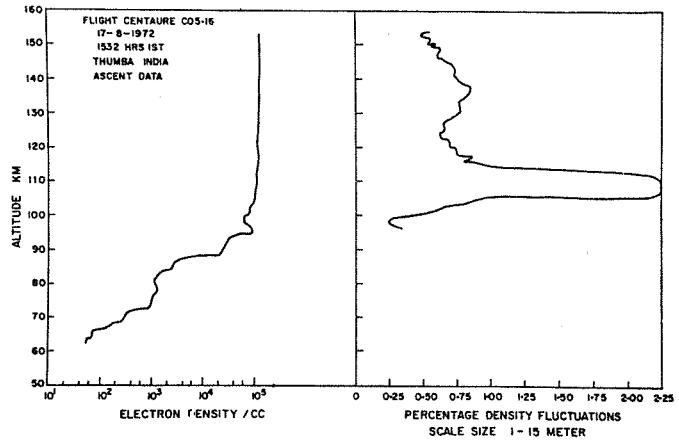


Fig. 5

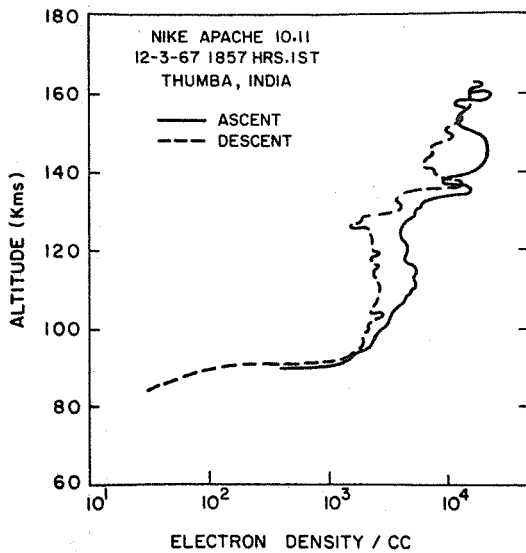


Fig. 6

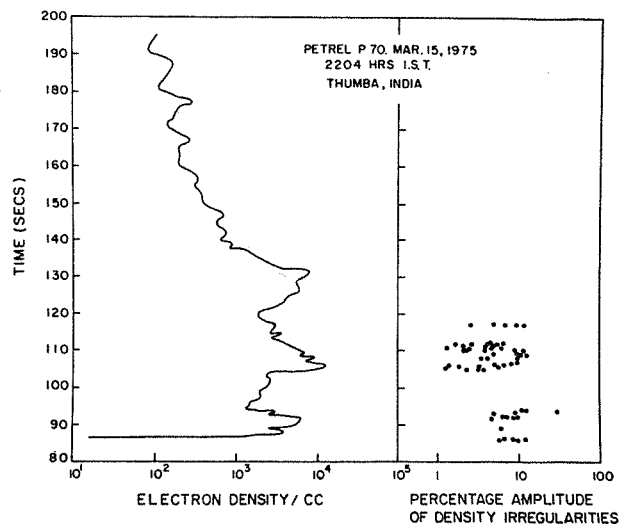
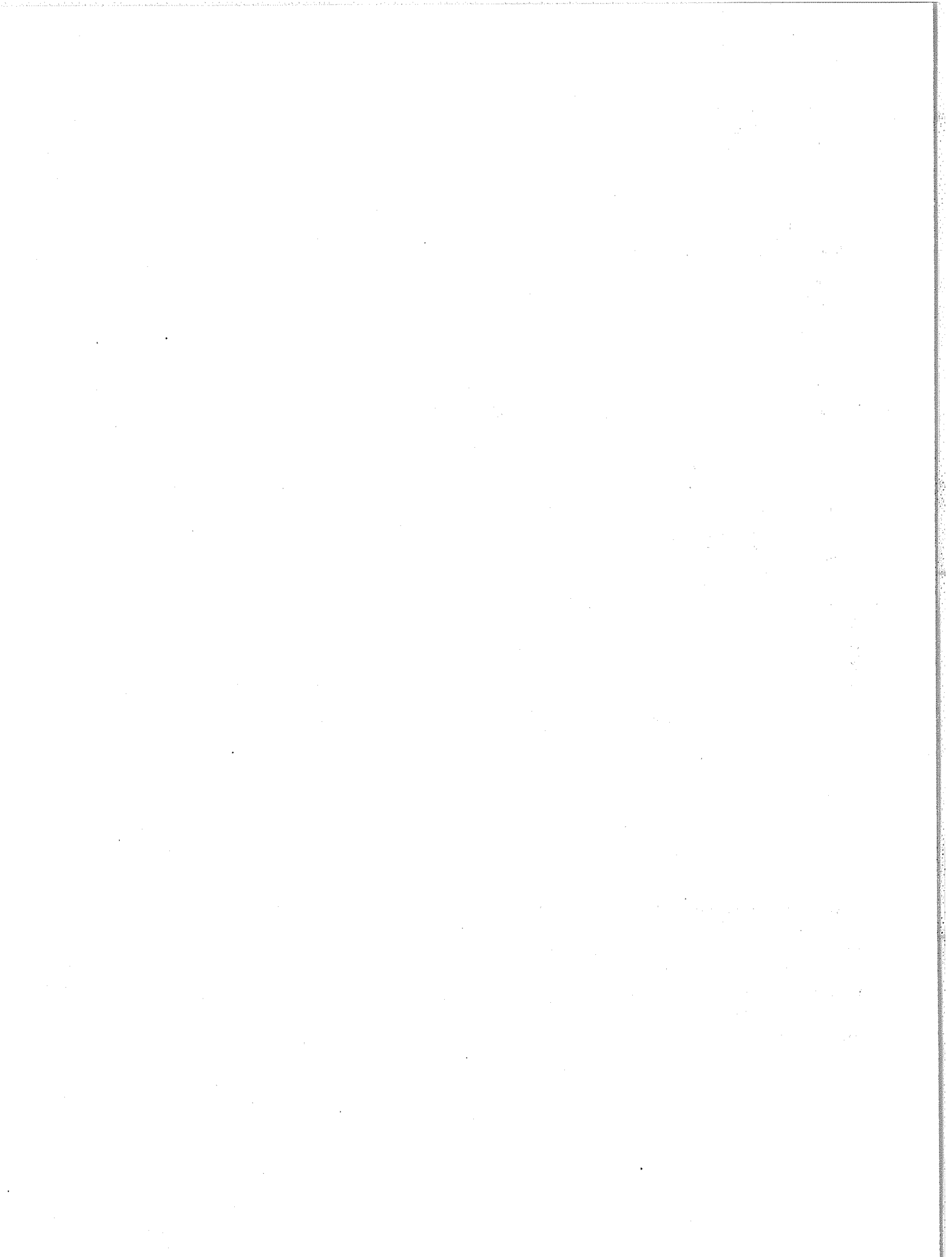


Fig. 7

- Fig. 4 Electron density/height profile obtained by a rocket launched near noon ($\chi = 0^\circ$).
- Fig. 5 Electron density/height profile obtained by a rocket launched during the afternoon ($\chi = 45^\circ$).
- Fig. 6 Electron density/height profile obtained by a rocket launched in the evening ($\chi = 95^\circ$).
- Fig. 7 Electron density/height profile obtained by a rocket launched near midnight.



Section 1.3 Topside

1.3.1 Rocket and Satellite Measurements Compared with the

IRI-79 Electron Density Profiles

H. Neske, S. Ramakrishnan, C. Rebstock

Fraunhofer- Institut für Physikalische Messtechnik,
Heidenhofstraße 8, D-7800 Freiburg, FRG

Experimental evidence from several rocket flights at locations between the equator and high latitudes, and from two satellites, is compared with the latest version (IRI-79) of the International Reference Ionosphere. Differences appear at certain locations and are discussed.

The purpose of this paper is to compare average electron-density distributions as predicted by the IRI /Rawer, 1980/ with in situ measurements of densities. This is in no way a complete comparison but only a study for selected times and locations, of such cases as were available to us. Electron densities have been measured by the impedance Probe technique, providing an absolute accuracy of better than 10% /Neske and Kist, 1974/. Measurements from rockets and satellites in three different latitude ranges were taken for comparison. In the following, the rocket data are considered first, because these are more suitable for comparing with altitude profiles at a given location. Satellite data, on the other hand, provide a global coverage. Wherever possible we have used IRI profiles adjusted to measured peak data. Where such data were not available, we used the CCIR predictions as given in an IRI subroutine.

The two low-latitude profiles /Neske and Kist, 1973/, measured with an interval of four days in the middle of the afternoon above Kourou (Figure 1), show in one case a marked valley between E- and F-layers, whereas in the other case a slightly structured monotonic increase is observed. It is difficult to decide which should be considered as "typical". The IRI profile corresponds clearly to the monotonic shape, which is quite well reproduced (by a factor of less than 2).

For mid-latitudes an example is given in Figure 2. It was obtained in a flight in the American JAMPIC project /Lorse et al., 1978/. After normalizing the ionosonde data at the height of the sporadic E-layer, the in situ measurements of densities for ascent and descent are in good agreement with the sounder results. Taking the peak values, as given by the CCIR predictions, for hmF2 and h'pF2 (345.2 km and $6.2 \cdot 10^{11} \text{ m}^{-3}$ respectively) the discrepancy between the IRI profile and measurement is up to a factor of 4 at around 190 km altitude (dots). Using, however, the actual values as measured by the ionosonde (380 km and $9 \cdot 10^{11} \text{ m}^{-3}$) the agreement is much better. The plotted IRI profile (crosses) includes, furthermore, an adjustment of the F-layer thickness parameter for best fitting of the measured curve. Hence inaccuracies in the CCIR peak prediction are, in this case, mainly responsible for the deviation.

Although the quality of data used for deriving the IRI model was much better at low and middle latitudes than at higher ones, it seemed worthwhile to attempt a check at high latitudes too. Figure 3 shows the composite profiles for four rocket launches obtained during the Polar High Atmosphere programme /Neske, 1980/, which was performed under different geophysical conditions over Andenes (magnetic dip 77.4°). The mean profile given by IRI for these three months has a completely different shape; in particular, the deviation at 140 km is more than two orders of magnitude. This is probably due to the

fact that high-latitude conditions differ from those implied in a smoothed description of shape parameters.

We further compare IRI values with in situ measurements of satellites under three sets of conditions described below.

(1) The highly exsentric orbit of the Japanese satellite TAIYO /Mirac, 1975/ provides a quasi height profile at low latitudes. We show, in Figure 4, two examples of measurements with which the calculated IRI profile can be compared directly. In these cases the decrease in density at higher altitudes is smaller for IRI than for the measured ionisation. This may be due to the particular construction of the IRI model in which some compromise had to be found at higher altitudes when fitting a global function for the scale heights of Bent and Ilwelyn /1970/; this was done so as to obtain better accuracy in the lower part of the topside F-Region (IRI being limited to heights below 1000 km). The discrepancy between IRI and measurement at 800 km corresponds to a factor of 2, increasing to 4 for the extrapolation to 1200 km. Unfortunately, the actual values of hmf2 and Hmf2 were not known, so that the extrapolation to the actual peak could not be carried out. We have seen above, that such a correction of the CCIR predictions is sometimes important.

(2) We determined height gradients with data from two satellites, TAIYO and AEROS-B, which made simultaneous measurements during (night time) encounters /Neske et al., 1979/. Four cases are shown in Figure 5; here the gradients of the density on the top side, as given by measurement and IRI, are in good agreement. These are all cases of rather small gradients on the topside. Under other conditions, much greater actual gradients occur, which are then rather different from the smoothed average /Neske et al., 1979/. The deviation of the absolute values in Figure 5 reflects the variability of the ionisation rate, or transport phenomena.

(3) Finally the sun-synchronous satellite AEROS-B /Lämmerzahl and Bauer, 1974/ provided a global coverage of the electron density for two local times, 15h30 and 03h30, at low and middle latitudes. For a period covering the month of August together with the last week of July 1974 (small crosses), and for the longitude sector $280^{\circ} \text{ E} \pm 10^{\circ}$, measurements and IRI were compared in different latitude ranges ($\pm 5^{\circ}$) and in altitude ranges from 220 to about 880 km, as shown in Figure 6, for night- and day-time. We see, in general, agreement between median IRI profiles and the naturally scattered density distributions as observed. The day/night variation seems to be correctly reproduced and, inside the dispersion range, also the latitudinal variations. Two points should be noticed: first, during day and night, the model gives densities which are too low at 60° midip; second, during day-time, the density at 40° S midip is somewhat lower than predicted.

Conclusions:

Quite naturally, when the IRI-79 shape of the electron density profile is adjusted to measured peak values (hmf2 and Hmf2) the agreement with measured profiles is considerably better than when the CCIR predictions are taken as input values. Absolute comparison under the latter conditions depend on the accuracy of the CCIR model, which is known to be rather different in different geographic regions. Under the first conditions the profile functions are in good agreement in the low and middle latitude ranges. For high latitudes and for high altitudes, the model deviates considerably from our experimental results.

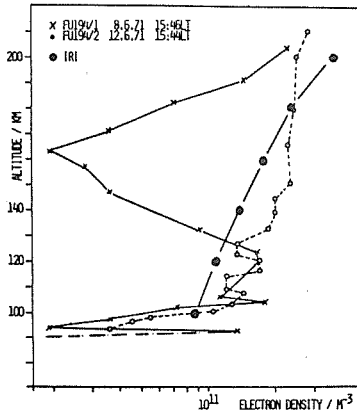


Fig. 1 Two electron profiles over Kourou (5°N, 307°E) 4 days apart.

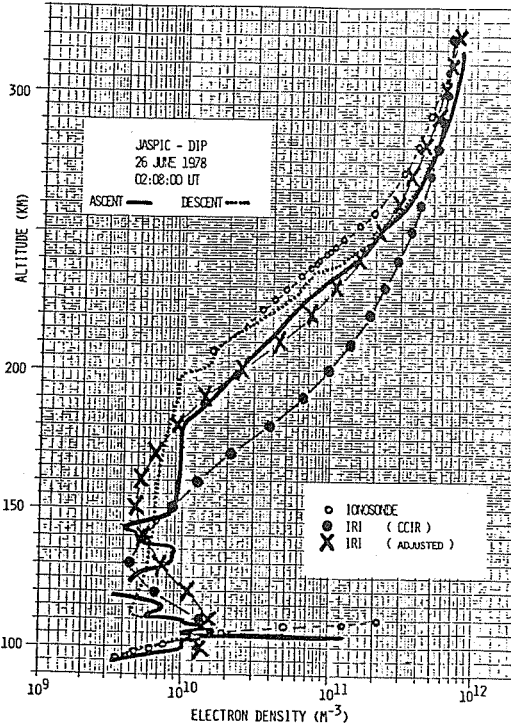


Fig. 2 Electron densities for ascent and descent over Wallops Island (38°N, 285°E) and data from the ionosonde.

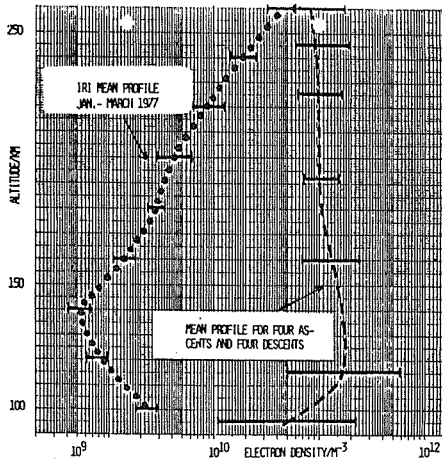


Fig. 3 Mean profile based on four rocket launches over Andenes (69°N, 16°E). Time period January through March 1977. Local times around 22:00

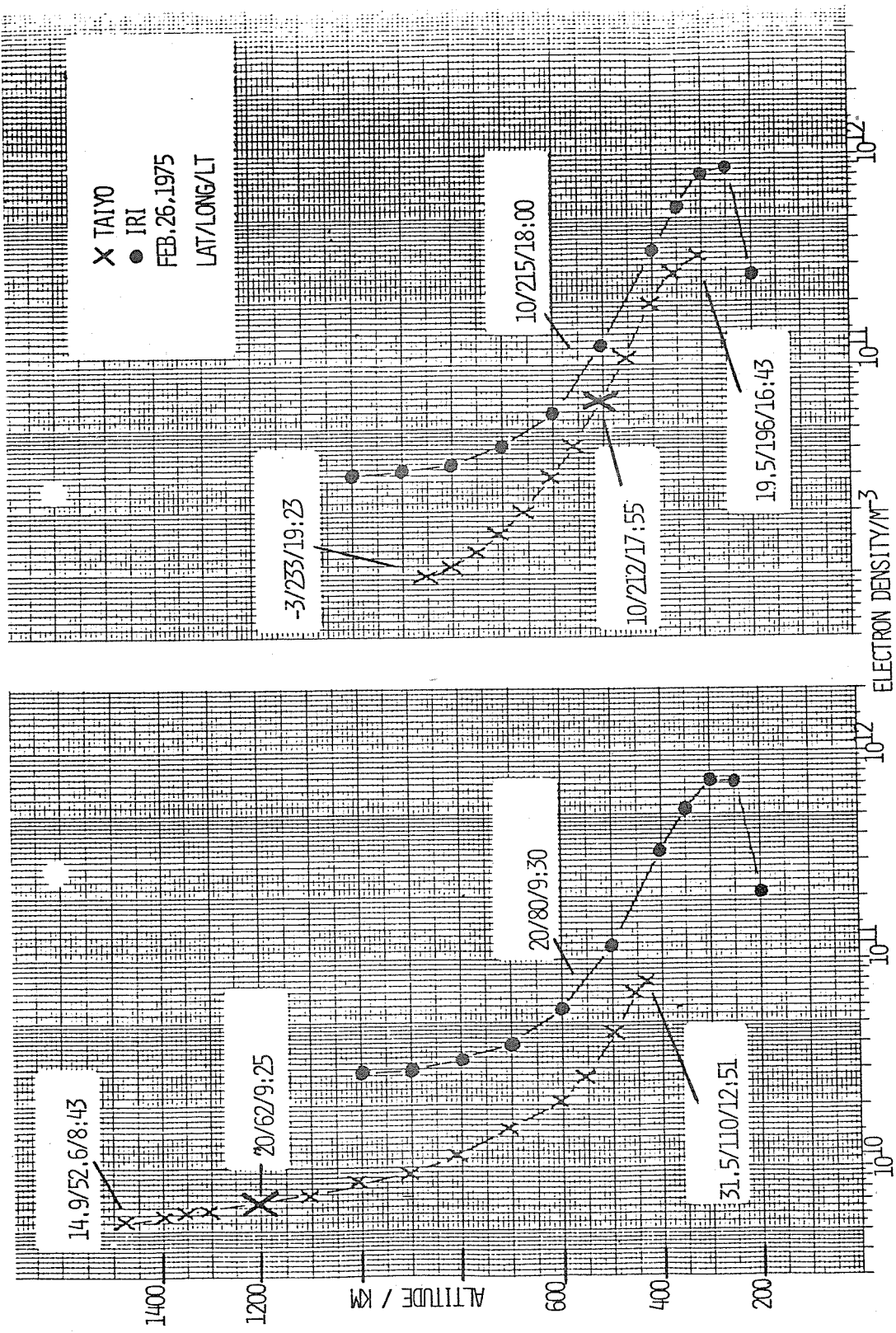
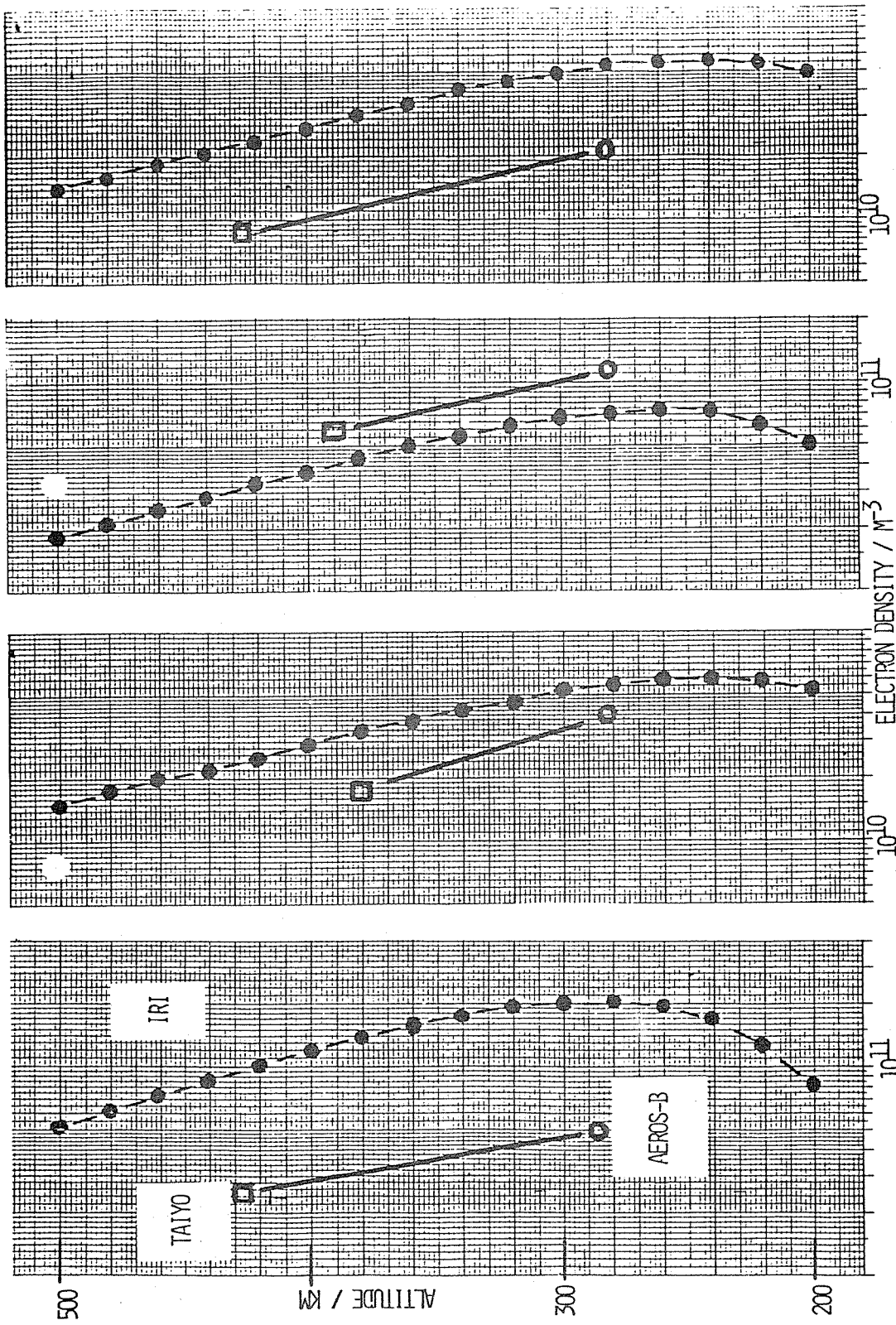


Fig. 4 Quasi height profiles from TAIYO satellite at low latitudes.



DAY/LAT/LONG/LT : 193/31N/29E/4,6H

195/31S/24E/4,5H

195/30S/29E/4,6H

196/29S/23E/4,6H

Fig. 5 Density gradients measured by two satellites during night time encounters at low latitudes.

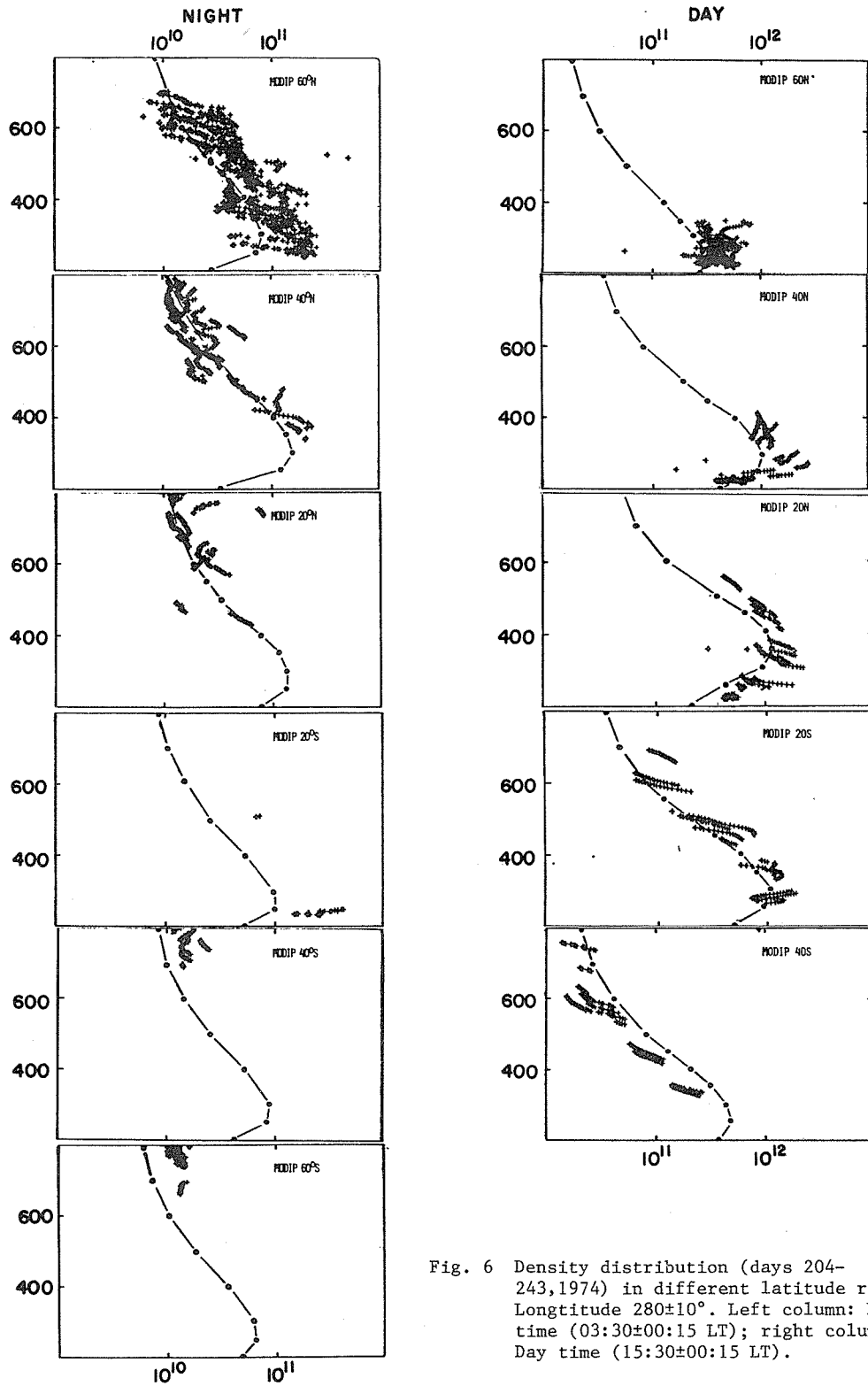
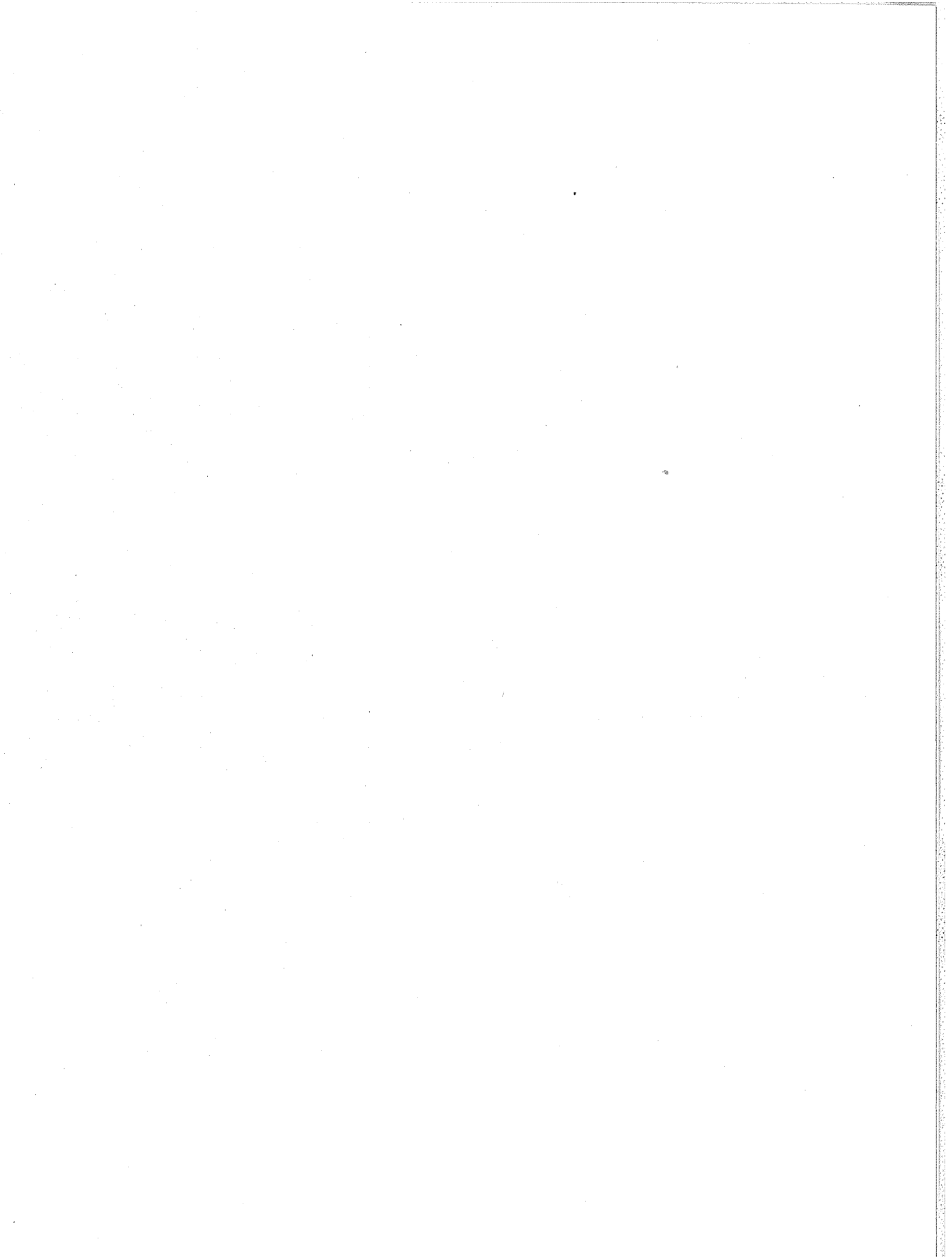


Fig. 6 Density distribution (days 204-243, 1974) in different latitude ranges. Longitude $280 \pm 10^\circ$. Left column: Night time ($03:30 \pm 00:15$ LT); right column: Day time ($15:30 \pm 00:15$ LT).



1.3.2 Comparison between Plasma Densities Measured with the
AEROS-B and S3-1 Satellites and the IRI Model

C.R. Philbrick¹, F. Lämmerzahl², E. Neske, A. Dumbs³

¹Air Force Geophysics Laboratory, Hanscom AFB, Mass., USA

²Max-Planck-Institut für Kernphysik, Heidelberg, FRG

³Fraunhofer-Institut für Physikalische Ferntechnik,
Freiburg, FRG

Abstract: Measurements by a mass spectrometer on satellite S3-1 have been compared with those from an impedance probe and from a retarding potential analyzer on AEROS-B in order to investigate the relationship of the instruments response to ionospheric total and partial densities. Conversion of the mass spectrometer data into absolute ion densities is based on a large number of correlated ionosonde observations of the f_oF_2 critical frequency. Results of the two different probes on AEROS-B were extensively intercompared and the impedance probe is considered to provide very accurate electron density. The perigees of the two satellites were both over the northern polar region in November 1974 and many crossings at the same latitude and longitude occurred. Among these crossings, five cases were located which met restrictive conditions minimizing the effects of spatial and temporal variability. The ratio of the densities measured when the two satellites were closest to these crossing points exhibits a mean of 1.00 with 6% standard deviation, and the relative composition of molecular and atomic ions agrees within about 20%. Density variations found to be correlated with invariant magnetic latitude, rather than to be strongly dependent on altitude, in the F-region. Data are compared with the International Reference Ionosphere model values for density and ion composition in the F-region.

1, Introduction

The basic properties of the ionospheric plasma, such as density, temperature and composition have been investigated by many different probing techniques using ground-based sounding facilities as well as satellite and rocket-borne instrumentation. Various efforts to cross-check such measurements so as to obtain a better estimate of their reliability and accuracy have been reported /Taylor and Wrenn, 1972; Roble et al., 1978/.

In-orbit intercalibration is particularly important to ion mass spectrometers for determining their absolute sensitivity to ambient total ion number densities. A reliable calibration cannot be achieved in a laboratory experiment, owing to the inherent difficulties in simulating the ion flow conditions applicable to an instrument on an orbiting spacecraft. Any effects of discrimination between different masses that the analyzer may produce are evaluated in the laboratory and taken into account in analysis of the data. The factor for converting ion currents into number densities, however, is usually derived from normalizing the summed currents of all ion masses to the total plasma density as obtained from some other experiment. If such an experiment is included on the same satellite or rocket, then in-flight calibration of an ion mass spectrometer is straightforward /Hoffman et al., 1973, 1974/. The variability of the ionosphere, however, makes it difficult to make comparisons between measurements from different satellites, or between a satellite and ground-based ionosonde or incoherent scatter radar observations, which are close enough to be correlated.

An ion mass spectrometer which collected a large number of ion composition measurements in the altitude range between 150 km and 500 km was onboard the S3-1 satellite. Five measurements were located when this satellite passed very near the AEROS-B satellite which, among other experiments, carried an impedance probe and a retarding potential analyzer. At the crossings, both satellites were passing the same latitude and longitude within a few minutes of each other, and at altitude separations small compared to the plasma scale height. Five cases met rather restrictive conditions designed to minimize the effects of spatial and temporal variability, and these allowed a direct intercomparison between the density and ion composition measurements from these satellites. Excellent agreement was found between absolute number densities and percentage composition, which gives additional confidence in the accuracy of both data sets.

The orbital plane of the AEROS-B satellite corresponded to local times near 0400 and 1600, and that of the S3-1 to times near 1100 and 2300. The time difference between the orbit planes means that crossings will only occur at high latitude, and for these cases the crossings are near 79°N. At this high latitude, the ionospheric plasma is often highly irregular, and it has been found that comparisons in terms of invariant latitude appear to be more important than do altitude differences of tens of kilometers in the 250 km to 400 km altitude range.

The importance of reliable plasma measurements for establishing empirical reference models of the ionosphere is obvious. Analysis of data obtained from AEROS has shown that the ionospheric global behaviour as described by the current CCIR program /CCIR, 1974/ needs to be corrected /Noor Sheikh et al., 1978/, in particular, to account for longitudinal effects in the equatorial region that are stronger than predicted /Neske et al., 1980; Lämmerzahl et al., 1979b/. The AEROS data base has also been incorporated in IRI by Rawer et al., /1978a/ and Rawer /1980/. The S3-1 ion data represent a unique set of lower and upper F-region composition measurements, of almost complete global coverage, which are excellently suited for modelling the ionospheric composition pattern. Comparisons with the IRI, both for single observations and on a statistical basis, demonstrate a need for further improvement in ionospheric modelling. A few of these results are presented.

2, The Experiments

This study is based on measurements obtained from a mass spectrometer (ion composition) on the S3-1 satellite, and from an impedance probe (electron density) and a retarding potential analyzer (densities of major ions) on the AEROS-B satellite. The AEROS experiments have been described by Neske and Kist /1974/ and by Spenner and Dumbs /1974/. The mass spectrometer was of similar design to an earlier flown instrument /Philbrick, 1974/. Details on the three experiments and data evaluation procedures are published elsewhere /Philbrick et al., 1980/.

AEROS was a cooperative German-U.S. aeronomy satellite program designed to obtain simultaneous measurements of the most important properties of the neutral gas and the plasma in the upper atmosphere, together with the flux of ionizing solar radiation in the extreme ultraviolet, in order to investigate the coupling between the atmospheric components and its control by solar energy /Lämmerzahl and Bauer, 1974; Lämmerzahl et al., 1979a/. The second of two satellites, AEROS-B, was launched in July 1974 and provided measurements until September 1975 when it reentered the atmosphere.

In-situ electron density on AEROS-B was obtained by a rf impedance probe (IF) designed to measure the modified upper hybrid resonance frequency. This frequency as actually measured is directly related to the electron density of the ambient plasma in a rather large sensitive volume determined by the 180 cm length of the sensor. During each cycle

of six data points at one second intervals, the resonance phase conditions and the dc-bias voltage were altered for diagnosis of the plasma interaction on the probe. The effect of an ion sheath on the measured density was shown to be negligible, and a mean spread in the densities of 4% was observed over a cycle. The high degree of internal consistency gives confidence in the reliability of this technique. The accuracy of the absolute values of the electron density is generally better than 10% and, for the densities considered in this paper which are generally greater than 10^{11}m^{-3} , the accuracy should be near 5%.

The ion mode of the retarding potential analyzer (RPA) on AEROS-B provided the temperature and densities of the major ions every 18 seconds, corresponding to a 140 km spatial resolution. The sensor was of planar geometry and the scan period of 1 s was synchronized with the spin phase to provide measurements at angles within $\pm 30^\circ$ of ram direction. The measured current-voltage curve was analyzed using a fitting procedure in which the free parameters were the assumed four constituent densities ($\text{H}^+ = \text{mass } 1$, $\text{He}^+ = \text{mass } 4$, $\text{O}^+ = \text{mass } 16$, and molecular ions = mean mass 31), the temperature, and the spacecraft potential. When the residuals became too large the results were rejected. The total ion density has been compared with the electron density from the impedance probe on the same satellite. A difference of 20 to 30%, by which the RPA values are systematically lower than those of the IP data, is explained as due to a transmission loss in the RPA grid assembly for ion flow; therefore, the partial densities from the RPA must be corrected by a corresponding common factor, but this correction has not been made in the results presented.

The S3-1 was the first in a series of three satellites designed to provide a scientific study of the properties of the upper atmosphere, and to emphasize investigations of the coupling between the neutral atmosphere and the ionosphere over the altitude range between 150 and 500 km. The near polar orbit was highly eccentric with a perigee near 150 km and initial apogee near 4000 km. During the period from early November 1974 through June 1975, low altitude data were obtained that cover almost all latitudes and four ranges of local time, near 1100, 2200, 0700 and 1700. Among the several experiments carried on the satellite was a mass spectrometer which measured both the neutral atmosphere and ionosphere species densities. The five ion masses that it was tuned to measure were N^+ , O^+ , N_2^+ and O_2^+ .

Calibrations with various gas mixtures showed that the mass discrimination of the quadropole was less than 5% over the mass range. The conversion of the collected ion currents into absolute density was derived from a comparison of flight data and ground-based ionosonde data. Approximately 50 cases were identified where good correlation between ionosonde observations from a worldwide distribution of stations and the satellite measurements should exist. The criteria applied to select these cases was that the satellite should be at the F_2 peak, as determined by the satellite altitude profile of summed ion current, and simultaneously be crossing a latitude and longitude box of $5^\circ \times 5^\circ$ centered about an ionosonde station, and further that the foF2 critical frequency should have been measured within about 5 minutes of the crossing. The comparison between the foF2 determined electron density and the summed ion current yielded the instrument sensitivity to ions. Standard deviation was $\pm 26\%$ and no long-term trend of changing sensitivity was detected. Based on the consideration of the calibrations and the in orbit performance, the ion densities reported should be better than $\pm 15\%$ and the relative composition better than $\pm 10\%$ for densities greater than 10^8m^{-3} .

3. Comparison of Experiments

The ion mass spectrometer (MS) results from the S3-1 satellite have been compared with the impedance probe (IP) and retarding potential analyzer (RPA) results from the AEROS-B satellite /Philbrick et al., 1980/.

The results of that comparison for five nearly coincident sets of measurements showed excellent agreement for both total density and ion composition. In figure 1 the measurements obtained near one of the crossings of the S3-1 and AEROS-B satellites are shown. The molecular ion densities (H_3O^+ , N_2^+ , O_2^+) from the MS have been summed so that they can be compared with the RFA measurements of molecular ions. The O^+ profiles for the RFA and MS instruments and the total ion density (MS) and electron density (IP) are shown for comparison. Arrows indicate the crossing point of the orbits. In Figure 2a and 2b the same orbit intersection is shown, but the results are shown versus invariant latitude and the intersection of the orbits is shown in geodetic and corrected geomagnetic coordinates. The invariant latitude display of the data was found best to depict the correlations between the measurements. At these high latitudes the altitude is less important than invariant latitude in describing the density distribution of the F-region ions.

A study of the five cases of comparable results from the two satellites /Hilbrich et al., 1980/ resulted in a ratio between the AEROS-B and S3-1 total densities of 1.00 ± 0.06 , and agreement between the molecular and atomic ion concentrations within about $\pm 20\%$.

4. Comparison of Measurements to IRI Model

Figure 1 includes the altitude profiles for electron density and molecular ion density from the IRI model corresponding to the conditions for the intersection of the orbits. The general agreement between the IRI and the measurements is reasonably good considering that the ionospheric variability at these high latitudes is large. Other comparisons of the electron (or total ion) density given by the IRI model and MS measurements have been made and generally good agreement has been found near the peak of the F2-region, but some significant differences have been found in the F1-region.

Figures 3 and 4 display a comparison between the ion composition measurements and the IRI composition. The two cases chosen for comparison represent summer daytime and winter nighttime mid-latitude conditions. The latitude, solar zenith angle (λ), and other conditions stated on the figures were chosen to allow the closest comparison between the satellite measurements, the IRI model, and the original rocket data summary of Manilov and Semenov /1978/ on which the IRI composition was based. In the summer daytime case, Figure 3, each of the satellite mean profiles represents between 70 and 110 independent measurements per 10 km altitude interval and, in the case of Figure 4, between 150 and 250 measurements per 10 km interval. The rocket summary, and hence the IRI model, represents the summary of a total of 43 profiles which had to be distributed by season, solar zenith angle and other parameters. The rocket derived composition summary thus cannot be expected to have the statistical significance that we can now obtain from the satellite data. Unfortunately, the differences are surprisingly large. This may be due to the fact that the rocket observations were obtained at a few places and hours but satellite data from a large manifold. We conclude that for constructing improved models of ionospheric composition it is essential to include data from satellites as have now become available. The consistency of the data sets from the satellites S3-1 and AEROS-B is an encouraging result in view of an improved model.

Acknowledgements

We wish to thank N.E. Gardner, B. Delorey, L.J. Ziemba and H. Wolf for their efforts in the data computations. The helpful discussion and comments by F. Kawer and F.S.W. Champion are appreciated. Data used in connection with this article were obtained from WDC-A for Solar-Terrestrial Physics (Ionosphere). This work was completed while one of us (C.R.F.) was staying at the Max-Planck-Institut für Kernphysik as a visiting scientist. This work has been sponsored in part by the Bundesminister für Forschung und Technologie through DFVLR.

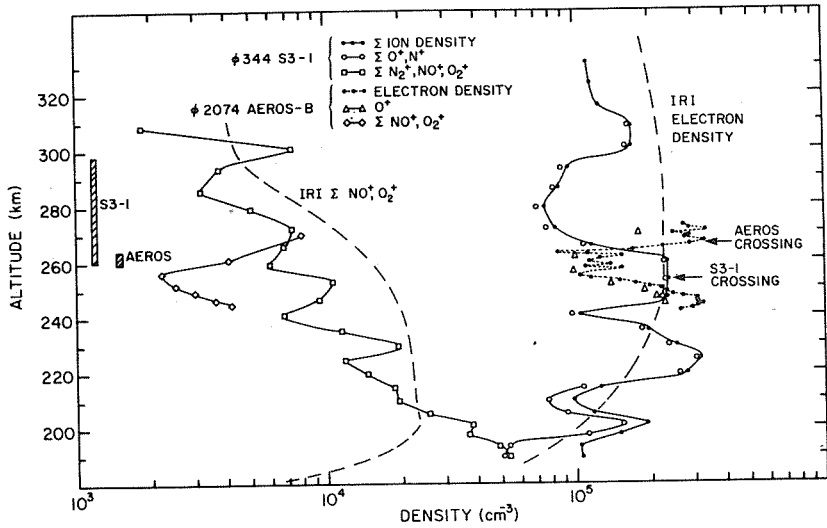


Fig. 1

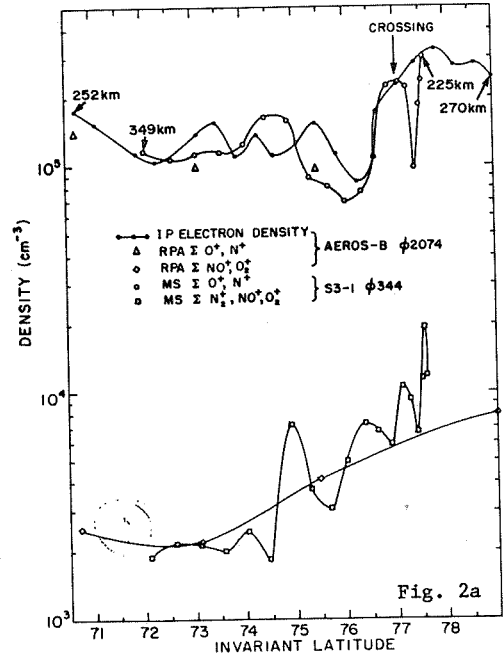


Fig. 2a

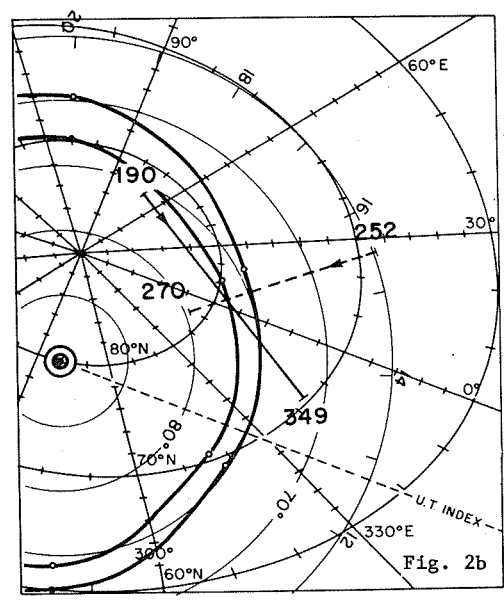


Fig. 2b

Fig. 1 Plasma density and partial ion density height profiles from AEROS-B and S3-1 experiments near a crossing point of the two satellites, within 7 min from each other, on 29 Nov 1974. IRI model densities (option Chiu) are shown for comparison. Regions where the satellites passed through the auroral oval are marked by bars. $K_p = 1+$.

Fig. 2a Comparison of densities from AEROS-B and S-31, at the same crossing point as in Fig. 1, plotted versus invariant magnetic latitude.

Fig. 2b Satellite trajectories near the crossing point projected in both geodetic and corrected geomagnetic coordinates. The two lines represent the limits of the auroral oval for low geomagnetic activity [Whalen, 1970].

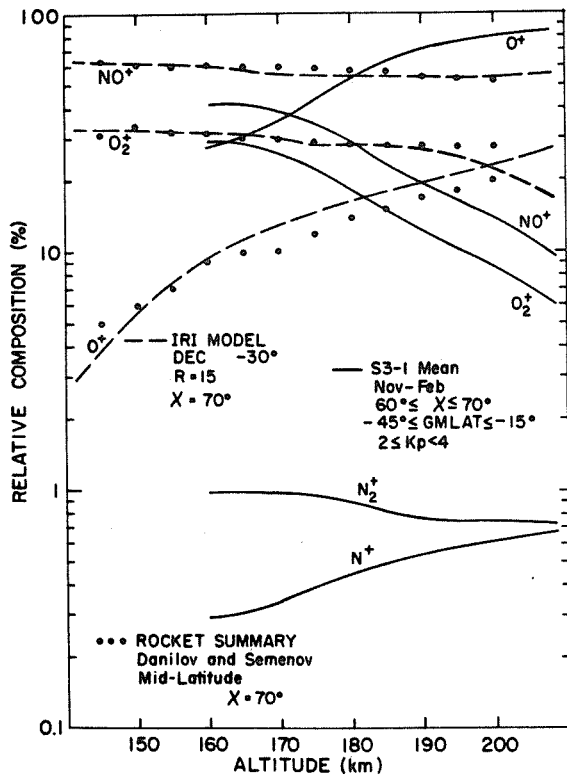


Fig. 3

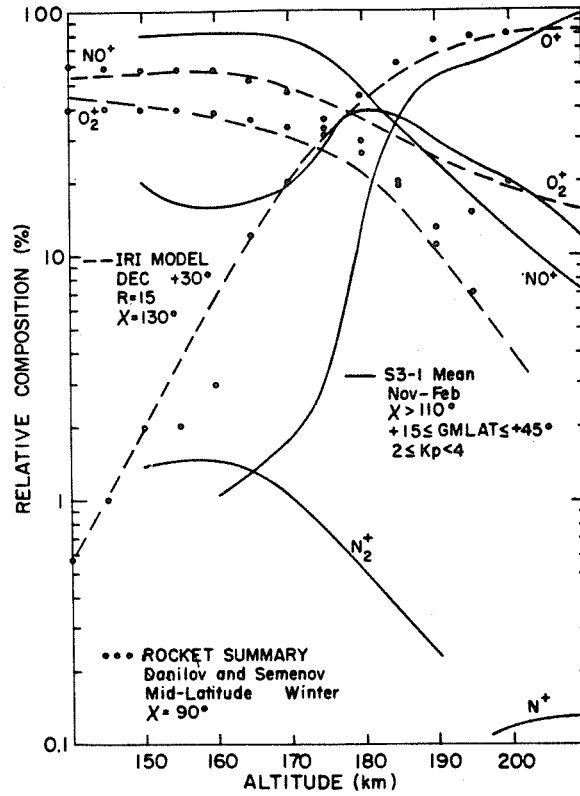


Fig. 4

Fig. 3 Summer mid-latitude daylight composition of the lower F-region ionosphere. Mean densities from S3-1 measurements are compared with the IRI model [Rawer, 1980] and the original rocket summary [Danilov and Semenov, 1978].

Fig. 4 Winter mid-latitude nighttime composition of the lower F-region ionosphere.

1.3.3 Comparison of Theoretical Electron Density Profiles at the Magnetic Equator with IRI Model and Incoherent Scatter Data

T.Yu. Leshchinskaya¹, A.V. Mikhailov²

¹Academy of Sciences, IZMIRAN, 142092, Moscow, USSR

²Inst. of Applied Geophysics, Hydrometeorological Service, 107258, Moscow, USSR

Abstract: For some quiet days, four seasons and different levels of solar activity, comparisons have been made between noon equatorial IRI profiles, Jicamarca incoherent scatter data, and a theoretical distribution of electron concentration. It is shown that in the equatorial F2 region the IRI model describes the shape of electron density profiles with insufficient accuracy. On the other hand, given the present-day knowledge of the main aeronomic parameters, it is possible to describe satisfactorily the electron density distribution in the F2 region at the magnetic equator.

1, Introduction

In accordance with the suggestion of Rawer et al., /1978/ concerning the verification of the IRI model, comparisons have been made for noon equatorial profiles with Jicamarca incoherent scatter data for rather quiet conditions, different seasons and two levels of solar activity: minimum 1964 to 1966 /McClure et al., 1970/, and maximum 1967 to 1969 /Clark et al., 1976/. The IRI profiles were adjusted to the experimental values of NmF2 and hmF2.

2, Comparison of the IRI with observations

It can be seen from Figure 1 that, as a rule, the observed F2 layer is thicker below hmF2, between 200 and 250 km, therefore the observed density values are sometimes 2 or 3 times greater than those given by IRI. Also the model and observed scale heights above hmF2 differ by a factor of 2..4. At low solar activity, this factor is less than at higher level. It should be mentioned also that IRI admits no dependence on solar activity of the scale height above hmF2, although the experimental scale heights are found to vary with changes in the upper atmosphere temperature.

Thus, when comparing with adjusted IRI profiles, it is found that IRI describes the profile shape, and its variations with solar activity in the equatorial F2 region, with insufficient accuracy. If IRI were computed with unadjusted peak values then absolute differences in density could exceed those given in Figure 1.

3, Theory

On the other hand calculations based on the physical processes that are responsible for ionosphere formation are being developed. Near noon the following basic processes play a role in the formation of the equatorial F2-region: photoionization (mainly of atomic oxygen), charge transfer from O⁺ to molecular ions, and electrodynamic drift of plasma. Plasma lifted upwards by the $E \times B$ force up to the F2-maximum diffuses downward along magnetic field lines.

An approach similar to that of Hanson and Moffett /1966/ for stationary conditions at noon is applied. Account is taken of photoionization of O, O₂ and N₂, charge transfer from O⁺ to O₂⁺ and NO⁺ with temperature dependent rate constants /Ferguson, 1969; McFarland et al., 1973/.

Photo-chemical equilibrium and the thermospheric model MSIS /Hedin et al., 1977/ are assumed in the calculations. The EUV spectrum and its variation with solar activity as given by Ivanov-Kholodny and Firsov /1974/, is accepted but the integral flux is approximately doubled /Schmidtke et al., 1977/. The difference between geomagnetic and geographic coordinate systems is taken into account.

Calculated values of hmF2 are found 20 to 30 km higher than those observed. To obtain agreement between model and experimental values, for higher solar activity the exospheric temperature in the MSIS model must be lowered by 100 K. This conclusion is confirmed by direct measurements of the ion temperature T_i /Clark et al., 1976/; at the heights considered T_i does not differ appreciable from T_n . In our calculations we admit MSIS values for lower solar activity, but for $F(10.7) = 100$ we deduce 100 K from the MSIS value; T_e is put equal $T_i = T_n$. It is well known that electrodynamic drift effects influences the electron density profile at the geomagnetic equator /Hanson and Koffett, 1966/. In order to determine the vertical drift velocity v_z use is made of semi-empirical relations first deduced by Ivanov-Kholodny and Mikhailov /1976/. These connect the F2-peak data with aeronomic parameters:

$$\begin{aligned} \log NmF2 &= A_1 \log n(O) + E_1 \log \beta + C_1 \sqrt{v_z} + D_1 \\ hmF2 &= A_2 \log n(O) + E_2 \log \beta + C_2 \sqrt{v_z} + D_2 \end{aligned} \quad (1)$$

where $n(O)$ is the number density of atomic oxygen and β the loss coefficient.

The coefficients depend on solar activity $F(10.7)$ by a quadratic relation $a \cdot F^2 + b \cdot F + d$ (coefficients in Table 1).

Table 1

Determination of the Coefficients A, E, C and D in Eq.(1)

	a	b	d		a	b	d
A_1	0.0	0.0	1.0	A_2	6.94-4	1.26-2	40.38
E_1	-4.52-6	4.83-4	-0.45	E_2	-7.30-4	3.46-1	14.46
C_1	7.76-7	-1.16-4	-0.09	C_2	1.86-3	-5.77-1	71.77
D_1	-6.12-5	1.72-2	-5.30	D_2	-1.03-2	1.93	104.06

(For 400 km. Units: cm^{-3} for densities, m/s for velocity, km for height).

Comparison of the computed and observed drift velocities at Jicamarca /Woodman, 1970/ shows that the mean error in v_z is 2.4 m/s, which is roughly equal to the experimental inaccuracy /Fejér, 1979/. It should be noted that a time lag of 1.5 h is admitted between the response in F2 to a change in v_z . The results of our calculations are shown as broken lines in Figure 1. They represent the observed profiles rather well and reflect the change in profile shape with variations of solar activity.

4. Conclusion

The IRI model does not provide a satisfactory representation of electron density profiles at the magnetic equator. Probably this is due to the limitations of experimental data available for the equatorial iono-

sphere and its great variability. On the other hand our semi-empirical aeronomic theory makes it possible to describe satisfactorily the electron density distribution in the F2-region at the geomagnetic equator.

Discussion remark:

The author pointed out that neutral wind induced changes were not included in the present model, only the vertical component of electrodynamic plasma drift. K. Rawer stated that the Bent-results used for establishing the IRI topside model contain a dependence on solar activity via the value of $R_m F_2$ which appears in the equations.

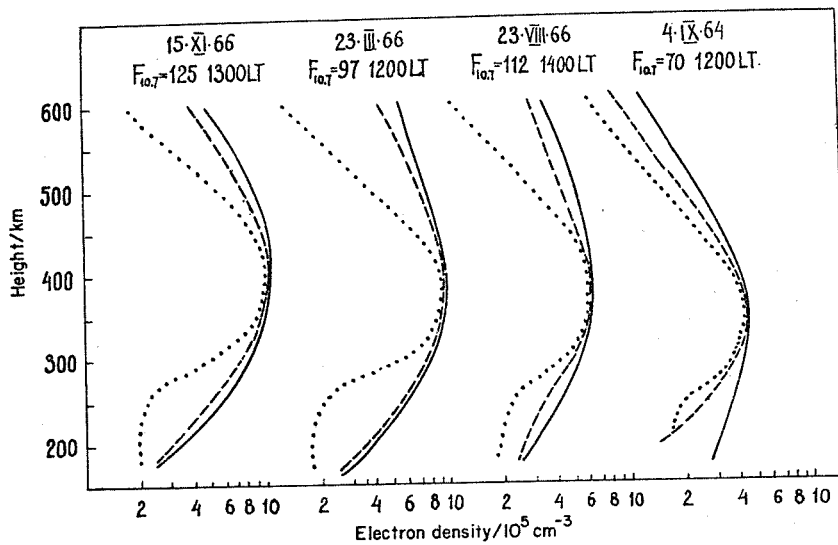


Fig. 1a

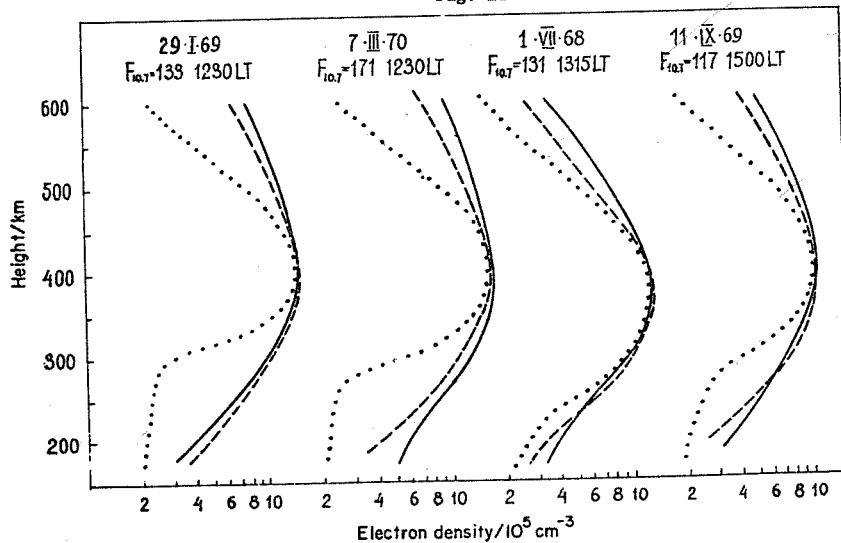


Fig. 1b

Fig. 1a, b Equatorial noon profiles obtained by incoherent scatter (full), by aeronomic computations (broken) and with IRI (dotted).

1.3.4 Intercomparison of Various Measurements of Thermal Plasma
Densities at and near the Plasmapause

D.V. Williams¹, M.J. Rycroft, A.J. Smith², V.V. Bezrukikh,
K.I. Gringauz³, N.C. Maynard⁴, M.J. Morgan, T.W. Thomas⁵

¹Board of Studies of Geophysical Sciences, The University,
Southampton, SO9 5NH, England

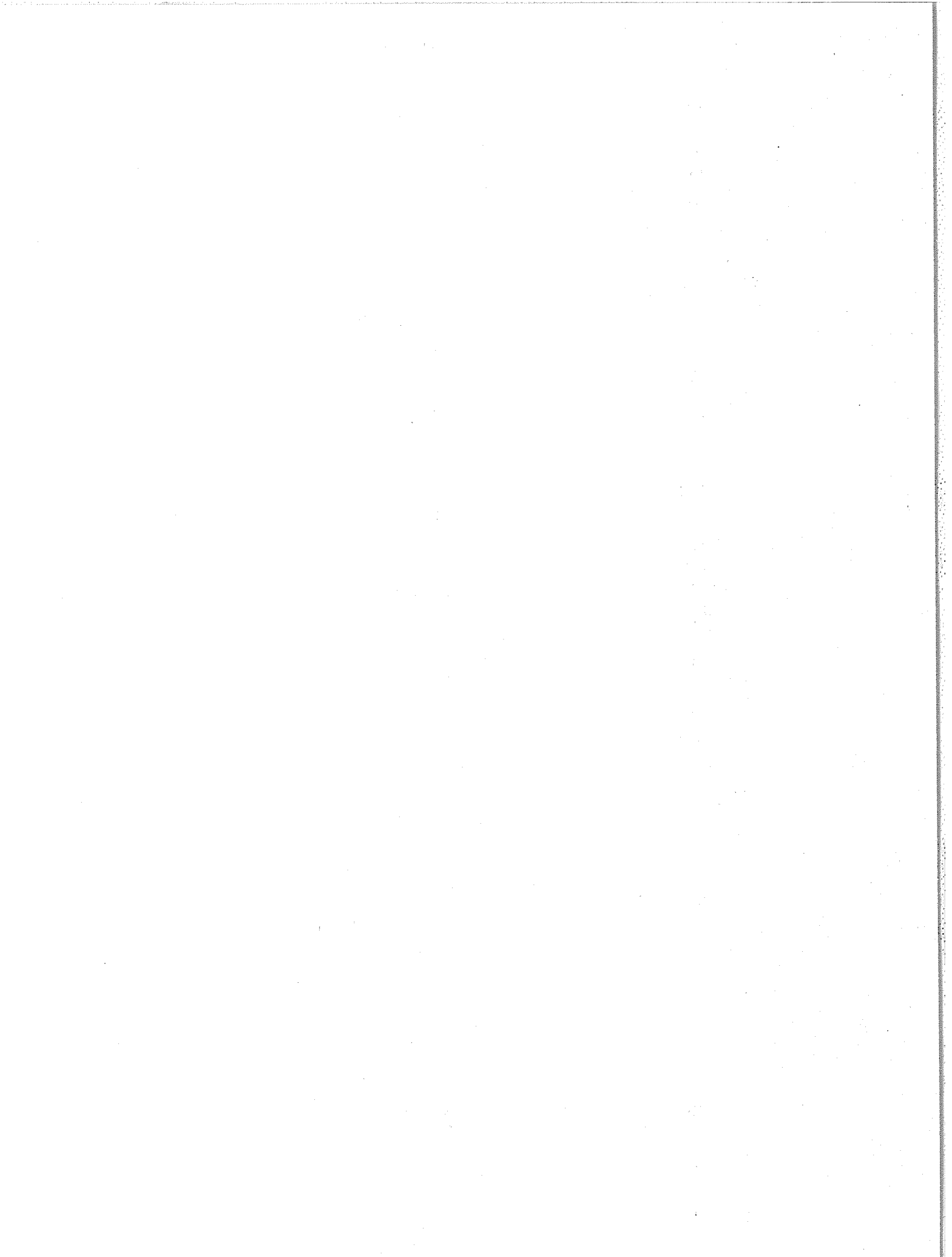
²NERC British Antarctic Survey, Cambridge CB3 0ET, England

³Space Research Institute of the USSR Academy of Sciences
(IKI), Moscow, USSR

⁴NASA Goddard Space Flight Center, Greenbelt, Maryland 20771,
USA

⁵Dartmouth College, Hanover, New Hampshire 03755, USA

This paper was withdrawn by the authors after pagination; thus the next paper
begins on page 75. Ed.



1.3.5 Comparison with IRI of Electron Density and Temperature at the Magnetic Equator

G.F. Deminova, L.A. Yudovich

IZMIRAN, 142092, Troitsk, Moscow region, USSR

Abstract: The height distributions of the electron and ion densities N_e and N_i and of the electron temperature T_e at the geomagnetic equator are calculated for quiet geomagnetic conditions, near noon in the height interval 100 to 2000 km, and for three levels of the solar flux index $F(10.7)$. The results of the calculations are compared with the observed data obtained at the Jicamarca incoherent scatter station, and with N_e profiles given by the IRI model. It is found that the IRI model, when applied to noon conditions at the geomagnetic equator, underestimates the peak height $hmF2$ and gives a half-thickness of the F-layer that is less than observed. The results of our calculations are in better agreement with the observed data.

For quiet geomagnetic conditions near noon at the geomagnetic equator and for three levels of the solar flux index $F(10.7) = 100, 150$ and 200 we computed the ionospheric parameters by analytical solution of the set of plasma equations in the steady-state approximation. Five ion species O^+ , H^+ , O_2^+ , NO^+ and N_2^+ were taken into consideration.

The Jacchia /1977/ model of the neutral atmosphere is used. The rates of chemical reactions and of cooling were taken from Torr and Torr /1979/ and Schunk and Nagy /1978/. The heating was calculated according to Swarts and Nisbet /1972/, but their expression for the heat production was increased by a factor of 2.

For the calculation of T_e above 400 km, one must assume a value of T_e at some fixed height as a boundary condition. We assumed at $h = 1000$ km $T_e = 2500^\circ, 3000^\circ$ and 3500° for $F(10.7) = 100, 150$ and 200 respectively. We based these rough assumptions on data given by Mahajan and Pandey /1979/.

The calculated height profiles of N_e and T_e were compared with those obtained by incoherent scatter at Jicamarca near the geomagnetic equator. They are shown in Figure 1. On the left, the electron and ion concentrations obtained from a self-consistent solution of the system of the equations for charged particles are shown by solid lines. (Here $N(XY^+) = N(O_2^+) + N(NO^+) + N(N_2^+)$). The dots, circles and crosses denote observed data obtained during geomagnetically quiet periods, and on days when $F(10.7)$ was close to 100, 150 and 200.

The N_e profiles given by IRI-78 with the observed values of $NmF2$ and $hmF2$ are shown as dashed lines. The half-thickness of the IRI profiles is - almost a factor of 2 - smaller than the observed one, as well as the results of our calculations. If, on the other hand, we use Chiu's /1975/ formulas we get values of $hmF2$ substantially lower than those observed. For $F(10.7) = 100, 150$ and 200 respectively, the observed values of $hmF2$ are approximately 400 km, 450 km and 490 km while Chiu's model gives 280 km, 320 km and 360 km. The discrepancy in peak density is somewhat less. Note the good agreement between calculated and observed values of $hmF2$. The calculated values of $NmF2$ lie within the spread of the individual measured values. Both parameters do not depend markedly on T_e . This is accounted for by the dominating role of electro-dynamical drift in the equatorial F-region. Calculation lead to the following asymptotic expressions for $hmF2$ and $NmF2$ /Deminov et al., 1977a, b; Deminova et al., 1979/:

$$hmF2 = h_0 + \frac{1}{2} H \cdot \ln \left[\frac{R_E}{D_0 \sqrt{\pi}} (2WL_0H)^{1/2} \right] \quad (1)$$

$$NmF2 \approx Q_m \left(\frac{\pi H}{2 W L_m} \right)^{1/2} \quad (2)$$

where D_0 and L_0 are the diffusion and recombination coefficients at a fixed height h_0 , H is the scale height of the neutral atmosphere, R_E is the Earth's radius, W is the vertical plasma drift velocity, Q_m and L_m are respectively the rate of ion production and the recombination coefficient at the height $hmF2$.

The results of the calculations and of their comparison with the observed data clearly show the dependence of plasma density profiles upon solar activity. For example, for $F(10.7) = 100$ we find $hmF2 = 400$ km and $NmF2 = 9.5 \cdot 10^{11} m^{-3}$ while for $F(10.7) = 200$ we get 490 km and $1.7 \cdot 10^{12} m^{-3}$.

On the right of Figure 1 the temperatures T_e are plotted. The solid lines are the calculated profiles of T_e , and the data observed at Jicamarca are shown as dots, circles and crosses for the dates identified in the caption. The neutral temperature is taken from Jacchia /1977/, T_e and T_n are approximately equal near the F2-peak. At heights from 150 to 350 km, T_e decreases with height and exceeds T_n by up to 1200K. The results of the calculations are in good agreement with the observations. The upper level where T_e begins again to differ from T_n depends on the level of solar activity. At $F(10.7) = 100$, T_e begins to increase above 500 km, and at $F(10.7) = 200$ above 650 km. Though, as mentioned above, the upper boundary condition is rather uncertain, by computation with different assumptions for the topside temperature we found only a small effect of these assumptions on the upper height where T_e began to increase.

Thus, different from our computations, the IRI model, for noon conditions at the geomagnetic equator, underestimated the peak height $hmF2$ and gives smaller thickness of the F-layer than observed. The equatorial maximum of T_e near 300 km is also appearing in IRI.

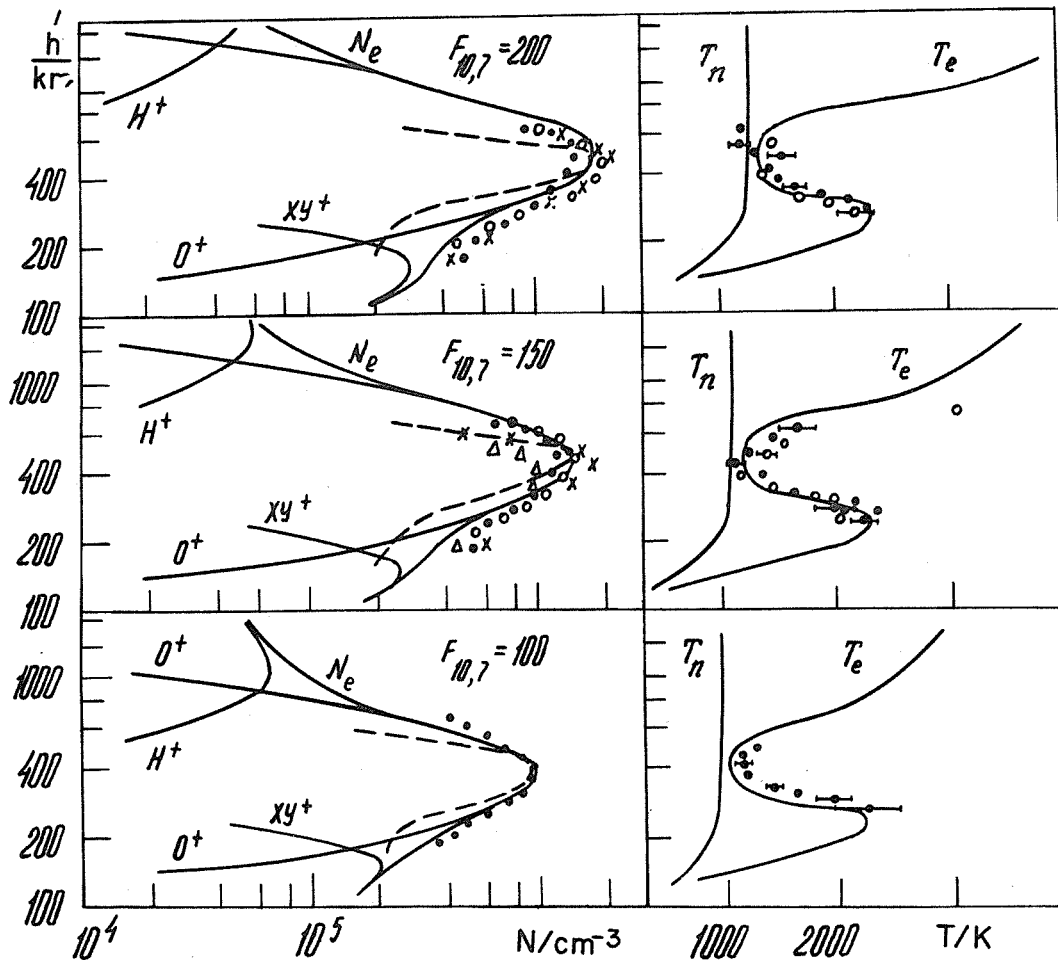


Fig. 1 Left: Observed (Jicamarca, individual symbols) and computed (full lines) electron and ion density profiles and, for comparison, IRI (broken lines). Right: Observed (individual symbols) and computed electron temperature T_e . Neutral temperature T_n after Jacchia [1977]. On top (high solar activity): dots 31 Mar. 1967, circles 29 Dec. 1967, crosses 7 Mar. 1967. Middle panel (medium activity): dots 24 Jan. 1967, crosses 21 Oct. 1968, crosses 4 Jan. 1967, triangles 21 June 1968. Bottom panel (low activity): dots 28 Aug. 1968.

Section 1.4 Variability

1.4.1 Variability of the Equatorial F-Region

K. Bibl

University of Lowell, Center for Atmospheric Research,
Lowell, MA 01854, USA

Abstract: Although the study of the equatorial F-region dynamics has become important because of the need to understand the Spread-F phenomenon, systematic investigations of the variations in the equatorial F-region parameters are scarce. Comparison of older statistical data from three equatorial stations in Africa with data from a new Digisonde, operating for more than one year on a West-Pacific island, shows striking similarities in the seasonal behavior of the variation of ionospheric parameters even though the new station was almost antipodal to the African stations.

It is necessary to separate the solar and lunar tidal effects from the travelling or standing waves induced by solar particle dumping in both auroral zones. Solitons, non-linear waves with propagation speeds dependent on their amplitude, may be created by the clash of two acoustic gravity waves traveling in opposite directions towards the equator. They might be responsible for the extreme changes in the shape of the diurnal curve of the critical frequency, in the height of the F-layer maximum and in the minimum height during the night hours. Their variance is of the order of the average values.

For Kwajalein, I.I., the seasonal dependence of the variance in $h_p F$, the height of the electron density maximum, is presented in a provisional analysis of the amplitudes for different wave periods. For the sensitive hour, 2000 Local Mean Time, the virtual profile of the F-region ionization is given and compared with the Spread-F occurrence.

1, Introduction

As background measurements for a planned combination of rocket and monostatic and bistatic experiments designed to study the equatorial Spread-F phenomenon, routine ionospheric sounding has been carried out from August 1977 to August 1978 at the island Roi-Namur near Kwajalein in the Marshall Islands at 9°N, 167°E, only 2° North of the geomagnetic equator. Although the main purpose of the operation of the new Digisonde 128 Es, described by Bibl and Reinisch /1978/, was to monitor the occurrence of Spread-F conditions, and to measure the spectral properties and the location of the coherently reflected Spread-F echoes, sufficient data were collected and scaled to permit an analysis of the predominant periods in the motion of the F-region heights.

2, Large Scale variations in the Ionospheric F-Region

Although non-negligible variations of the ionospheric parameters occur anywhere, the variability itself is a function of locality /Bibl, 1964a/ and is particularly large at the magnetic equator. Figure 1 shows F-region virtual profiles for Kwajalein, I.I. at 20 h LMT, represented by the virtual height at sounding frequencies 2.0, 3.0, 4.0, 5.0 and 6.0 MHz. While the true minimum heights are pretty well approached by the virtual minimum height at night, the thickness given by corresponding electron densities might be too large by a factor of 2. However, in virtual heights the daytime and seasonal changes can be more easily detected. While in earlier investigations we preferred the parameter $h'F_{3000}F_2$ for detecting variations, in the present study we chose instead the "parabolic height" $h_p F_2$.

But both parameters allow a good estimate of the nighttime F-layer shape and height range if the minimum height h_m in F is also known. While thickness and h_pF2 are positively correlated, the critical frequency f_oF2 and h_pF2 very often show a negative correlation. There are exceptions, very often induced by the so-called G- or lunar-layer or F3-stratification after Bibl /1958/ of which Figure 2 shows a nighttime example.

We have found positive correlations for Spread-F occurrence with high minimum heights, but more with rapid increases occurring slightly before 20hLMT. As Figure 1 shows, the changes in height from day to day usually follow a continuous trend for several days, but sometimes there are enormous changes between consecutive days.

2,1 First Order Difference

In the following we consider hourly changes of ionospheric parameters with emphasis on rather short term, non-regular, e.g. wave-like phenomena. In order to avoid regular, long periodical influences (diurnal and tidal ones) we have subtracted from all hourly differences in h_pF the median difference for the month. I.e. we replace the actual hourly change:

$$1 \Delta 1 h_pF(t) = h_pF(t) - h_pF(t-1) \quad \text{by the reduced hourly change:}$$

$$1 \bar{\Delta} 1 h_pF(t) = 1 \Delta 1 h_pF(t) - \overline{1 \Delta 1 h_pF(t)}. \quad (1)$$

As examples, the hourly distributions of $1 \bar{\Delta} 1 h_pF2$, together with the hourly medians for August/September 1977 and August 1978, are represented in Figures 3 and 4. We feel that the increase of variation from 1977 to 1978, specifically at the evening rise and collapse before and after 20 h LMT, is connected with the increase in solar activity. The corresponding distribution functions of f_oF2 and $h_{min}F$ are shown in Figures 5 and 6.

2,2 Longer period and higher order differences

In the following we shall consider h_pF2 in more detail building up higher order differences. Since day and night conditions are very different we have split the normalized differences into two components identified as day (D: 06 to 19 h LMT) and night (N: 20 to 05 h LMT). (In the following Figures open boxes mean $\bar{m}D$ and filled boxes mean $\bar{m}N$). The detrended differences $1 \bar{\Delta} 1 h_pF(D)$ and $1 \bar{\Delta} 1 h_pF(N)$ have been integrated in the following way:

$$2 \bar{\Delta} 1 h_pF(t) = 1 \bar{\Delta} 1 h_pF(t) + 1 \bar{\Delta} 1 h_pF(t-1); \quad 3 \bar{\Delta} 1 h_pF(t) = 2 \bar{\Delta} 1 h_pF(t) + 1 \bar{\Delta} 1 h_pF(t-2);$$

$$4 \bar{\Delta} 1 h_pF(t) = 2 \bar{\Delta} 1 h_pF(t) + 2 \bar{\Delta} 1 h_pF(t-2); \quad 1 \bar{\Delta} 2 h_pF(t) = 1 \bar{\Delta} 1 h_pF(t) - 1 \bar{\Delta} 1 h_pF(t-1);$$

$$2 \bar{\Delta} 2 h_pF(t) = 2 \bar{\Delta} 1 h_pF(t) - 2 \bar{\Delta} 1 h_pF(t-2) \quad (2)$$

Our algorithms act as frequency filters: With $1 \bar{\Delta} 2$ one prefers periods of 1.6 to 3.2 h (with an arc sin distribution in case of constant amplitude); with $2 \bar{\Delta} 2$ periods of 3.2 to 6.4 h. Longer periods can only be estimated from $3 \bar{\Delta} 1 h_pF(t)$ and $4 \bar{\Delta} 1$ which will be large for periods greater than six and greater than eight hours. This method /Bibl, 1958/ quickly gives an easy survey of the dynamical properties in a set of data. For all five quantities defined in Equation (2) distribution functions deduced from h_pF2 measurements at Kwajalein, are presented in Figures 7a...h. These statistical distributions clearly show a seasonal variation on which is superposed an increase in variance with the increasing solar activity.

3, Results

A tabular summary of the distribution functions presented in Figures 7a...h is shown as a table in Figure 8. In a given line the variance is measured as the difference of the quartiles for day (D25) or night (N25),

of the deciles for day (D10) and night (N10). The last column gives the expected deviation, namely $2/3$ of the vectorial sum of the three main components $2\Delta 1$, $2\Delta 2$ and $4\Delta 1$.

In all months we see the prominence of the four six hour periods, $2\Delta 2$ hpF. Because of the different expectance values, dependent on the phase of the wave relative to the sample times, about $2/3$ of the measured difference in the quartile values can be taken as the median amplitude. This gives about 50 km expected amplitude for the average 4 to 6 h periods. In July this value is exceeded during both day and nighttime hours, while in January the nighttime hours show a clear minimum. For the daytime, there seem to be two minima, one in August/September and one in February/March. At night the 2 to 3 h periods are maximum in May and show minima in January and April, while the amplitudes for the day hours are rather constant over the year. Longer periods (7 to 8 h) show a broad maximum during April to July and a minimum from August to January, although the lack of data during October and November limits our knowledge of the behavior during these months. The fact that the amplitudes do not grow substantially in the transition from a three hour sampling difference $3\Delta 1$ hpF, to a four hour span, $4\Delta 1$ hpF2, indicates that periods of over eight hours are eliminated as intended.

These results compare very well with an analysis of data from three equatorial stations in Africa generated two sunspot cycles earlier /Bibl, 1967/. Figure 9 shows, for the African station Iwiro, similar distribution functions of detrended MUF3000F2 differences for the month of August (comparable to Figures 7 and 14 for Δ hpF2). The same 4 to 6 h periods are obviously strong.

Even the seasonal behavior of the detrended foF2 before and after the average maximum events, synchronized using the superposed epoch method, is quite similar to the new findings. Figure 10 shows the average difference of the foF2 up to nine hours before and after a maximum (25 values). Maximum amplitudes of the longer periods occur in July, while the shorter periods show a secondary maximum in May.

We believe that the values given in Figure 15 are representative of the variability of the F-region peak for periods during the rising sunspot cycle at the equator. A correction factor of $2/3$ should be applied for all D25 and N25 values to obtain the average variability for the three period groups.

4, Conclusions

Our results may be used for predicting probable deviations from average behavior:

(i) The expected actual F2-layer peak value /Paul, 1980/ may deviate from the predicted value by the 'total D25 or N25 number' listed in the last column of Table I (for hpF2).

(ii) If, at a certain time, season and location, a measurement has been taken and if the trend has been established by prior measurements or by using the IRI prediction of the diurnal behavior, then the expected change within one, two, or three hours can be estimated by $1\Delta 2$, $2\Delta 1$ and $3\Delta 1$.

For temperate latitudes the predominant changes have shorter quasi-periods so that an analysis of $1/4$ hour data is required /Bibl, 1964b/.

Acknowledgement: The equipment used to collect these data has been developed for U.S. Defense Nuclear Agency (DNA) under Contract DNA001-76-C-0268 and been operated under Contract DNA001-77-C-0187. The same contract also supported the scaling of the data by Mrs. Claire LeClair. Programming and analysis of the presented data was carried out by Mr. William Kersey, and drafting by Mr. Alfred Cognac with research funds of the University of Lowell Center for Atmospheric Research.

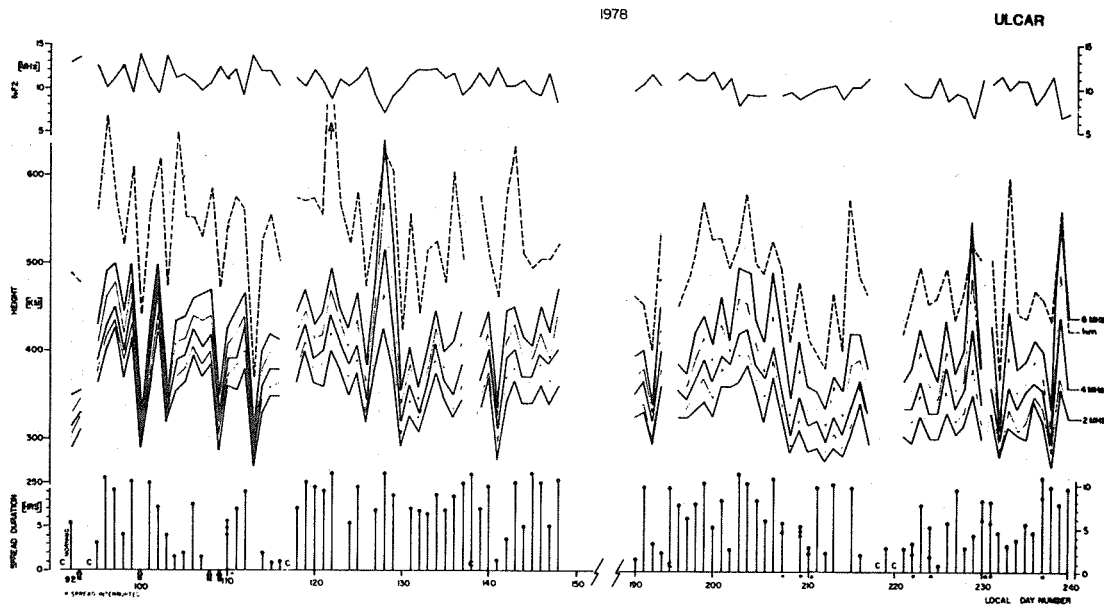


Fig. 1 Virtual F-region profiles at Kwajalein, M.I. (Apr. ... Aug. 1978).

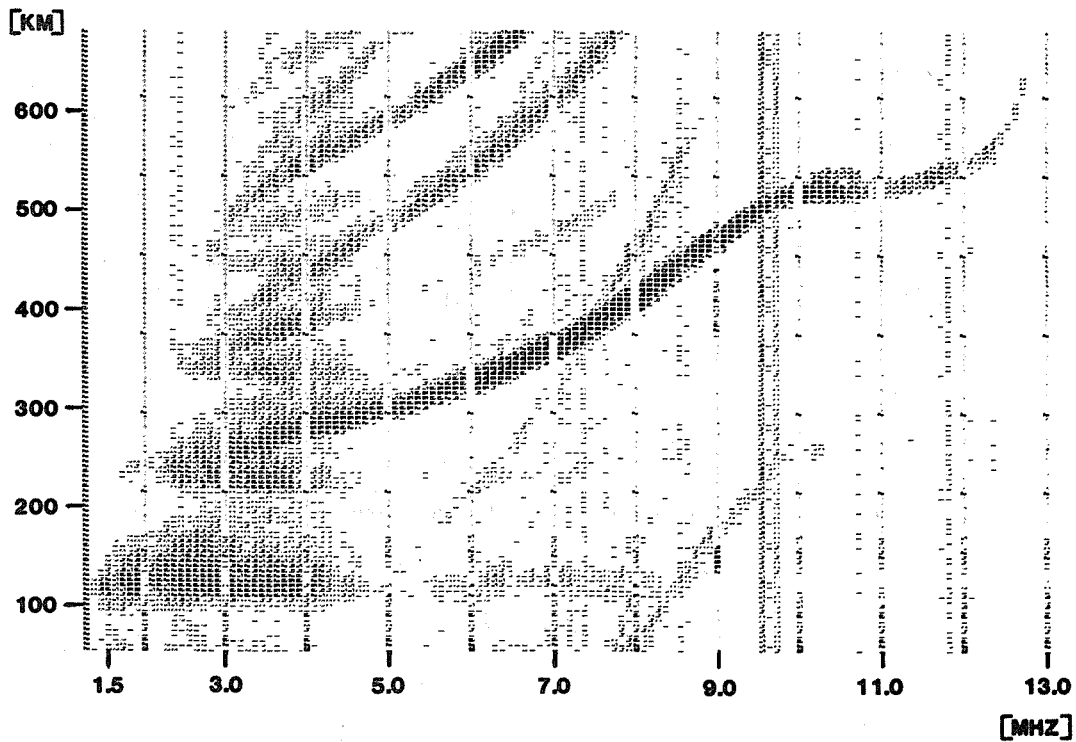


Fig. 2 Night ionogram with distinct G-layer (Kwajalein 23 May 1978, 1830 LMT).

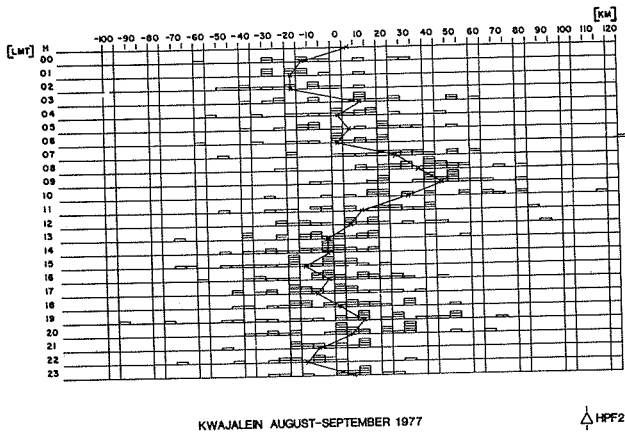


Fig. 3

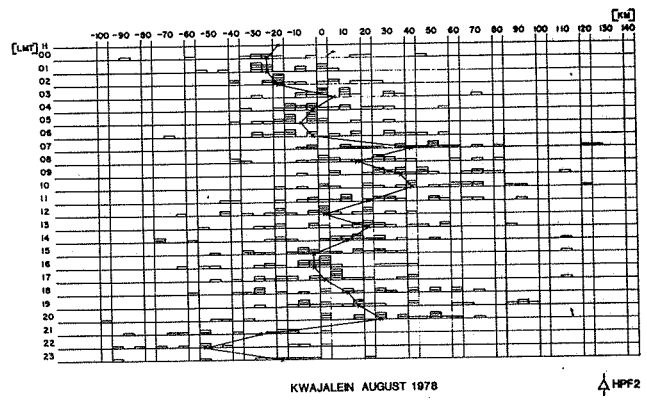


Fig. 4

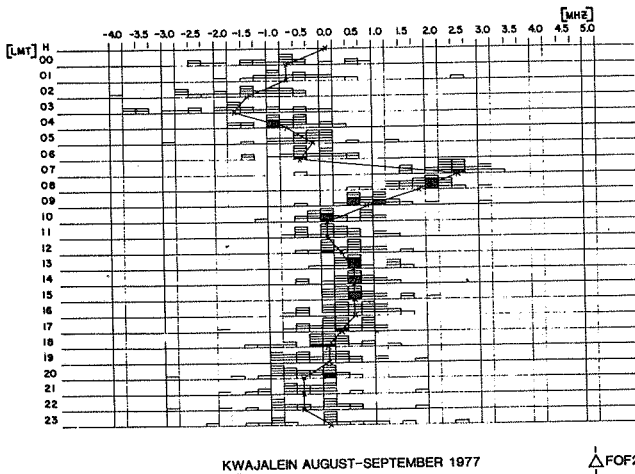


Fig. 5

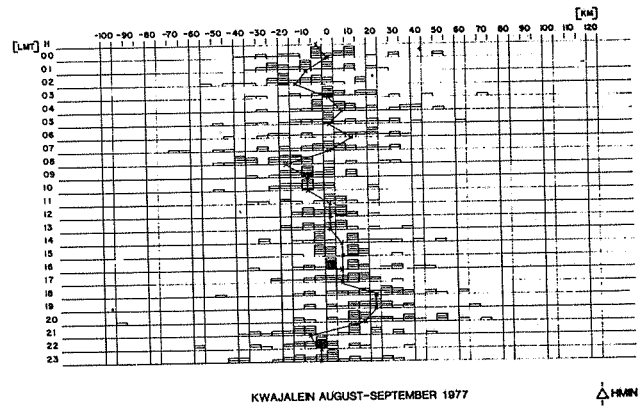


Fig. 6

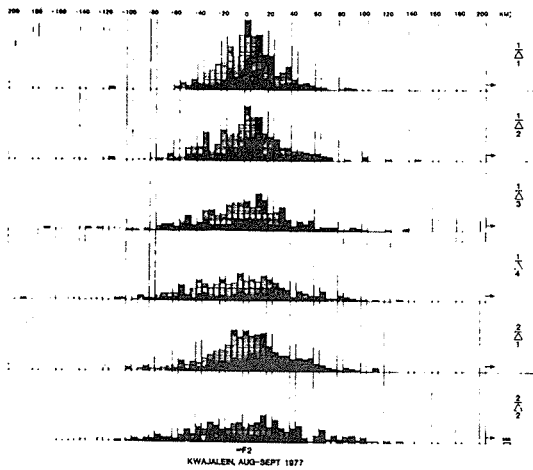
Figs. 3 - 6 Reduced hourly change Δ of f_{oF2} , monthly.

Fig. 3 ... for hpF2, Aug./Sept. 1977

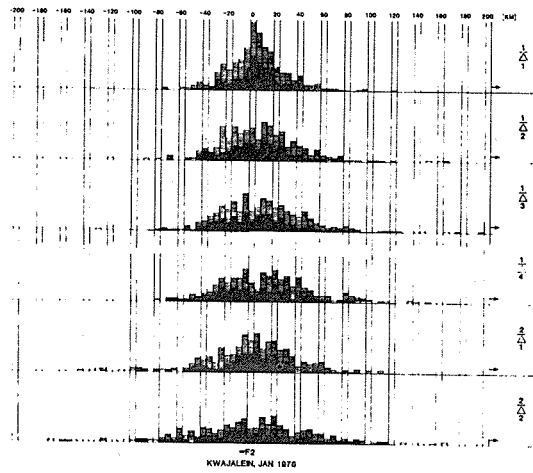
Fig. 4 ... for hpF2, Aug. 1978

Fig. 5 ... for foF2, Aug./Sept. 1977

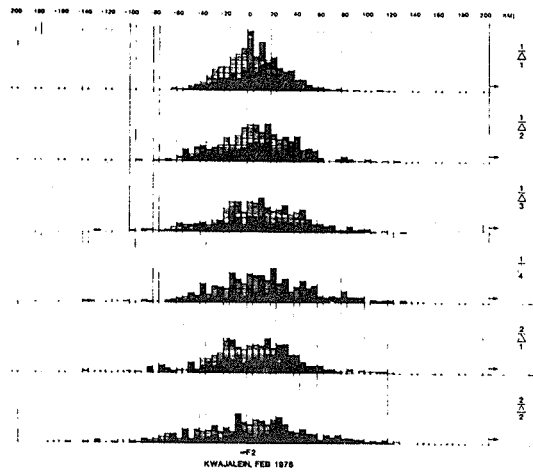
Fig. 6 ... for h'minF2, Aug./Sept. 1977



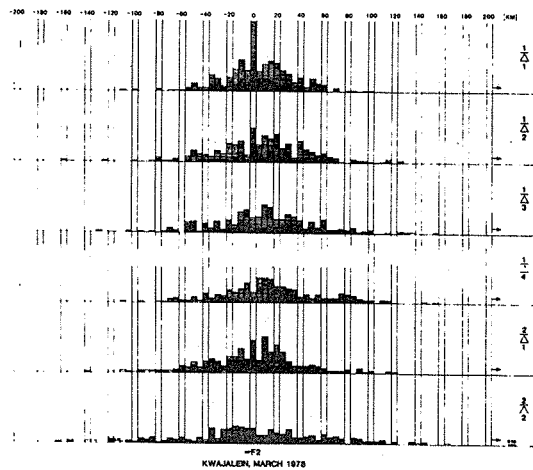
a) Aug./Sept. 1977



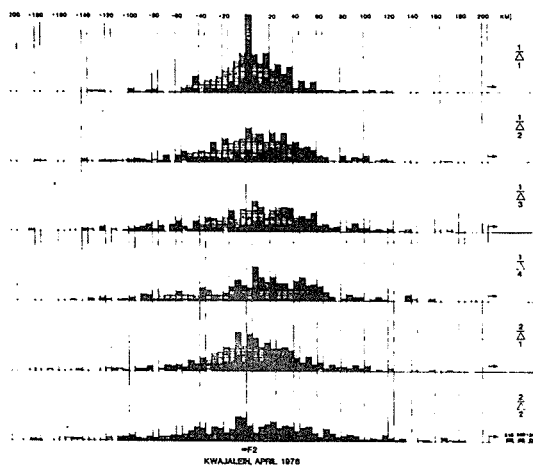
b) Jan. 1978



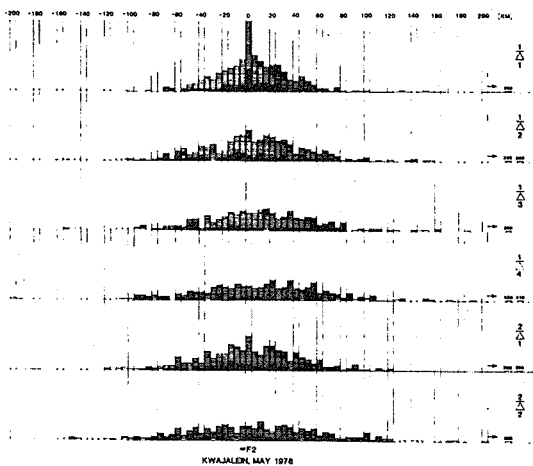
c) Feb. 1978



d) Mar. 1978

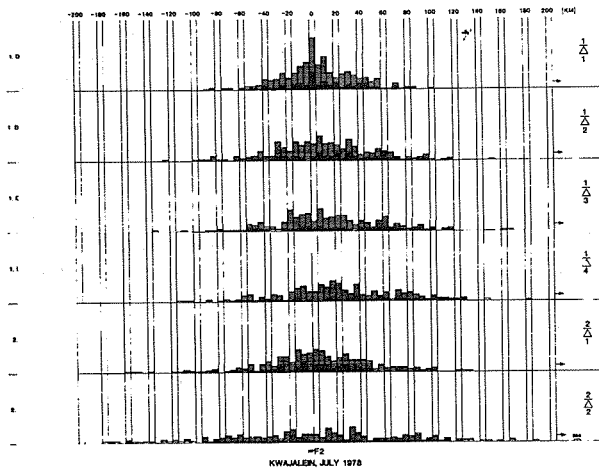


e) Apr. 1978

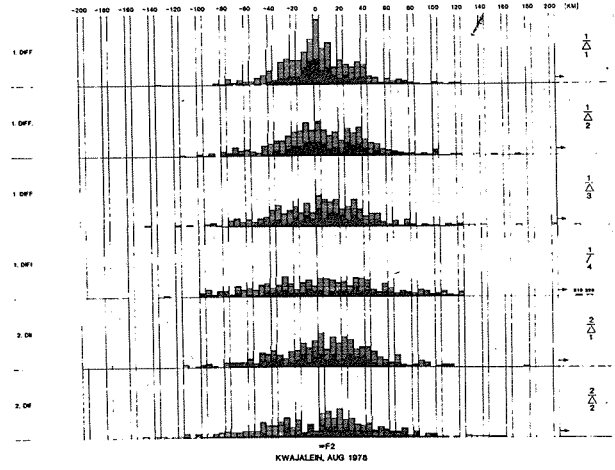


f) May 1978

Fig. 7--See overleaf for caption



g) July 1978



h) Aug. 1978

Figs. 7a...h Monthly over-all statistics of detrended $\bar{\Delta}hpF2$ (1 to 4h) reduced second order changes. From top to bottom: 1st difference over 1h; 1st difference over 2h; 1st difference over 3h; 1st difference over 4h; 2nd difference over 1h; 2nd difference over 2h. (Symbol $\frac{b}{\Delta a}$ identical with $a\bar{\Delta}b$ in text).

- a) Aug./Sept. 1977
- b) Jan. 1978
- c) Feb. 1978
- d) Mar. 1978

- e) Apr. 1978
- f) May 1978
- g) July 1978
- h) Aug. 1978

KWAJALEIN M.I.		1E1	2E1	3E1	4E1	1E2	2E2	hpF2 Total
AUG	M25	30	35	40	45	40	55	55
SEP	D25	30	40	45	45	40	70	60
77	M10	60	75	80	90	80	125	120
	D10	65	80	90	90	95	160	135
JAN	M25	25	35	45	45	30	40	45
78	D25	35	50	55	45	55	85	75
	M10	55	75	80	85	70	100	100
	D10	65	90	90	80	105	155	140
FEB	M25	30	40	45	50	40	55	55
78	D25	30	45	50	55	45	75	70
	M10	65	80	90	100	75	115	115
	D10	65	85	100	110	95	150	140
MAR	M25	30	40	55	65	40	65	65
78	D25	30	50	45	40	45	70	60
	M10	75	100	110	115	95	165	150
	D10	85	100	110	100	105	155	140
APR	M25	25	65	70	85	85	85	85
78	D25	40	50	65	60	55	80	75
	M10	80	120	145	150	100	180	175
	D10	75	105	120	120	110	170	155
MAY	M25	30	65	95	95	65	85	95
78	D25	35	50	55	60	55	75	75
	M10	80	125	140	145	110	185	180
	D10	80	100	115	120	105	160	150
JUL	M25	40	60	65	80	40	95	85
78	D25	40	50	50	45	55	70	75
	M10	85	95	115	145	100	150	150
	D10	75	100	105	120	110	185	170
AUG	M25	25	35	40	45	40	55	55
78	D25	35	40	40	50	50	75	70
	M10	60	75	80	80	90	120	115
	D10	65	80	90	95	105	160	140

Fig. 8

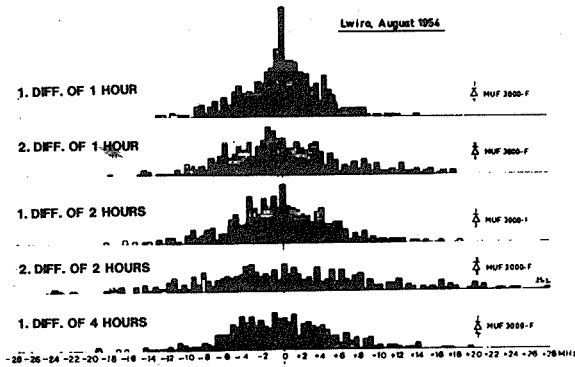


Fig. 9

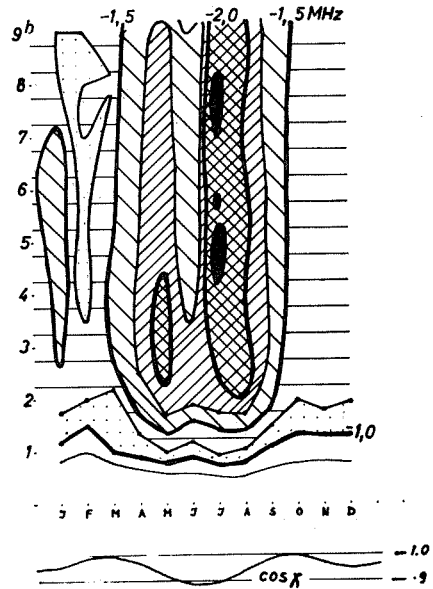


Fig. 10

Fig. 8 Variance table of the different changes in hpF2 for Kwajalein, M.I.

Fig. 9 Detrended differences of MUF 3000 F2 for Lwiro, Aug. 1954.

Fig. 10 Decay after average maximum in foF2 for Lwiro, year 1954.

1.4.2 Construction of Electron Density Profiles for the Flare-
Disturbed Ionosphere with Data from Doppler Measurements

I.N. Odintsova, V.D. Novikov

IZMIRAN, Troitsk, Moscow Region, 142092, USSR

Recent investigations show that the E- and F-regions of the ionosphere suffer considerable changes during solar flares. The study of these effects is of a great importance for the prediction of radio wave propagation and radiation risks, and it can help also to evaluate the spectral distribution of EUV radiation during a flare.

For this purpose one needs reliable models of the disturbed ionosphere, in particular the electron density profiles $N(h)$. Two methods for constructing model profiles are available:

- a) theoretical calculations based on atmospheric models and measurements of solar fluxes during the various types of flares;
- b) use of ionospheric measurements made by various radiophysical techniques during flares /Mitra, 1974/.

The variations in the upper ionospheric profile during the initial phase of a flare are particularly interesting. Although fast variations of EUV radiation are often observed during this phase /Donnelly, 1976/, there are very few data concerning profile changes.

Donnelly /1968/ constructed $N(h)$ profiles for the proton flare of August 28, 1966 using SFL records. However, the method was rather complicated and did not find wide application.

A comparison of $N(h)$ profiles constructed for the flares of 21 and 23 May 1967 from SFL records and from incoherent scatter measurements /Thome and Wagner, 1971; Mitra, 1974/ shows that the profiles do not coincide precisely due to differences in the reaction times.

Recently we developed a method for constructing $N(h,t)$ profiles for the initial phase of a flare, which is based on Doppler measurements /Novikov, 1977; Novikov and Odintsova, 1979/. It was shown that Doppler sounding on several frequencies, together with ionosonde data, can provide acceptable spatial resolution. In a simple case it is sufficient to have three frequencies, corresponding to reflections from the E-, F1- and F2-regions. As an example, we shall consider the flare of August 28, 1966. Donnelly /1968/ observed it with near vertical sounding on three frequencies 3.3, 4.0 and 5.054 MHz (Figure 1, solid curves).

We used a simple model for the undisturbed ionosphere consisting of parabolic E- and F2-layers with a linear increase of electron density N in the F1-region. This model is a good enough approximation in most cases, but one also uses standard models of the undisturbed ionosphere e.g. the IRI.

The general expression for the Doppler shift Δf in the case of vertical sounding is

$$\Delta f = - \frac{2f}{c} \int_0^{h_m} \frac{dn}{dt} dh \quad (1)$$

where n = refractive index, h_m = height of reflection, c = speed of light. Other expressions can be derived from Equation (1) e.g./Davies, 1970/:

$$\Delta f = \frac{h_m - h_o}{c} \left(-x + \frac{1+x^2}{2} \ln \frac{1+x}{1-x} \right) \frac{df_o}{dt}, \quad (2)$$

$$\Delta f = \frac{h_m - h_o}{c} \int \left[-2x + (1+x^2) \ln \frac{x+1}{x-1} \right] \frac{df_o}{dt} \quad (3)$$

Equation (2) refers to the reflection from a parabolic layer with critical frequency f_o , and Equation (3) takes into consideration double propagation through the same layer with reflection occurring from higher layers. Here $x = f/f_o$, h_o and h_m are the heights of the base and the peak of a layer. If the sounding frequency corresponded to a reflection from the F1-region, the following approximate expression was used

$$\Delta f \approx \frac{2f}{c} \frac{dh}{dt} = \frac{2f}{c} \frac{dh}{dN} \frac{dN}{dt} \quad (4)$$

From Equations (1) to (4) we obtained the $\Delta f(f)$ dependence in analytical form /Novikov and Odintsova, 1976/. For the abovementioned model of the ionosphere, Equation (2) may be rewritten as

$$\int_0^t \Delta f dt = \frac{f(h_m - h_o)}{c} K_y \Big|_0^t \quad (5)$$

where $K_y = \left(\frac{y}{2} - \frac{1}{2y} \right) \ln \frac{y+1}{y-1}$; $0 < f < f_o E$; $y = 1/x$; $t = 0$ at the start of a flare. The integral in Equation (5) can be obtained graphically from curve 1 in Figure 1. Since K_y is a function of dimensionless argument it is convenient to construct the curve K_y and to solve Equation (5) graphically.

For the calculation of electron density variations in the F1-region it is necessary to obtain the curve $\Delta f(t)$ with a reflection from the F1-region, and to correct for the contribution of the E-region from that curve. For this purpose we calculate $\frac{df_o E}{dt}$ from Equation (2) and substitute it in Equation (3) so as to obtain the changes in Δf , at frequencies 4.0 and 5.054 MHz, that are caused by variations in the E-region. Subtracting these values of Δf from the curves 2 and 3, respectively, we obtain the $\Delta f(t)$ changes caused by electron density variations in the F1-region only (dashed lines in Figure 1). To construct $N(h)$ profiles in the F1-region, we use the expressions given by /Novikov, 1977 and Novikov and Odintsova, 1979/, and make the calculations successively for separate parts of the $N(h)$ profile. The results for the flare of 28 August 1966 are shown in Figure 2b. Every profile consists of two linear parts corresponding to experimental records on 4.0 and 5.054 MHz. The profiles constructed by this method are in good agreement with those obtained by Donnelly /1968/ (Figure 2a).

We used the same method to construct $N(h)$ profiles in the F1-region during some other flares. SFD records were obtained for the path Fort Collins (USA) - Havana (Cuba) at 10 and 15 MHz /Belii et al., 1977/. In those calculations we neglect the electron density changes at and below the E-region peak. This is no longer valid when the critical frequency of the E-region is close to the transmitter frequency. $N(h)$ profiles for the flare at 1838 UT on 15 Feb. 1978, were obtained by the ionosonde just before the flare, and 5 minutes later; the latter is in good agreement with the profile calculated at SFD maximum (Figure 3). Enhancement of electron density in the E- and lower F-region is a typical feature in the initial phase of a flare.

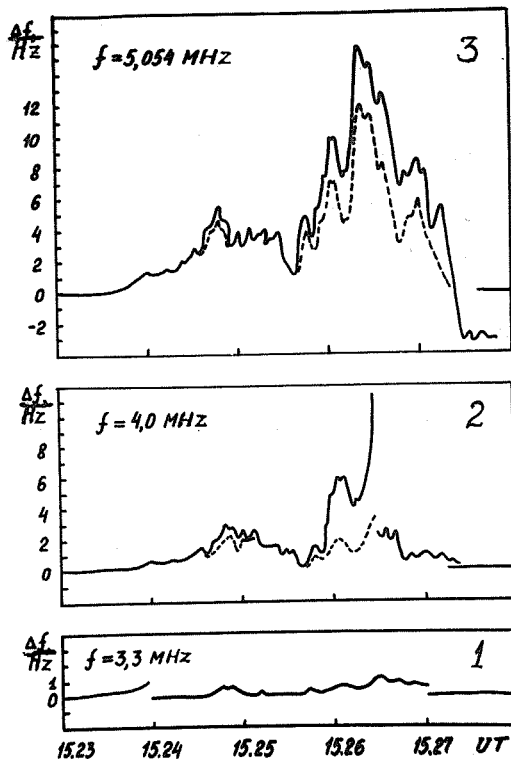


Fig. 1

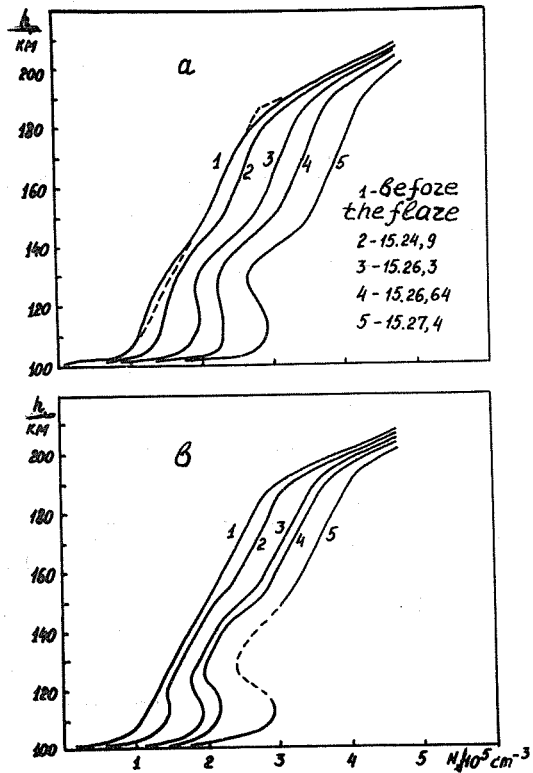


Fig. 2

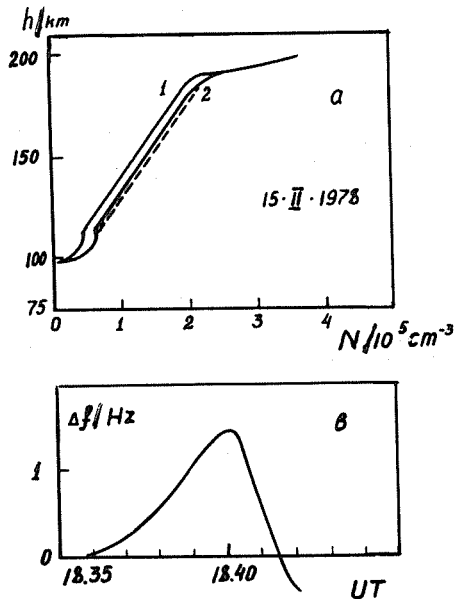


Fig. 3

- Fig. 1 Donnelly's [1968] Doppler observations of the flare of 28 Aug. 1966 (full lines) and those computed from the adjusted model (broken lines).
- Fig. 2 Electron density vs. height profiles obtained at different instants (parameter at the curves) from the data in Fig. 1: (a) by Donnelly [1968]; (b) by our method.
- Fig. 3 Doppler observation (bottom) and deduced profile change (1 to 2) for the flare of 15 Feb. 1978.

CHAPTER 2 PLASMA TEMPERATURES

Section 2.1 Electron Temperature

2.1.1 Comparisons of Isis and AE Satellite Measurements of

Electron Temperature with the International Reference Ionosphere

L.H. Brace and R.F. Theis

NASA/Goddard Space Flight Center, Laboratory for Planetary Atmospheres, Greenbelt, Maryland 20771, USA

Abstract: Empirical models of ionospheric electron temperature T_e , based on satellite Langmuir probe measurements, are compared with the International Reference Ionosphere (IRI) temperatures. Models at 300 and 400 km were derived from measurements made in 1976 and 1977, respectively, when Atmosphere Explorer-C was in circular orbit at these altitudes. Models at 1400 and 3000 km were derived from the ISIS-2 and ISIS-1 satellite in 1972 and 1970, respectively. These comparisons reveal that the reliance on solar zenith angle and the fixed vertical temperature gradients assumed in the IRI model prevent it from adequately describing the diurnal, seasonal and altitudinal variations of T_e in the upper F-region. In future versions of the IRI we suggest that vertical temperature gradients be made variable with local time, altitude and the McIlwain L value to better account for the effects of conjugate photoelectron heating, field aligned heat conduction and the heat content of the overlying plasmasphere. The existing satellite data base is adequate to define the necessary temperature gradient field.

1, Introduction

The thermal structure of the ionosphere has been the subject of extensive study over the past 20 years since orbiting spacecraft opened up this region to in situ investigation. A recent review summarizes the current theoretical and empirical knowledge about F-region electron temperatures /Schunk and Nagy, 1978/. The electron temperature, T_e , in the region below about 300 km is determined in daytime by a balance between electron heating by photoelectrons and electron cooling by elastic and inelastic collisions with ions and neutral gas /Hanson, 1963; Dalgarno et al., 1963/. Heat conduction within the electron gas is less important at these altitudes, but not negligible /Hoegy and Brace, 1978/.

In the upper F-region and throughout the plasmasphere, electrons are heated in the daytime by photoelectrons which escape the F-region and travel along the magnetic field toward the conjugate ionosphere. Since collisions with neutrals and ions are less frequent at these higher altitudes, local cooling is less effective, and T_e rises until it is limited by field aligned heat conduction into both underlying F-regions where the heat is lost to ions and neutrals.

In this paper we compare empirical models of T_e /Brace and Theis, 1980/, based on satellite Langmuir probe measurements from Atmosphere Explorer C, ISI-1 and ISIS-2, with temperatures given by the International Reference Ionosphere, IRI /Rawer et al., 1978a; Rawer and Ramakrishnan, 1978/. We discuss the similarities and differences in these models in terms of the physical processes noted above, and suggest improvements in future IRI models.

2, The Satellite Models of Te

The Langmuir probe technique has been described extensively /Findlay and Brace, 1969; Brace et al., 1973/ and various results from these experiments have been reported /Brace and Reddy, 1965; Brace and Spencer, 1964; Brace et al., 1967; Brace, 1970; Brace and Theis, 1974; Mahajan and Pandey, 1978, 1980/. The Te models used in this paper, and the modelling technique itself, are described more extensively by Brace and Theis /1980/. The modelling method employs spherical harmonics to describe the dip latitude and local time variation at fixed altitudes at equinox and solstice. Thus far, models have been derived from the Langmuir probe Te measurements from AE-C, ISIS-1 and ISIS-2. Figure 1 illustrates the time intervals and altitudes from which data were selected to derive the models used here. Figure 1 also shows the corresponding levels of solar activity represented by the yearly average sunspot number, R.

The ISIS-1 Te models employed subsets of the 1969-71 data acquired between 2000 and 3600 km altitude, a region where the vertical temperature gradients are small compared with the latitude and local time structure. The average altitude of 3000 km was assigned because the spacecraft spends so much time near apogee (3600 km). The ISIS-2 models used appropriate subsets of the 1971-73 data to model the 1400 km behavior of Te. The circular orbit of ISIS-2 at 1400 + 50 km, made this choice obvious. During its circular orbit phase AE-C provided data at a number of nearly fixed altitudes between 205 and 410 km. We have modelled the 300 km and 400 km data.

3, Comparison with the IRI Model

The IRI model values used in the paper were calculated using the subroutine IRIFO 6, 15.8.79 provided by Bilitza /private communication/ and based upon the equations for Te given in the URSI-COSPAR IRI description /Rawer et al., 1978a/. We recognize that the IRI Te model was not intended to represent the region above 1000 km, but we will compare them with the ISIS models at higher altitudes because such comparisons may be helpful in future efforts to extend the IRI model upward.

In order to compare the satellite models with the IRI, we have plotted them both as functions of local time in Figures 2, 3a and 3b. The satellite model profiles are shown in solid lines and the corresponding IRI profiles are shown dashed. To match the solar activity of the IRI to the corresponding satellite models we employed the mean sunspot number of the data set as indicated in Figure 1.

4, Discussion

The differences in the IRI and the satellite models of Te result primarily from the decision in formulating the IRI model to make Te dependent upon solar zenith angle. It is clear on the basis of the processes of thermal balance, that the local solar zenith angle is a controlling variable for Te in the ionosphere below about 300 km, where Te is determined by local heating and cooling processes. However, in the upper ionosphere and plasmasphere, the effects of conjugate photoelectrons, interhemispheric heat conduction, and plasmaspheric heat capacity are also important. These factors cannot be described by local solar zenith angle alone. The satellite models demonstrate this clearly in the form of the smaller diurnal variations observed at high altitudes and the lack of seasonal differences in the diurnal variations. In this section we describe these differences in more detail.

4.1 The differences at low altitude

For the reasons noted above, the IRI does not describe the diurnal variations accurately (Figure 2) or the season effects on the diurnal variations (Figures 3a and 3b). The equatorial region has the greatest problem because it exhibits the most complex and asymmetrical diurnal structures. The IRI fails to describe the rapid rise at dawn and the

early morning peak near 07 h. This peak is not as evident at mid-latitudes (Figures 3a and 3b) because the daytime temperature does not return to the very low equatorial values. The origin of this morning peak is the less effective local cooling provided by the low early morning electron densities.

The exaggerated seasonal effects in the IRI model are evident in Figures 3a and 3b in the length of the period of enhanced daytime T_e in summer and winter. In contrast, the satellite models at 300 and 400 km show only seasonal differences that are very slight as a result of the conjugate heating effects which prevent local heating and cooling from completely dominating T_e .

4.2 The differences at high altitude

The differences with the IRI noted at low altitude are amplified at 1400 and 3000 km. The IRI was not intended to accurately describe T_e at these altitudes, but it is instructive to make these comparisons because they illustrate the underlying assumptions in the model which cause trouble even at the lower altitudes.

The midday and midnight T_e of the IRI at 1400 km are in good agreement with the ISIS-2 data (1400 km model). This is probably because the IRI was matched to the AEROS satellite measurements /Spenner et al, 1974/ which are consistent with the ISIS-2 measurements. The Explorer 22 Langmuir probe data, acquired at 1000 km in 1964 and 1965 /Brace and Reddy, 1965; Brace et al., 1967/ were also fully consistent with the AEROS data, but, because of its circular orbit, Explorer 22 provided better measurements of seasonal and diurnal structure.

In contrast to the agreement at 1400 km, the IRI temperatures at 3000 km are much too high in daytime and too low at night. These differences arise from the extension of the IRI model to altitudes where the assumed vertical T_e gradients no longer are correct (2K/km in daytime and no vertical gradient at night). Ignoring the possible effects of differing solar activity, the satellite models suggest a more appropriate daytime value of 1K/km between 1000 and 3000 km. T_e measurements from the S3-3 satellite /Rich et al., 1979/ suggest that the afternoon plasmasphere is nearly isothermal at about 5700 K between 5000 and 8000 km altitude, although a zero vertical gradient is not consistent with conductive heat flow from the plasmasphere into the ionosphere. At night, the midlatitude vertical gradient implied from the satellite models remains about 1K/km. Even larger vertical gradients in T_e are characteristic of mid-latitude regions below 1000 km as measured by the incoherent scatter data of Millstone Hill /Evans et al., 1978/. Gradients of 2K/km are typical of the nighttime ionosphere there.

The differences at higher altitudes are even more evident in the failure of the IRI to follow the local time variation at dawn and dusk. The IRI T_e retains its solar zenith dependence when extrapolated to 1400 and 3000 km, while the satellite models show relatively insignificant differences between the diurnal variations in the winter and summer hemispheres. In addition, the 3000 km satellite data show that the 40° field line cools very slowly at night, never cooling completely to the exospheric temperature. A similar result was reported from Explorer 32 Langmuir probe results at 2600 km above the equator /Brace, 1970/ on an even shorter field tube. The daytime Explorer 32 values of 4700 K and nighttime values of about 2000 K agree well with the 3000 km model equatorial values derived from ISIS-1.

5. Conclusions

The variations of T_e with local time and season are not well described by the IRI, even below 1000 km where the model is intended to apply. In particular, the characteristic steep increase at sunrise

followed by a peak T_e at about 0700 hours are not represented by the IRI model. The IRI model also exaggerates the differences in the diurnal variation of T_e at mid-latitudes in winter and summer. Such seasonal differences are shown by the satellite models to be relatively unimportant, a result that is consistent with the influence of inter-hemispheric transport of photoelectrons and heat rather than exclusive control of T_e by local heating and local cooling. However, even local heating and cooling processes produce asymmetrical diurnal variations because the slow build up of Ne in the morning causes reduced local cooling of electrons to ions at this time.

Successful modelling of the F-region may require coupling of T_e and Ne using satellite or radar models of their relationship /Brace and Theis, 1978; Spenner and Wolf, 1975; Mahajan, 1977/. An example of such a model, based on daytime Atmosphere Explorer-C measurements at solar minimum /Brace and Theis, 1978/, is shown in the form of contour plots in Figure 4. Equation (1) gives the analytical form of the model.

$$T_e = P_1 + (P_2 h + P_3) \exp (P_4 h + P_5 N_i + P_6 h N_i) \quad (1)$$

where T_e = electron temperature / K, N_i = ion (or electron) density/cm⁻³, h = altitude/km. The coefficients P_n are $1.051 \cdot 10^3$, $1.707 \cdot 10^1$, $-2.746 \cdot 10^3$, $-5.122 \cdot 10^{-4}$, $6.094 \cdot 10^{-6}$ and $-3.353 \cdot 10^{-8}$ for $n = 1$ to 6 .

This model shows that T_e and Ne (or Ni) are inversely related in daytime above 200 kilometer where electron cooling by collisions with ions becomes an important determinant of T_e . At lower altitudes, the electrons are cooled primarily by elastic and inelastic collisions with the neutral gas, and the T_e height profiles become nearly independent of Ne.

Models such as this would provide more realistic estimates of T_e that would be, in effect, normalized for the actual Ne conditions given by measurements or models such as the IRI. However, it is important to recognize that the coefficients in Equation (1) may vary with solar activity, and the model does not apply at night or in regions of auroral precipitation or other non-EUV heat sources.

Once the lower F-region T_e is properly described by a density dependent model, the electron temperature at higher altitudes could be described by adopting vertical temperature gradients to reflect both local and conjugate solar zenith angles, the field line total electron content, and the temperature itself. It may be possible to achieve an acceptable approximation to the above by using a vertical gradient that is variable with only local time, altitude and L-value. The local time and L terms would account approximately for the conjugate heating and the heat content of the overlying plasmasphere, while altitude terms could approximate the changes in temperature gradient with temperature that are required to maintain a constant conductive heat flux along a given flux tube.

We suggest that the currently available data base between 300 and 3000 km, referenced here, is adequate to significantly improve the present IRI model below 1000 km and to guide the evolution of a T_e model for the overlying plasmasphere.

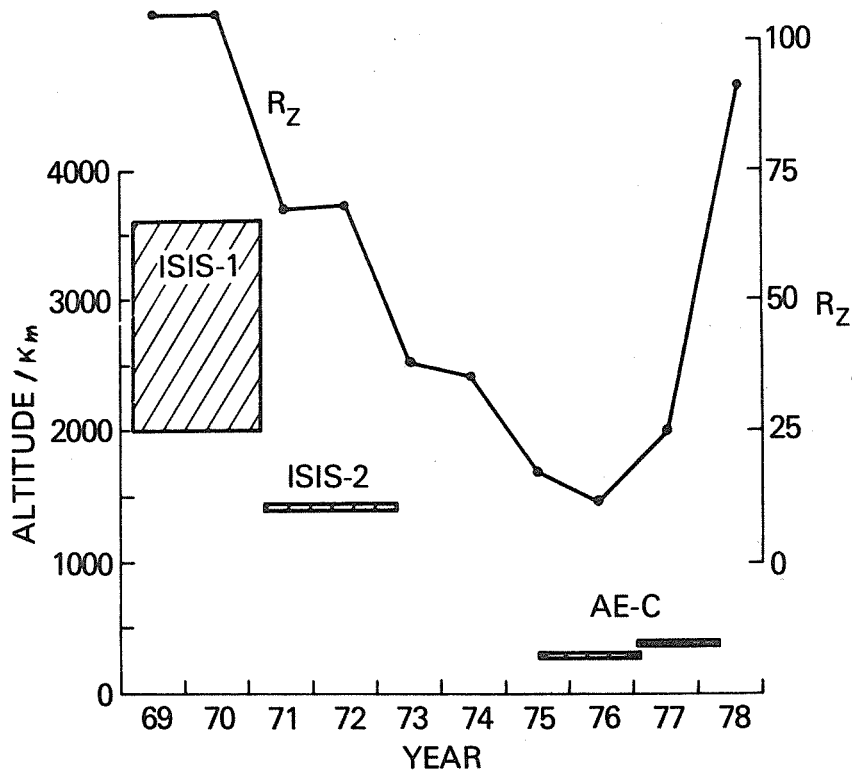


Fig. 1 The time interval and altitudes of the satellite data base employed in the T_e models. The ISIS-1 data in 1969-70 represented the 3000 km data base and correspond to high solar activity (sunspot number, R about 100). The ISIS-2 circular orbit data of 1400 km and the AE-C data at 300 and 400 km correspond to solar minimum conditions.

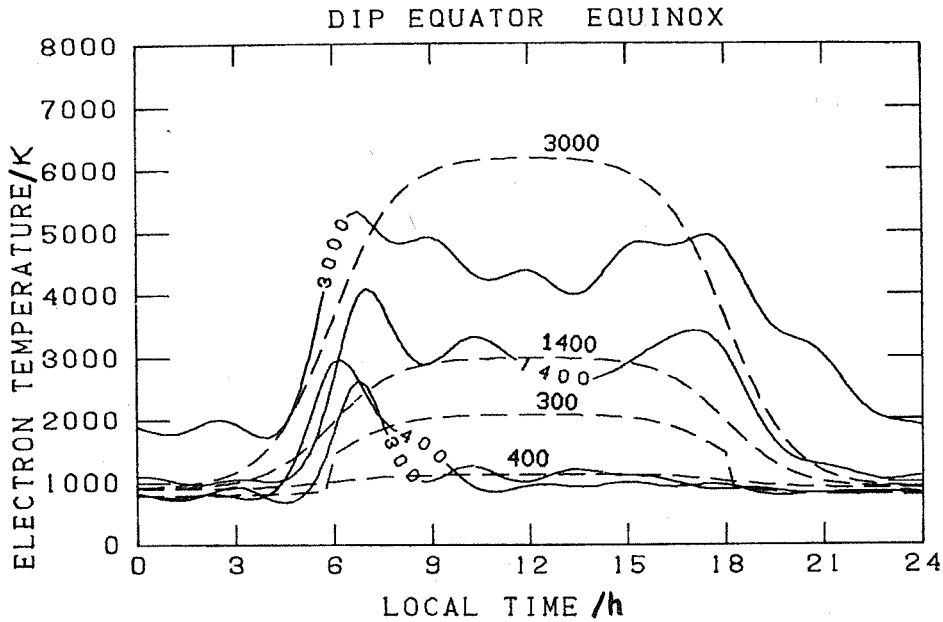


Fig. 2 Comparison of the satellite and IRI equinoxial diurnal variation of T_e at the dip equator. The asymmetries in the local time structure evident in the satellite models are not evident in the IRI which employs only solar zenith angle to represent the local time effects.

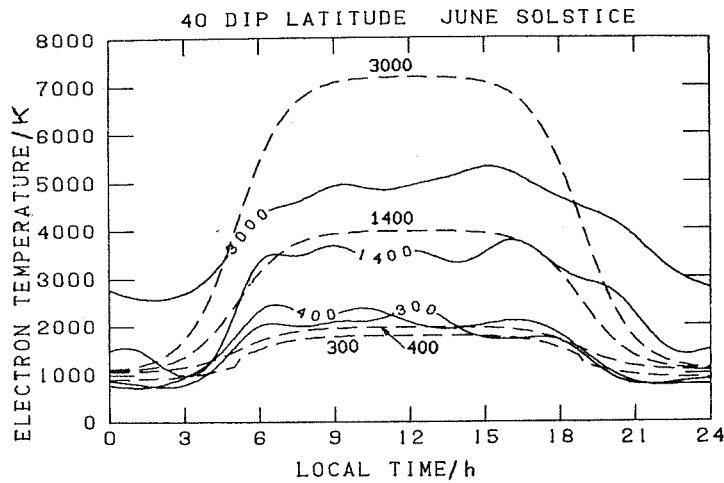


Fig. 3a

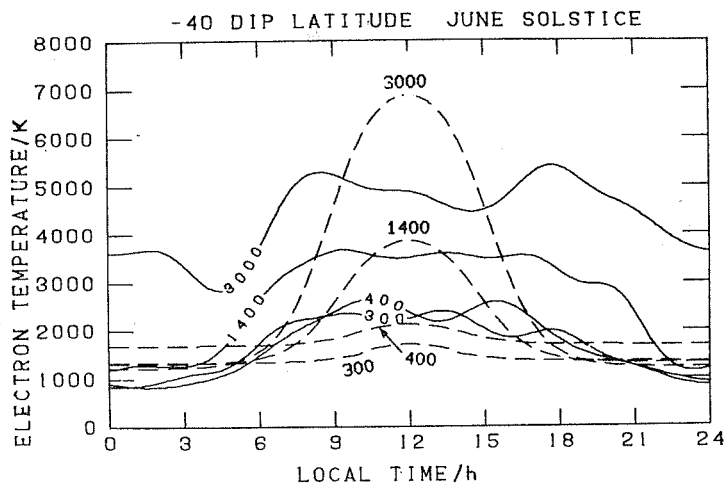


Fig. 3b

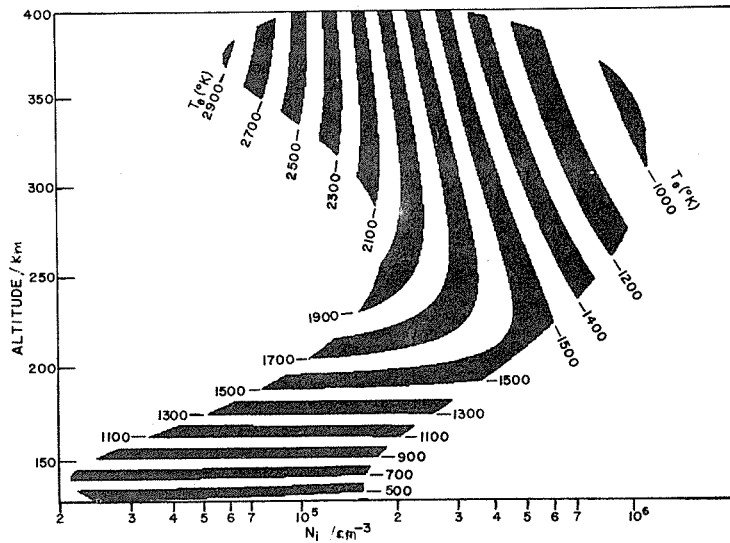


Fig. 4

Fig. 3a and b

Comparison of the satellite and IRI solstice diurnal variations of T_e at 40° north and south latitudes. The relatively small seasonal differences between $+40^\circ$ and -40° latitude are greatly overestimated by the IRI, again because of the use of solar zenith angle to represent the diurnal effects.

Fig. 4

An empirical model [Brace and Theis, 1978] of T_e as a function of N_e and height based on daytime AE-C measurements. Such a model could be used to define T_e where N_e is given by the IRI model or from measurements.

2.1.2 Proposal of Improvements of the Electron Temperature Model in IRI

K. Hirao

ISAS, University of Tokyo, Meguro-ku, Japan

Abstract: Only recently, the measurement of electron temperature in the ionosphere has become quite reliable for both space-vehicle and ground-based measurements. Many comparison studies have been achieved and carefully measured values now differ by less than 10%.

The number of data obtained so far seems to be sufficiently large to make possible systematic studies of an electron temperature model in the ionosphere, especially in middle and low latitude regions. At low latitudes the daytime electron temperature profile has normally a peak at around 220 km height and then a slight decrease with height up to around 350 km. Above this level it remains almost constant up to 500 km, beyond which it increases monotonically. However, in middle latitudes, daytime electron temperature profiles normally show a monotonic increase.

Nighttime temperature profiles show almost constant values above 200 km, with slight decrease around 350 km, and then an increase above 500 km in both middle and low latitude regions. In high-latitude regions, the electron temperature profile seems to be complicated between 100 to 200 km.

1, Introduction

Since the different methods of measurement have become reliable, recent electron temperature data obtained with satellites and sounding rockets can now be used for the construction of a reliable model. The sounding rocket data are particularly important for the bottom-side ionosphere. Figure 1 shows the distribution of incoherent back-scatter stations, and of the sounding rocket ranges used recently.

2, Sounding Rocket Data at the Kagoshima Space Centre (KSC), Japan

Rocket measurements of the electron temperature profile have been continuously carried out, since the early 70s, using identical radio frequency rectification probes on several rockets per year. The observation period almost covers one solar cycle. The probe used was specially developed to avoid the surface contamination effect, which sometimes caused some discrepancy in electron temperatures measured by Langmuir probes /Hirao and Oyama, 1972/, and to eliminate the effect of vehicle potential /Hirao and Oyama, 1970/. The earlier data for this period were analysed in order to obtain an experimental model of the electron temperature profiles over KSC /Hirao and Oyama, 1980/. The following characteristic features of the electron temperature profile have been found:

(i) There is a systematic diurnal variation of the electron temperature profile as shown in Figure 2. From evening to late morning, the profile is rather uniform except for a thin layer of high temperature at around 11 LT in winter. This layer might be related to the focus of the current system causing the geomagnetic diurnal variation /Oyama and Hirao, 1979/. It also might appear over the same geomagnetic latitude location in the winter hemisphere, but it is probably too exceptional to be included in IRI. The diurnal variation of the profile at KSC (20° geomagnetic latitude) is different from that at Jicamarca /Farley et al., 1967/ and at Millstone Hill /Evans and Holt, 1978/.

(ii) The profile shows almost constant temperature at heights of 300 to 350 km. The difference between the asymptotic electron temperature, and the exospheric temperature derived by the method of Jacchia /1971/, shows an almost linear relationship with solar radio flux $F(10.7)$. An

increase in the temperature difference is accompanied by a decrease in solar radio flux as shown in Figures 3a and 3b. Therefore the solar activity dependence of electron temperature at around 300 to 350 km height can be determined. The peak electron temperature at around 220 km also shows solar activity dependence.

(iii) In the bottom side, there is one characteristic point at 170 km where almost all the profiles show an inflection point; the temperature gradient there is about 20 K/km in the daytime profile. Another point to be mentioned is that the electron temperature becomes almost equal to the model neutral temperature at about 90 km height.

3, Satellite Encounter Data between AEROS-B and TAIYO

From March to September 1975 two satellites, AEROS-A and TAIYO, flew simultaneously under quiet solar conditions. There were many vertical encounters mainly over the South-Atlantic geomagnetic anomaly region at around 15 and 04 h LT. An encounter analysis with comparison of the electron temperatures from both satellites was made by Spenner et al., /1979/. An encounter was defined by allowing a longitude difference of 15° , a time difference of half an hour, and a latitude difference of less than 1° , but the allowed height difference was only 100 km or less. At night good correspondence of the electron temperatures measured by the two satellites was found; the dispersion was about 5% or less after making altitude-corrections based on the Spenner and Plugge /1978/ Model, which was derived from the data obtained by AEROS-A, incorporated in IRI 1978. This shows that the Spenner-Plugge Model is quite reasonable for night-time conditions.

The daytime results were not so good. It was suggested that the disagreement might be caused by the complicated situation over the South-Atlantic geomagnetic anomaly. However, a re-analysis has been made by the author who assumed a sharper gradient in the electron temperature profile. The result is shown in Figure 4; there is an improved coincidence with about 10% dispersion resulting from adopting a -10K/km gradient at around 300 km. This value is quite reasonable as compared with the profiles obtained at Jicamarca /Farley et al., 1967/.

Therefore, another gradient than in the model derived from the results of AEROS-A is needed at certain latitudes. Actually, the height gradient of the electron temperature 250 km over KSC is about 8 K/km in the afternoon.

4, Comparison with IRI 1978 and the above-described Data

The electron temperature profile calculated by the IRI 1978 program for the KSC geomagnetic latitude is shown in Figure 5, as well as the measured average profile for KSC. Of course, as the solar cycle effect influences the KSC data, it is not realistic to compare the two profiles because IRI 1978 does not include any solar cycle effect. However, some possible improvements to IRI 1978 can be pointed out.

(i) In the bottom side, the electron temperature has been found to be equal to the model neutral temperature at a height of around 90 km in the daytime. At night, the plasma density is so low that the electron temperature cannot be measured by the usual probe technique.

At around 120 km, the electron temperature profile shape is quite different from that of the model neutral temperature; this might be due to the existence of a not yet identified heat source. In IRI 1978 it is assumed that the electron temperature coincides with the neutral temperature at a height of 120 km. This problem must be reexamined. Also, considering our data, we have some doubts about the linear interpolation with height as applied in IRI in daytime.

(ii) As far as the magnitude of electron temperature is concerned, a solar cycle dependence is clearly observed in the data at KSC, which

is probably a typical location at low geomagnetic latitude. The comparison shows that the model temperature is rather low generally. Also, the peak in the electron temperature profile in the equatorial F-region as given by IRI occurs at rather high altitude compared with KSC data and, possibly, the Jicamarca data. The height of the minimum in the temperature profile, however, agrees nicely with the data of both stations.

(iii) The rate of temperature decrease with height in the F-region is fairly small in daytime. It is shown in Figure 5 for KSC. The comparison with Jicamarca data gives the same conclusion. Our intercomparison analysis of the AEROS-B and TAIYO data also shows that the gradient of the profile should be reexamined.

5, Conclusions

The electron temperature profile in IRI 1978 was based on incoherent back scatter data as well as the AEROS-A satellite data. Reliable data on electron temperature profiles obtained by sounding rocket were probably scarce when the work for IRI started. As a result, the profile in the bottom side was not derived from measured data. As for the solar cycle effect, it was assumed in IRI that no clear solar cycle effect existed. At KSC, however, some clear solar cycle effects have been recognized.

To improve IRI 1978, it is necessary to use more data sources, particularly from the many sounding rocket ranges as well as incoherent scatter stations shown in Figure 1. The electron temperature measurement technique has become quite reliable in recent years. The electron temperature profiles which have been obtained at widely distributed rocket ranges should be used for improving the IRI profile.

Editor's Note: The reason why no solar cycle effect was assumed in IRI was that the only incoherent scatter station with a long series of regular measurements, Millstone Hill, shows no clear cycle effect at all. It may, however, be that different conditions exist in the equatorial region.

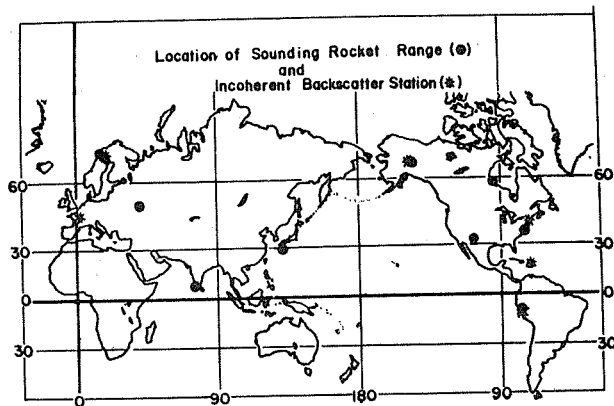


Fig. 1

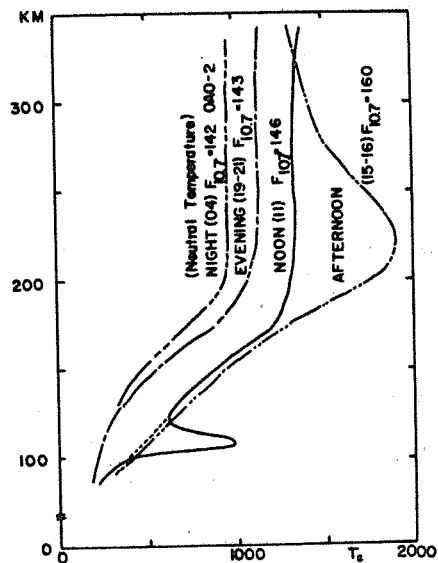


Fig. 2

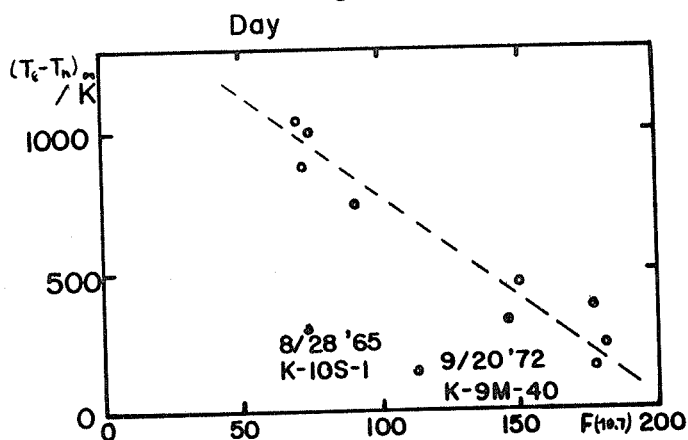


Fig. 3a

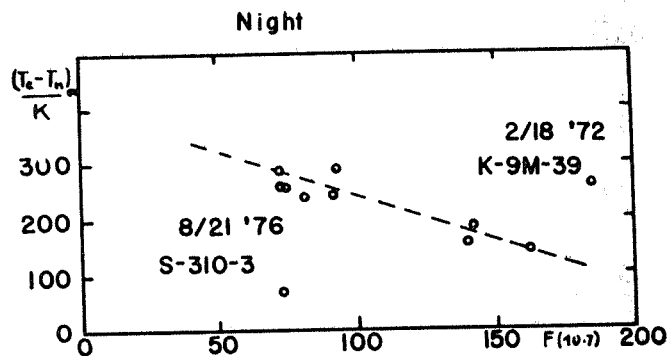


Fig. 3b

Fig. 1 Distribution of sounding rocket ranges and incoherent scatter stations.

Fig. 2 Average electron temperature profiles over KSC (Kagoshima Space Center, Uchinoura).

Fig. 3a and b Difference of electron and neutral temperature at 300 to 350 km height depending on solar activity (Covington-index $F(10.7)$): a) Day; b) Night.

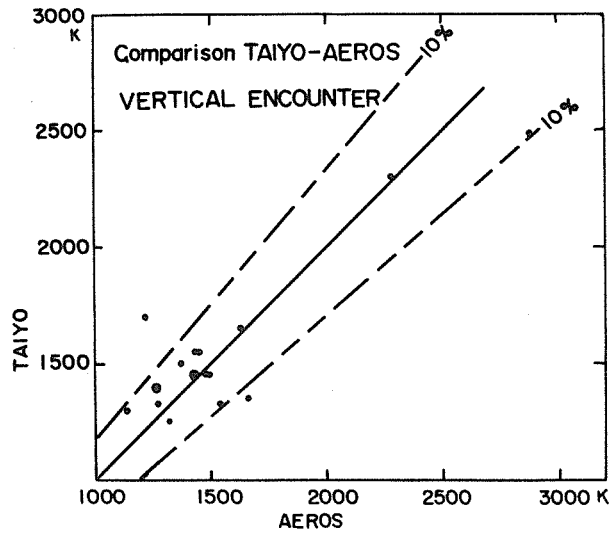


Fig. 4 Comparison of simultaneous electron temperature measurement at AEROS - TAYO encounters. (AEROS data were corrected to TAYO height).

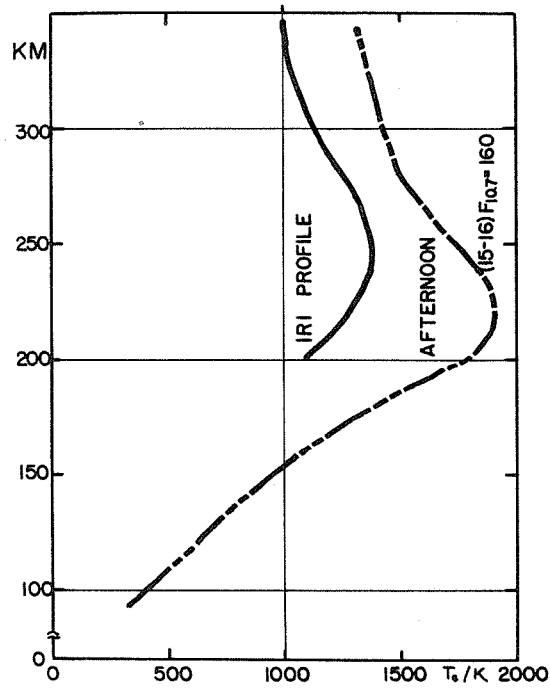


Fig. 5 Afternoon low latitude electron temperature profile after IRI (full line) and from rocket profiles at KSC (broken line).

2.1.3 Verification of the International Reference Ionosphere on Electron Temperature Profiles Obtained by Various Methods below 200 km

Yu.K. Chasavitin and N.M. Klyueva

USSR State Committee for Hydrometeorology and Control of
Natural Environment, Moscow, USSR

Abstract: Electron temperature profiles of IRI have been compared with the Te profiles obtained in Volgograd and other middle latitude sites by probe and incoherent scatter techniques, and with some empirical models of Te developed independently of IRI. To establish the latitude range in which IRI can be used, the model Te profiles have been compared with the corresponding experimental profiles obtained at high and low latitudes. As a result of such comparisons, the defects of a model are noted and its feasibility under different geophysical conditions is considered.

1, Introduction

The International Reference Ionosphere (IRI-1978) /Rawer, 1977; Rawer et al., 1978a,b/ is the most complete empirical model available at present. It presents space-time variations of ionospheric parameters in analytical form. The comparison of parameters given by IRI with experimental data obtained under appropriate conditions, and with data from models other than IRI is of great interest. This paper describes a comparison which has led to conclusions concerning the reliability of IRI under various geophysical conditions, for electron temperature parameters only.

2, Comparison with the Experimental Data (Middle Latitudes)

IRI-1978 and some experimental results are compared on the basis of a large mass of electron temperature data, which has already been described and analysed, obtained using rockets and incoherent scatter in the 100 to 200 km height region /Chasovitin and Klyueva, 1975; Klyueva, 1978/. To test IRI, 50 Te profiles have been selected from these data. Nearly half of them were obtained from Volgograd MR-12 rocket ascents /Andreeva et al., 1971; Chasovitin et al., 1974; Klyueva et al., 1978/; the remainder stems from Kagoshima, Wallops Island, Cape Kennedy (rocket data), and Millstone Hill, St. Santin and Arecibo (measurements by incoherent scatter). The profiles were randomly selected for quiet and weakly disturbed days ($K_p < 4$), but mainly with regard to different seasons and times of day. For every experimental electron temperature profile Te a model profile Tem calculated from IRI-1978 /Rawer et al., 1978a/. For the comparison the deviations of the experimental from the model values of Te at fixed heights are calculated as

$$\delta Te = (Te - Tem) / Tem$$

The results for three heights between 130 and 200 km are given in Figure 1. All the data are grouped according to the solar zenith angle intervals (χ) shown in the Figure and the values of δTe are related to the mean value of χ for this set of experiments. The points in Figure 1 show the data for different stations without regard to the season, since no important peculiarities have been identified with various seasons. We arrive to the following conclusions: The δTe values at 130 km, based on probe measurements, display great scatter and they exceed the values from incoherent scatter by considerable amounts. This reflects a well-known fact that, at lower heights, the probe electron temperature data exceed the values measured by the incoherent scatter technique. The mean values of δTe (curve 1) calculated only from probe measurements for $\chi < 115^\circ$ range between 40 and 80%. The incoherent scatter data

are close to those of the model, and the mean values of δT_e (curve 2) are approximately zero. This is natural, because, in the model, T_e and T_n were assumed to be equal at 120 km (T_n is the neutral gas model temperature) and, as is known, incoherent scatter measurements at lower heights give T_e values close to T_n . There is no great difference between probe and incoherent scatter data at 160 and 190 to 200 km, and therefore all the data are considered together. The following feature was noticed in the daytime at $\chi < 40^\circ$: positive values of δT_e dominate for the stations situated at geomagnetic latitudes ϕ greater than 40° , whereas negative or almost zero values are characteristic of lower latitude stations ($\phi < 40^\circ$). The mean values of δT_e calculated separately for the first and the second group of stations (marked 3 and 4, respectively in Figure 1) illustrate this feature which we shall explain below. It should be noted that in these height regions, there is satisfactory agreement between the IRI and experimental data in the 40° to 75° range of zenith angle; most of deviations are within the limits of scatter of the individual T_e values. In other intervals of χ the agreement is worse, but nearly 80% of the deviations are within the range of permissible scatter. To illustrate this, the experimental and model profiles of electron temperature for different stations and various geophysical conditions are shown in Figures 2 and 3. These profiles confirm the peculiarities and conclusions pointed out above.

3. Comparison of Models (Middle Latitudes)

The IRI model has been compared with other empirical electron temperature models for middle latitudes, which have been developed independently of IRI. The dependence of T_e on the solar zenith angle at fixed heights was determined for various models. Models /Chasovitin and Klyueva, 1975; Klyueva, 1978/ based on probe rocket and incoherent scatter measurements obtained in the range of the 20° to 53° geomagnetic latitudes, and also a model derived from St. Santin incoherent scatter data /Belinskaya et al., 1976/ have been compared with IRI. At heights greater than 140 to 150 km, electron temperature models based on probe data /Chasovitin and Klyueva, 1975/ and on incoherent scatter data /Klyueva, 1978/ only differ slightly from each other so that both could be combined to one more general model. The dependence of electron temperature on the solar zenith angle in summer for these models and for IRI is shown in Figure 4; the results are similar for other seasons. From Figure 4 it leads us to the following statements: At 130 km all the models nearly coincide except for model IV, based on probe data (curve 2), which usually overestimates the electron temperature, especially when $\chi = 60$ to 100° . At high altitudes the dependence of electron temperature on the solar zenith angle has peculiar features for different models. Thus, T_e increases by 350 K in IRI at 200 km in passing from night to day for $\phi = 51^\circ$ and 43° (geomagnetic latitude, curves II and III) and nearly by 800 K for $\phi = 29^\circ$ (curve I). For model curve IV, which can be regarded as an average for the range $\phi = 20$ to 50° , the electron temperature variation from night to day at the same altitude is 700 K. This variation and the dependence of T_e on χ agree with model I and differ from models II and III. In model V for St. Santin, in passing from night to day at 200 km, the electron temperature increases by 900 K, which is in contrast to the variation for curve III of IRI, though this curve corresponds to model V. Thus, at 200 km in the daytime, curve IV is in satisfactory agreement with curve I ($\phi = 29^\circ$), whereas curve V is not; all these curves differ greatly from curves II ($\phi = 51^\circ$) and III ($\phi = 43^\circ$). In reality curve V ought to have been in agreement with curves II and III which relate to similar geomagnetic latitudes, and curve IV ought to lie somewhere between curves I and II. At this altitude at night, curves II, III, IV and are in satisfactory agreement, whereas the electron temperatures of model I are somewhat lower. The above features are also observed at 160 km. The features described in this paper are confirmed by the analysis of electron temperature profiles appropriate to the models under consideration (Figure 5). From all this we conclude that IRI at middle geomagnetic latitudes does not correctly reproduce

the transition of electron temperature in passing from night to day; near $\phi = 40$ to 50° the values of T_e are underestimated in the daytime (mostly in summer). It can further be noted that the electron temperature variations for IRI are very small (curves I and II) in passing from winter to summer, even though the solar zenith angle varies from 63° to 17° . This is in contrast with the data obtained from the other models, according to which T_e at 200 km, varies by 200 to 300 K.

4, Latitudinal Electron Temperature Variations

To study the accuracy of IRI at different latitudes, the electron temperature model values have been compared with the experimental data obtained in different latitude zones. For this purpose, latitude variations of T_e have been calculated from IRI at fixed heights, at noon and midnight, along the geomagnetic meridian $\lambda = 0^\circ$. Equinox data are shown in Figure 6 (curves I); for other seasons electron temperature values differ only slightly as mentioned above, and a similar latitude dependence is observed. Figure 6 shows that the electron temperature at noon suddenly changes at $\phi = 40^\circ$. This is associated with the sudden change in the IRI-parameter H_0 in the daytime at this latitude, which is caused by the transition from the formulae for the upper to those for the lower part of ionosphere: H_0 equals 200 km at $\phi \leq 40^\circ$, and 350 km at $\phi > 40^\circ$. Generalized electron temperature data from the sources referred to in para 3 above were analyzed for stations located in the geomagnetic latitude range 20° to 53° in order to find evidence for the existence of such discontinuity at $\phi = 40^\circ$. Mean values of T_e for these stations and appropriate conditions are given in Figure 6 and are numbered 1 to 5. It is seen that there is no discontinuity in the mean values at $\phi = 40^\circ$, which are greater than those of IRI in the geomagnetic latitude range 40° to 50° . Thus, the IRI daytime model at $\phi = 40^\circ$ to 50° does not represent the true latitude variation, and leads to electron temperatures which are too small. From Figure 6, one can see that the features described in sections 2 and 3, as well as the defects of the model, can be explained by the discontinuity mentioned above.

In Figure 6, the plots marked III and IV give electron temperatures obtained at high latitude (Port Churchill) /Chasovitin and Klyueva, 1978/ and low latitudes, respectively. Comparison with T_e model profiles is shown in Figures 7 and 8; the plots marked IV in Figure 6 pertain to experiments 1, 3 and 7 in Figure 8. Figure 7 shows the experimental profiles of T_e obtained from Heiss Island /Chasovitin and Klyueva, 1978/, and Figure 8 shows the rocket profiles obtained at low latitudes; both Figures also give the appropriate profiles of IRI. Naturally, when making comparisons with isolated experiments, it is impossible to draw firm conclusions about applicability of the IRI at high and low latitudes; we shall just give a rather tentative summary: In some cases, in polar regions, the T_e model profiles are in satisfactory agreement with the experimental profiles selected for quiet and weakly disturbed conditions. This agreement is most commonly observed at $\chi > 90^\circ$; in other cases, electron temperature experimental values can be 1,5 to 2 times greater than the model values, or even greater. Data for low latitudes given in Figures 6 and 8 show that satisfactory agreement between model and experimental profiles is sometimes observed, preferentially with solar zenith angles between 70° and 90° . The greatest differences (by a factor of 2 or more) were observed at small zenith angles. We feel that the particular conditions in the polar and equatorial ionosphere should be studied further.

5, Conclusions

Having compared electron temperature profiles of IRI with experimental data and some other models, we can draw the following conclusion: IRI is in a rather good agreement with the experimental data in the geomagnetic latitude range 20° to 55° at 140 to 200 km for solar zenith angles 40° to 75° . Under these conditions, the majority of the

differences are within the range of 20% to 30%. The agreement is worse for other zenith angles, but still nearly 80% of the deviations are in the range of permissible scattering. At night, IRI is generally in satisfactory agreement with other models. Electron temperatures given by IRI in the daytime at $\phi = 40^\circ$ to 50° are incorrect; this arises from discontinuity in the H_0 parameter at $\phi = 40^\circ$ at the transition from one formula to another, so that in this range the latitudinal variation is not correctly reproduced. There, the model values are greatly underestimated, particularly near noon, and the electron temperature variations in passing from night to day are too small. However, the elimination of this fault will provide a better agreement with other models. The IRI gives only small variations of electron temperature in passing from winter to summer at the same local time, this is in disagreement with the experimental data for the daytime.

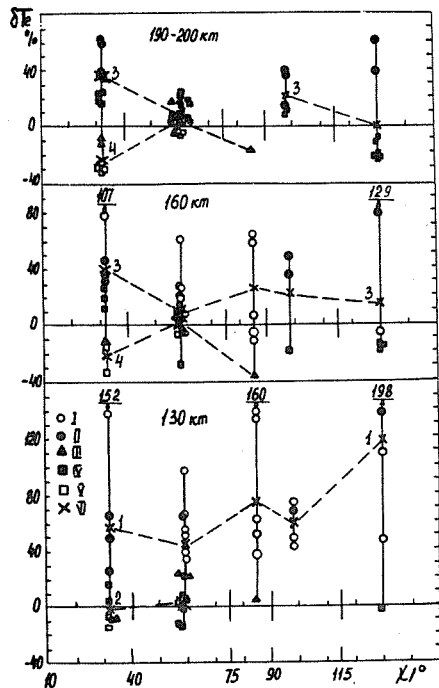


Fig. 1

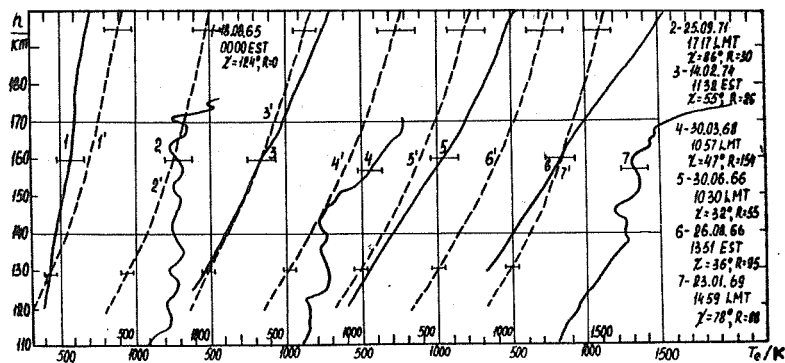


Fig. 2

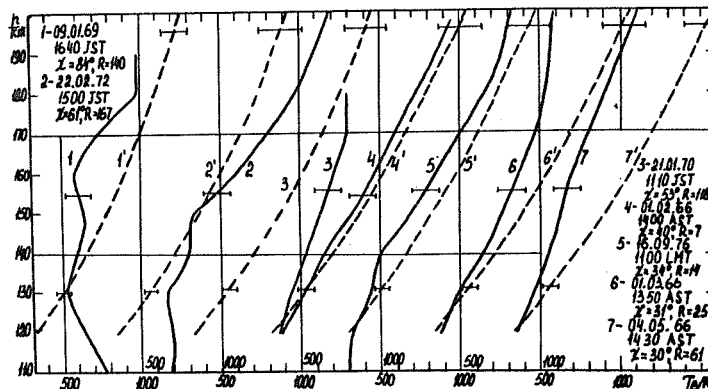


Fig. 3

Fig. 1 Relative deviations of experimental electron temperature values from model values at three fixed heights and various intervals of zenith angle. I: Volgograd; II: Wallops Island and Cape Kennedy; III: Kagoshima; IV: Millstone Hill and St. Santin; V: Arecibo; VI: Mean values.

Fig. 2 Experimental electron temperature profiles for middle ($>40^\circ$) latitude stations. 1 and 3: Millstone Hill [Evans, 1970; Roble et al., 1978]; 2, 4 and 7: Volgograd [Andreeva et al., 1971; Chasovitin et al., 1974]; 5 and 6: St. Santin and Wallops Island respectively [Carr et al., 1967; Pharo et al., 1971]; 1', 2' ... 7' represent the corresponding profiles given by IRI-78.

Fig. 3 Experimental electron temperature profiles for middle ($>40^\circ$) latitude stations. 1, 2, 3 and 5: Kagoshima [Hirao & Oyama, 1972; Oya et al., 1970; Watanabe & Obayashi, 1977]; 4, 6 and 7: Arecibo [Mahajan, 1967]; 1', 2' ... 7' represent the corresponding profiles given by IRI-78.

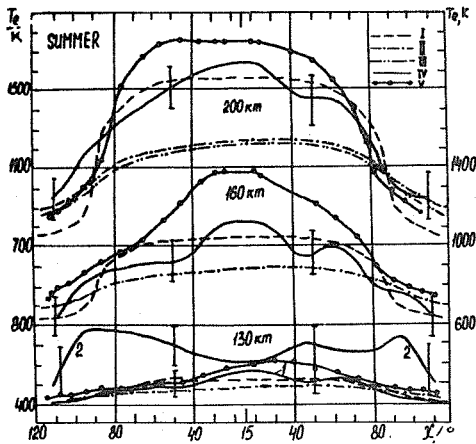


Fig. 4

Fig. 4 The dependence on solar zenith angle of model electron temperatures at three fixed heights in summer (ψ latitude, λ longitude, ψ geomag. latitude).

- I: IRI-78, $\psi = 40^\circ$, June, $R = 60$, $\lambda = 100^\circ$ ($\phi = 29^\circ$);
- II: IRI-78, $\psi = 40^\circ$, June, $R = 60$, $\lambda = 280^\circ$ ($\phi = 51^\circ$);
- III: IRI-78, $\psi = 40^\circ$, June, $R = 100$, $\lambda = 2^\circ$ ($\phi = 43^\circ$);
- IV: Models (5, 9);
- V: Model (2).

Note that for 130 and 160 km Models II and III are coincident. At 130 km the curves marked 1 and 2 are based respectively on incoherent scatter and probe data but, at 160 and 200 km, the full lines are based on a generalized model.

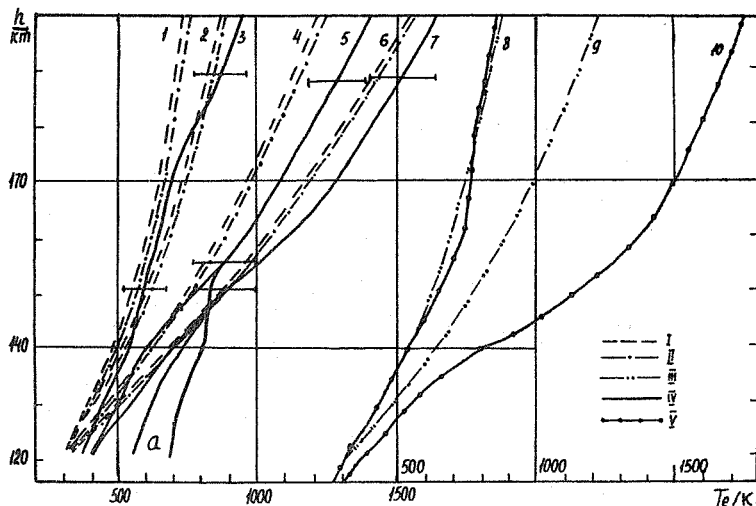


Fig. 5

Fig. 5 Model electron temperature profiles for winter and summer at noon and midnight. Key to identification of the curves:

- I: IRI-78, $\psi = 40^\circ$, $R = 60$, December
 - 1: $\psi = 100^\circ$ ($\phi = 29^\circ$), midnight;
 - 2: $\psi = 280^\circ$ ($\phi = 51^\circ$), midnight;
 - 4: $\psi = 280^\circ$ ($\phi = 51^\circ$), noon
 - 6: $\psi = 100^\circ$ ($\phi = 29^\circ$), noon
- II: IRI-78, $\psi = 40^\circ$, $R = 60$, June; 1, 2, 4 and 6: as for I above.
- III: IRI-78, $\psi = 40^\circ$, $R = 100$, June.
 - 8: $\lambda = 2^\circ$, ($\phi = 43^\circ$), midnight;
 - 9: as for 8 above, noon.
- IV: Models (5, 9).
 - 3: Midnight, winter and summer;
 - 5: Noon, winter; 5a from probe data;
 - 7: Noon, summer, 7a from probe data.
- V: Model (2).
 - 8: Midnight;
 - 10: Noon

Fig. 6 Variation of electron temperature with latitude along the meridian $\lambda = 0^\circ$, at noon and midnight during the equinox.

- I: IRI-78, $R = 100$, September;
- II: Mean values of T_e at:
 - 1: Kagoshima; 2: Arecibo; 3: St. Santin
 - 4: St. Santin (2); 5: Millstone Hill (5,9).
- III: Experimental data from Fort Churchill (6)
- IV: Experimental data from low latitudes. The noon and midnight values are indicated by white and black points respectively.

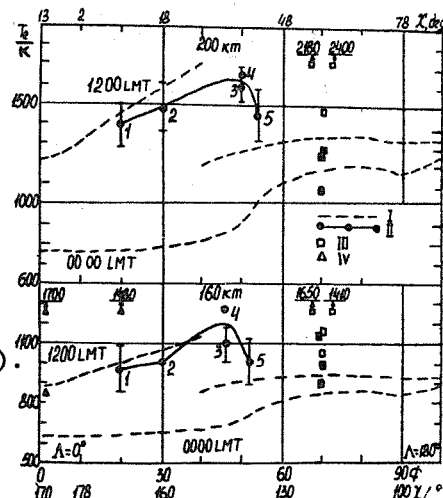


Fig. 6

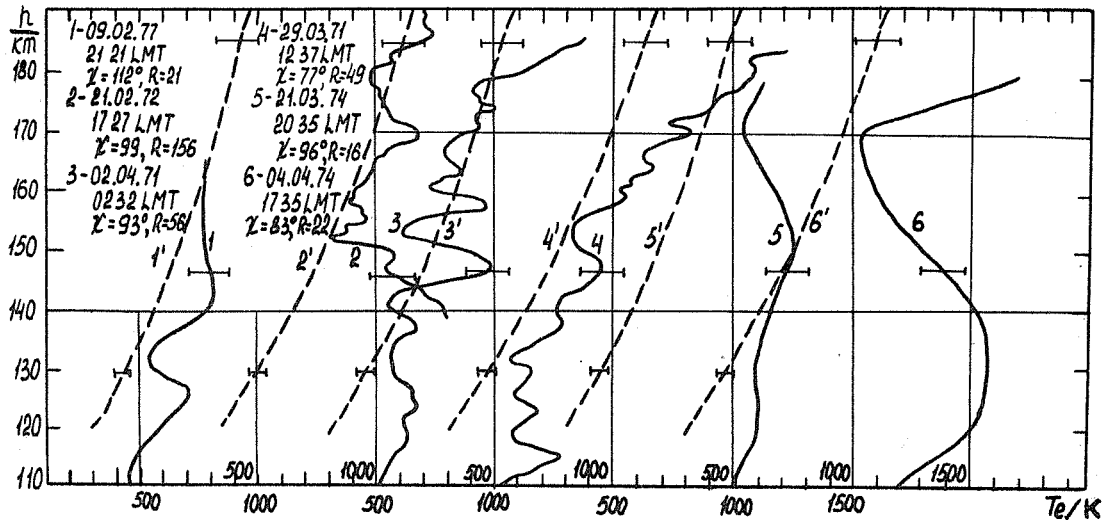


Fig. 7 Electron temperature profiles. 1 to 6: Rocket measurements made at Heiss Island; 1' to 6': The corresponding IRI model profiles.

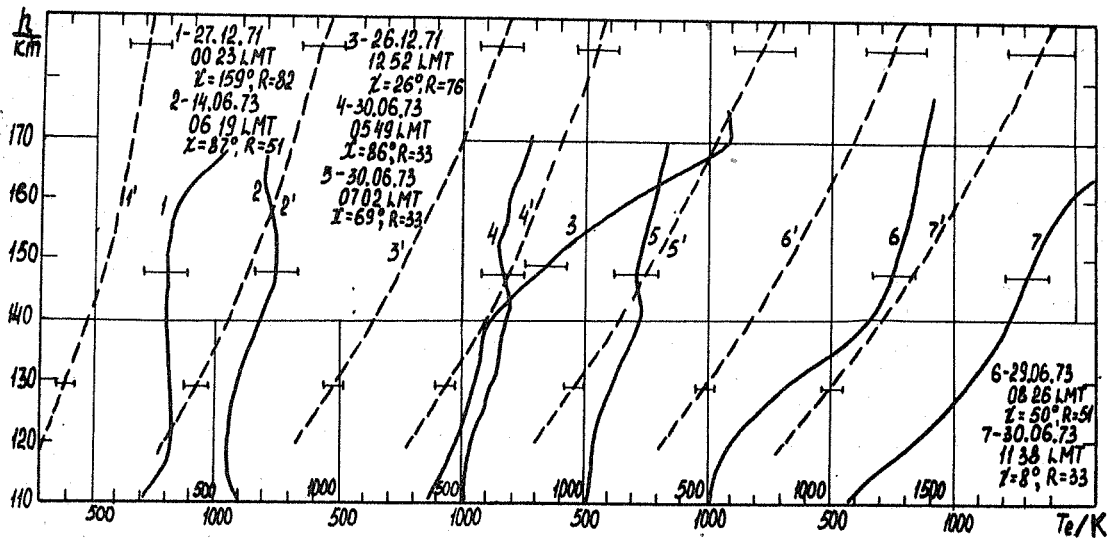


Fig. 8 Electron temperature profiles.

1 to 7: Rocket profiles obtained by the research ships "Professor Zubov" and "Professor Vize" at the following locations:

- | | |
|-----------------------------------|-----------------------------------|
| 1. $01^\circ 39'N, 24^\circ 10'W$ | 4. $16^\circ 59'N, 28^\circ 10'W$ |
| 2. $02^\circ 34'S, 24^\circ 56'W$ | 5. $16^\circ 59'N, 28^\circ 10'W$ |
| 3. $00^\circ 11'S, 24^\circ 24'W$ | 6. $16^\circ 39'N, 28^\circ 06'W$ |

1' to 7': The corresponding IRI model profiles.

2.1.4 Electron Temperature Modelling in the F-Region and Topside of the Ionosphere: A Proposal for Improving the IRI

K.K. Mahajan and V.K. Pandey

Radio Science Division, National Physical Laboratory,
New Delhi - 110012, India

Abstract: The electron temperature (T_e) model in the International Reference Ionosphere gives an average behavior of T_e in the altitude range 200 to 1000 km at all latitudes. The model is based on the latitudinal profiles of T_e , obtained from the AEROS-A measurements, combined with standard height profiles from various incoherent-scatter stations. The IRI does not include any effects due to solar activity, seasonal and day-to-day changes in T_e and variable electron density N_e . From incoherent scatter Radar and satellite probe measurements, it is now well known that large day-to-day and seasonal changes occur in T_e in the F-region which are due to changes in N_e . In the topside, T_e exhibits large solar activity and day-to-day changes because of changes in the heat flux (ϕ) conducted down from the protonosphere. The heat flux is, however, now known to be related to changes in electron concentration at heights around 400 km in the topside ionosphere. Empirical relations between N_e and T_e in the F-region, and N_e and ϕ_c in the topside, are now available for low as well as high solar activity conditions. These relations are used to compute model T_e values which are compared with measurements. A good agreement is seen between these model values and the measured values. It is proposed that these empirical relations be incorporated in the IRI for modelling T_e .

1, Introduction

The International Reference Ionosphere (IRI) compiled by Rawer et al. /1978a/ provides a continuous description of the main plasma parameters describing the ionosphere in space and time. Basically IRI is an electron density model; however, it also contains representative vertical profiles of other physical parameters characterizing the ionospheric plasma such as electron temperature, ion temperature and the relative ion composition.

The electron temperature (T_e) model in the IRI represents an average behavior of T_e as a function of altitude and latitude. It is based on the AEROS-A satellite measurements reported by Spenner and Plugge /1978/, together with the standard height profiles obtained from the incoherent scatter measurements at various observatories. The IRI, however, does not include solar activity, seasonal, diurnal and day-to-day changes in the electron temperature, which have been seen by many workers in the past. The solar activity effect in the topside T_e , for example, has been identified by Brace et al., /1968/ and by Mahajan and Pandey /1979/. The seasonal changes in T_e in the F-region have been reported by Evans /1973/. Diurnal and day-to-day variability in T_e has been seen in both the satellite and radar measurements made by many workers.

Thus, in view of the above effects, which cause large variability in T_e , the IRI model for T_e needs to be improved.

However, in addition to the IRI, there are at present three more empirical models for electron temperature given by Mahajan /1977/, Brace and Theis /1978/ and Mahajan and Pandey /1980/. The first two models are limited to the F-region altitudes, and are based upon the observed negative correlation between N_e and T_e . The empirical models of daytime T_e given by Mahajan /1977/ is based on the incoherent scatter radar measurements of N_e and T_e at Arecibo and St. Santin for low and medium solar activity conditions. The model of Brace and Theis /1978/ is based on Langmuir probe measurements on AE-C satellite for solar minimum condition. The electron temperature model of Mahajan and Pandey /1980/ is for the topside ionosphere where the negative correlation observed

between the protonospheric heat flux (ϕ_c) and topside Ne has been used as the basic input. This paper combines the F-region and the topside Te models of Mahajan /1977/ and Mahajan and Pandey /1980/ to give a model for heights between 200 and 1000 km for periods of low F(10.7) = 75 and medium F(10.7) = 150 solar activity conditions. The model is valid for low and mid-latitudes.

2. Physical Mechanisms Controlling Te

The electron temperature Te, in the ionosphere is sensitive mainly to three physical processes, namely electron heating by photoelectrons, electron cooling by heat transfer due to conduction /Banks, 1969; Schunk and Nagy, 1978/. In the F2 region, for heights between 200 to 300 km, the effects of thermal conduction are rather small and the heating rate is proportional to the concentration of thermal electrons (Ne), while the cooling rate is proportional to the product of electron and ion concentration (i.e. to Ne²). As the heating and cooling rates are nearly equal, it is obvious that between 200 and 300 km Te must be inversely proportional to Ne, as has been seen from several experimental measurements /Mahajan, 1967, 1977; Waldteufel, 1971; Spenner and Wolf, 1975; Prölls et al., 1975/. We have used the Ne-Te relationship observed by Mahajan /1977/ to generate tables of Te for various values of Ne for heights between 200 and 300 km. Tables 1(a) and 1(b) reproduced as Figures 1(a) and 1(b) give the values of Te for low and medium solar activity conditions, respectively.

Above about 300 km, the heat conducted down from the protonosphere (ϕ_c) becomes a major influence in determining Te /Geissler and Bowhill, 1965; Evans and Mantas, 1968; Mahajan and Pandey, 1979/. The heat flux ϕ_c is related to the energy spectrum of the photoelectrons escaping from the F-region. As the energy spectrum of these photoelectrons depends on the concentration of electrons in the escaping region, it is expected that ϕ_c will be inversely related to Ne in the escaping region. This indeed has been observed by Mahajan and Pandey /1980/, from various incoherent scatter radar measurements of Te and Ne, who developed following empirical relations between Ne and ϕ_c at 400 km in the topside ionosphere for different solar activity conditions:

Low solar activity:

$$\phi_c = (7.42) \cdot 10^9 - (2.94) \cdot 10^4 \cdot N_e \quad (1)$$

Medium solar activity:

$$\phi_c \begin{cases} = (2.33) \cdot 10^{10} - (4.08) \cdot 10^4 \cdot N_e & ; N_e < 5.2 \cdot 10^5 \\ = 2.0 \cdot 10^9 & ; N_e > 5.2 \cdot 10^5 \end{cases} \quad (2)$$

where ϕ_c is in units of eV cm⁻²s⁻¹ and N_e is in cm⁻³.

3. The Modelling Procedure

The application of the model requires a knowledge of the electron concentration profile between 200 and 400 km. Once the Ne-h profile is known, the following steps are taken:

- I. Electron temperature is read in Tables 1(a) and 1(b), in the height range from 200 to 300 km, for the observed values of Ne and interpolated for the appropriate condition of solar activity.
- II. Heat flux ϕ_c is obtained from Equations (1) and (2) with the particular value of Ne at 400 km.
- III. Having obtained Te at 300 km from step (I) and ϕ_c from step (II), the temperature gradient (dTe/dh) is obtained at 300 km from:

$$\phi_c = 7.7 \cdot 10^5 T_e^{5/2} (dT_e/dh) \cdot \sin I \quad (3)$$

IV. The temperature gradient at 300 km is used to calculate T_e at a height Δh above 300 km.

V. By assuming that ϕ_c remains constant with height above 300 km, the T_e profile is built up in steps Δh in the topside ionosphere up to 1000 km.

The validity of this assumption and its possible effects on the model T_e values will be discussed in Section 5.

4. Comparison of our Model and the IRI Model with Measurements

We shall compare our model and the IRI model with some actual measurements of T_e made by various incoherent scatter radars. Figures 2a and 2b show two such comparisons for St. Santin (44.6°N) and Malvern (52.1°N) during a period of medium solar activity. The data for St. Santin have been taken from CNET data booklets, and for Malvern from Hey et al., (1968). It can be noted that the observed values of T_e agree fairly with our model. However, there are large differences between the observed profiles and the IRI model. One can indeed pick out cases with very low and very high N_e values where the disagreement with IRI is greatest. However, when one selects a case where the N_e profile is nearest to the average behavior, there is good agreement between IRI and the measurements. This is demonstrated in Figure 3a which shows a comparison of our and the IRI model with Millstone Hill (42.6°N) observations (Evans, 1969) during a period of low solar activity. The IRI model shows a significant disagreement with the Millstone Hill observations (Evans, 1974) in Figure 3b which refers to a period of medium solar activity. Our model shows an excellent agreement with the Millstone Hill observations both in Figure 3a and Figure 3b. This was expected because the input data used for obtaining the empirical relations in Equations (1) and (2) have been taken from the Millstone Hill observations.

Figures 4a and 4b show a comparison of our model with observations at Arecibo (18.3°N) for low as well as medium solar activity conditions. The data for low solar activity are taken from Ho and Moorcraft (1971), and for medium solar activity from Hagen and Hsu (1974). The IRI model is also shown and it gives values for T_e that are lower than those for Arecibo at low solar activity, and higher at medium solar activity.

5. Discussion

In developing the present model based on the negative correlation between N_e and ϕ_c , we have assumed that the protonospheric heat flux observed at 400 km remains constant at the altitudes of interest (viz. 300 to 1000 km). This assumption is not strictly correct as the protonospheric heat flux varies with altitude. Thus, the present model needs to be improved so as to take into account the variation of ϕ_c with height in the altitude range 300 to 1000 km. This feature is demonstrated in Figure 5, which shows the comparison of the T_e profile observed at Millstone Hill (Evans, private communication) with that obtained from a constant and an altitude dependent protonospheric heat flux. It is quite clear that, in the topside ionosphere, the observed T_e profile agrees better with the T_e profile obtained by varying ϕ_c with height.

The present T_e models provide T_e for two specific levels of solar activity, namely low and medium. For intermediate levels of solar activity, a detailed correlation study is needed between N_e and T_e in the F-region, and N_e and ϕ_c in the topside. (to estimate T_e for intermediate solar activity by interpolating between the model T_e values for low and medium activity). The above models ought yet to be extended to high solar activity ($F(10.7) = 200$).

The present models are applicable only to middle and low (but not to equatorial) latitudes where the thermal conduction plays a major rôle in controlling the T_e profile. Because the nearly horizontal magnetic field lines at equatorial latitudes inhibit the heat flow, the behavior of the equatorial ionosphere is appreciably different from that deduced from measurements at middle latitudes.

Acknowledgements

We are grateful to J.V. Evans for supplying us with the unpublished values of N_e and T_e measured with the incoherent scatter radar at Millstone Hill during 1975.

Fig./Table 1a. Low Solar Activity ($F(10.7) = 75$)

<u>Height</u> km	<u>Ne/10⁵ cm⁻³</u>									
	1.0	2.0	3.0	4.0	5.0	6.0	7.0	8.0	9.0	10.0
200	2080	1800	1530	1260	990	860	860	860	850	850
210	2140	1850	1610	1340	1130	970	940	920	920	890
220	2200	1900	1690	1430	1270	1070	1020	980	960	920
230	2250	1950	1760	1540	1400	1170	1110	1040	990	950
240	2300	1990	1820	1640	1500	1280	1200	1100	1030	970
250	2330	2040	1890	1720	1590	1390	1280	1170	1060	990
260	2350	2080	1950	1800	1650	1490	1230	1210	1080	1000
270	2340	2120	2000	1870	1670	1520	1270	1190	1080	1010
280	2330	2150	2050	1920	1680	1530	1280	1140	1070	1020
290	2320	2180	2090	1950	1680	1520	1280	1100	1040	1020
300	2310	2190	2120	1960	1650	1510	1260	1060	1030	1030

Fig./Table 1b. Medium Solar Activity ($F(10.7) = 150$)

<u>Height</u> km	<u>Ne/10⁵ cm⁻³</u>											
	2.0	3.0	4.0	5.0	6.0	7.0	8.0	9.0	10.0	11.0	12.0	13.0
200	1670	1610	1550	1520	-	-	-	-	-	-	-	-
210	1860	1800	1720	1680	1620	1550	1500	-	-	-	-	-
220	2020	1920	1890	1840	1760	1710	1670	1610	-	-	-	-
230	-	2120	1980	1970	1910	1870	1870	1740	1680	1610	-	-
240	-	2270	2130	2140	2050	1980	1930	1820	1790	1710	-	-
250	-	-	2310	2230	2150	2070	2000	1930	1850	1780	1700	1640
260	-	-	2380	2300	2220	2130	2050	1970	1870	1800	1720	1660
270	-	-	2450	2330	2240	2150	2060	1960	1860	1760	1660	1600
280	-	-	2490	2360	2260	2160	2070	1930	1780	1710	1620	1550
290	-	-	2510	2370	2250	2140	2060	1870	1730	1630	1550	-
300	-	2670	2530	2380	2240	2130	2030	1810	1690	1560	1550	-

Fig. 1 Model of T_e as function of $Ne/10^{11} m^{-3}$ and height, for low and medium solar activity.

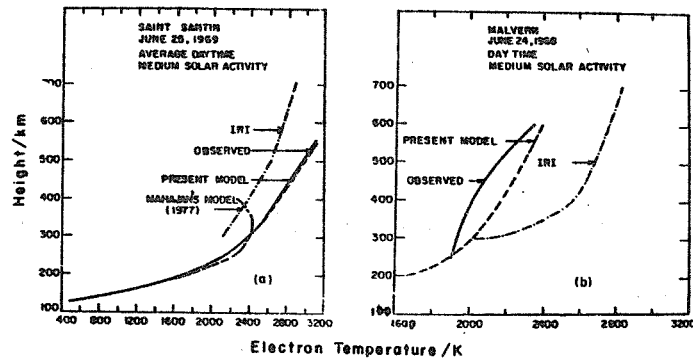


Fig. 2

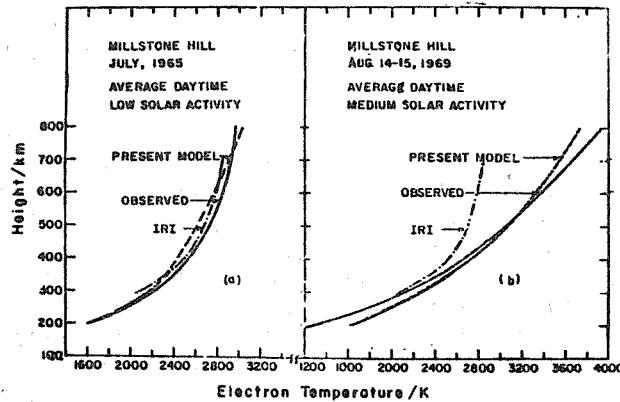


Fig. 3

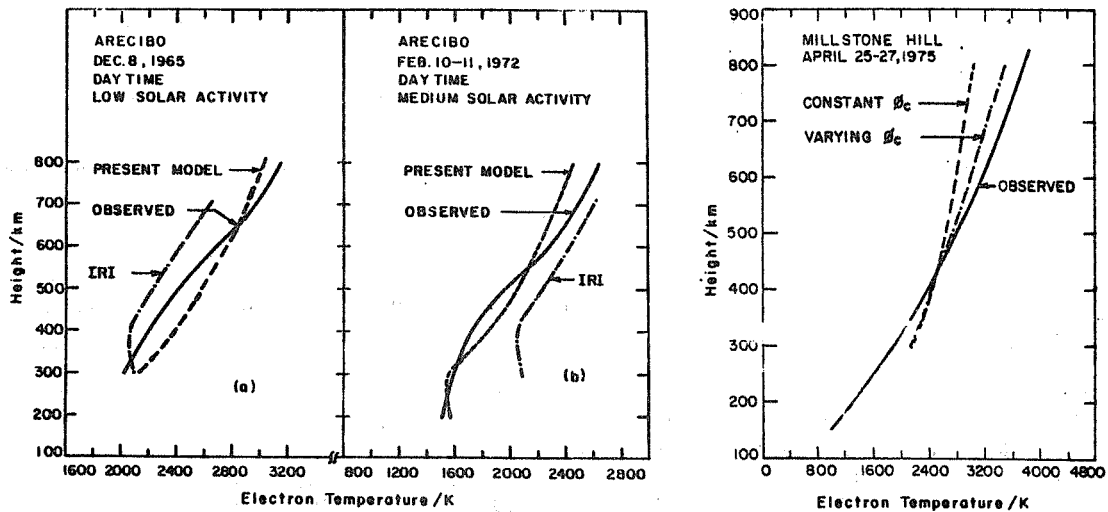


Fig. 4

Fig. 5

- Fig. 2 Comparison of our model and the IRI model with actual T_e measurements at (a) St. Santin (44.6°N) and (b) Malvern (52.1°N) during a medium solar activity period.
- Fig. 3 Comparison of the T_e profiles obtained from the present model and the IRI model with the observed T_e profile for Millstone Hill (42.6°N) during (a) low and (b) medium solar activity conditions.
- Fig. 4 Comparison of the T_e profiles obtained from the present model and the IRI model with the observation at Arecibo (18.3°N) during (a) low and (b) medium solar activity conditions.
- Fig. 5 Comparison of observed T_e profile with T_e values obtained by using constant and altitude varying conduction flux.

2.1.5 Estimation of a Model Electron Temperature Distribution
based on Absorption Measurement

K.B. Serafimov

Central Laboratory for Space Research, Sofia 1000, Bulgaria

Abstract: A method was suggested for determining the electron temperature profile using measurements of the cosmic noise absorption. This method needs supplementing with additional information from various other measurements. A combination of A2-absorption measurement, ionogram and the IRI model opens another way for checking IRI Te-profiles.

Cosmic noise absorption, measured by the A-2 method, gives an opportunity to arrive at an absolute determination of the vertical profile of the electron temperature in the ionosphere, if some shape is assumed. From the expression for the absorption A in a thin plasma (i.e. by electron-ion collisions) we find:

$$A = \frac{\text{const}}{f^2} \int N_e^2 T_e^{-3/2} dh \quad (1)$$

Given an independent measurement of electron density N_e , we can obtain the electron temperature T_e with sufficient precision in the near-maximum part of the F2-layer. With Serafimov and Kutiev /1979/, for $T_e(h)$ we assume a profile consisting of two linear sections, thus characterized by four parameters a to d. With this model we find an equivalent mean value of N_e^2 for the above integral. Pulling this averaged factor before the integral we can solve the remaining integral (with our T_e -profile) in closed form /Nestorov and Serafimov, 1963/ which gives one relation between a to d containing A.

We still need three other relations for determining all four parameters a to d. One stems from the coincidence of T_e with the neutral temperature T_n at the lower boundary ($h = 100$ km), another one from the transition between the two model lines /Serafimov and Kutiev, 1979/. The additional information still needed is taken from an in situ measurement by a suitable satellite (at greater altitude). So we get a to d and a temperature profile around the F2-peak. The most readily available method to obtain the averaged electron density square is using ground-based ionosonde data combined with a model of N_e above the F2-peak, for example the one developed by Serafimov /1977, 1979/. IRI can be used very successfully particularly when NmF and hmF are obtained by ionogram reduction.

Otherwise, profiles of $T_e(h)$ and $N_e(h)$ obtained from IRI could be used directly in Equation (1) in order to obtain a theoretical value of the absorption for each frequency f. In this case IRI appears as a means for testing our use of the A-2 method.

Section 2.2 Ion and Electron Temperatures

2.2.1 The Atmospheric Explorer C Ionospheric Temperatures:

Dependences and Representation

D. Bilitza

Fraunhofer-Institut für Physikalische Messtechnik,
Heidenhofstrasse 8, D-7800 Freiburg, FRG

Abstract: The huge amount of AE-C measurements of electron and ion temperatures was used to investigate their dependences on different ionospheric parameters. This data analysis led to models depending on altitude, geomagnetic latitude, magnetic local time and season. No longitudinal trends were visible in these data. The solar activity dependence needs further investigation, especially by combining all existing reliable electron temperature data. These models use 96 coefficients each, and represent the original data with an average deviation of 8% for the electron temperature and 7% for the ion temperature.

1, Introduction

All modelling attempts to represent ionospheric electron and ion temperatures have so far been restricted by the limited amount of available data /e.g. Spenner and Flugge, 1978; Dorling and Raitt, 1976; Rawer et al., 1978/. Due to the particular satellite orbits, there were gaps in local time, latitude or altitude. Ground-based measurements, which became practicable with the incoherent scatter technique, are restricted to the geophysical conditions of the measuring station.

For the International Reference Ionosphere (IRI) /Rawer et al., 1978a/, satellite and ground-based measurements were combined to give global temperature models. Even so, there are still some shortcomings, as shown in Figure 1, showing the temporal behavior at 20° latitude and 400 km altitude for summer and winter. There is good agreement at 03 h and 15 h where AEROS-data were available for constructing the IRI model. But there are obvious discrepancies in the sunrise and afternoon sectors, and there are significant seasonal changes.

2, Atmospheric Explorer C (AE-C) Data Base

Due to the extended mission time and the chosen orbit, the data of the AE-C satellite is homogenous in most of the important ionospheric parameters. Figure 2 shows that this is valid for the seasonal, temporal and longitudinal coverage, whereas the latitudinal coverage shows a slight preference for the northern hemisphere. The altitude coverage exhibits two maxima at 300 and 400 km. This is due to the year-long circular orbits at these altitudes, which were achieved by using the integrated propulsion system. The vast majority of the measurements were made during medium solar activity, namely in the years 1975-1977.

The measurements used in this study cover the time period from the end of 1973 to the middle of 1978. Electron temperatures were measured by Brace's CEP, and ion temperatures by Hanson's RPA /Radio Science, special issue, 1973/. All data obtained with these two instruments were considered as far as they lie inside the temperature range of 100 K to 6000 K, and in the height range 125 to 1025 km. With these restrictions, there remained about 630 000 electron temperature data points and 400 000 ion temperature data points; that is, about 10 times the amount of data used for IRI-78.

3, Dependences on Ionospheric Parameters

The dependence on six geophysical parameters was tested: altitude, geomagnetic latitude, longitude, geomagnetic local time, season and the Covington index. The geomagnetic local time is based on a magnetic dipole grid and is therefore the adequate time variable relating to geomagnetic coordinates. A short FORTRAN Computer-program for the calculation of the geomagnetic local time, for a given Universal Time, is listed in the Appendix. The well-known latitudinal, altitudinal and temporal behavior of the temperatures /e.g. Schunk and Nagy, 1978; Pilitza, 1979/ was reproduced by the AE-C measurements and is not further discussed in this paper.

3.1 Longitudinal Variation

Longitudinal variations as high as 400 K have been reported by Spenner and Plugge /1979/ for the AEROS satellite data. These were not introduced into IRI. Figures 3 and 4 show the daytime AE-C longitudinal variation for equatorial electron temperature and ion temperature at middle latitudes. No significant longitudinal zones, altitudes and times did disclose any characteristic variation with longitude for either the electron or the ion temperature.

3.2 Seasonal Variation

The importance of seasonal variation is visible in Figure 5 which shows midday latitudinal profiles of the electron temperature at 400 km for summer and winter. Up to about 30° latitude, the winter temperatures are higher than the summer values. For higher latitudes this trend is reversed. This shape is caused by interhemispheric plasma flow from the summer to the winter hemisphere, which shifts the temperature minimum into the summer hemisphere. Besides this seasonal variation, there is only a very slight hemispherical difference as seen in Figure 6, where the winter profile of Figure 5 is reversed in latitude. One might, therefore, take account of seasonal changes by collecting all the summer data in one hemisphere, and all the winter data in the other one.

3.3 Solar Activity Variation

The heat gain and loss of the electron gas both increase with increasing solar activity: the gain due to the increasing solar EUV fluxes and the loss due to the increasing electron density. For higher altitudes a third term becomes important, namely the heat conduction down from the protonosphere, which is also increasing due to the higher escape flux of electrons. For altitudes above 500 km, Mahajan and Pandey /1979/ have reported a general increase with increasing solar activity for the ISIS-1 and EXPLORER 22 satellites. For lower altitudes the loss term, which is proportional to the square of the electron density, becomes the dominant factor and one would expect a decrease in temperature with increasing solar activity. But this is only true for winter when the electron density reaches its seasonal maximum. In the summer months the electron temperature values show a slight increase with increasing solar activity. The same observations were reported by Evans /1973/ for Millstone Hill incoherent scatter measurements.

But this is only a simplified description and Figure 7 shows that further investigations must be made before solar activity changes can be included in an empirical model. This winter plot for the latitude of Arecibo (Puerto Rico) combines AE-C and incoherent scatter data and shows that the electron temperature seems first to increase before it shows the expected decrease. The ion temperature stays almost constant with increasing solar activity as is shown in Figure 8 for middle latitude at noon.

4, Empirical Models

Based on this data analysis, all the AE-C temperatures were collected in boxes defined by the height interval 50 km, the latitude interval 10° and the time interval 2 hours. All data measured between the 90th and 170th day of the year were taken as summer data and collected from the northern hemisphere, and all the other data from the southern hemisphere. Of the so defined 3888 boxes 2509 (65%) were taken in account for the electron temperature model, and 2609 (67%) for the ion temperature model. The rest were filled with less than 50 values and were considered not sufficiently representative.

Then mean values and standard deviations (RMS) were calculated for each box. The rms-percentage-deviation was, in general, below 15% and reached 30% in regions with steep temperature gradients as, for example, for the sunrise period (geomagnetic local time: 04 h to 06 h) and for latitudes close to 30° on both sides of the equator. For the ion temperature, the RMS-deviation is only in a very few cases higher than 20% of the corresponding mean value. Different model functions have been tested for this data set. The best results are given by the following functions:

- power series in cosines and sines of the geomagnetic latitude
- diurnal, semi-diurnal and tetra-diurnal cosine and sine terms of the geomagnetic local time
- hyperbolic series of the altitude.

The 96 model coefficients for both models are listed in Tabel 1 together with the corresponding model terms.

The temperature is finally given by:

$$T_{e/j} / K = 1000 \cdot \sum_{j=1}^{ab} a_j^{e/j} f_j$$

The average percentage deviation from the AE-C mean values is 8% for the electron temperature and 7% for the ion temperature. Figures 9 to 11 show these models together with the AE-C mean values and the RMS-deviations. Figure 11 shows the very good representation of the different electron temperature/altitude profiles. In Figures 10 and 11 latitudinal profiles for the electron and ion temperature are presented. The seasonal variation (= interhemispheric variation) given by the AE-C data is well reproduced by our models for both sets of temperatures.

The validity range is about -60° to $+60^\circ$ geomagnetic latitude. Above these latitudes the day-to-day variations become so large that other influences have to be considered before further empirical modelling can go on.

Discussion remark:

K.K.Mahajan pointed out that in the F-region as well as in the top-side ionosphere electron temperature is finally controlled by the electron density though heat flux down from the protonosphere dominates at greater heights.

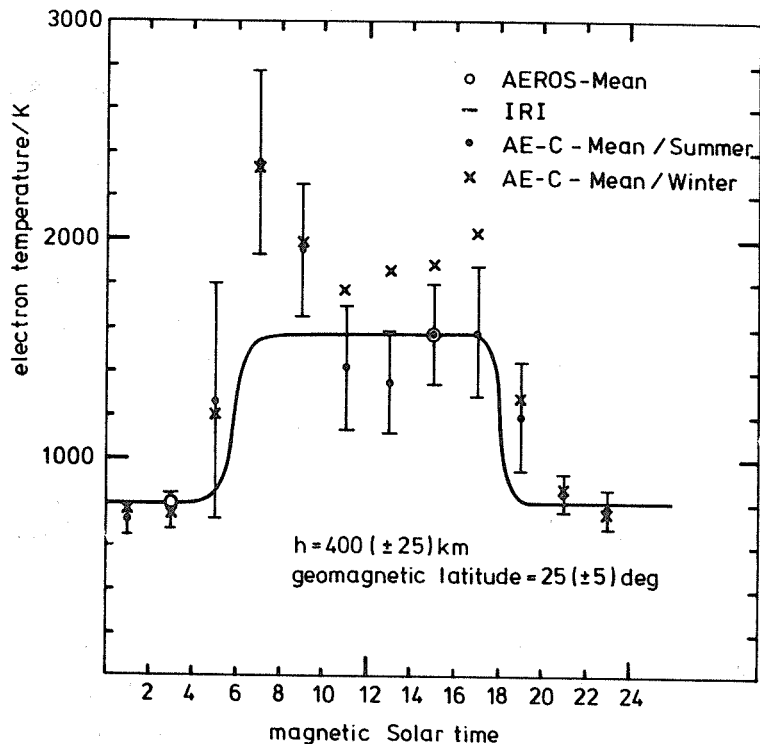


Fig. 1

Fig. 1 Comparison between the diurnal variation of the AE-C satellite data and the IRI model, (IRI is based on AEROS measurements).

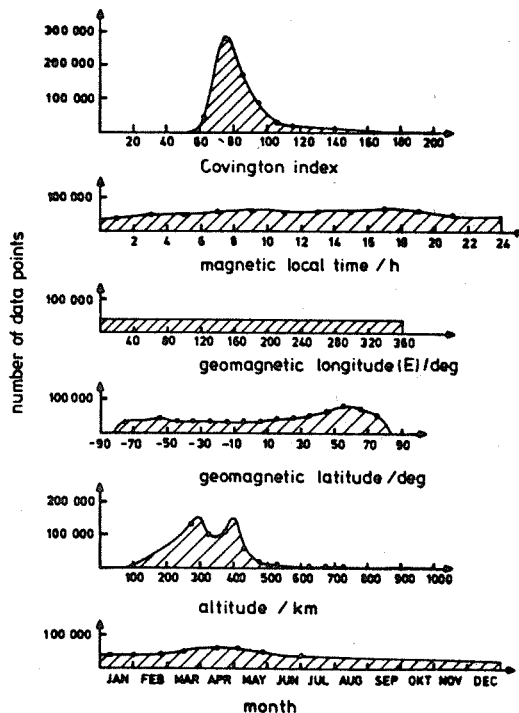


Fig. 2

Fig. 2 Data coverage of the AE-C mission for some important ionospheric parameters.

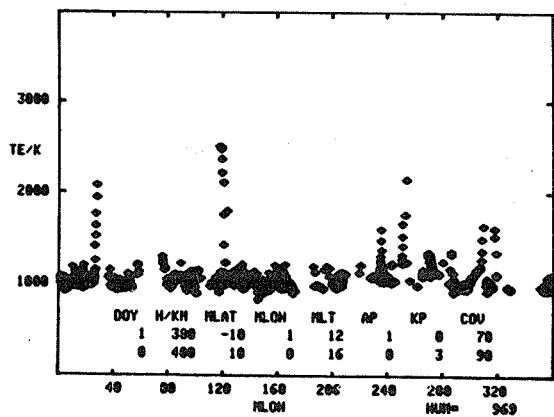


Fig. 3

Fig. 3 Longitudinal variation of the electron temperature at the magnetic equator during midday at 400 km altitude (AE-C data).

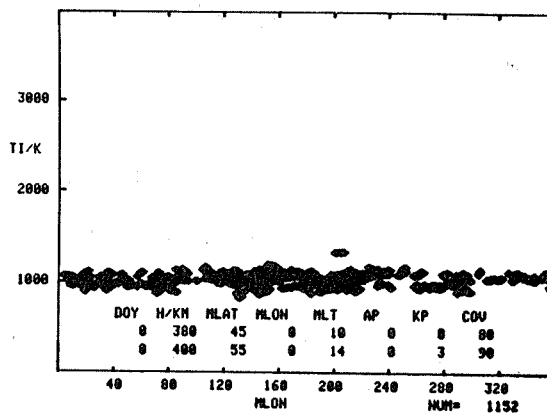


Fig. 4

Fig. 4 Longitudinal variation of the ion temperature at middle latitudes during midday at 400 km altitude (AE-C data).

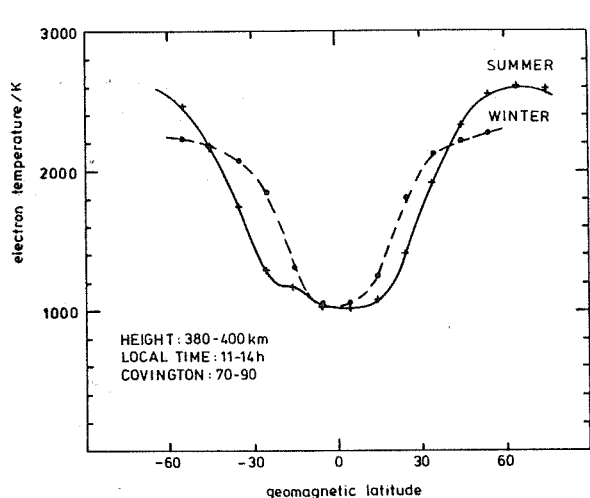


Fig. 5

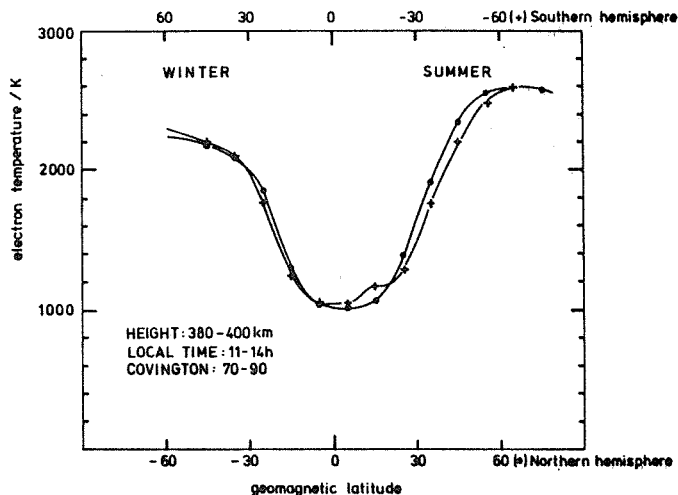


Fig. 6

Fig. 5 Latitudinal profiles of the electron temperature at 400 km altitude during noon for summer and winter (AE-C data).

Fig. 6 Interhemispheric differences of the electron temperature after the exclusion of seasonal effects (same as Fig. 5 with the winter profile reversed in latitude).

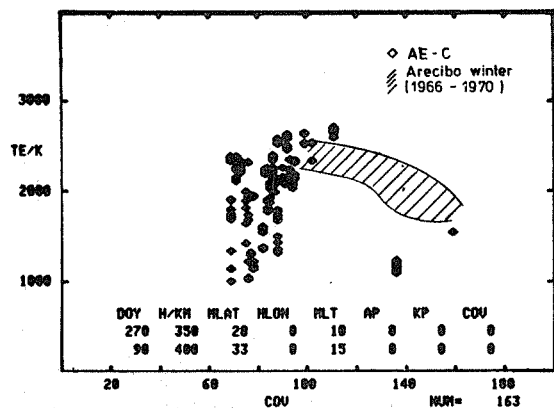


Fig. 7

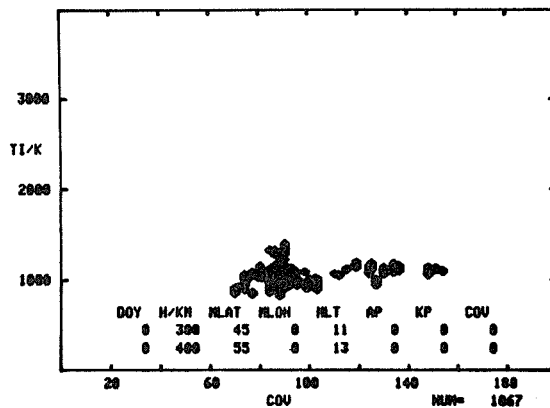


Fig. 8

Fig. 7 Solar activity variation of the electron temperature during noon at 400 km altitude including AE-C and Arecibo data.

Fig. 8 Solar activity variation of the ion temperature during noon at 400 km altitude (AE-C data).

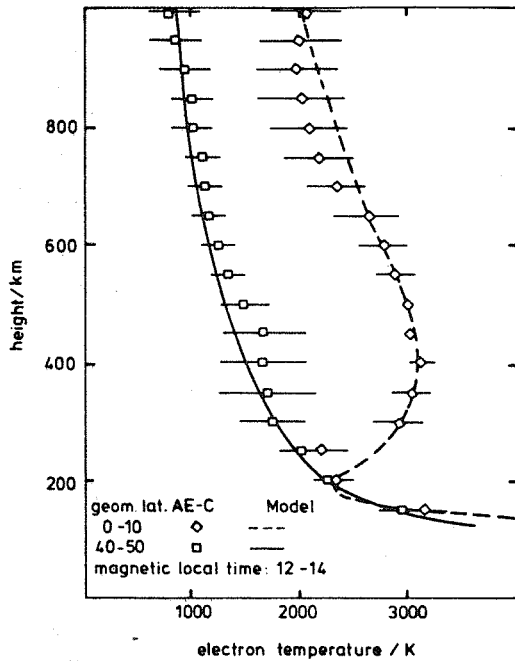


Fig. 9

Fig. 9 Model and AE-C mean values for the electron temperature at noon for equatorial and middle latitudes.

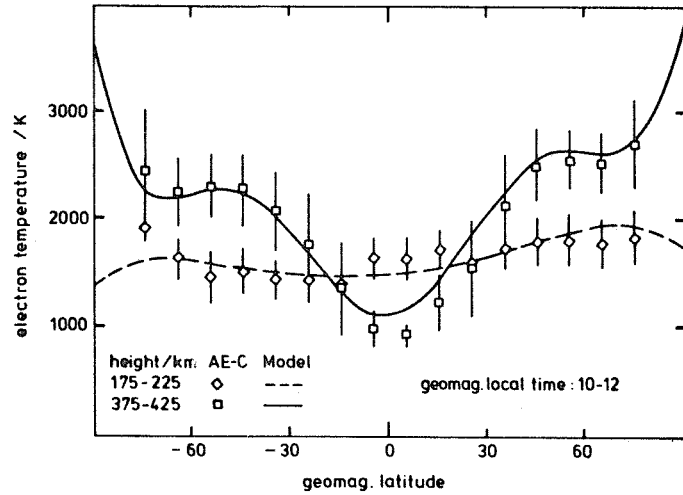


Fig. 10

Fig. 10 Model and AE-C mean values for the electron temperature during noon at 200 and 400 km altitude.

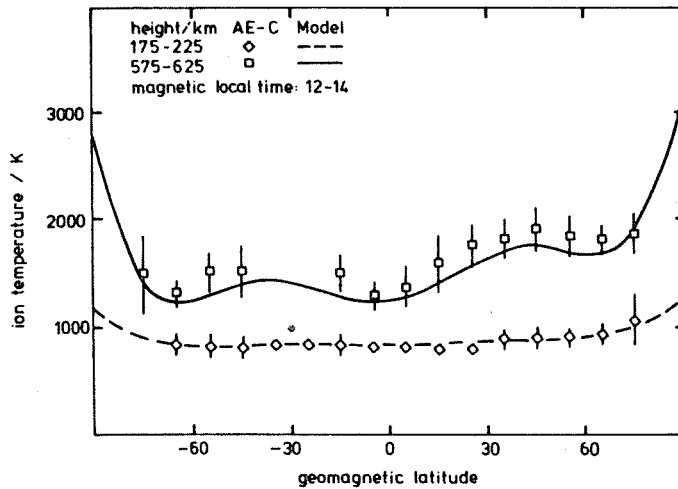


Fig. 11 Model and AE-C mean values for the ion temperature during noon at 200 and 600 km altitude.

Table 1 Model coefficients for electron and ion temperature

	a ^e electron temperature	a ⁱ ion temperature	model functions f _j
1	-.3358740E 03	.9906284E 00	1 x = h/100
2	-.6412821E 01	-.3049664E 01	1/X
3	-.3203497E 00	.2382582E 01	1/(X·X) h = altitude/km
4	.5127223E 01	.1237424E 00	1/(X·X·X)
5	-.1328166E 01	.3638997E 01	cos ₂ ∅ ∅ = geomagnetic
6	.3381968E 03	-.7645646E 00	cos ₂ ∅ latitude
7	.1846130E 01	-.1368674E 01	cos ₃ ∅
8	.1495915E 02	.2194481E 02	cos ∅ · cos q
9	.1333760E 02	.1832292E 02	cos ₂ ∅ · sin q q = t/24.360
10	-.3689317E 02	-.4668504E 02	cos ₂ ∅ · cos q
11	-.2199329E 02	-.3767337E 02	cos ₂ ∅ · sin q
12	-.4388884E 01	-.4113288E 01	cos ₂ ∅ · cos 2q t = magnetic
13	-.2570671E 01	-.2267290E 01	cos ₂ ∅ · sin 2q local time
14	.2043260E 02	.2320683E 02	cos ₃ ∅ · cos q
15	.7914203E 01	.1930351E 02	cos ₃ ∅ · sin q · 1
16	.4313878E 01	.3755526E 01	cos ₃ ∅ · cos 2q
17	.2522843E 01	.1722568E 01	cos ₃ ∅ · sin 2q
18	.2000630E 00	.5006589E 00	cos ₃ ∅ · cos 3q
19	.3632239E-01	.5322000E 00	cos ₃ ∅ · sin 3q
20	.3215081E 00	.6470600E 00	sin ∅
21	-.1398544E 00	-.3039238E 00	sin ∅ · cos q
22	-.3505225E 00	-.2542804E 00	sin ₂ ∅ · sin q
23	.3398679E 03	.1211601E 01	sin ₂ ∅
24	-.6815014E 00	-.3091343E 01	sin ₂ ∅ · cos q
25	-.2000354E 01	-.2566834E 01	sin ₂ ∅ · sin q
26	.6978825E 00	.7315934E 00	sin ₂ ∅ · cos 2q
27	.2200378E 00	.2842279E 00	sin ₂ ∅ · sin 2q
28	-.2771191E 02	-.4745862E 02	
29	.8632736E 02	.4056699E 02	
30	-.6638417E 02	-.1879764E 01	
31	-.3195663E 02	-.1266817E 03	
32	-.1086786E 03	-.1324840E 03	
33	.8739856E 02	.2734424E 03	
34	.1427998E 03	.2631538E 03	
35	.4007463E 02	.3151476E 02	
36	.2082120E 02	.1272292E 02	
37	-.4427658E 02	-.1368709E 03	
38	-.2432663E 02	-.1298712E 03	• 1/X
39	-.4255315E 02	-.2962019E 02	
40	-.2277191E 02	-.8841489E 01	
41	.1035672E 01	-.3144746E 01	
42	-.4085462E 00	-.4010081E 01	
43	-.1762616E 01	-.4163472E 01	
44	.4568237E 00	.1973166E 01	
45	.3213736E 01	.2509285E 01	
46	.0000000E 00	.0000000E 00	
47	-.1035548E 02	.1688126E 02	
48	.2119308E 02	.1918030E 02	
49	-.7373666E 01	-.5476406E 01	
50	-.1095351E 01	-.1097859E 01	

Table 1 cont.

	a^e electron temperature	a^i ion temperature	model functions f_j
51	.1501077E 03	.1261199E 03	
52	-.3831550E 03	-.1232017E 03	
53	.2700867E 03	.2137534E 02	
54	.2994405E 01	.2337860E 03	
55	.2448044E 03	.3024512E 03	
56	-.3910170E 02	-.5203628E 03	
57	-.2551194E 03	-.5856938E 03	
58	-.1021360E 03	-.7574243E 02	
59	-.5999553E 02	-.2518782E 02	
60	.4828246E 01	.2655803E 03	
61	-.1845251E 02	.2797507E 03	" $\cdot 1/X^2$
62	.1114461E 03	.7286549E 02	
63	.6783919E 02	.1661172E 02	
64	-.4451051E 01	.6416303E 01	
65	.4171057E 00	.9509613E 01	
66	.5200229E 01	.9681511E 01	
67	-.1145819E 01	-.3735500E 01	
68	-.8138241E 01	-.6785177E 01	
69	.0000000E 00	.0000000E 00	
70	.3575121E 02	-.2804993E 02	
71	-.5467485E 02	-.4452098E 02	
72	.1791576E 02	.1263747E 02	
73	.2654136E 01	.1425881E 01	
74	-.1577780E 03	-.1011870E 03	
75	.3836948E 03	.1079866E 03	
76	-.2611238E 03	-.2678857E 02	
77	.1395706E 02	-.1368674E 03	
78	-.1548326E 03	-.2138656E 03	
79	-.1102847E 02	.3156904E 03	
80	.1077704E 03	.4053516E 03	
81	.7696506E 02	.5597430E 02	
82	.5392638E 02	.1772145E 02	
83	.2334969E 02	-.1645084E 03	
84	.7063438E 02	-.1878884E 03	" $\cdot 1/X^3$
85	-.8492555E 02	-.5480295E 02	
86	-.6118703E 02	-.1173001E 02	
87	.3709023E 01	-.4223662E 01	
88	.3701853E 00	-.7025101E 01	
89	-.4913782E 01	-.7377697E 01	
90	.1187514E 01	.2205447E 01	
91	.6253740E 01	.5518394E 01	
92	.0000000E 00	.0000000E 00	
93	-.2735152E 02	.1438439E 02	
94	.3958183E 02	.3181740E 02	
95	-.1234585E 02	-.9011836E 01	
96	-.2330353E 01	-.7199816E 00	

Appendix

FORTRAN program for calculation of the geomagnetic local time in hours (decimal) for given universal time (UT/sec), geodetic latitude and longitude (XLAT, XLONG/deg) and day of the year (DAY)

```
REAL FUNCTION (UT, XLAT, XLONG, DAY)
C  CALCULATES GEOMAGNETIC LOCAL TIME (HRS), UT=GMT(SEC),
C  XLAT/XLONG=GEODETIC LATITUDE/LONGITUDE(DEG)
C  DAY=DAY OF YEAR
RAD=57.29578
FLAT=XLAT/RAD
FLONG=XLONG/RAD
DELTA=0.409207 * SIN((DAY-80.0) * 3.14159/184.0)
BETA=(180.0-UT/240.0)/RAD
PX=COS(FLAT) * COS(FLONG)
PY=COS(FLAT) * SIN(FLONG)
PZ=SIN(FLAT)
SX=COS(DELTA) * COS(BETA)
SY=COS(DELTA) * SIN(BETA)
SZ=SIN(DELTA)
P1=0.35117 * PX-0.91483 * PY-0.19937 * PZ
P2=0.93358 * PX+0.35837 * PY
S1=0.35117 * SX-0.91483 * SY-0.19937 * SZ
S2=0.93358 * SX+0.35837 * SY
THETP=ATAN2(P2,P1)
THETS=ATAN2(S2,S1)
FMLT=(THEPT-THETS+3.141593)/.2617994
IF (FMLT.GT.24.0) FMLT=FMLT-24.0
IF (FMLT.LT.0.0) FMLT=FMLT+24.0
RETURN
END
```

2.2.2 Comparison of the Ion Density and Temperature Data Obtained by the RPA on CGC-6 and the IRI Model

Ts.P. Dachev, M.S. Trendafilov, D.G. Goshev

Central Laboratory for Space Research, BAN,
Bul. Russki No.1, Sofia 1000, Bulgaria

Abstract: A comparison is made between the ion concentration and temperature data as measured by the RPA on board CGC-6 and as calculated using the IRI model. The analysis refers to 100 orbits in the region $+50^\circ$ dip latitude and all longitudes. The discrepancies between the model and measured quantities at different values of the magnetic declination are carefully analyzed. The graphs show that these discrepancies at large absolute values of the magnetic declination are connected with the direction of the neutral winds. In this paper we consider the possibility of including in future IRI models the magnetic declination as a factor which determines the magnitude and direction of interaction between neutral winds, and the distribution of ion concentration and temperature at different seasons and local times.

1, Introduction

The theoretical determination of ion and electron concentration and temperature and ion composition is still an unsolved problem in spite of the existence of longterm ground and satellite measurements. The IRI model /Rawer et al., 1978a/, and its latest modification IRIAL-7, December 1979, appears to be a universal program for computing the parameters mentioned above, together with complementary information about neutral temperature in the height range of 70 to 1000 km. The model could be considerably improved and enlarged if we took into consideration, and included in it, results from satellite in situ measurements; these reveal mainly space variations generated by global changes in the configuration of the Earth's magnetic field, and the interactions between the ionospheric plasma and the dynamics of the neutral atmosphere /Hanson et al., 1970/.

In the present study a comparison is made between the ion concentration and the temperature data as measured by the RPA on board the CGC-6 satellite /Mayr et al., 1978/, and those calculated from the IRI model for specifically selected transits of the satellite; the comparison will confirm the necessity of taking into consideration the magnetic declination /Eyfrig, 1963; Kohl et al., 1969; Dachev, 1978/ as one of the necessary factors for a more accurate prediction of the ionospheric parameters at a fixed local time and season.

2, Results

Data on ion density and temperature, which are interpreted in this paper are obtained by a RPA on board the CGC-6 satellite /Dachev et al., 1980/. Transits numbered from 3480 to 3631 within the interval February 1 to 11, 1970 are considered. The satellite perigee at these transits is located in the northern hemisphere at $60^\circ - 70^\circ$ dip latitude. The local time of equatorial passage varies between 22 30 and 00 30 LT. The satellite height is about 600 km in the magnetic equator region.

The data for the ion concentration and temperature are taken from the original photofilms received from the World Data Center-A by our laboratory, and introduced as an array into a computer for fixed dip latitudes in the interval $+50^\circ$. By averaging the original data for position and time of the satellite, the geographical and time characteristics needed as inputs into IRI were determined. As solar activity measure the Zürich sunspot number for February 1970 was taken. The IRIAL-7 program was used

together with a special magnetic tape containing the CCIR coefficients for deducing the foF2 and M3000/HMF2 values. The results obtained from the comparison of data obtained by the longitude of orbit No 3568 are shown in Figure 1. The measurement was made on Febr. 7, 1970 when geomagnetic conditions were quiet (Kp = 2.25, Ap = 2 and R = 104). The sunspot number was near the average for that period. In the upper part of the Figure the electron concentration as computed by the IRI model is shown with a solid line; the concentration of the oxygen ions from data obtained by the RPA on board the OGO-6 satellite is plotted with crosses and the total ion concentration is shown with a thin line. In the lower part of the Figure, the comparison between the measured and computed values of the electron temperature is shown. The computed temperature values according to the IRI model are shown with a solid line and the temperature measured by the satellite is shown as a dotted line. The changes of the parameters TNOR, NNCR and NNCRREC⁺, shown in Figure 2, are defined as follows:

$$TNOR = \frac{Ti(OGO) - Ti(IRI)}{Ti(IRI)} \% ; \quad NNCR = \frac{Ni(OGO) - Ni(IRI)}{Ni(IRI)} \% ;$$

$$NNCRREC^+ = \frac{NiO^+(OGO) - NiO^+(IRI)}{NiO^+(IRI)} \% \quad (1)$$

The parallel interpretation of the results given in Figures 1 and 2 shows a change in the sign of TNOR and NNCR near the magnetic equator, while NNCRREC⁺ reaches its maximum value near -10° dip latitude. The differences between the measured and calculated O⁺ ion concentrations are very great and attain values of 4000 cm⁻³. At the same time it is seen that the O⁺ ions are dominant over the whole latitude range (Figure 1); the maximum concentration of other types of ions, mainly H⁺ and He⁺, occurs at about 40° dip latitude and is not greater than 30% of the total ion density. A similar comparison is shown in Figure 3, for orbit No 3507 which differs from No 3568 only in the sign and magnitude of the magnetic declination DMAG. As in Figure 1 a change in the measured and calculated values near the magnetic equator is seen. The variations of NNCR, TNOR and NNCRREC⁺ are similar to those in Figure 2, but the extreme values appear to occur at different dip latitudes.

3, Discussion

The differences, shown in Figures 1 and 3, between the values of ion concentration and temperature obtained using the IRI model, and those obtained by the RPA on board the OGO-6 satellite are due to differences which were observed in the sign and magnitude of the magnetic declination for both orbits. For orbit No 3507 the declination is negative and has a maximum value, while for orbit No 3568 it is positive. These conditions are favourable for a large vertical plasma drift, generated by zonal neutral winds /Serafimov et al., 1980; Kumar and Hanson, 1980/. The direction of the drift component in both hemispheres is shown in Figures 1 and 3. It is seen that, in the regions where the vertical drift is upwards, the experimental values of concentration are higher than those obtained by the IRI model, and vice versa. In the same regions, after Kishbeth et al. /1977/, the behavior of ion temperature is related to the adiabatic heating and cooling of the plasma.

4, Conclusions

The observed differences between the experimental and theoretical values of the ion concentration and temperature are strongly dependant on the geographical longitude and the magnetic declination of the place. This suggests the need for an improvement of the IRI model which would take account of the values of magnetic declination and longitude together with a model of wind motions in the neutral atmosphere at a fixed season and local time.

Acknowledgements: The authors are grateful to Prof. F. Rauer for giving them an opportunity to work with the latest modification of the IRI model, and to A. Vassileva and M. Minkova for the technical assistance during the preparation of this paper.

Discussion remarks:

K. Rauer pointed out that the CCIR model used to describe the planetary behavior of the peak is too much smoothed. This is particularly serious in the equatorial region where high peaks occur at slightly variable latitude.

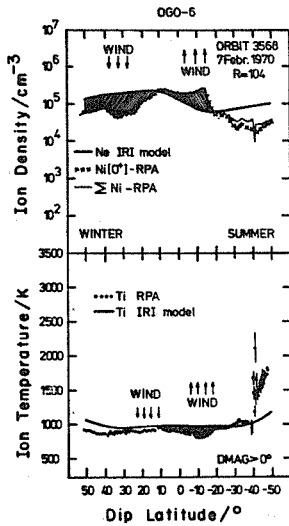


Fig. 1

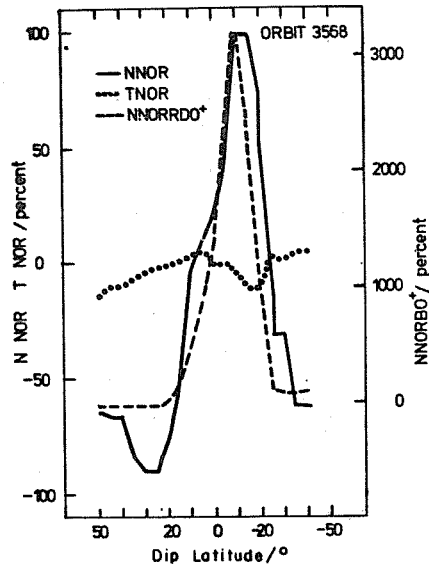


Fig. 2

Fig. 1 Comparison of IRI with OGO-6 measurements of ion concentration and ion temperature under conditions where the magnetic declination (DMAG) was positive. Ionospheric plasma drift due to zonal neutral winds is indicated by arrows.

Fig. 2 Percentage variations of the parameters of Equation (1) with dip latitude.

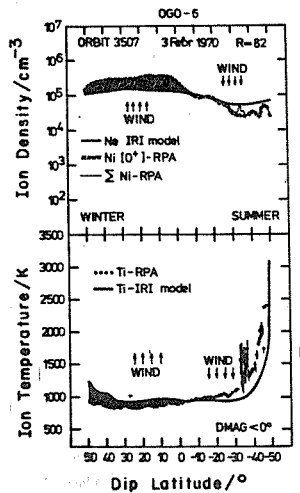


Fig. 3 Comparison of IRI with OGO-6 measurements as in Fig. 1 but for negative declination.

2.2.3 Comparison of the IKI with Ion Temperature and Ion Density as Measured during Very Quiet Geomagnetic Conditions on board the Geophysical Rocket "Vertical-6"

F. Lencze, K. Kovács¹, I. Apa'thy, I. Szemerey²,
V. Afonin, V. Lezrukih, N. Shutte³

¹Geodetical and Geophysical Research Institute Hungarian Academy of Sciences, Sopron, Hungary

²Central Institute for Physics, Hungarian Academy of Sciences, Budapest, Hungary

³Institute for Space Research, Academy of Sciences of the USSR, Moscow, USSR

Abstract: During a magnetically quiet time ion temperature and ion density up to 1500 km were measured on 25 Oct. 1977 during the flight of the geophysical rocket "Vertical-6" by means of a group of five retarding potential analyzers, looking into different directions of space. The results when compared with the International Reference Ionosphere 1978 show that both the ion temperature and the ion density are lower than the values predicted by the Reference Ionosphere, the difference decreasing with increasing altitude.

1, Introduction

The geophysical rocket "Vertical-6" was launched on 25th October 1977 at 1515 LMT, at middle latitude in the European part of the USSR in the framework of the complex investigation of the upper atmosphere organized by Inter osmos. The trajectory of the rocket was very close to the vertical, the deviation being not greater than about 3°. The rocket was stabilized along three axes with an accuracy of +3° and reached an altitude of 1500 km. The measurements, discussed here, were carried out by means of a group of five retarding potential analyzers (RPA) looking into different directions in space.

The experiment is particularly interesting for two reasons: on the one hand, rocket experiments reaching an altitude of 1500 km are rare, and on the other hand the date is in the minimum of the solar cycle during a period of very low activity. At the launch day the relative sunspot number was 28, Covington's solar radio flux index was 88.1. Geomagnetically the conditions were extremely quiet ($K_p = 0$). We thus had the exceptional situation of completely undisturbed conditions.

2, Methods of Analysis

The ion temperature and ion density were determined, by multi-parameter curve fitting partly from the characteristic curves of the analyzer looking upwards and partly from the data given by one of the RPAs looking in the horizontal direction /Knudsen, 1966; Moss and Hyman, 1968; Hanson et al., 1970/. The model values have been computed using the procedures given in the International Reference Ionosphere 1978 /Rawer et al., 1978a/, however, when calculating the ion temperature, the smoothing procedure designed to keep it less than the electron temperature has been not used, as it was clear in advance that the ion temperature would satisfy this condition. As regards the determination of the total ion density in the height range between $h_m F_2$ and 1000km, for the harmonized Bent-model the maximum electron density has been computed by means of the subroutine IONDEM, i.e. after the simplified equations of Chiu.

3, Results and Proposed Improvements

The ion temperatures obtained from the measurements were compared with the model values computed for the time of the apogee of the trajectory in Figure 1; the neutral temperature, computed on the basis of CIRA /1972/ is also plotted. Below about 550 km the computed values of ion temperature differ considerably from the measured ion temperature which approaches the neutral temperature. Above this altitude the measured data show a steep gradient and the model approaches the observed ion temperature at about 700 km. Then the model deviates more and more from the measured data with increasing height showing the largest difference at about 800 km. Above this height the computed values again approach gradually the observed values. The difference between the measurements and the average model may be due to the quiet conditions.

In figure 2 the computed values of electron density and the measured total ion density are shown. It can be seen that the computed electron density is **greater** than the observed value along the whole profile, the difference decreasing somewhat with increasing height. However, the shapes of the two profiles are practically identical. The difference between both profiles may be due largely to the Chiu value of foF2 being too great.

I would be not proper to suggest any improvement of the IKI on the basis of only one experiment; therefore the discussion has been confined to the presentation of results.

Editor's remark:

The shape of the observed instantaneous temperature profile might be strongly influenced by atmospheric gravity waves. As for electron density the agreement with an average profile could not be better due to the known large variability.

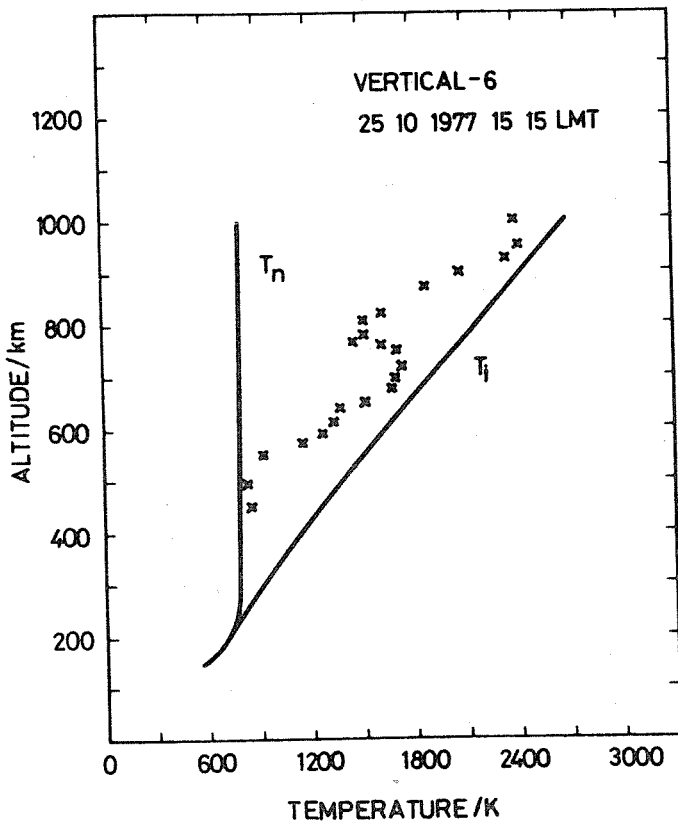


Fig. 1 Variation of the neutral and ion temperatures (T_n , T_i) with altitude computed for the time of apogee with CIRA 1972, and the International Reference Ionosphere 1978, respectively (full lines). The measured ion temperature is denoted by crosses.

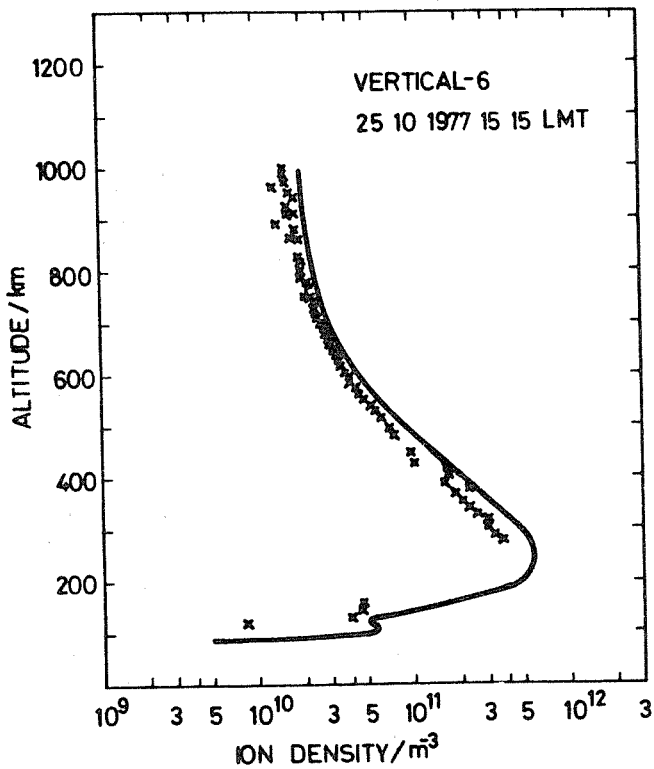


Fig. 2 Electron density profile computed on the basis of the International Reference Ionosphere 1978 for the time of apogee (full line). Measured total ion densities are denoted by crosses.

2.2.4 Observation of N_e , T_e and T_i by Incoherent Scatter

Technique during a Period of Low Solar Activity

V.I. Taran, E.V. Rogozhkin, D.A. Dzyubanov

Kharkov Polytechnical Institute, USSR

Abstract: Altitude dependencies of N_e , T_e and T_i for 1975 obtained at the research incoherent scatter facility of the Kharkov Polytechnical Institute (operating frequency 150 MHz, parabolic antenna, diameter 100 m) are compared with model dependencies. The measured values of N_e at the peak and lower levels are in good agreement with the model, while those of T_e and T_i are different than given by the model.

1, Measurement and Reduction

An incoherent scatter facility for research has been created at the Kharkov Polytechnical Institute operating at a frequency of about 150 MHz /Taran, 1976/. It has two channels, which makes it possible to transmit and receive pulses with a peak power of 2 MW, and feeds a parabolic Cassegrain antenna, whose diameter is 100 m. The system noise temperature is less than 500 K.

To determine electron density and temperatures, autocorrelation functions were determined from the return signals. For altitudes up to 400 to 500 km, double pulses are used and the autocorrelation function is measured directly. For greater altitudes, so as to increase the signal/noise ratio long pulses of about 1 ms are used at a pulse repetition frequency of 25 Hz. Integration time, determined by the experimental conditions, can vary from 1 to 3 min. The electron density is calculated either from the measured power profile of the scattered signal, allowing for the temperature ratio, or from extreme points of the power profile when sounding with linearly polarized signals. In the former case the electron density profile obtained is normalized either to vertical sounding data or to Faraday rotation data. Since the autocorrelation function is measured at the intermediate frequency one can identify the Doppler shift of the carrier frequency caused by the ionospheric plasma drift along the line of sight.

2, Comparison with IRI

To compare the results for 1975 with the preliminary IRI /Rawer et al., 1975/, average 3-day data were used representing winter, summer and equinox periods.

Figure 1 shows the altitude-time variation of electron density as contours of constant plasma frequency; solid arrows identify local sunrise and sunset, dashed arrows sunrise and sunset at the geomagnetically conjugate point. Apart from the well-known seasonal/diurnal variations, the daytime F-region peak electron density is about 10% greater in winter than in summer, and the peak altitude is 40 km lower. In summer, when the sunset at the conjugate point leads the local sunset, an increase in electron content can be observed at that time, as well as at that of local sunset. As for electron temperature, in summer (Figure 2) the start of the morning rise is related with the local sunrise, but in winter with the sunrise at the conjugate point. The ion and electron temperature variations (Figure 3) are, in general, similar. Below 300 km the ion temperature shows little diurnal variation, because of thermal equilibrium between ions and neutrals; as the altitude increases the ion temperature approaches the electron temperature. Figure 4 shows the comparison between noon experimental and model electron density profiles (at the left hand), and between the kinetic

temperatures of charged particles. In Figure 4a (June) there is no great difference between model and experimental values of electron density at the F-region peak, the altitude of which differs by only 20 km. The F1-layer is very clearly seen in the experimental data. Particularly at lower heights the measured electron temperature is lower than the model values. As for the ion temperature, up to 400 km the measured values are equal, but for greater altitudes they are higher than the model values. There are no great differences between the vertical gradients of kinetic temperatures.

In autumn (Figure 4b) fairly good agreement of electron density values is seen for altitudes above the peak. The measured temperature of charged particles differs from the model values by 200 to 400 K, while the values of the vertical gradient do not differ much.

In winter (Figure 5), both in the daytime and at night, the measured electron density does not differ much from the model values in the lower ionosphere, but above the peak this difference increases with altitude, experimental values being lower than the model ones.

One of the general differences between the experimental and the model values is that the amplitudes of measured seasonal variation of the altitude of the F-region peak are greater than those in the model; besides, in all seasons the measured nighttime electron and ion temperatures are equal.

Some of the differences may be due to experimental errors and to the fact that the actual and the local geophysical conditions do not coincide. The latter factor is apparently real, since the geomagnetic field was disturbed on nearly all the days of the measurements.

Discussion remarks:

K. Rower pointed out that the IRI (electron density) scale height formula provides transition to infinity at great heights. Apparently, the transition, assumed after Alouette 1 data, should occur at even higher altitude.

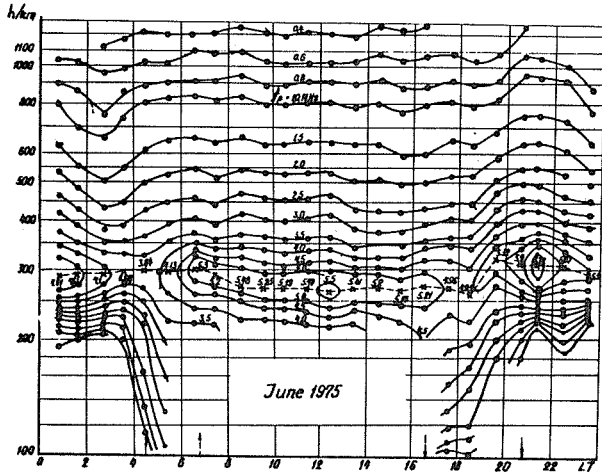


Fig. 1 Contours of equal plasma frequency measured at Kharkov, June 1975. Sunrise and sunset at Kharkov are indicated by solid arrows, and at the conjugate point by dashed arrows on the abscissa.

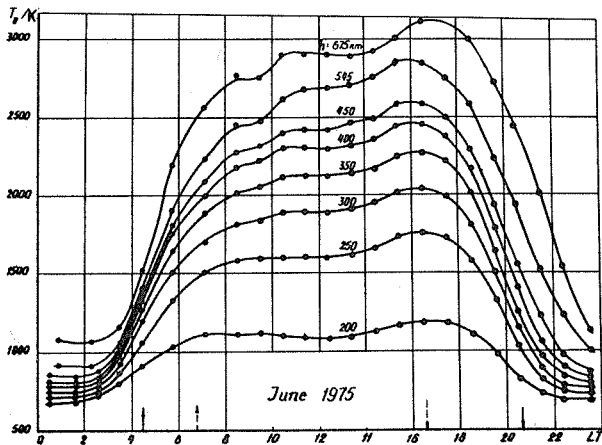


Fig. 2 Electron temperature measured at Kharkov, June 1975.

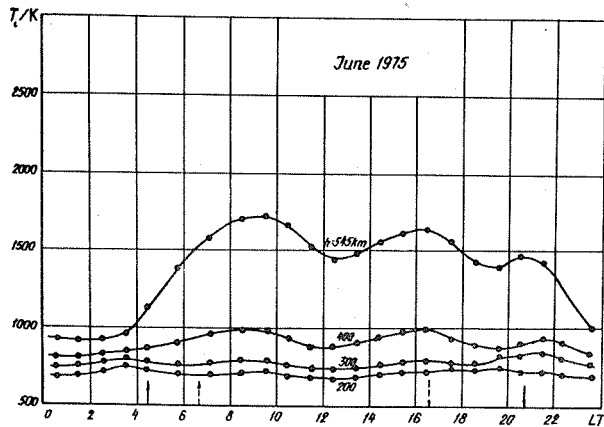


Fig. 3 Ion temperature measured at Kharkov, June 1975.

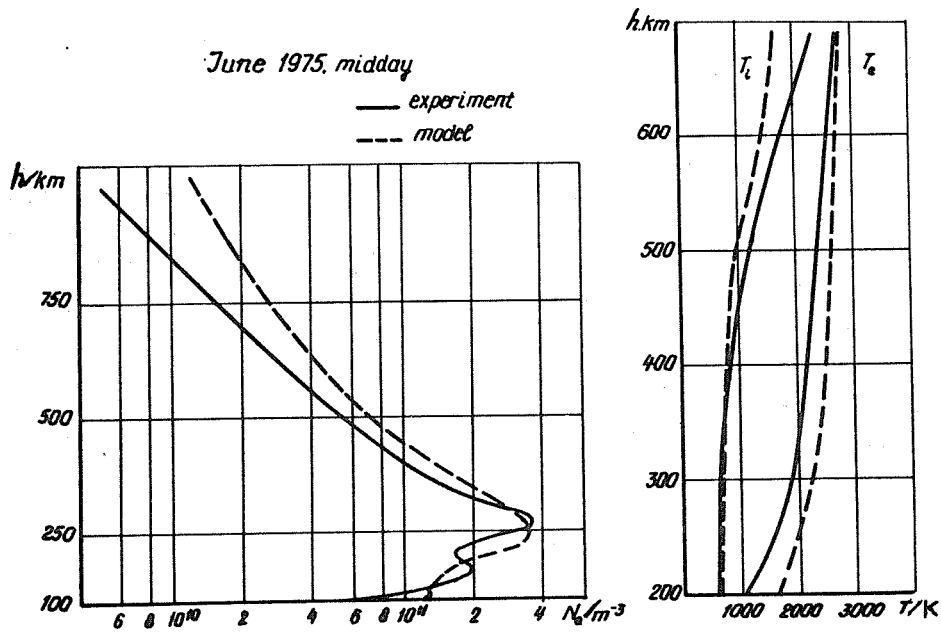


Fig. 4a

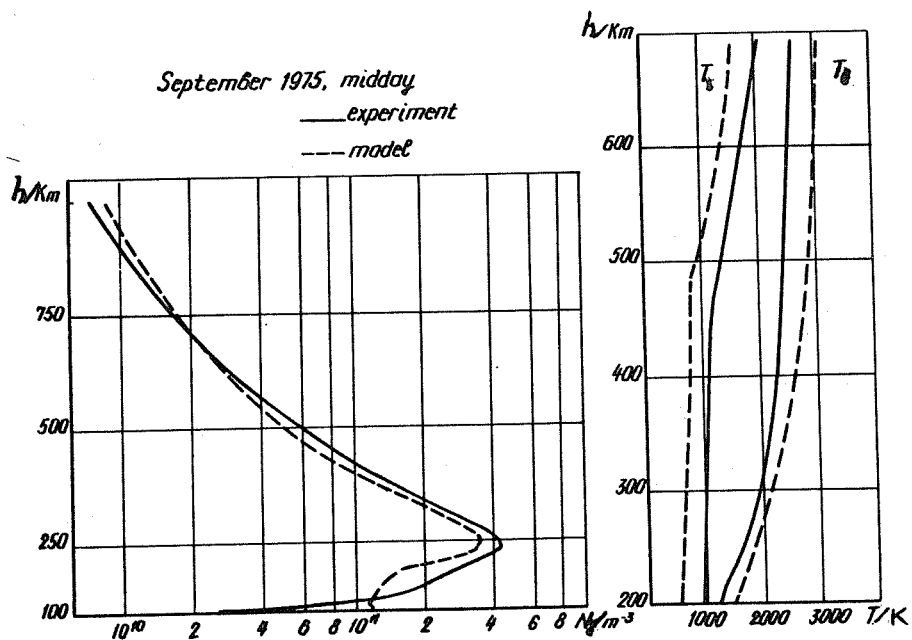


Fig. 4b

Fig. 4 Comparison between electron density (left) and kinetic temperature (right) profiles. The measured profiles are shown as full lines and those based on the IRI model by dashed lines. (a) June 1975; (b) September 1975, both for noon at Kharkov.

December 1975

— experiment

--- model

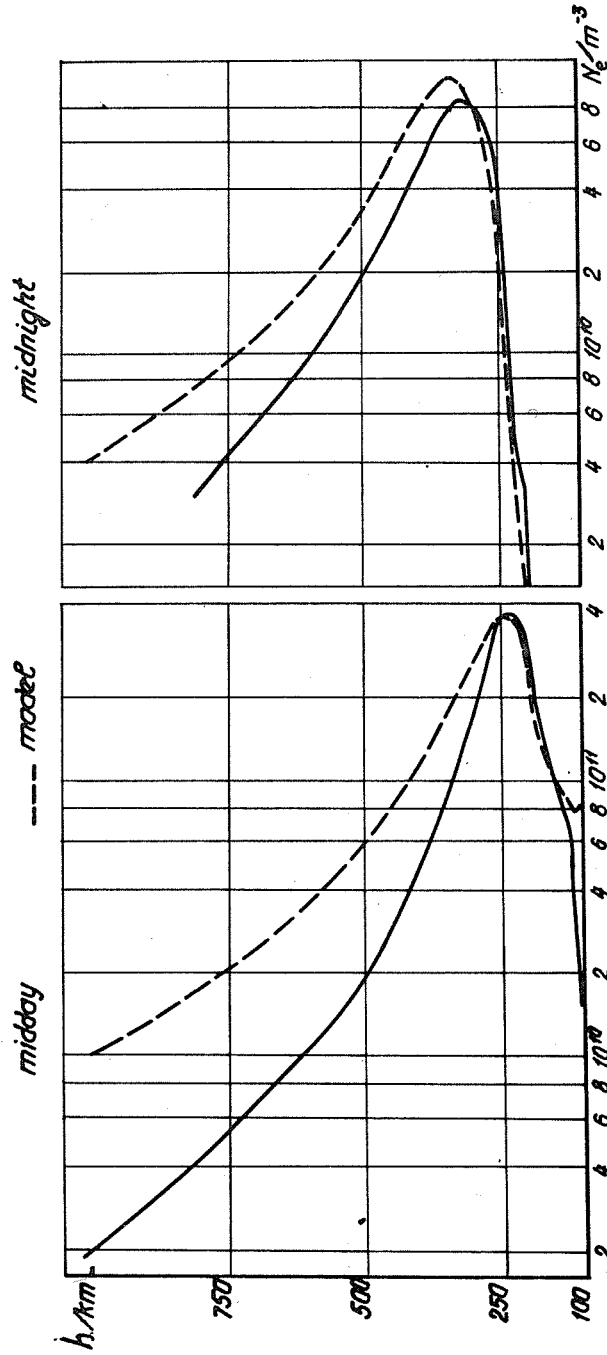


Fig. 5 Comparison between measured (full lines) electron density profiles, and those based on the IRI model (dashed lines) at midday (left) and at midnight (right). Kharkov, December 1975.

Section 2.3 Variability

2.3.1 Studies of the Topside Ionosphere Using the Satellite

"Interkosmos-19"

(I) The Ionospheric Satellite "Interkosmos-19"

M.M. Gogoshev¹, A. Kiraga, Z. Klos², K. Kubat³
Yu.V. Kushnerevsky, V.V. Migulin⁴, K.B. Serafimov¹,
P. Triska³, M.D. Fligel⁴, J. Similauer²

¹Central Laboratory for Space Research, Bulgarian Academy of Sciences

²Space Research Centre, Polish Academy of Sciences

³Geophysical Institute Czechoslovak Academy of Sciences

⁴Institute of Terrestrial Magnetism, Ionosphere and Radio Wave Propagation, Academy of Sciences, USSR

The possibility of constructing a global ionospheric model depends on the systematic study of the parameters and processes occurring around the main peak of the ionosphere. The scientific instrumentation of a new satellite in the Interkosmos program is adapted to this task. Interkosmos-19 was launched on 27 Febr. 1979 into an 74° elliptical orbit with apogee of 996 km, perigee of 500 km and period of 100 min /Pravda, 1979; Migulin, 1979/. It is stabilized along three axes, with the main axis oriented towards the centre of the Earth (Figure 1) /Kushnerevsky and Vasilev, 1980/.

The primary aims of the 'Ionosonde-IK' space-craft were:

- 1) to study global electron density distribution in the topside ionosphere, its dependence on local time, and connections with solar and geomagnetic activity;
- 2) to study ionisation processes, particle precipitation, and the generation of optical emissions and various kinds of plasma waves for a study of ionosphere and magnetosphere interactions;
- 3) to study the interactions of particles with other ambient plasma components.

The USSR built topside sounder IS-338, installed in the satellite, operates in the range of frequencies from 0.3 MHz to 15.95 MHz. Local electron densities from 10^8 to $2 \cdot 10^{12} \text{m}^{-3}$ and temperatures from 500 to 10^4K are obtained using the probing device P-4 (Bulgaria, USSR). In addition, spherical ion traps provide data on positive ion densities from 10^8 to $2 \cdot 10^{12} \text{m}^{-3}$. A high-frequency probe KM-3 (USSR, Czechoslovakia) measures electron temperatures from 600 to 12000 K and the distribution of thermal electron velocities. In the KM-3 device a microprocessor controls the programming and preliminary data processing.

Corpuscular fluxes are known to play an essential role in the ionization balance of the upper atmosphere, in the polar auroral zones of the northern and southern hemisphere in particular, and also in electromagnetic phenomena occurring in the ionospheric plasma; the soft electron spectrometer SF-3 (USSR) records electrons in the energy ranges 10 to 150, 50, 120, 500, eV; 1.5 and 15 keV, and the background level of radiation. The differential spectrometer "Pero-31" (USSR) detects more energetic electrons in the following ranges: 40 keV, 0.1, 0.3 to 0.6, 0.6 to 1.9, 0.9 to 1.2, 1.2 to 2.0, 2.0 to 3.0 MeV and protons from 1 to 5, 10 to 30 and above 30 MeV. The electrophotometer EMO-1

(Bulgaria) measures the natural emission intensities at 630 nm, 427.8 nm and 557.7 nm, in order to study the physical processes in the polar oval and in the equatorial regions.

It is another aim of IK-19 to investigate the man made and natural electromagnetic wave phenomena and noise in the ionospheric plasma in a wide frequency band. Of primary interest are the problems connected with the time/frequency development of wave phenomena and the mechanisms which stimulate them. For this purpose, receiving and analysing devices for electromagnetic radiation in the band from 70 Hz to 6.0 MHz installed on IK-19. The low frequency analyzer ANCh-2ME (USSR, Czechoslovakia) covers electric and magnetic components of very low-frequency waves and noise in the range from 70 Hz to 20 kHz. Furthermore, while analyzer ANCh-2ME records the antenna impedance, radio-frequency spectrometer IRS-1 (Poland) in the band 0.6 to 6.0 MHz and HF analyzer AVCh-2 (USSR) for 0.1 to 5.0 MHz are designed to study natural and man made waves and noise in the ionospheric plasma. IRS-1 has a bandwidth of 36 kHz and sweeps the whole band in 2 or 10 s. AVCh-2 records processes taking place in the plasma in real time, i.e. in the whole frequency band and permits further studies with large frequency and time resolutions. Devices IRS-1 and AVCh-2 operate with the same antenna, a 15 m dipole.

A coherent radio-beacon M4K-3 (Czechoslovakia) completes the scientific instrumentation of the satellite. It operates on three frequencies: 40.008 MHz (modulation 100.2 and 1000.2 kHz), 180.036 MHz (modulation 100.02 kHz) and 360.072 MHz (modulation 100.02 kHz).

Transmission to ground of the scientific information is accomplished by the digital and analogue telemetry system ETMS-A (Hungary, Poland, USSR, Czechoslovakia). The digital system uses direct transmission or storage (30, 120, 960 min). Analogue telemetry is received at Appatits, Moscow, Norilsk, Panska-Was (Czechoslovakia) and Habana (Cuba).

In March 1980, IK-19 had been in operation for a year, after more than 5000 orbits. According to the data hitherto processed, one may draw a few conclusions concerning the present solar cycle 21: In the equatorial zone in March, 14 to 16 h LT, the electron density at the maximum of cycle 21, at 500 km, has increased by four, compared with the solar minimum activity years /Chan and Colin, 1969/; at altitudes 900 to 1000 km it has even increased by almost 20 times.

(II) First Results of a Statistical Evaluation of Electron
Temperature Measurements on Board the Interkosmos-19
Satellite

J. Smilauer¹, V.V. Afonin²

¹Geophysical Institute of Czech. Academy Sci., Prague, CSSR

²Space Research Institute, Academy of Sciences, Moscow, USSR

Abstract: During a period including the magnetic disturbance of 10/11 Mar. 1979, electron temperature measurements made on board the satellite 1979-020A are statistically analyzed. A comparison of two representative 16-hour means of the electron temperature vs. invariant latitude dependence clearly shows that magnetic activity causes an increase in the electron temperature.

1, Introduction

On board the Interkosmos-19 satellite, electron temperature (T_e) was measured by the radiofrequency method. A planar probe has been used with its plane perpendicular to the satellite's velocity vector. One type of measurement was a series of 16-hour runs of continuous recordings with 0.64 s time resolution that were available for the first three weeks of satellite operation. Since both the perigee position and the right-ascension of the ascending node have not changed too much during this time, the dependence of T_e upon the invariant latitude, and especially the influences of geomagnetic activity on T_e could be studied.

2, Results

For every run, containing almost ten complete orbits, a sorting of T_e according to the invariant latitude has been made independently for the ascending and descending branches of the orbit, differing in local magnetic time; for each interval of one degree in latitude, the mean values and RMS-deviations have been calculated. Several conclusions can be drawn: a) During the nighttime (around 02 LMT) and for a quiet period, the mean T_e for invariant latitudes up to 60° is about 2000 K, and the RMS-deviations are very small, typically 150 K. In disturbed periods the scatter of the equatorial T_e values becomes slightly higher, up to 400 K; b) During the daytime (around 15 LMT), the average T_e increases to about 3000 K and the scatter is about 200 K, increasing for disturbed periods up to 600 K.

For a comparison in geomagnetically disturbed and quiet periods, the run No. 170, obtained under disturbed conditions, and the run No. 226, for quiet conditions, have been compared ($\bar{D}_{st} = -75$ nT, $\sum K_p = 85$ and $D_{st} = 7$ nT, $\sum K_p = 13$, respectively). The results are shown in Figure 2 for nighttime and in Figure 3 for daytime. Differences against mean T_e are given in the lower parts of the plots, the positive values corresponding to the increase of T_e for the disturbed period. For checking purposes, upper parts of Figures 2 and 3 show the differences in the altitude and geomagnetic time, which are obviously not substantial. During the disturbance from 10 to 11 March 1979, electron temperature in the nighttime sector increased in the whole range of invariant latitudes from $40^\circ N$ to $40^\circ S$ by about 300 K, and the boundary of subauroral enhancements was shifted down to about 45° ($L = 2.2$). The daytime T_e also showed a slight increase, but its nature appears to be somewhat different since the two maxima are shifted towards higher latitudes. This tendency more clearly shown in the comparison of run 170 with the "quiet set" (runs 226, 299 and 328) indicates a slower heat convection across the field lines in the daytime sector, and higher boundaries of subauroral enhancements. It can be concluded that magnetic activity must be taken into account as one of the parameters needed for an electron temperature model.

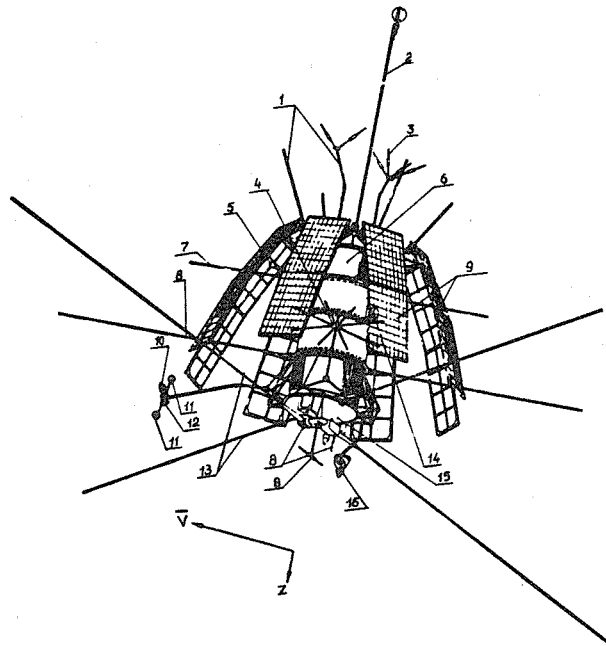


Fig. 1 Exploded view of satellite "Intercosmos-19". 5 - P-4 probe; 10 - KM-3 probe; 15 - module with scientific experiments.

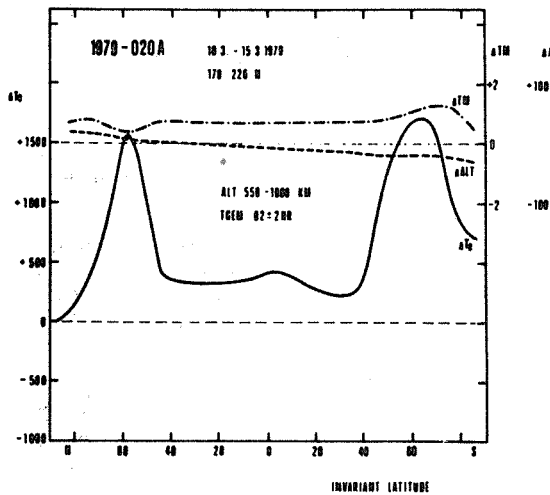


Fig. 2a

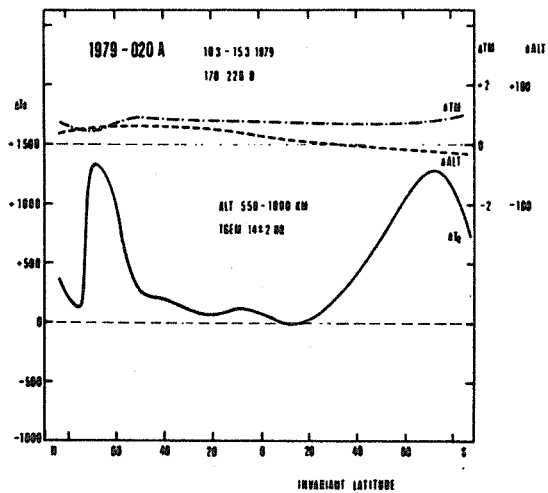


Fig. 2b

Fig. 2 Increase of $T_e(\Delta T_e)$ during the disturbed period. Also shown are the differences in altitude, ΔALT , and in local magnetic time, ΔTM . a) Night (around 02 LT); b) Day (around 14 LT).

2.3.2 Extremely High F-Region Electron Temperatures During the Present Maximum of Solar Cycle No. 21 (extended abstract)

M. Gogoshev, G. Moraitis, Ts. Gogosheva, B. Komitov
 B. Taneva-Mendava, T. Markova, I. Mendov, Ts. Pashova,
 K. Kunev, S. Spasov

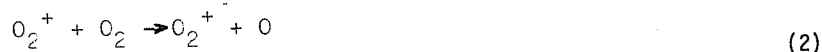
Central Laboratory for Space Research, Bulgaria

The oxygen line at 630 nm, emitted from the polar aurora but also from the atmosphere at mid and low latitudes, is an important indicator of the aeronomic and dynamic processes in the F-region. Because of its relatively low thermal excitation level (1.96 eV), even very small energy inputs can be detected using this line. Observations of 630 nm were made, at intervals of 7.5 min, at the mid-latitude observatory at Stara Zagora using a tilting filter photometer. The threshold sensitivity of the system was 5 Rayleigh, and care was taken to confirm the absolute calibration. Our long series of observations allows us to compare the absolute emission values between solar maximum (1979) and solar minimum (1973) conditions. For the early night hours, the ratio of maximum to minimum emission was as high as 5 to 6, whereas the corresponding ratio was less than 3 for the Covington index (of solar 10.7 cm radio emission). After midnight the emission ratio decreased considerably.

Except during twilight, the intensity of the 630 nm line depends entirely on the dissociative recombination of O_2^+ in the reaction:



which is limited by:



In twilight periods, photodissociation in the Schumann-Runge continuum is important:



but collisional excitation of atomic oxygen, occurring during the cooling down of the hot electron gas, also makes a remarkable contribution.

We can now estimate the contribution made by the three mechanisms. Observations made using photometers on the Vertical-6 and -7 rockets have shown that it is possible to separate the different generating mechanisms. It was found that, during twilight, the photodissociation excitation is most important, followed by dissociative recombination. However, the Vertical-6 and -7 data refer to low and moderate solar activity respectively, and a review would be desirable. Dissociative recombination (Equation 1) depends on both the F2-layer electron density and the concentration of O_2 molecules, and also on the concentration of N_2 molecules. The two molecular concentrations represent the main quenching factor for the metastable species $O(^1D)$. The density of excited oxygen atoms and, by integration, the intensity of the red (tripled) line, can be computed if the profiles of the relevant species are known. We use Jacchia's /1977/ model for the neutrals, and the IRI electron density profile adapted at Athens and Sofia. With the reaction constants of Serafimov et al., /1977/ and the algorithms explained in Gogoshev and Komitov /1980/, we were able to compute the emission contributions due to photodissociation to dissociative recombination. The observed intensity shown in Figures 1 and 2 is equal to the sum of the two components, but after midnight only. Before midnight it is much greater. Even when assuming neutral models with extremely high (atomic and molecular) oxygen densities we were unable to explain the observed red line intensities.

As an explanation for the discrepancy we suggest the existence of relatively high electron temperatures after sunset. These, in conjunction with the high intensities of atomic oxygen, would cause excessive excitation, and hence emission of the red line airglow. Considering the energy transferred to the neutrals by collision with hot electrons, and using Manta's /1973/ reaction coefficients, we were able to compute from our emission intensities a hypothetical electron temperature as shown in Figure 3. When the excess is particularly great, as in Figure 1, electron temperatures of up to 2500 K are needed, even several hours after sunset. During the maximum of Solar Cycle No 21, we found at least 15 cases of excessive radiation of this kind.

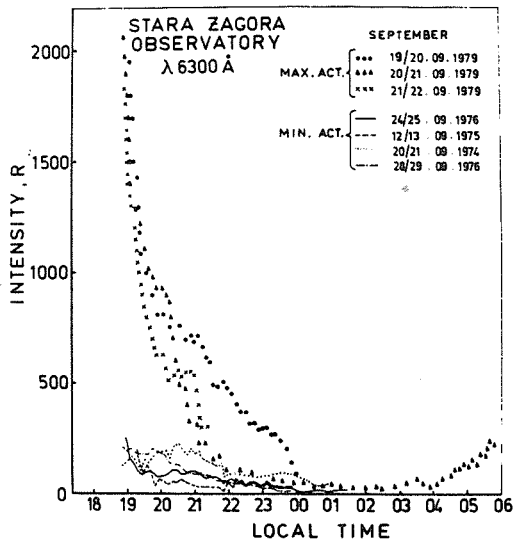


Fig. 1

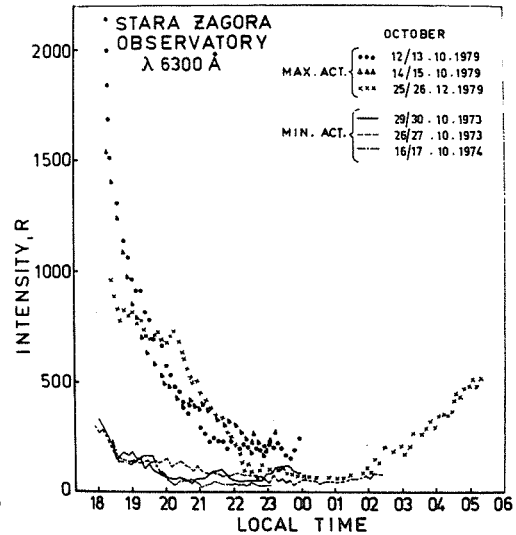


Fig. 2

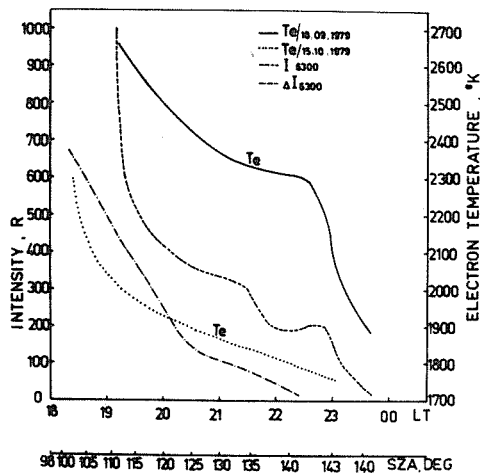


Fig. 3

Fig. 1 Observed intensities of oxygen line 630 nm for dates in September of 1979 sunspot maximum conditions (dots, triangles, crosses) and during the preceding minimum (curves of different type). Aeronomical computations yielded values as observed after midnight throughout.

Fig. 2 Same as Fig. 1 for October dates indicated.

Fig. 3 6300Å intensities (lefthand ordinate) and therefrom computed T_e (righthand) for two dates in 1979 (sunspot maximum).

CHAPTER 3 IONOSPHERIC STRUCTURE

Section 1 Ionic Composition

3.1.1 Ion Composition in the D- and Lower E-Regions with Particular Emphasis on Cluster Ions

E. Kopp

Physikalisches Institut Bern,
Sidlerstrasse 5, CH-3012 Bern, Switzerland

Abstract: A review is given of present-time experimental knowledge concerning ion composition in the lowest ionosphere, in particular of the cluster ion populations and the relevant chemistry. It appears premature to establish a detailed model on the presently available experimental information.

1, Introduction

The positive and negative ion composition of the Earth's lower ionosphere is divided into two completely different regions. The upper part is dominated by molecular ions (NO^+ and O_2^+) and electrons, and the lower part by positive cluster ions and the presence of negative ions other than electrons. The primary sources of ionization produce electrons and positive molecular ions. The complexity of the ion composition in the ionosphere below 70 km is caused mainly by processes such as three-body ion-neutral reactions producing secondary ions and O_2^- by attachment of electrons to O_2 . The composition of positive and negative secondary ions is highly variable owing to temperature changes and to the variations of the minor constituents No , $\text{O}(^3\text{P})$, $\text{O}_2(^1\Delta\text{g})$, H_2O and H .

The positive metallic ions Fe^+ , Mg^+ , Al^+ , Si^+ , Na^+ etc. constitute a special class of ions. Metallic ions are observed in the E- and F-regions. We know from in situ ion composition measurement and ground based observations with Na and K Lidars, and from meteor radars and meteor trail spectra, that metallic ions have their sources in the ablation of the incoming meteoric dust particles. Metallic ions disappear very rapidly below an altitude of approximately 90 km, but have been observed as high as 700 km in the F-region. They do not contribute a major part to the total positive ion density below 100 km. The chemical loss processes for metallic ions are not yet well understood, because present rocket mass spectrometers are not sensitive enough to detect the three-body reaction products of metallic ions. In the lower ionosphere between 60 and 100 km, the life times of positive and negative ions are generally so short that transport processes may be neglected, except for metallic ions and nighttime negative ions. However, transport in the mesosphere and lower thermosphere is important for the main part of minor constituents, especially NO , $\text{O}_2(^1\Delta\text{g})$, O and H_2O .

The main aeronomic effect arising from differences in ion composition is the change of the bulk or effective positive ion recombination coefficient (e.r.c.). Of particular interest is the change of e.r.c. in the lower D-region at heights below the transition of molecular ions to the main cluster ions $\text{H}^+(\text{H}_2\text{O})_n$ located between 70 and 90 km. In the region of dominant positive cluster ions, the e.r.c. decreases because the dissociative recombination rate is at least one order of magnitude faster for cluster ions than for NO^+ and O_2^+ .

Mul and McGowan /1979/ have recently published new electron dissociative recombination rates for NO^+ and O_2^+ . The rates derived for 300 K are 2.3 and $1.9 \cdot 10^{-7} \text{cm}^3 \text{s}^{-1}$ with a temperature dependence of $T^{-0.5}$. The NO^+ value is now close to the O_2^+ value, being about a factor of 2 lower as compared with the rate constant of $4.5 \cdot 10^{-7} (T/300 \text{ K})^{-0.85}$ derived by Oppenheimer et al., /1977/ from the results of Walls and Dunn /1974/.

2. Positive Ion Composition

Positive ion composition measurements have been made in the lower ionosphere with rocketborne mass-spectrometers at various latitudes, and in conditions with different solar and geomagnetic activities. All spectrometers have used a special pumping system. The measurements carried out since 1963 /Narcisi and Bailey, 1965; Krankowsky et al., 1972; Goldberg and Blumle, 1970; Zbinden et al., 1975/ have all shown the same general feature - the lower D-region is dominated by cluster ions $\text{H}^+(\text{H}_2\text{O})_n$. The main cluster ions observed in these earlier flights were $\text{H}^+(\text{H}_2\text{O})$ and $\text{H}^+(\text{H}_2\text{O})_2$, and much less of $\text{H}^+(\text{H}_2\text{O})_3$. These measurements were all made with instruments using a plate with a center orifice for ion sampling and an ion draw-in potential of at least -5 V. There was soon doubt whether these ions were real or were partially caused by break up of heavier clusters. The reasons for a break up of loosely bound cluster ions are collisions in the shock layer in front of the instrument, or collisions with ions accelerated by the large draw-in potential. To overcome these effects, new modified instruments were flown using a conical inlet geometry and reduced draw-in potential /Kopp et al., 1978; Arnold and Krankowsky, 1979/. Results from a daytime, midlatitude, positive ion composition measurement during a 1976 rocket flight above Wallops Island are shown in Figure 1 /Kopp et al., 1978/. The results are typical for a quiet, summer, daytime condition. Below 83.5 km the dominant ions are $\text{H}^+(\text{H}_2\text{O})_3$ and $\text{H}^+(\text{H}_2\text{O})_4$ in nearly equal abundance. Above the transition height, molecular ions are dominant with slightly higher NO^+ densities in the D-region. The decrease with increasing altitude of $\text{H}^+(\text{H}_2\text{O})_3$ and $\text{H}^+(\text{H}_2\text{O})_4$ above the transition height is very fast. Up to an altitude of 93 km, the cluster ions $\text{H}^+(\text{H}_2\text{O})$, $\text{H}^+(\text{H}_2\text{O})_2$, $\text{NO}^+(\text{H}_2\text{O})$ and $\text{NO}^+(\text{CO}_2)$ are still present well above the height where $\text{H}^+(\text{H}_2\text{O})_3$ and $\text{H}^+(\text{H}_2\text{O})_4$ disappear. $\text{H}^+(\text{H}_2\text{O})_n$ and NO^+ clusters are terminating or intermediary ions of the NO^+ and/or O_2^+ hydration chain. The hydration loss of NO^+ and O_2^+ above the transition heights is possible, but hydration time is clearly larger than the life time of molecular ions as determined by dissociative recombination. The measured metallic ions at about 90 km have not been included in Figure 1.

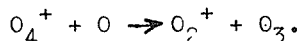
The main ion production in the midlatitude daytime D- and lower E-regions is direct ionization of NO by Ly- α radiation, and direct ionization of excited molecular oxygen $\text{O}_2(^1\Delta_g)$ in the wavelength region 111.8 to 102.7 nm /Hauffman et al., 1971/. The variation of the ultraviolet radiation at 100 nm is typically by a factor of 2 within a solar cycle period. The much larger variability of the total ion and electron density of the daytime midlatitude D-region is thus caused by NO and $\text{O}_2(^1\Delta_g)$ density variations and by temperature effects.

The main problem in understanding the presence of water cluster ions in the lower D-region is to find a fast reaction path for NO^+ and O_2^+ hydration. All recent mass spectrometric measurements in the D-region have now also found the intermediary NO^+ cluster ions $\text{NO}^+(\text{H}_2\text{O})$, $\text{NO}^+(\text{H}_2\text{O})_2$ and $\text{NO}^+(\text{CO}_2)$, as already proposed in an early hydration scheme by Fehsenfeld and Ferguson /1969/, Dunkin et al., /1971/, Heimerl and Vanderhoff /1971/, and Niles et al., /1972/. The main difficulty with this scheme was that NO^+ hydration to $\text{NO}^+(\text{H}_2\text{O})_3$ with switching to $\text{H}^+(\text{H}_2\text{O})_3$ was too slow. Johnson et al. /1975/ have shown that NO^+ can produce $\text{NO}^+(\text{H}_2\text{O})$ much faster by the reaction path $\text{NO}^+ \rightarrow \text{NO}^+(\text{CO}_2) \rightarrow \text{NO}^+(\text{H}_2\text{O})$. The forward

reaction rate constant has a strong $T^{-4.4}$ temperature dependence. The NO^+ hydration scheme which is used to predict the $\text{H}^+(\text{H}_2\text{O})_n$ distribution is shown in Figure 2. Similar fast chains are proposed for $\text{NO}^+(\text{H}_2\text{O})_2$ and $\text{NO}^+(\text{H}_2\text{O})_3$ production. The strong temperature dependence of the NO^+ hydration time is essentially assigned to the forward and backward rate constant of reactions $\text{NO}^+(\text{H}_2\text{O})_n + \text{X} + \text{M} \rightleftharpoons \text{NO}^+(\text{H}_2\text{O})_{n-1} + \text{X} + \text{M}$ ($\text{X} = \text{N}_2, \text{O}_2, \text{CO}_2$). Rates and the temperature dependence have only been measured for the first ($n = 0$) three body reaction with CO_2 and N_2 /Johnson et al., 1975; Turner and Conway, 1976; Smith et al., 1977/. The implication of the fast reaction path with the intermediate ion $\text{NO}^+(\text{H}_2\text{O})_{n-2}$ has been examined in model calculations using model temperature profiles by Thomas /1976/ and Reid /1977/. The NO^+ hydration model is able to reproduce qualitatively the daytime, quiet, D-region ion composition at midlatitudes, but cannot explain the large gradients of $\text{H}^+(\text{H}_2\text{O})_3$ and $\text{H}^+(\text{H}_2\text{O})_4$ observed at 83.5 km (see Figure 1). Several calculations designed to determine temperature of equilibrium constants at different temperatures from ion composition results have recently been published /Chakrabarty, 1979; Arnold and Krankowsky, 1977/. For all the published ion composition results, an independent and accurate temperature profile with a height resolution less than 1 km was not available. Simultaneous measurements of temperature and ion composition, and further laboratory studies at low temperature, are needed in order to find the appropriate method of deducing mesospheric temperatures from ion composition results, and to improve the understanding of the observed gradients of cluster ion densities.

O_2^+ production is the dominant ion source in the lower ionosphere under disturbed conditions at mid- and high latitudes. A characteristic ion composition for an auroral situation is shown in Figure 3 from a measurement of the Heidelberg group above Kiruna /Björn et al., 1980/. $\text{H}^+(\text{H}_2\text{O})_3$ and $\text{H}^+(\text{H}_2\text{O})_4$ are still the dominant ions in the lower D-region, but the molecular ions are not completely lost by hydration. Their relative concentration in the lower D-region is of the order of 10% or more of the total positive ion density. The transition height from cluster ions to molecular ions is located at 71 km that is more than 10 km below the level of the midlatitude quiet day. Above this altitude, molecular ions NO^+ and O_2^+ are dominant, but $\text{H}^+(\text{H}_2\text{O})$ and $\text{H}^+(\text{H}_2\text{O})_2$ are still produced up to an altitude of 79 km from O_2^+ hydration. The $\text{H}^+(\text{H}_2\text{O})_n$ concentrations are only slightly below those of the molecular ions. The ratio NO^+/O_2^+ is larger than 1 in a disturbed condition owing to the increase of NO and the increased loss for O_2^+ in a charge exchange reaction with NO.

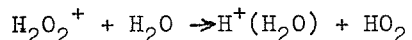
An extended O_2^+ hydration scheme is shown in Figure 4. Terminating ions are $\text{H}^+(\text{H}_2\text{O})_2$ and $\text{H}^+(\text{H}_2\text{O})_3$. The initiating reaction is a three-body association of O_2^+ with O_2 to O_4^+ which does not react with CO_2 . The loss of O_4^+ is due to switching with H_2O to $\text{O}_2^+(\text{H}_2\text{O})$ and the reaction:



This reaction short-circuits the $\text{H}^+(\text{H}_2\text{O})_n$ production at altitudes where atomic oxygen concentration exceeds that of water vapor. Model calculations of the positive ion composition in the high latitude disturbed D-region by Swider and Narcisi /1974, 1975/ and Swider /1977/ are in good agreement with the AFGL-measurements /Narcisi et al., 1972/. One of the remaining difficulties with the O_2^+ hydration scheme is still to match the observed $\text{H}^+(\text{H}_2\text{O})_n$ to $\text{H}^+(\text{H}_2\text{O})_{n-1}$ ratios. The production rates of $\text{H}^+(\text{H}_2\text{O})$ and $\text{H}^+(\text{H}_2\text{O})_3$ in the models are, in general, too small to explain the corresponding observed water cluster ion densities.

Traces of ions at mass 63, 81 and 99 amu were found in recent ion composition measurements and were interpreted as $\text{H}^+(\text{H}_2\text{O})\text{CO}_2$ /Swider and Narcisi, 1975; Kopp et al., 1978/. These ions support another faster production channel for heavier $\text{H}^+(\text{H}_2\text{O})_n$ ions over intermediate loosely bound $\text{H}^+(\text{H}_2\text{O})_n$ clusters /Swider and Narcisi, 1975; Chakrabarty et al., 1978/.

Several ion composition measurements during disturbed conditions have observed H_2O_2^+ ions at heights between 75 and 85 km /Arnold and Krankowsky, 1974; Zbinden et al., 1975; Herrmann and Philbrick, 1980/. H_2O_2^+ is directly produced from O_2^+ by a charge exchange reaction with neutral H_2O_2 . The loss of H_2O_2^+ by the reaction



should not be neglected as a direct source of oxonium ions. The NO calculations by Swider /1978/ from 10 different ion composition measurements show a variability of the NO concentration between 10^{13} and 10^{15}m^{-3} at heights between 95 and 105 km. Occasionally, NO densities higher than 10^{14}m^{-3} are also observed as low as 70 km in the D-region. The NO density in the mesosphere is higher in winter anomalies and at high latitudes. An increase of mesospheric NO affects the positive ion composition because of the increase of NO^+ production and the loss of O_2^+ ions from charge exchange with NO. Positive ion composition profiles during a D-region winter anomaly above Wallops Island are shown in Figure 5. The high electron and molecular ion densities down to a height of 77 km are typical for a winter anomaly caused by large mesospheric NO densities from vertical and/or horizontal transport and from a temperature increase in the mesosphere. $\text{H}^+(\text{H}_2\text{O})_3$ and $\text{H}^+(\text{H}_2\text{O})_4$ are equally abundant and are the major ions below the transition height at 77 km. Their production is mainly hydration of NO^+ .

The parameter f^+ , the ratio of positive cluster to molecular ions in the D-region, is important for the determination of an effective electron loss coefficient in the lower ionosphere. f^+ -values from a selection of the 40 - 50 D-region mass spectrometer results are shown in Figures 6 to 8 and Table 1. The transition height between the regions of predominant cluster ions ($f^+ = 1$) is located between 70 and 92 km. The variability of this transition height and the gradient of the cluster ion density are associated with significant changes of mesospheric temperatures and densities of minor constituents NO, $\text{O}_2(^1\Delta_g)$ and $\text{O}(^2p)$. In those cases where variations of the electron production rates are caused by variations in the ion/electron pair production rates attributable to particle precipitation and X-ray radiation, the variations of the f^+ parameter are associated with the increase of O_2^+ production and higher $\text{O}(^2p)$ densities below 90 km. Such conditions are limited to the high latitude D-region.

The transition height of molecular ions to cluster ions ($f^+ = .5$) in the summer daytime D-region (see Figure 6) decreases from 87 km at high latitude to 82.5 km at the equator. This decrease is caused by the summer temperature decrease at mesospheric heights from the equator to high latitudes and, consequently, the decrease of hydration time for NO^+ and O_2^+ . The f^+ values of 4 of the 5 available mass spectrometer measurements during daytime anomalous winter conditions at midlatitude are shown in Figure 7. Their transition region is around 77 km: well below 80 km. The lowering of the transition region in a winter anomaly is caused by the strong mesospheric temperature increase and the enhancement of NO densities at 80 to 100 km. High latitude winter results in the northern hemisphere do not show significant day/night variations of the f^+ ratio under disturbed conditions. The dominance of ionisation by particles and X-rays during magnetically active periods at high latitudes lowers the transition height of molecular ions to cluster ions to altitudes between about 83 km for weak auroras and about 72 km, the lowest height observed during a PCA event or with hard particle precipitation (see Figure 8).

Only one positive ion composition measurement of the high latitude, winter, nighttime D-region during undisturbed conditions is available for comparison. The transition height obtained from this measurement above South Uist is located at 92 km, at least 8 km above the region for disturbed conditions.

Nighttime summer and winter measurements in midlatitudes and the equatorial region are still missing, as well as the reference measurements for the winter anomaly and undisturbed high latitude winter D-region.

3. Negative Ions

The relatively large atmospheric ambient air density in the lower mesosphere permits formation of negative ions by three-body attachment of electrons to O_2 . N_2 does not form stable negative ions. The electron attachment rate to O_2 was measured in the laboratory by Chanin et al. /1959/ and is sufficiently fast to account for the D-region negative ion production. Fehsenfeld et al., /1967, 1969/ have conducted laboratory investigations of the reaction in which O_2^- ions are lost in a complicated sequence of reactions with mesospheric minor constituents O_3 , CO_2 , NO , H and H_2O . Most of the negative molecular and atomic ions such as O^- , O_2^- , O_3^- , O_4^- , CO_3^- , CC_3^- , CC_4^- , CH^- have a short chemical lifetime. Important loss processes for these ions are photo-dissociation during daytime from visible sunlight and reactions with $O(^1P)$, H , O_3 and $C_2(^1\Delta g)$. The total daytime negative ion density decreases rapidly above a certain height, normally located between 80 and 85 km. The decrease of the negative ion density is associated with an increase of the $O(^1P)$ density above this height and the increased loss of the short-lived ions, in particular O_2^- and O^- .

The observations of negative ions in the D-region come from a few mass spectrometer measurements of the Heidelberg and the AFGL groups /Narcisi et al., 1971; Arnold et al., 1971/. The ions observed were CO_3^- , NO_3^- , Cl^- , C_2^- , and high mass negative cluster ions were interpreted as $NO_3^-(H_2O)_n$ /Narcisi et al., 1972/. These results were controversial because the Heidelberg observation could not confirm the $NO_3^-(H_2O)_n$ observation. The cluster ions measured by the Heidelberg group were found at lower heights between 78 and 85 km, below the cut-off of negative ions. The observations of these flights, particularly for the ions Cl^- and HCO_3^- of the Heidelberg measurements, were also not consistent with the prediction of theoretical models. However, the density ratios of negative to positive ions are in good agreement with theoretical models.

A new measurement of D-region negative ions during the eclipse in 1979 is now available /Kopp et al., 1980/. The observation has been made with a high resolution magnetic sector field mass spectrometer of the University of Bern. The molecular and atomic ions observed were mainly CO_3^- , Cl^- , O_2^- , NO_3^- and O^- . A large variety of negative cluster ions was observed, mainly in the upper D-region between 75 and 85 km.

In a D-region model of Mitra and Rowe /1972/, negative ions are divided into two classes, X⁻ and Y⁻. All negative ions with a short chemical lifetime of the order of 10^2 s or lower belong to class X⁻. Important ions in this class are O_2^- , O^- , O_3^- , CO^- , CC_3^- , CO_4^- and OH^- . Most of these ions have fast daytime loss reactions due to their photodissociation by visible light from the Sun and to reactions with O , H , O_3 and $C_2(^1\Delta g)$. The ions in class Y⁻ have a much longer chemical lifetimes, typically 10^4 to 10^6 s. They do not react with O , $C_2(^1\Delta g)$, and H and are, in general, also more resistant to photodissociation. Important ions of the Y⁻ group are NO_3^- , HCC_3^- , $NO_3^-(H_2O)_n$, $HCC_3^-(H_2O)_n$ and cluster ions of the X⁻ group. It is now recognized that Cl^- , which is a well-confirmed principal negative D-region ion, has production and loss reactions which differ from those of the ions of classes X⁻ and Y⁻. The two-ion model of Mitra and Rowe /1972/ can be extended to a three-ion model including Cl^- as shown in Figure 9. The main neutral chlorine component of the stratosphere and mesosphere is HCl /Turco, 1977/. Production of Cl^- is mainly due to the charge exchange reactions of O_2^- and O^- with HCl . The loss of Cl^- arises from the reaction with atomic hydrogen and clustering with water vapor. The three-ion model of

Figure 9 is useful for calculating the day-night variation and the effect of atomic oxygen on the negative to positive ion ratio shown in Figure 10. The upper boundary of negative ions is determined by atomic oxygen, and the day-night variation are due to changes in photodissociation loss and reduced nighttime $O_2(^1\Delta g)$ densities below 80 km.

The nature, the production rate, and the variability of negative cluster ions of the day- and night-time D-region are not known. Nevertheless, it is expected that the production of negative cluster ions depends on temperature and on minor constituents such as NO, H_2O and H. From laboratory and in situ measurements, the negative cluster ions of the D-region should be $NO_3^-(H_2O)_n$, $CO_3^-(H_2O)_n$, $HCCO_3^-(H_2O)_n$ and cluster ions of O_2^- and O^- .

4, Conclusions

Theoretical models for NO^+ and O_2^+ hydration have been extended, but the model predictions still do not satisfactorily match the measured $H^+(H_2O)_n$ distributions. The determination of atmospheric temperature from H^+ ion composition measurements will not be possible until a set of simultaneous temperature and ion composition measurements becomes available.

The loss reactions and models of metallic ions in the D-region are based only on theoretical models. Practically no in situ measurements are available for a study of the metallic ion loss processes.

The nature and the variability of D-region negative ions are not at all clear. Recent measurements have shown the need for even more complex models of the D-region negative ion chemistry.

Additional positive ion composition measurements in the nighttime summer and winter low latitude D-region and reference measurements for the winter anomaly and the disturbed high latitude lower ionosphere are needed for the model of the electron loss rate in the lower ionosphere.

Discussion remarks:

K. Rower noted the importance of rather simple parameters for comparing with a descriptive model like IRI. One such parameter would be the transition height between positive molecular ions and clusters, another one the transition height between electrons and negative ions or clusters. The author insisted that the atomic oxygen density is the decisive parameter. Rower asked finally whether extreme values could at least be given. The author felt this might be too difficult at present time.

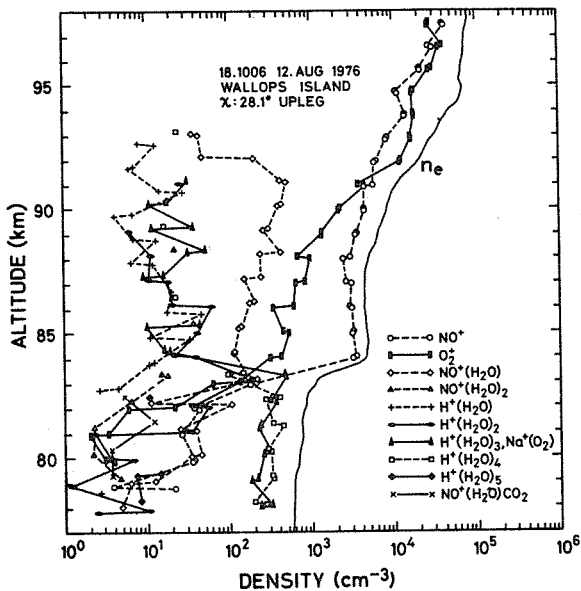


Fig. 1 Measured electron and ion density profiles in the summer daytime D-region above Wallops Island.

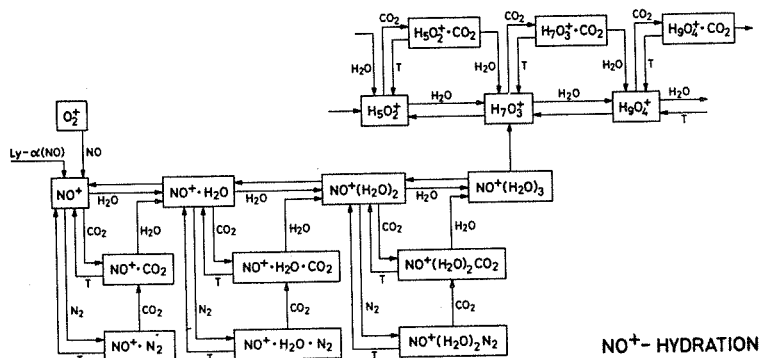


Fig. 2 Schematic diagram of production and loss reactions for NO^+ in the D-region.

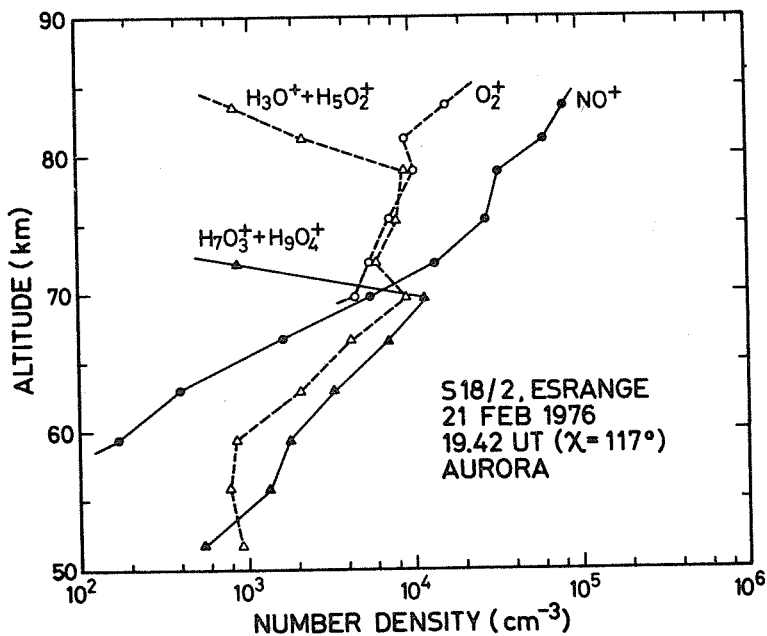


Fig. 3 Measured number densities of NO^+ , O_2^+ and proton-hydrated ions in the winter nighttime, high latitude D-region for disturbed conditions.

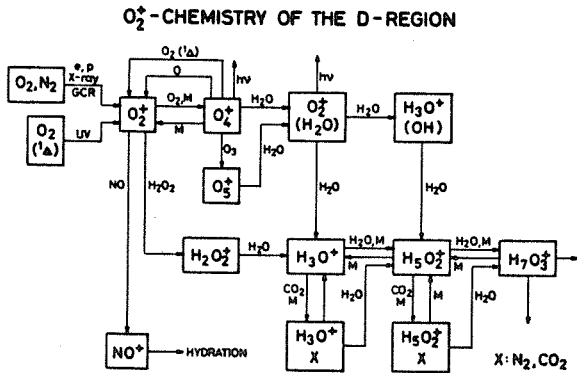


Fig. 4

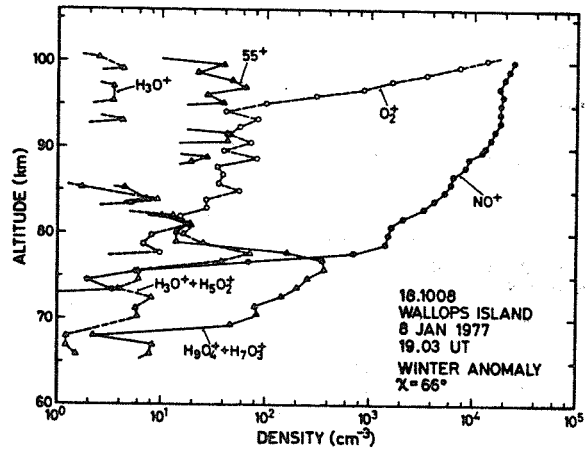


Fig. 5

Fig. 4 Schematic diagram of the production of proton-hydrated ions from O_2^+ in the D-region.

Fig. 5 Measured ion densities of NO^+ , O_2^+ and protonhydrates in the winter midlatitude daytime D-region with anomalous radio wave absorption.

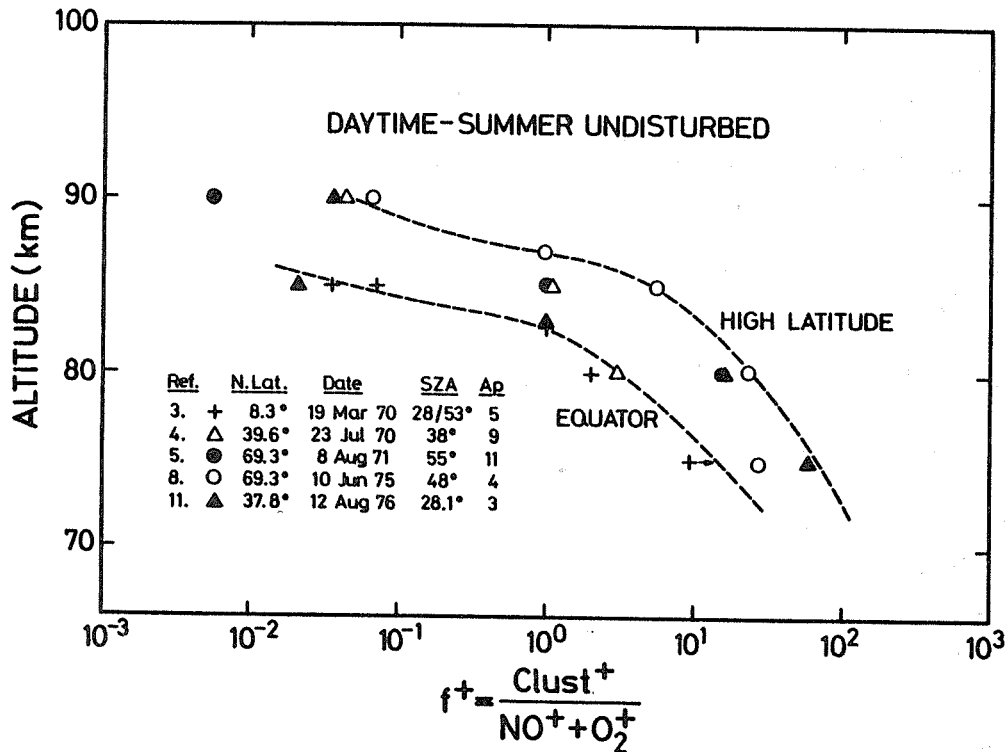


Fig. 6 Ion density ratio f^+ of the summer undisturbed D-region from positive ion composition measurements (3,4,5,8,11).

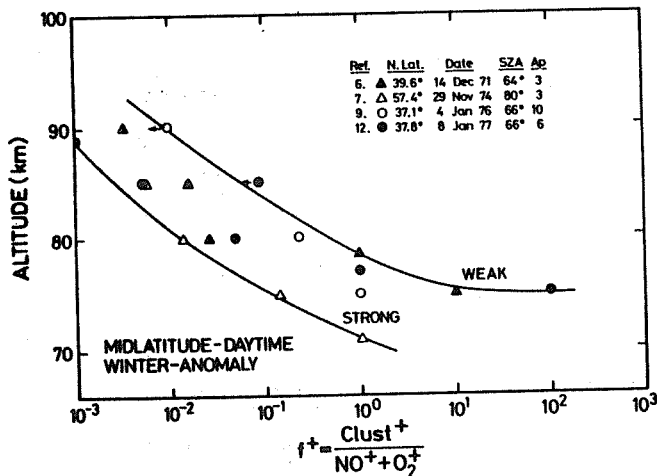


Fig. 7 Ion density ratio f^+ of the anomalous, daytime midlatitude D-region from positive ion composition measurements in winter (6,7,9,12).

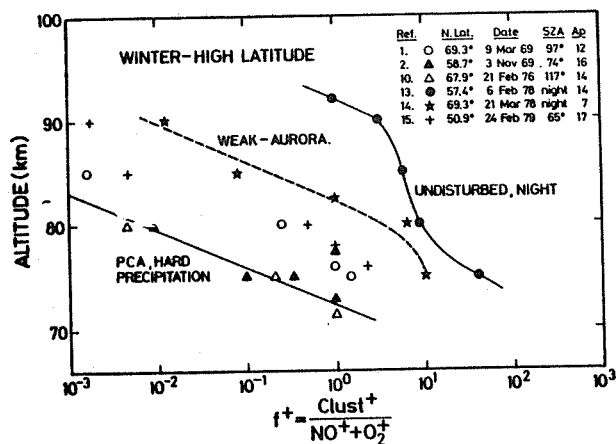


Fig. 8 Ion density ratio f^+ in the high latitude winter D-region from positive ion composition measurements (1,2,10,13,14,15).

THREE ION MODEL FOR NEGATIVE D-REGION IONS.

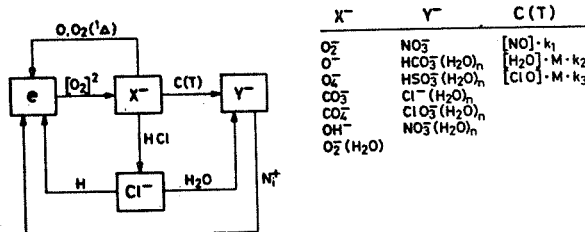


Fig. 9 Three ion model for the negative D-region ions.

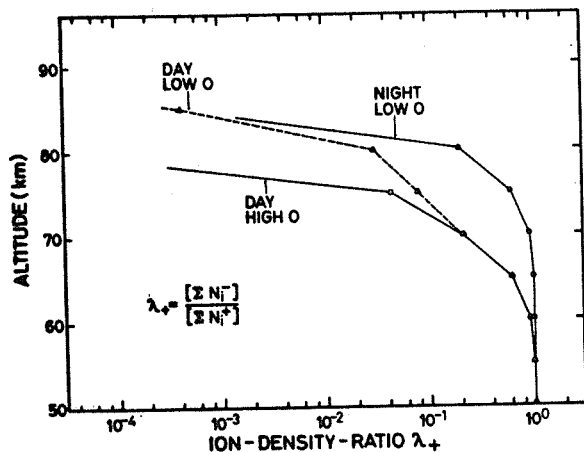


Fig. 10 Ion density ratio λ_+ of the total negative to the total positive ion density calculated from the three ion model of Fig. 9.

Table 1

CONDITION	ALTITUDE/km FOR 3 DIFFERENT CLUSTER TO MOLECULAR ION RATIOS IN THE D-REGION		
	$f^+ = 0.1$	$f^+ = 1$	$f^+ = 10$
Summer daytime			
- equator	84.5	82.5	76.5
- midlatitude	87	85	80
- high latitude	89	87	83.5
Winter daytime			
- anomalous, midlatitude	79	77	75
Winter high latitude			
- night, undisturbed	94	92	85
- night, weak aurora	86	82.5	75
- day/night PCA, hard particle precipitation	76	72.5	69

References to Figures 6, 7, 8:

- (1) Krankowsky, D., et al., 1972, Radio Sci. 7, 93.
- (2) Swivler, W., and R. S. Narcisi, 1975, J. Geophys. Res. 80, 655.
- (3) Goldberg, R. A., and A. C. Aikin, 1971, J. Geophys. Res. 76, 8352.
- (4) Johannessen, A., and D. Krankowsky, 1974, J. Atmos. Terr. Phys. 36, 1233.
- (5) Johannessen, A., and D. Krankowsky, 1972, J. Geophys. Res. 77, 2888.
- (6) Zbinden, P., et al., 1975, PSS 23, 1621.
- (7) Arnold, F., and D. Krankowsky, in: Grandal, B., and J. A. Holtet(eds): Dynamics and Chemical Coupling between the Neutral and Ionized Atmosphere, 1977, 93.
- (8) Arnold, F. and W. Jovs, 1979, Geophys. Res. Letts. 6, 763.
- (9) Arnold, F. and D. Krankowsky, 1979, J. Atmos. Terr. Phys. 41, 1127.
- (10) Bjorn, L. G., et at., 1979, J. Atmos. Terr. Phys, 41, 1185.
- (11) Kopp, E. et al., 1978, Space Res. 18, 245.
- (12) Meister, J., et al., 1976, Space Res. 18, 245.
- (13) Arnold, F., ESA Report SP-152, 1980, 479-495.
- (14) Arnold, F., ESA Report SP-152, 1980, 479-495.
- (15) Eberhardt, P., et al., 1980, Trans. Am. Geophys. Un. 61, 311.

3.1.2 A Proposed Improvement of IRI Using the O⁺ - H⁺ Transition Level

I. Kutiev, K. Serafimov, M. Karadimov¹, K. Heelis²

¹Central Laboratory for Space Research, Moskovska 6, Sofia, Bulgaria

²University of Texas at Dallas, Box 688, Richardson, Tx 75080, USA

Abstract: The transition level (TL) between the O⁺ and H⁺ dominated regions in the topside ionosphere is examined in terms of its latitude, longitude and local time variations.OGO-6 data show that in the nighttime winter midlatitudes, between -10° to -40° dip latitude, a sharp trough in the TL surface occurs, at altitudes changing from 1100 down to 600 km. At the dip equator, as well as at dip latitudes higher than -40°, the TL surface throughout the night remains at the same altitude as at sunset namely about 1100 km. Summer midlatitudes exhibit strong variability of the TL surface, the latter having the altitude variation of 200 km at +30° dip latitude. There is evidence that, on the winter side, the TL surface descends within an hour after sunset from 1100 km to 600 km.

1, Introduction

The behavior of the O⁺ - H⁺ transition level (TL) has recently been studied by various investigators. Titheridge /1976/ examined C⁺ - H⁺ transition level variations at low solar activity, and Miyazaki /1979/ and Kutiev et al. /1980/ did so for low and high solar activity respectively. The common result of these studies is that, in the daytime the transition level (TL) height reaches 1000 to 1200 km, and in nighttime it drops to 600 km. In this period the TL exhibits strong latitude and longitude dependence reflecting the dynamics of the O⁺ ions. Thus, the TL could be a good tool for studying a number of phenomena occurring in the nighttime topside ionosphere such as the equatorial E x B ion drift, the global wind system at F-region heights, variations of the plasmopause position, etc. Also a knowledge of TL temporal and spatial variations should be of help in ionospheric modelling because the vertical distribution of ion density is essentially characterized by TL.

In this paper the data obtained from the OGO-6 satellite are considered in terms of the nighttime behavior of TL. These data are quite uniformly spaced in latitude, longitude and altitude in the ranges +60° to -60°, +180° to -180°, and 600 km to 1100 km, respectively. Thus, the morphological behavior of the TL can be examined only when it lies within these ranges. The examination of the data base shows that, during the solar maximum period 1969/1970, the TL frequently occurred outside these intervals, since it was not encountered by the satellite. There are, therefore, portions of the globe over which the precise behavior of the TL is unknown. These regions can be identified and the nature of the TL in adjacent areas may in many cases lead to a reasonable expectation of its behavior in regions where it is not directly observed. Figure 1 shows the location of all TLs encountered by OGO-6 around the summer solstices of 1969 and 1970. The position of the TL is plotted for all encounters in the local time region between 21 h and 04 h. The data coverage outside this region is quite small; it is expected that within this interval the local time variation of the TL altitude will be very small.

2, Results

Let us consider first the data in the southern (winter) hemisphere in Figure 1. In the longitude region between 60° and 150° (referred to as

region A) there exists a well-defined banded structure with bands that appear to be parallel to the dip equator. The fact that the TL has not been located in certain regions within the volume sampled by the spacecraft means that in these regions the TL lies below 600 km or above 1100 km. Observations of the individual C^+ and H^+ number densities may be used to determine whether it lies above or below. In the longitude region -30° to $+60^\circ$ (referred to as region B) the banded structure is even more pronounced in the southern hemisphere. There is a distinct lack of TL encounters between the two bands, and investigation of individual C^+ and H^+ number densities showed that, in this region, the TL lay below 600 km altitude. In the longitude region -180° to -30° (referred to as region C) no banded structure exists as in regions A and B. This simply means that the TL usually lies above 600 km at all latitudes.

The greatest variability in the TL altitude is seen at the equator. In the dip latitude region -15° to $+30^\circ$ and the altitude region of 900 km to 1100 km, the distribution of C^+ and H^+ may be considerably affected by neutral winds and $E \times B$ drifts leading to a large variability in the TL altitude. Figure 2 is a plot of TL altitude observations versus dip latitude for region A showing a minimum in TL at about -30° dip latitude. The region below 700 km does not have such uniform sampling as at higher altitudes such that we were unable to define the precise nature of the TL surface. Nevertheless, the minimum is well shown by the rapid changes in the TL altitude in the narrow dip latitude regions -15° to -5° and -60° to -45° . The changes are such that, in moving equatorward in the region -15° to -5° , the TL altitude changes from about 700 km to 1100 km and, in moving poleward in the region -45° to -60° , it changes from about 700 km to about 1100 km.

Figure 3 shows the altitude variability of the TL versus dip latitude in region B. Here the features described in region A are retained but the position and variability is confined to the region from 1000 km to 1100 km. A minimum in the TL altitude is still evident at -30° dip latitude, but here there are large changes in the TL altitude in the regions -20° to -5° and -50° to -35° . Thus the trough or the minimum in the TL surface appears to be narrower in region B than in region A.

Figure 4 is a plot of the TL heights versus dip latitude in the region C. The minimum still appears at -30° , but is less pronounced. The points are scattered and it is difficult to draw the average surface. However, the mean altitude at the TL minimum tends to be higher than in the regions A and B. At the same time the poleward slope of the TL surface is shifted equatorward to -40° dip latitude. Region C appears to have the narrowest TL trough.

In the northern (summer) hemisphere the TL altitude shows great variability. No pronounced minimum can be seen in Figures 2, 3 and 4, but the TL points can be found as low as 800 km around $+30^\circ$ dip latitude. The examined altitude range, with dip latitudes above $+30^\circ$, is not sampled uniformly by the satellite and the exact behavior of the TL surface is not known. Around the dip equator, the TL surface lies above 1100 km as shown in Figures 2 and 3. TL altitudes were encountered by the satellite over the dip equator for the region C, which may lead to the conclusion that, for most of the cases there, the TL surface lies below 1100 km.

As mentioned above the local time variations of the TL surface have been ignored. This is justified because, after a detailed examination of a probable altitude/local time dependence within the narrow dip latitude bands in different longitude regions, no such dependence was found in the local time interval from 21 h to 04 h. Referring to the TL points encountered before 1830 local time and not plotted here it is easy to reach the conclusion that, in winter midlatitudes (-20° to -40° dip latitude), the TL drops from about 1100 km down to 600 to 700 km between

18h30 and 21h00 local time. Moreover in the altitude range from 1050 km to 900 km for this dip latitude range, no TL has been encountered between 19h40 and 21h00 local time. This means that the TL surface over midlatitudes falls rapidly after sunset and attains its normal nighttime level probably within an hour or so. The IRI-79 programs together with the CCIR numerical map were run in order to examine the predicted behavior of the TL surface in the nighttime midlatitude and equatorial ionosphere.

3. Comparison with IRI

Present computations of the TL under conditions similar to those with OGO-6 measurements show no longitude dependence, as indicated in Figure 5 by a thin line. The average TL surface taken from Figures 2, 3 and 4 is also shown for comparison. The dashed line in Figure 5 represents the F2-peak ion density altitude, which is given by the CCIR program and is independent of the IRI. On the other hand, the CCIR program strongly affects the IRI vertical models of ion density. There is a distinct lack of agreement between measured and computed TL altitudes. In the equatorial region ($\pm 25^\circ$ dip latitude) the TL-IRI altitude (as shown in Figure 5) ranges between 370 and 395 km, i.e. more than 600 km lower than the measured TL altitudes. For the winter midlatitude region, poleward from -25° dip latitude, the TL-IRI altitude is close to the minimum of the measured TL altitude.

On the summer side, the lack of measured TL points does not allow us to say how the TL-IRI model differs from the actual situation. However, the trend of the measured curves A, B and C above 900 km at $+30^\circ$ dip latitude seems to indicate an altitude difference of at least 300 km.

The dynamics of the ionosphere not taken into account in the IRI-TL models should be responsible for the great discrepancy between measured TL altitudes and those computed using this model. In the equatorial region some evidence for interhemispheric ion transport has been given elsewhere /Bailey et al., 1973; Heelis et al., 1978/. Such a transfer of O^+ ions from the summer to the winter side through the equator would raise the TL altitude in a way that would give the TL measured values. The trough on the winter side represents typical midlatitude nighttime conditions where the ionosphere descends due to the recombination in the F-layer and the consequential downward fluxes of O^+ from above. In that case IRI predicts the TL behavior fairly well. The poleward increase in the TL altitude is a result of the H^+ upward fluxes near the plasmapause. Here the O^+ scale height should increase because of the increased polarization of the electric field that couples electrons and ions /Banks and Kockarts, 1973/.

In conclusion, the TL surface examined using the RPA data of OGO-6 exhibits a behavior which differs considerably from that based on computations using the IRI-79 ion density model. The discrepancy is especially dramatic around the dip equator and near the midlatitude troughs. Further improvements of the model are needed, in particular the inclusion of the dynamic characteristics.

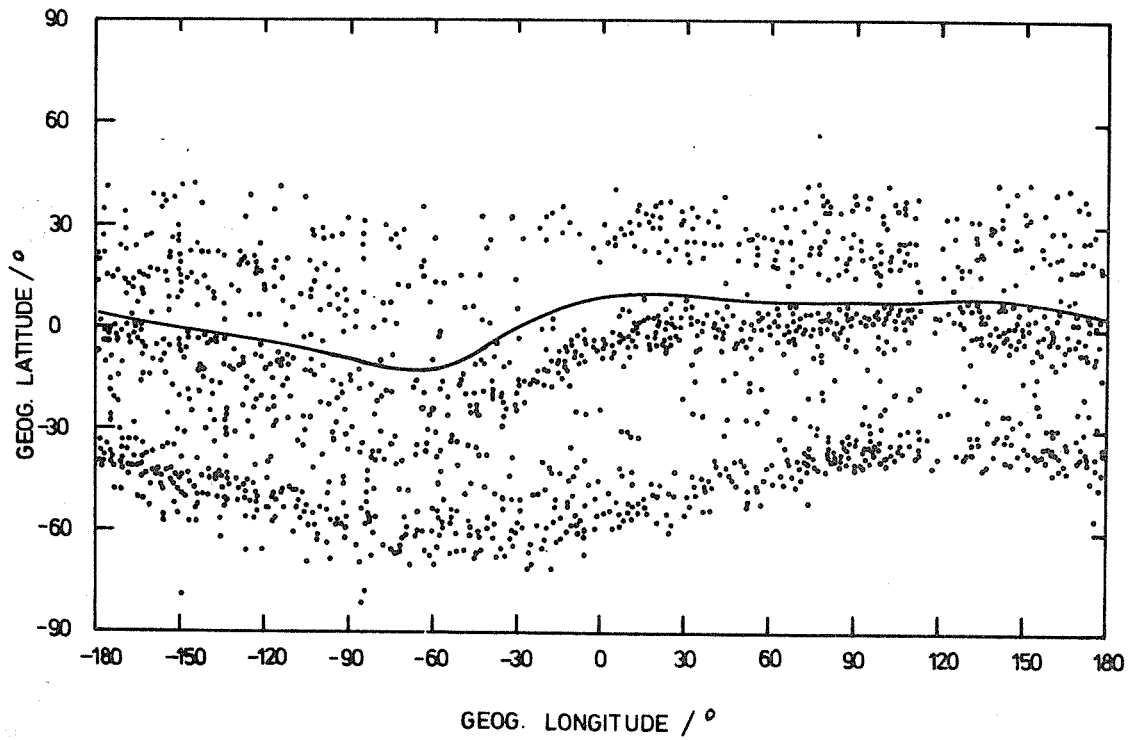


Fig. 1 Complete nighttime transition level encounters in the summer months of 1969 and 1970. The full curve represents the geomagnetic equator.

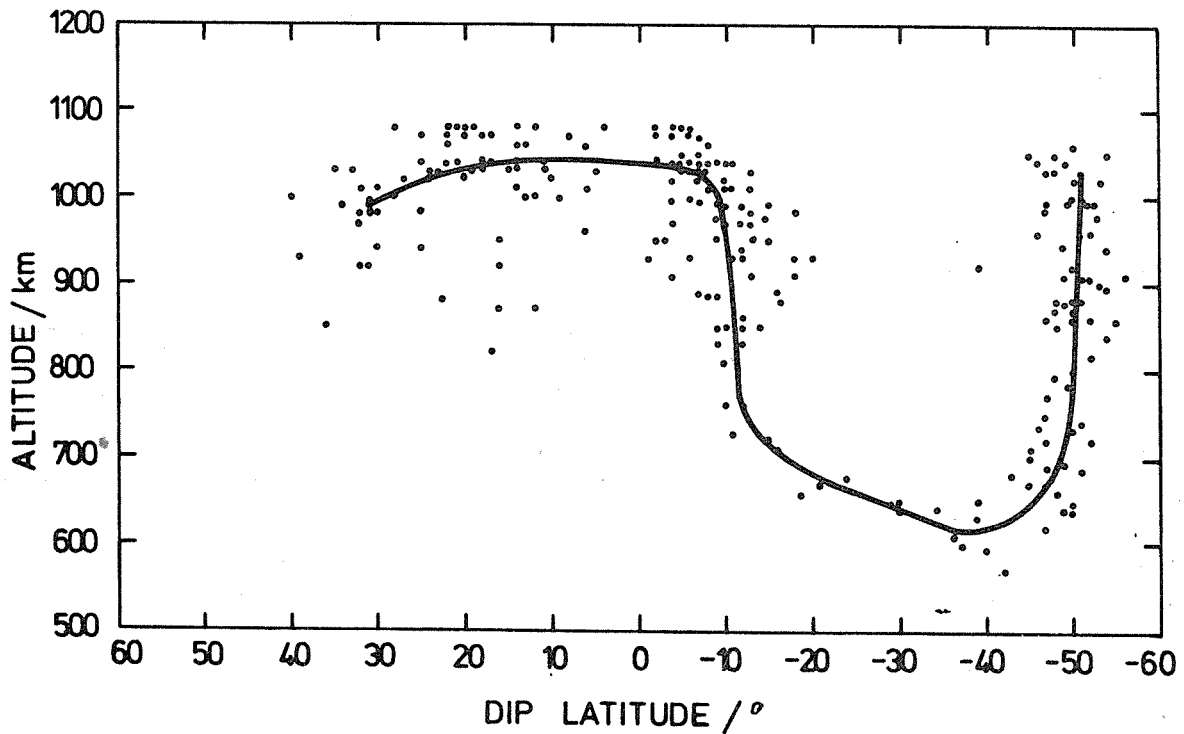


Fig. 2 Altitude versus dip latitude plot of TL points in the region A (60° to 150° longitude). An average TL altitude curve is drawn with full line.

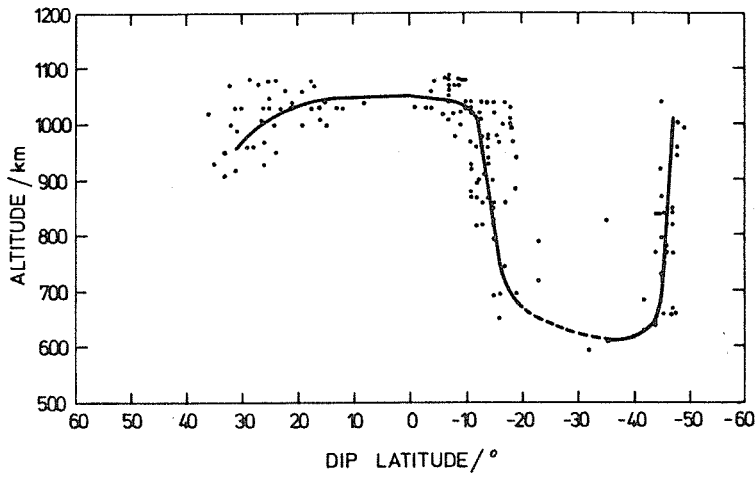


Fig. 3 As in Fig. 2 for region B (-30° to +60° longitude).

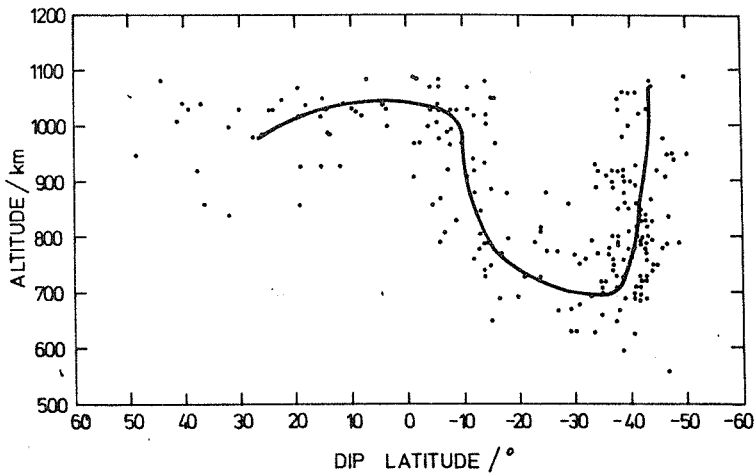


Fig. 4 As in Fig. 2 for region C (-180° to -30° longitude).

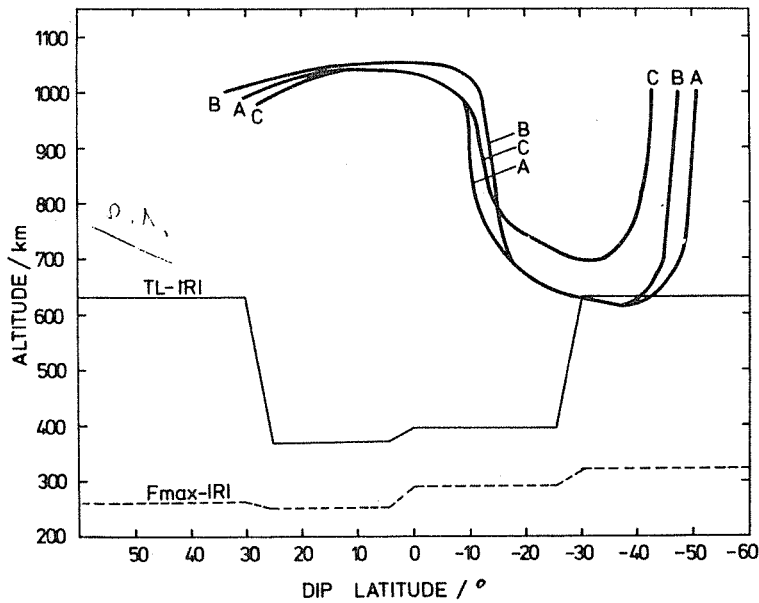


Fig. 5 Comparison between the average observed TL altitude curves for regions A,B,C (thick lines and computed altitudes (TL-IRI, thin line) and F max altitude as given by the CCIR program (dashed line).

3.1.3 Comparison of IRI with Vertical Profiles for the Ion and Electron Density and Electron Temperature Deduced on Board Vertical Rockets

K. Serafimov, I. Kutiev, L. Bankov, N. Bankov, Ts. Dachev,
B. Kirov, D. Teodosiev

Central Laboratory for Space Research,
Moskowska 6, Sofia, Bulgaria

Abstract: A comparison is made between the model profiles given by the last variant of IRI for Ne, Ni and Te and the values measured on board the rockets "Vertical"-3, -4, -6 and -7. The comparison covers the altitude interval 200 to 1500 km, and refers to the afternoon at middle latitudes near the autumn equinox. The observed discrepancies between the model and the measured values are analyzed, and an explanation is suggested connected with the dynamics of currents of magnetospheric and ionospheric origin.

1, Introduction

The 'Vertical' rocket program was designed to provide better technical possibilities for ionospheric investigations, as well as for some solar observations /Gringauz et al., 1968/. Since the first rocket with ionospheric payload (Vertical-3 in 1975), a number of rockets have been launched every year, in September or October, so that the measurements are capable of giving comparative data during a period of increasing solar activity.

In this paper we consider the vertical profiles of ion densities inferred from the spherical ion trap, and of the electron density and temperature inferred from a cylindrical Langmuir probe. The data have been taken from three rocket flights - Vertical 3, 4 and 6. All necessary information about the measurement is presented in Table 1. The instrumentation considered here was made by Bulgarian and Soviet research groups and was almost identical during all these flights /Serafimov, 1977/. The only exception was the use of a fourgrid spherical ion trap /Chapkunov et al., 1979/ on the Vertical-6 rocket. This latter improvement was favoured because it ensured a higher homogeneity of the ion collecting area and limited the perturbations which the analyzing grid introduced into the ambient plasma.

2, Results for Electron and Ion Densities

The comparison of the measured profiles with corresponding IRI models is shown on the Figures 1, 2 and 3. The most recent IRI-79 /Rawer, 1980/ program, together with CCIR F_L maximum characteristics, were adopted for geophysical conditions corresponding to the time of the measurements. All flights are carried out by day from the Volgograd rocket station (44°N, 49°E) at the same solar zenith angle of 67°.

Figure 1 present the vertical profiles of the ion and electron densities measured by the abovementioned instruments in the Vertical-3 rocket. The dashed line shows the ion density profile calculated by IRI using the CCIR values of hmF₂ and NmF₂. The profiles measured by different methods differ above 450 km, and this is due to the low velocity of the payload near the apogee. In this case the data for the electron concentration are more representative, and vice versa, below 250 km the data for the ion density seem more sensible. The IRI/CCIR profile coincides well with the measurements in the near maximum part of the F₂ layer. Above 350 km its values for the concentration are slightly lower; this may be due to the lower ion temperature and, therefore, smaller scale height.

Under 200 km the IRI/CCIR profile also gives lower values in comparison with the measured ion density.

A comparison of the measured Vertical-4 profiles of the ion (open circles) and electron (full circles) densities and those calculated by IRI is given in Figure 2. The continuous line shows the profile that was computed using CCIR data; the broken line shows the profile with given maximum electron density N_mF2 and its height h_mF2 . In this case CCIR gives values of N_mF2 and h_mF2 which deviate by about 40 km in height and a factor of two in maximum density. Again the IRI profile gives a lower density above the F2-layer maximum, and above 700 km it coincides with the measured profile of the electron concentration.

Figure 3 presents a comparison of IRI profiles and the measurements made by Vertical-6 /Serafimov, 1979/. Here the IRI profile reproduces well the measured ion and electron profiles when the values of N_mF2 and h_mF2 are assigned to it. In this case the calculated ion density above the maximum of F2-layer is slightly greater than the measured one. The measured profile itself changes abruptly its scale height at an altitude of about 600 km, which formally responds to a stationary rising flow of 10^9 cm^{-2} /Serafimov, 1979/. It is possible that such a non-stationary picture would give rise to the fact that the calculated ion density above the maximum exceeds the measured one. Below the maximum of the F2-layer, a "valley" with a minimum at 130 km is measured which is absent in the IRI profile.

3. Results for Electron Temperature

In the experiments considered here, the electron temperature has also been determined by a Langmuir probe. Figures 4, 5 and 6 show a comparison of the measured and the calculated T_e according to IRI for the three rocket flights. When calculating T_e according to IRI, the corresponding measured values of N_mF2 and h_mF2 have been introduced. In Figure 4 we have shown a comparison of T_e as calculated by IRI, (full line) and as measured by Vertical-3 (circles). Within the whole height range, T_e (IRI) is lower than the measured value, and above 300 km this difference exceeds 1000 K. It is seen that, above the F2-layer maximum, the calculated and measured gradients of the temperature differ considerably.

In the experiment with Vertical-4, the comparison between T_e (IRI) and the measured T_e is shown in Figure 5. Unlike the previous case, here the coincidence up to 1000 km is complete apart from insignificant difference in the temperature gradient above 700 km. Figure 6 shows the comparison using the data from Vertical-6. In this case the difference is greatest near the F2-layer maximum. In the height range up to 900 km, the calculated T_e is lower than the measured one.

4. Conclusions

The comparison of the IRI models for the ion density and the electron temperature with the corresponding measured values, obtained using the "Vertical" rockets, gives some idea about how far IRI presents satisfactory results. Unfortunately, the number of comparisons is not sufficiently great for a precise estimation of the reliability of the IRI profiles, but they serve as an preliminary test. The general conclusion drawn from these comparisons is that CCIR does not always give good values of N_mF2 and h_mF2 . In this work we have made an attempt to exclude the influence of CCIR, and the values of these quantities have been taken from the measurements. In this case the calculated ion density immediately above the F2-layer maximum was found to be lower than the measured one in two out of three experiments. This is probably due to the use of a lower value of the scale height or of the ion temperature.

The available data from the measurements give an opportunity for a comparison of the electron temperature as well. In two out of three cases (Figures 4 and 6) the electron temperature calculated according to IRI is lower than the measured one. The difference in the T_e height gradients above the F2-layer maximum is probably due to the variability of the heat flux coming from above, and this is connected with the total content and temperature of H^+ in the magnetic flux tube.

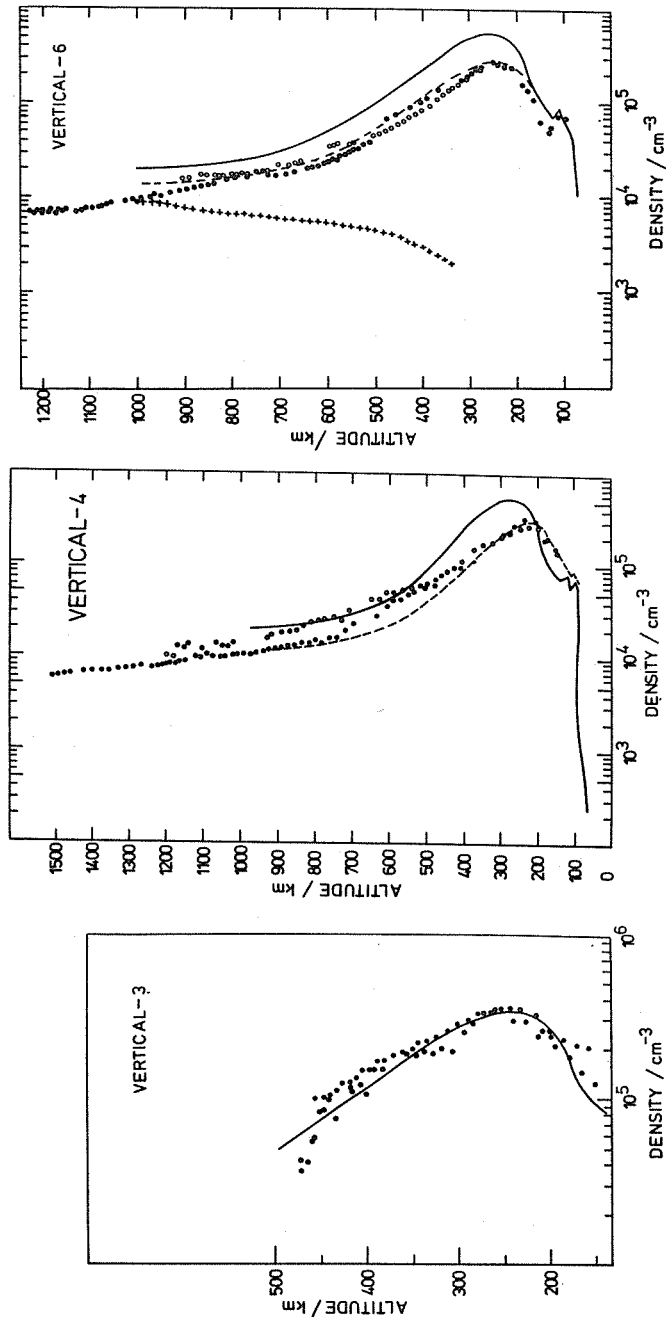


Fig. 1

Fig. 2

Fig. 3

Fig. 1 Electron and ion profiles. Open circles: ion density; full circles: electron density. IRI ion density profile with hmF2 and foF2 taken from CCLR (full line).

Fig. 2 The same as Fig. 1 Dashed line: IRI ion density with hmF2 and foF2 taken from measurement.

Fig. 3 Same as Fig. 2. Crosses: H^+ ion density profile.

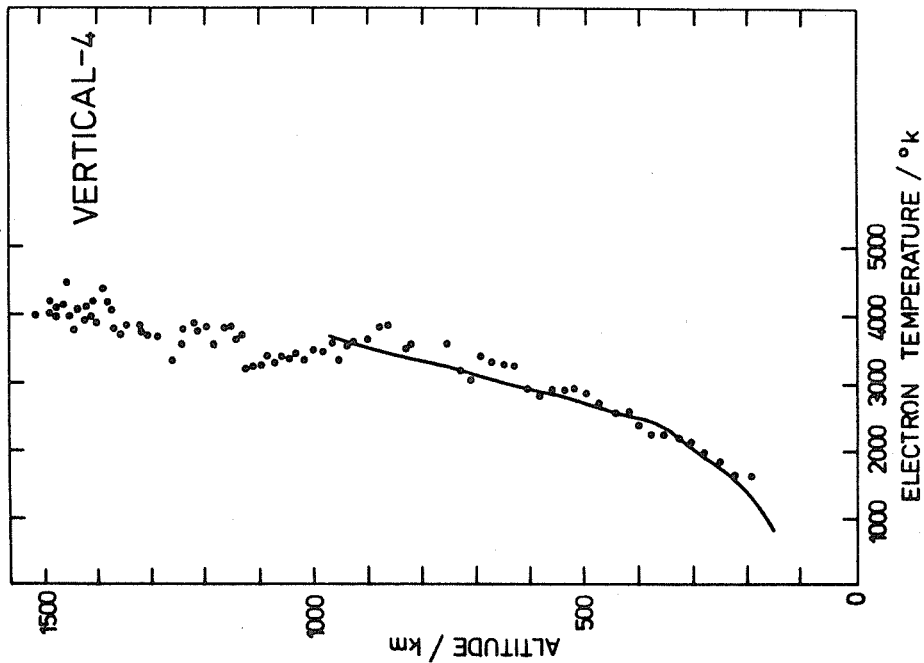


Fig. 4

Fig. 4 Full circles: electron temperature. IRI electron temperature (full line).

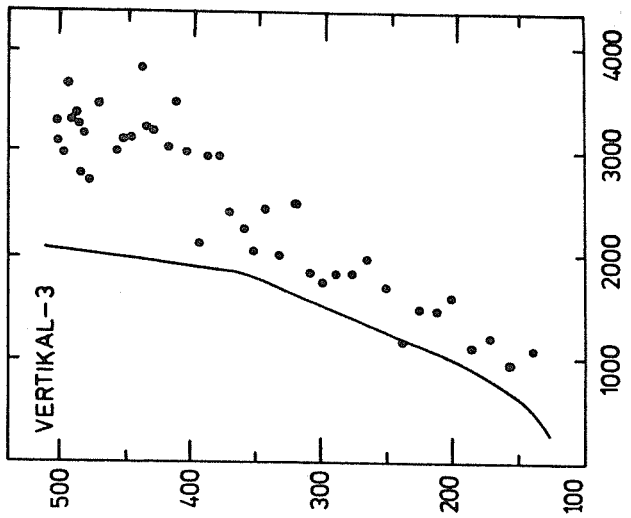


Fig. 5

Fig. 5 Full circles: electron temperature. IRI electron temperature (full line).

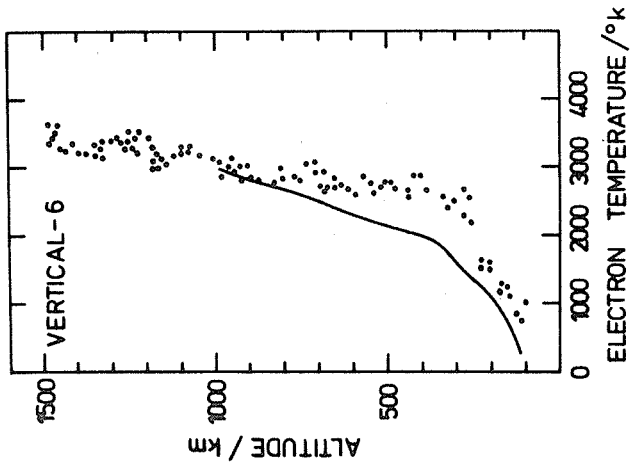


Fig. 6

Fig. 6 Full circles: electron temperature. IRI electron temperature (full line).

3.1.4 Empirical F-Region Model Development Based on S3-1 Satellite Measurements +

C.R. Philbrick

Air Force Geophysics Laboratory, Hanscom AFB/Mass., USA

Abstract: The ion mass spectrometer experiment on the S3-1 satellite collected measurements of the density of N^+ , O^+ , N_2^+ , NO^+ and O_2^+ in the altitude region 150 to 500 km for a period of approximately six months. Measurements from approximately 1800 orbits, which cover all latitudes for both summer and winter and four local time periods, have been studied to characterize the ionospheric variations. Mean profiles and median profiles with upper and lower quartile values, which show the data range, have been deduced from the measurements. The variation of the ion species densities with latitude, solar zenith angle, season, geomagnetic activity, and latitude has been compared with ionospheric models, such as the International Reference Ionosphere (IRI). Differences in profile shapes and relative composition from the IRI model are discussed. The response of the ionosphere to geomagnetic storm effects is shown in several cases where molecular ion densities can become dominant over atomic ion species to altitudes above 300 km.

1, Introduction

Several studies have been carried out toward the development of a useful model for predicting the mean ionospheric properties based upon various collections of data. The Bent-Ilewellyn /1973/, CCIR /1967/ and IRI /Rawer et al., 1978/ models rely heavily on the extensive data which have been collected by ground-based ionosondes and satellite topside sounders. Some in situ electron and ion density profiles from rockets and satellites have also been considered in formulating these models. The parameter which is best described by the models is the electron density near the peak of the F2-region, which is directly determined from the plasma critical frequency. However, there is significant uncertainty in the shape of the density profiles, particularly in the lower F-region. The only effort to date to empirically model ion composition has been that of the IRI model which is based entirely upon the summary of 41 rocket probes which was prepared by Danilov and Semenov /1978/.

Using the data base from the S3-1 satellite mass spectrometer, the initial stages of an empirical model for the altitude region between 150 and 500 km have been completed. This paper is an interim progress report on this development. Examples of the data, a general description of the modeling approach and initial results from the investigation are presented.

2, Experiment

The mass spectrometer experiment on the S3-1 satellite /Philbrick, 1976/ provided a data base of about 1800 orbits of ion density measurements covering the period November 1974 through May 1975. The density of the five primary ions, N^+ , O^+ , N_2^+ , NO^+ and O_2^+ , was measured each second, but this study only considers those measurements made each 10 seconds when the instrument axis was most closely aligned with the direction of motion of the spinning satellite. A comparison study of the ion density measured by the S3-1 as it passed through the F2 peak with ground-based ionosonde measurements of the foF2 provided an opportunity to test and calibrate the instrument performance. A total of 73 cases were located where the satellite was passing through the F2 peak within a $5^\circ \times 5^\circ$ latitude and longitude box centered on the ionosonde station, and an foF2 measurement was available within 15 mi-

minutes of the satellite overpass. No trend which would indicate a long term sensitivity change was observed and the standard deviation of the comparison was 26%. In another study /Hilbrich et al., 1972/ a direct comparison was made from five nearly coincident measurements with the AEROS-B impedance probe. The ratio between the measurements from the two satellites was $1.00 \pm .06$. Based on these studies and the laboratory calibrations, the reported ion densities should be accurate to better than $\pm 15\%$ and the relative ion composition accurate to better than $\pm 10\%$ for densities greater than $5 \cdot 10^8 \text{m}^{-3}$.

3, Measurements

Figure 1 shows an example of part of an orbit near perigee for day-time conditions. This orbit is typical for a geomagnetically quiet period even though some wave structure is observed in the southern midlatitude region. Note that the N^+ typically follows the C^+ response but at a density of about 1% of the C^+ on the day side. Also, the molecular ions have a generally similar behavior. Figures 2 to 4 show examples of some of the features which are commonly observed in the data set. These examples are included to indicate the quality of the data, show the variability of the ionosphere, and to provide clear examples of three of the features which occur in the F-region.

Figure 2 shows the results for orbit 1596 which occurred 15 orbits (less than one day) after the results of Figure 1, but these results were obtained near the peak of a geomagnetic storm corresponding to a $K_p = 7$. The left-hand side of the figure corresponds to latitudes within $\pm 30^\circ$ of the geomagnetic equator and the character of the measured profiles is similar to that of Figure 1 in the F1- and F2-regions. However, the right-hand side of the figure, which corresponds to geomagnetic latitudes between 30° and 70° , shows the strong effect of the storm. The F2 peak vanished, primarily because of the loss of C^+ due to the change in the $\text{C}^+ + \text{N}_2 \rightarrow \text{NO}^+ + \text{N}$ and $\text{C}^+ + \text{O}_2 \rightarrow \text{O}_2^+ + \text{O}$ reaction rates (followed by dissociative ion-electron recombination) in the presence of strong electric fields /Schunk et al., 1975/ and the large enhancement in the densities of N_2 and O_2 in the thermosphere. The N_2^+ ion density is increased due to the enhanced N_2 density and ionization rate from precipitating electrons. Between 60° and 70° geomagnetic latitude large spatial irregularities are observed with the O^+ density changing by more than a factor of 10 between measurements which are spaced horizontally by about 70 km. During this geomagnetic storm and others that have been examined, the cross-over from molecular to atomic ion predominance has been found as high as 400 km, instead of the normal case which is near 180 km.

Figure 3 shows an example of nighttime measurements which are characterized by the steep density gradient on the bottom side of the F2-region which generally becomes steeper at the lower geomagnetic latitudes. This orbit also shows the characteristic of the fountain effect, also called Appleton anomaly /Appleton, 1946/, over the magnetic equator. The molecular ion profiles exhibit the transport upward from the E-region into the F1-region directly over the magnetic equator.

Figure 4 gives an example of the ion density as the satellite passes through a strong auroral disturbance near the satellite's perigee. Over a range of a few degrees of latitude, the ion density is increased by more than a factor of 20 due to ionization by energetic particle precipitation.

4, Modeling Approach

The measurements for each ion species and for the total density have been divided into data bins with the following set of ranges:

Altitude/km: 150 to 160, 160 to 170, ..., 280 to 290, 290 to 310, 310 to 330, ..., 490 to 510.

Solar zenith angle: 60° , 60° to 70° , 70° to 90° , 90° to 110° , 110° .
 Magnetic index: $0 < k_p < 2$, $2 < k_p < 4$, $k_p > 4$.
 Latitude (geomagnetic): -90° to -70° , -70° to -60° , -60° to -45° , -45° to -15° ,
 -15° to 0° , 0° to $+15^\circ$, $+15^\circ$ to $+45^\circ$, $+45^\circ$ to $+60^\circ$,
 $+60^\circ$ to $+70^\circ$, $+70^\circ$ to $+90^\circ$.
 Season: Nov to Feb, Mar to Apr, May to Aug, Sep to Oct.
 Studies were also made by subdividing the data further to examine the dependence on sunspot number, AE index and DST index.

From examination of the data it was apparent that in order to develop a model of mean conditions, it would be necessary to eliminate some of the measurements which represented more unusual ionospheric conditions. These measurements which were outside of two standard deviations from the log mean of each bin were eliminated. Most of the analysis has included the calculation of the mean, median, and upper and lower quartile values for each data bin. The data bins that have been used generally contain between 50 and 800 measurements. Figure 5 shows an example of the mean curves for the total ion density in the latitude ranges from 0° to 15° and from 15° to 45° under nighttime conditions. Each point represents the mean of the logarithmic values for that data bin and the bars show the range of the upper and lower quartile values. In Figure 6 the altitude profiles between 150 and 270 km are shown for the five latitude divisions in the winter hemisphere at night. The curves show a strong variation with latitude. At higher altitudes, near the F2 peak, the highest density is near the equator and this profile has the strongest altitude gradient. The profile, corresponding to the auroral oval, 60° to 70° , is nearly independent of altitude. The major features of this latitude distribution are due to the constraints on the ion diffusion due to the Earth's magnetic field.

Figures 7 and 8 show the mean profiles for the ion species and the total ion density at midlatitudes under the conditions of winter night and summer day. Also shown in these figures is the appropriate IRI model mean profile for total ion density at 30° latitude. The mean of each independent data bin, represented by points on these curves, form relatively smooth profiles because of the large number of measurements within each bin. However, the shape of the IRI model profile is considerably different from the S3-1 profile in the lower F-region at night. The agreement between the IRI and S3-1 profiles is much better for the daytime comparison. The curves shown in Figures 7 and 8 represent the midlatitude mean densities. Examination of these profiles indicates the difficulty in obtaining suitable analytic expressions for representing the global mean features in the ion species densities. From our efforts to date, it appears that the total ion density profile for the S3-1 mean conditions can probably be represented analytically. Possibly these shape functions can be used with the much larger data base of other models, which contain a full range of solar and geophysical variations, by normalizing to the F2 peak density.

5, Conclusions

The area where the mass spectrometer measurements of S3-1 and other satellites can make a unique contribution to the modeling efforts is in describing the relative ion composition. Figures 9(a...d) show the relative ion composition for summer day and winter night conditions at midlatitude and high latitude for the five principle ion species. Examination of these figures lead to several interesting conclusions regarding the ion chemistry processes and the neutral species distributions, but these conclusions will not be discussed in this paper. The present reason for examining these cases of relative ion composition is to show that the species densities could be obtained from interpolation within a reasonable size table if an adequate total density model profile is available. This approach of using relative ion composition is the method currently used in obtaining species profiles from the IRI model. Some

comparisons of the S3-1 mean ion composition and the IRI composition model are made in another paper in this volume (1.3.2).

Acknowledgements

The major effort of organizing and analyzing the data has been done by R.H. Eshvani. The author gratefully acknowledges the efforts of R.E. McInerney, D. Belorey, E.J. Ziema, M.E. Gardner and discussions with K.S.W. Champion. The 1980 version of the IRI model (IRIFC7) was kindly supplied by K. Rawer. Data used in connection with this article were obtained from WDC-A (S.T.P.)

Editor's note:

It is shown in the last section of paper 1.3.2 /Philbrick et al./ that considerable discrepancies exist between rocket and satellite ion composition measurements at altitudes above 160 to 180 km, see Figures 3 and 4 of paper 1.3.2. The authors of this latter paper feel that compared with rocket data satellite measurements are not only made more often but also are now more reliable. Note that, for heights up to 200 km, IRI 78 is exclusively based on rocket measurements of ion composition.

+ Paper presented at 1981 Symposium on "The effects of the Ionosphere on Radiowave Systems" (jointly sponsored by N.R.L., O.N.R. and A.F.G.L.) held at Alexandria/Va. April 1981.

2-17 REV. NO. 1591.0
UNIT OF ORBIT 3/ 8/75

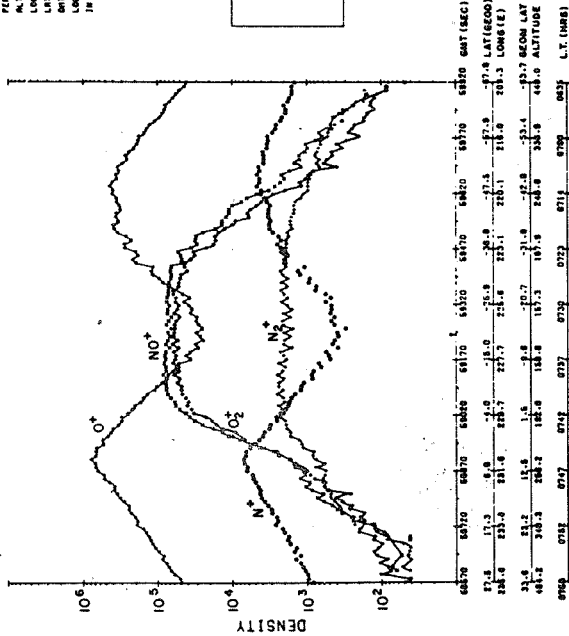


Fig. 1

2-17 REV. NO. 685.0
UNIT OF ORBIT 1/28/74

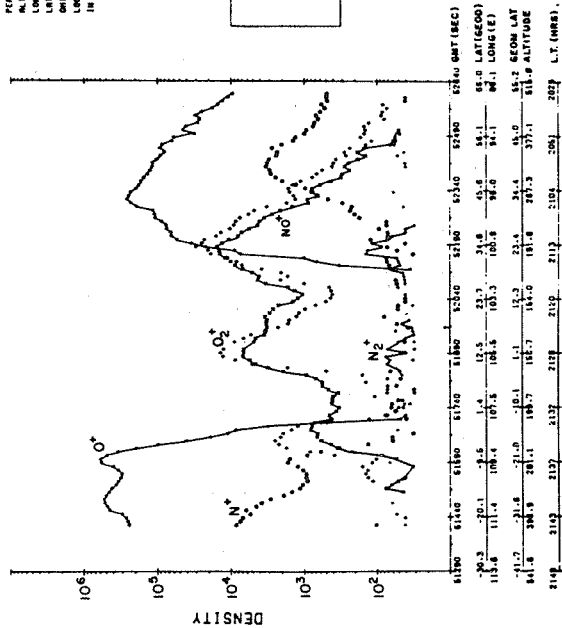


Fig. 2

2-17 REV. NO. 1586.0
UNIT OF ORBIT 3/10/75

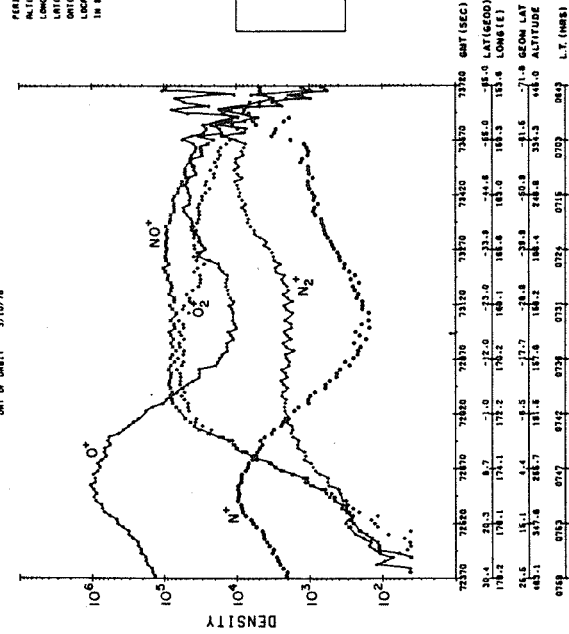


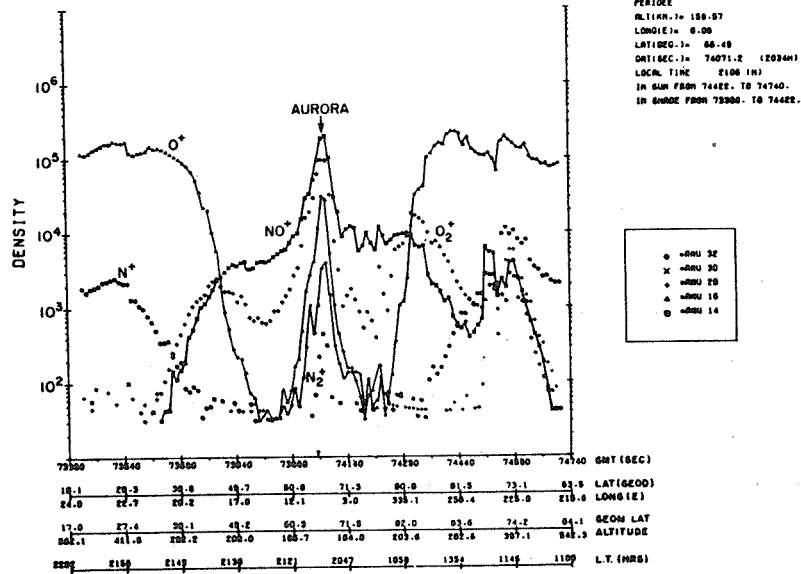
Fig. 3

Fig. 1 The species density (ions/cm³) profiles for N⁺ (14 amu), O⁺ (16 amu), N₂⁺ (28 amu), NO⁺ (30 amu) and O⁺ (32 amu) Measured by the S3-1 on orbit 1581 are shown. The scales show the GMT total seconds, latitude, longitude, geomagnetic latitude, altitude and local time.

Fig. 2 Species profile similar to those of Fig. 1 but for conditions corresponding to a geomagnetic storm.

Fig. 3 Species profile measurements similar to those of Fig. 1 but for nighttime conditions with perigee centered near the magnetic equator.

Fig. 4



PERIOD
 ALTITUDE: 150-57
 LONGITUDE: 0-90
 LATITUDE: 66-48
 GMT(SEC.): 74071.2 (2034H)
 LOCAL TIME: 2100 (H)
 IN GEAR FROM 74422 TO 74740
 IN GEAR FROM 73800 TO 74422

• -ORU 32
 x -ORU 30
 + -ORU 28
 * -ORU 16
 ○ -ORU 14

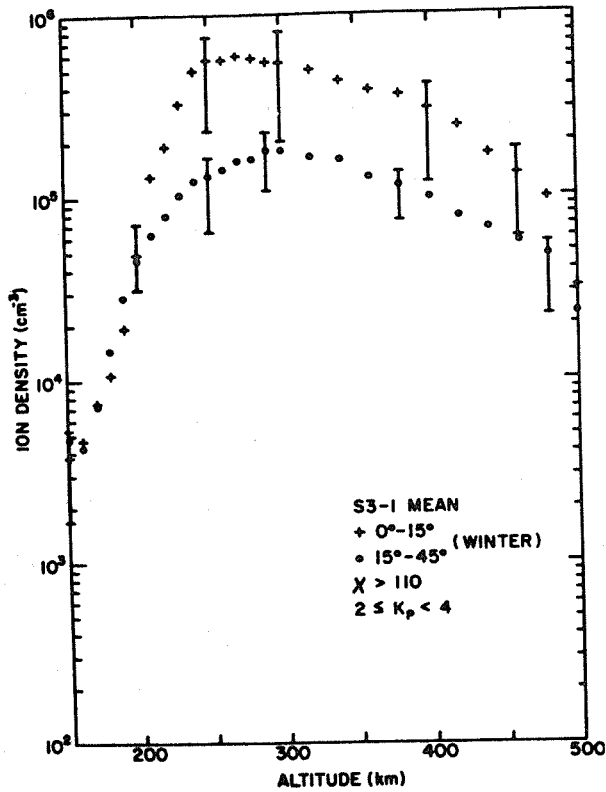


Fig. 5

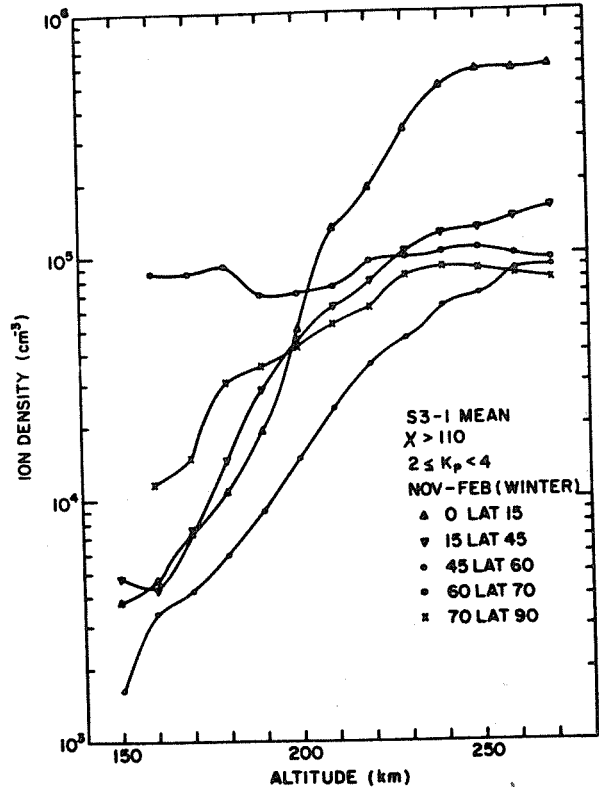


Fig. 6

- Fig. 4 Species profiles similar to those of Fig. 1 but for a period of enhanced auroral zone activity.
- Fig. 5 The mean ion density profiles for two latitude regions are shown together with bars representing the range of the upper and lower quartiles for the data bin.
- Fig. 6 The mean ion density profiles are shown for five latitude ranges in the winter hemisphere at night.

Fig. 7 The mean ion species and total density profiles are shown for midlatitude winter nighttime conditions together with the appropriate profile for total ion density from the IRI-80 model.

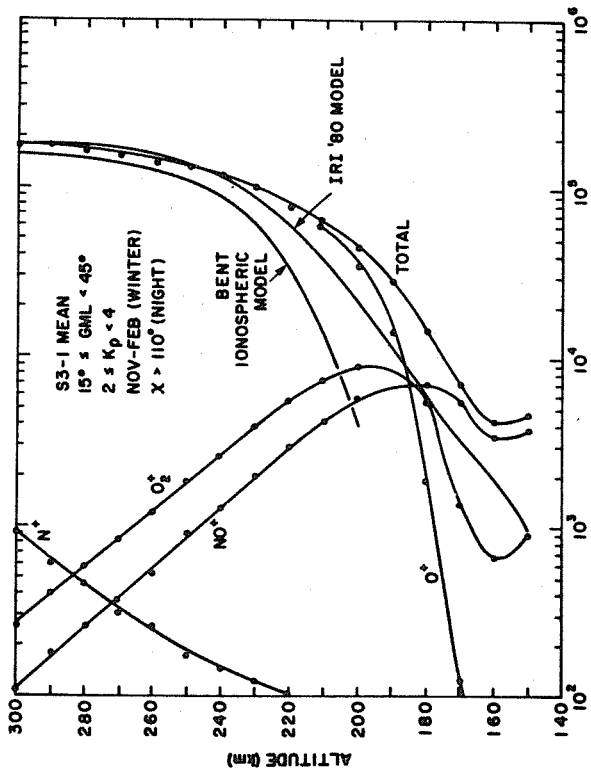


Fig. 7

Fig. 8 Ion species and total density profiles similar to those of Fig. 7 are shown for summer daytime conditions.

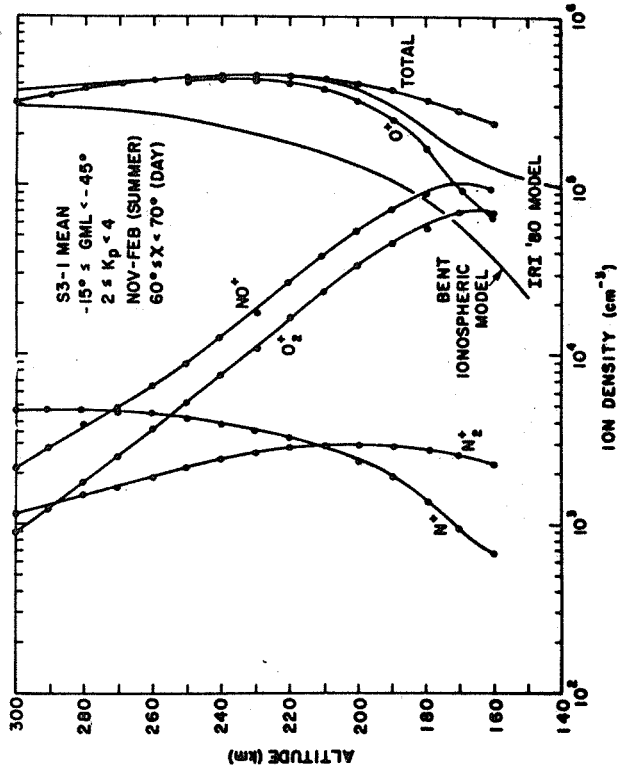


Fig. 8

Fig. 9 Relative ion composition percentages are shown for the F1 and lower F2 regions for the five species measured by the S3-1 satellite for four cases:

- (a) mid-latitude, day summer;
- (b) mid-latitude, night, winter;
- (c) high-latitude, day summer;
- (d) high-latitude, night, winter.

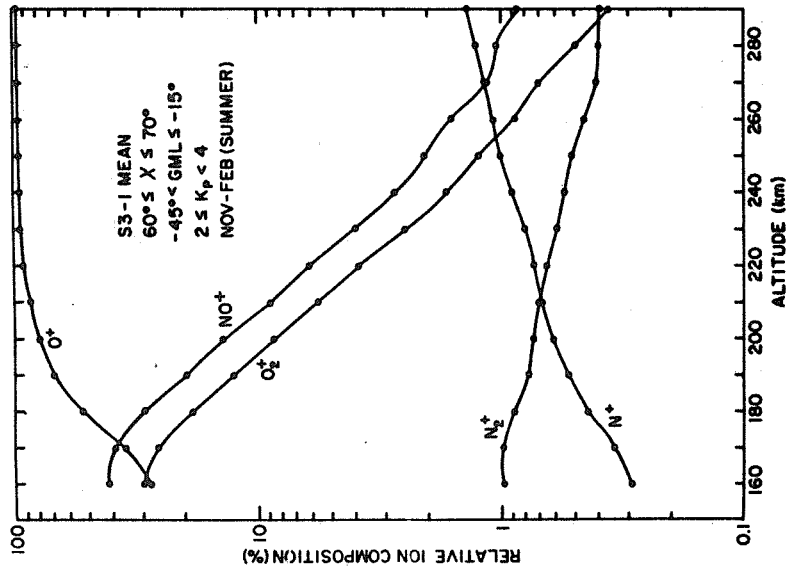


Fig. 9a

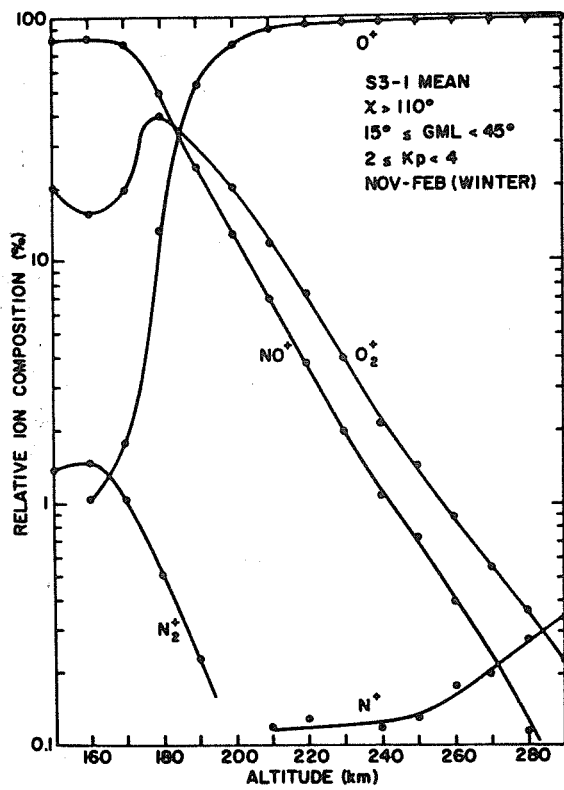


Fig. 9b

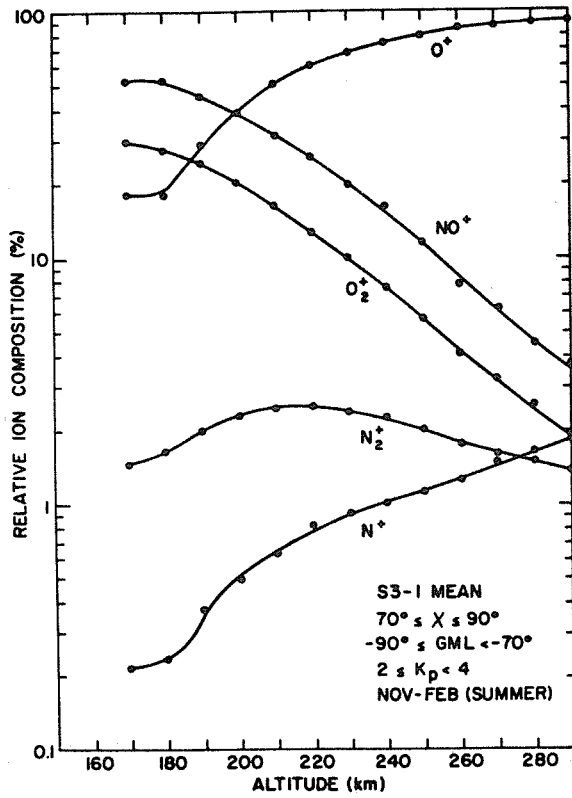


Fig. 9c

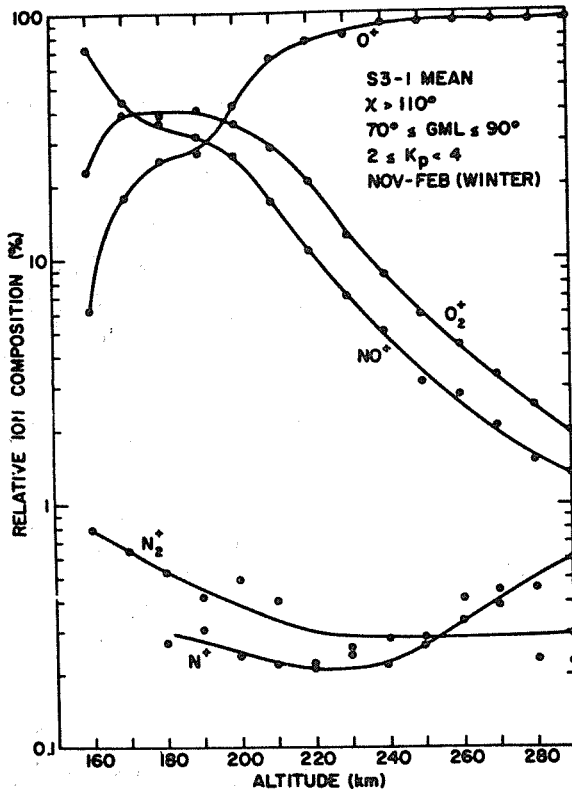


Fig. 9d

Fig. 9 Relative ion composition percentages are shown for the F1 and lower F2 regions for the five species measured by the S3-1 satellite for four cases: (a) mid-latitude, day, summer; (b) mid-latitude, night, winter; (c) high-latitude, day summer; (d) high-latitude, night, winter.

3.1.5 Temperature Control of Cluster Ion Concentration

Maria Dymek

Polish Academy of Sciences, Space Research Centre,
Warsaw, Poland

Abstract: In order to assess the chances of producing detailed models of the cluster ion population in the lower ionosphere, the effect of thermal breakup of $\text{NO}^+(\text{H}_2\text{O})_n$ ions is discussed. To this end two extreme cases were considered, both based on a complex chemical model. The reaction rate constants were either taken for a temperature of 300 K, or for a complete neglect of thermal breakup. When adopting a temperature of 300 K, which exceeds the real ionospheric temperature, thermal breakup leads to the disappearance of $\text{NO}^+(\text{H}_2\text{O})_n$ and seriously influences the concentration of $\text{H}^+(\text{H}_2\text{O})_n$ with $n > 3$. The uncertainty of the reaction rate constants and their temperature dependence prevent a standard model from being established. Even if this problem was resolved, the known variations of temperature near the mesopause should be taken as a warning against giving detailed indications in a standard model like III.

1, Introduction

In chemical reactions of cluster ions, heavy ions with low binding energies are both the reactants and the products. The dependence of reaction rates on temperature is strong, usually exponential, and this is due to the weak bonds.

Because of experimental difficulties, our present knowledge of the temperature dependence of the reaction rate constants is rather limited. Laboratory data were usually obtained at 300 K, while the temperature in the ionosphere may often be different. The use of these rate constants in model calculations very considerably influences the computed ion concentration profiles, notably at heights at which the ionospheric temperatures differ appreciably from 300 K, e.g. at the mesopause level.

The lack of laboratory measurements of the temperature dependence of the reaction rate constants for NO^+ clusters creates serious difficulties in the study of the ion chemistry of the lower ionosphere. A controversy exists, in particular, over the reaction rate constants for thermal breakup of $\text{NO}^+(\text{H}_2\text{O})_n$. The constants measured in the laboratory at 300 K are in the range from 10^{-20} to $10^{-18} \text{ cm}^3 \text{ s}^{-1}$; see Fehsenfeld et al., /1971/ and Picket and Teague /1971/. On the other hand, the binding energies of $\text{NO}^+(\text{H}_2\text{O})_n$, as measured by French et al. /1973/, are 0.79, 0.69 and 0.58 eV for $n = 1, 2$ and 3 , respectively. Reid /1977/ suggests that, since these energies are so high, the thermal breakup of these ions can be neglected at typical E-region temperatures.

In order to obtain upper and lower limits, the computations were made using the reaction rate constants corresponding to 300 K /Fehsenfeld et al., 1971/ on the one hand, and neglecting thermal breakup completely on the other. For a few reactions for which measurements exist, we also took account of the measured or estimated temperature dependences of the reaction rate constants. Three different 'standard' temperature profiles were considered; that given by Gurevich /1978/ lies between the two limits, WARM and COLL, given in CIRA 1972 (Figure 1 for 70° latitude) which are intended to represent the winter and summer mesosphere, respectively.

The set of chemical reactions adopted in the computations was fully explained in another paper /Dymek, 1980/.

2, Input Data

Density profiles of the neutral atmosphere constituents H_2 , O_2 , O and O_3 participating in photochemical processes were taken from CIR 1972,³ whereas the densities of $O_2(^1\Delta g)$, H_2O , CO_2 , CH , HC_2 and HO_2 were taken from the USA Handbook /1973/. For NO , Keira's /1971/ profile was used. Photoproduction rates in the ionosphere were calculated using the quiet Sun spectrum of Heroux et al., /1974/, for moderate solar activity (Covington index $F(10.7) = 120$). Absorption cross-sections and photoionization efficiencies were taken from Cshio et al., /1966/.

Ionization of excited $O_2(^1\Delta g)$ was also taken into account following Iaulsen et al., /1972/. The chemical reaction rates used in the computations were taken from Reid /1977/, Ferguson /1974/ and Rowe et al., /1974/.

The computations were made for two different temperature profiles called WARM and COLD; as for the H_2O concentrations Reid's /1975/ model WET was used.

3, Results of Computations

The effect of thermal breakup of $NO^+(H_2O)_n$ on the concentrations of NO^+ hydrates and of $H^+(H_2O)_n$ (with n greater than 3) was first computed either neglecting H_2O thermal breakup completely, or else assuming the large reaction rates found in the laboratory at 300 K. As could be expected, the 300 K thermal breakup of $NO^+(H_2O)_n$ leads to the disappearance of these ions, and also reduces the concentration of $H^+(H_2O)_n$ with $n > 3$ by a factor of more than 1000.

It has already been pointed out by Reid /1977/ and Rowe et al. /1974/ that the presence of hydrated protons in the ionosphere above 70 km is due to the reactions that convert $NO^+(H_2O)_n$ into $H^+(H_2O)_n$. This is the reason why a decrease of NO^+ hydrates, resulting from thermal breakup, is followed by a decrease in the $H^+(H_2O)_n$ concentration.

It appeared further that below 80 km the thermal breakup of $NO^+(H_2O)_n$ causes an increase in the concentration of the unhydrated NO^+ . When making comparisons with measured ion densities, it is important to note that artificial breakup of ions may produce erroneous results in ion composition measurements aboard rockets. The increase in the ambient temperature caused by the shock wave of the rocket may destroy the $NO^+(H_2O)_n$ ions, so that they are not recorded. In fact the measurements of Johannessen and Krankowsky /1974/, made at reduced rocket speed in the summer polar atmosphere (i.e. at low temperature), revealed the presence of $NO^+(H_2O)$ and $NO^+(H_2O)_2$. As a general rule, the more carefully recent experiments were made, the more cluster ions were found.

Both cases considered in this first approach are, of course, unrealistic, so that the computed range of variability is too large. A more realistic deduction should take account of a realistic temperature profile, and of the temperature dependency of the rate constants as far as the latter is known. For Figures 2a, b, the mean temperature profile of Gurevich /1978/ (curve 3 in Figure 1) was assumed. The solid curves represent the ion concentration profiles calculated with an allowance for temperature dependent reaction rates, while for the broken curves, fixed rates (namely corresponding to 300 K) were assumed. Because of the greater rate of breakup at higher temperature, the concentrations of cluster ions are notably higher in the first more realistic condition. According to Kebarle et al. /1967/, an increase in temperature causes also a decrease in the direct hydration rate, so that the rates of cluster formation and breakup both depend strongly on the temperature.

Comparison with the 300 K condition shows considerably greater densities of all clusters under realistic assumptions. Only at heights below about 75 km do the first and second hydrates of protons have greater densities at the higher temperature, as a result of enhanced thermal breakup of heavier ions. The possibility of such an effect was pointed out by Frankowsky et al., /1972/ when interpreting day - measurements of ion composition.

Finally, similar calculations were made for the temperature profiles WARM and CCIL of CIRA 1972 (curves 1 and 2 in Figure 1); the results show an increase of the concentration of both $H^+(H_2O)_n$ (with $n > 3$) and $NO^+(H_2O)_n$ when switching over from WARM to CCIL, see Figure 3.

4. Conclusion

Positive cluster ions in the lower ionosphere are subject to a very strong temperature control. Even when specific winter anomaly conditions are neglected, the range of temperature variation near the mesopause is so large that the different cluster concentrations may vary by orders of magnitude, particularly above 75 km. Thus large differences of concentrations measured under different conditions are not at all surprising. It appears therefore that, for an empirical model like IRI, it is inappropriate to specify relative abundances of clusters of different orders, rather than to give some percentage abundance of all the clusters together as compared with that of the molecular ions.

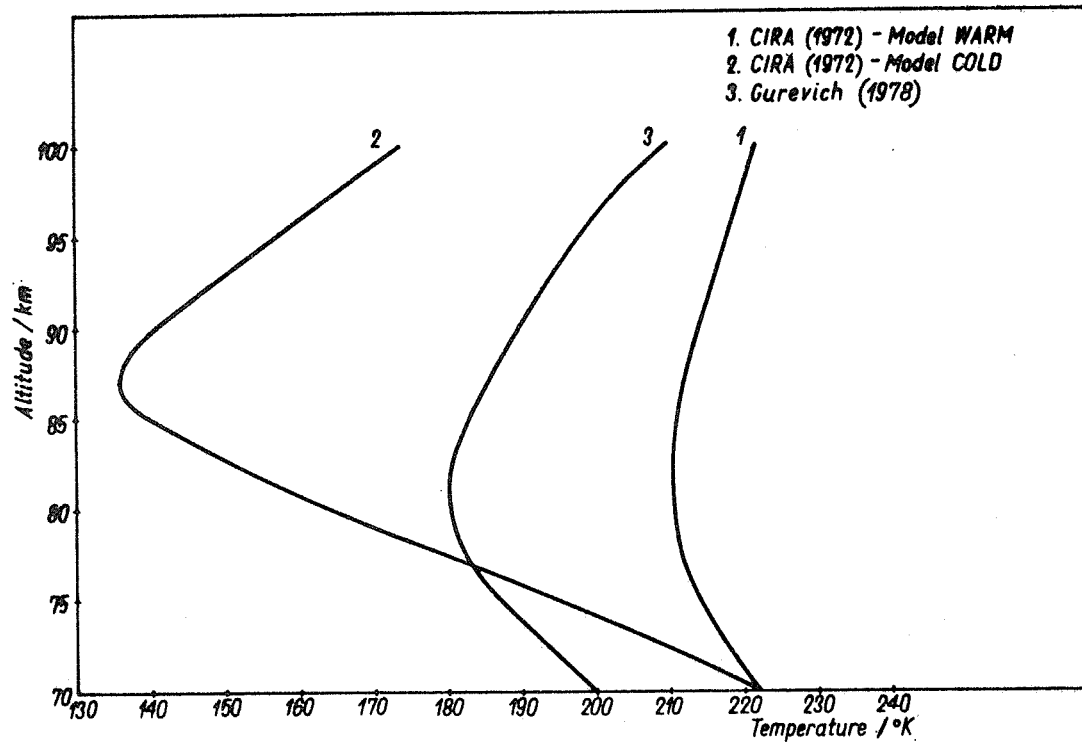


Fig. 1

Fig. 1 Three temperature profiles: CIRA (1972) WARM and COLD; Gurevich (1978).

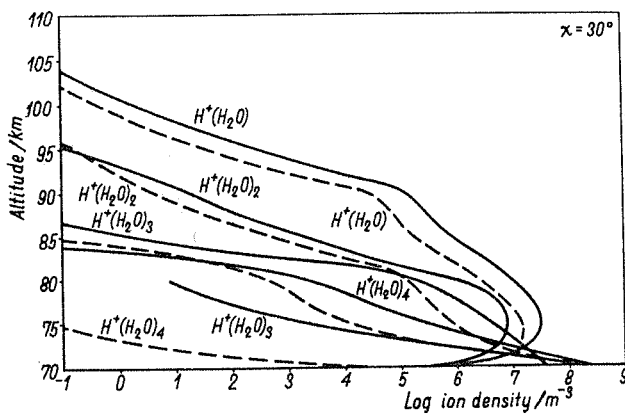


Fig. 2a

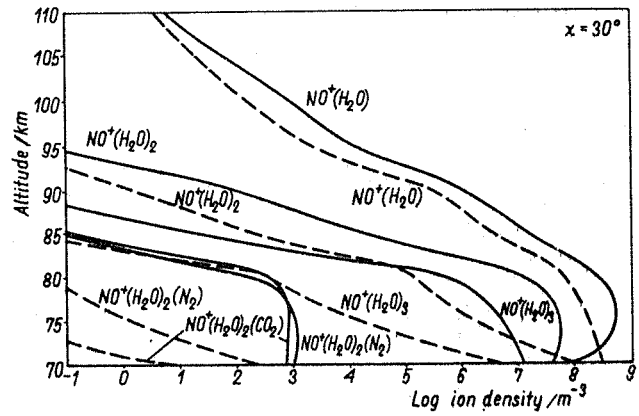


Fig. 2b

Fig. 2 Calculated profiles: a) water cluster ions; b) NO^+ clusters; taking into account temperature dependence of the reaction rate constants and the real ionospheric temperature (solid lines) or using the reaction rate constants for 300 K (broken lines).

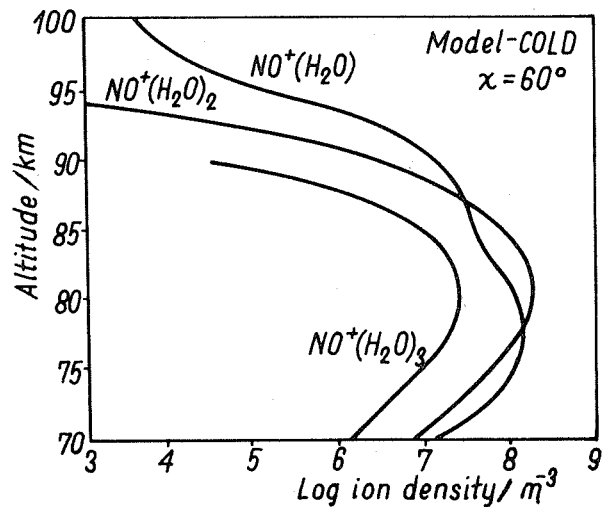
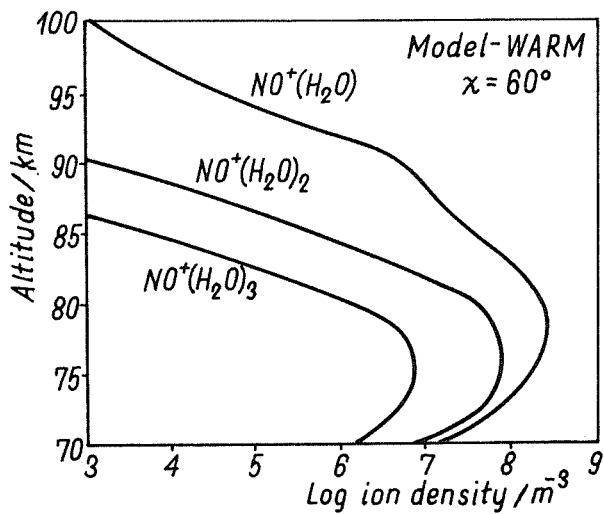
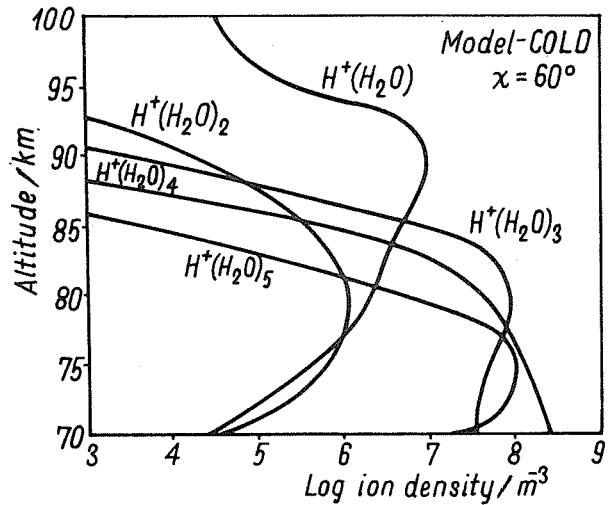
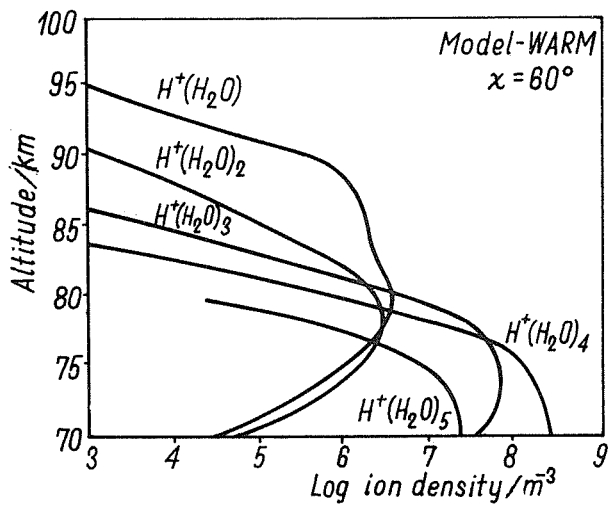
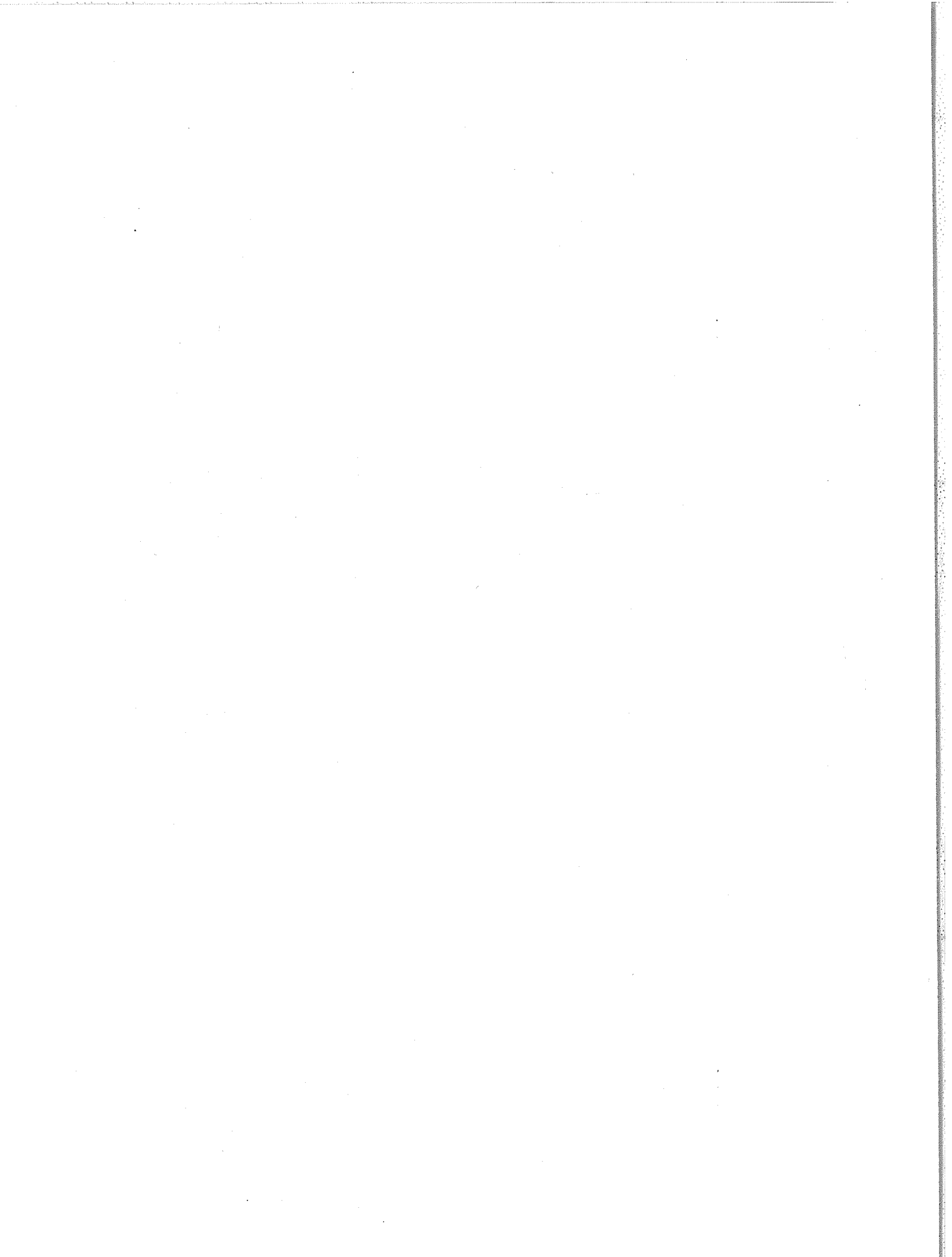


Fig. 3 Profiles of water cluster ions and NO^+ clusters calculated for temperature profiles WARM and COLD.



Section 2 Planetary Distribution

3.2.1 Proposal for "Mapping" the Spectral Components of foF2

A.K. Faul

Nat. Oceanic and Atmospheric Adm., Boulder/Colo., USA

Abstract: Several years ago a spectral analysis of the monthly median of the maximum plasma frequency in the F-region (foF2) was performed. All data reported for a period of at least three years at a given station were included in this analysis and some first results were published /Paul, 1978/. In relation to the "International Reference Ionosphere" the question was raised, whether at least the most significant components could be described by empirical relations with geographic or magnetic coordinates and sunspot numbers in the form of a computer program. This led to some further studies with major emphasis on the solar cycle dependence.

1, Introduction

In our particular /Paul, 1978/ analysis, a bandwidth of 1 cycle per year (a^{-1}) was used resulting in a spectral resolution of the same width. In this way the seasonal modulation of the diurnal variation could be represented by combining "carrier frequencies" and sidebands. For example, the semidiurnal variation appears as a triplet with sidebands $1a^{-1}$ above and below the carrier at 2 day^{-1} , i.e.: $2d^{-1} - 1a^{-1}$, $2d^{-1}$, $2d^{-1} + 1a^{-1}$. No attempt was made to resolve similarly the fine structure due to the solar cycle, because of the complexity of its spectrum and the scarcity of stations with sufficiently long data records. Amplitudes and phases of the spectral components obtained are therefore still slowly changing in time with the sunspot cycle. For comparison, the monthly Zürich sunspot numbers were passed through a filter with a bandwidth of $1a^{-1}$ corresponding to the bandwidth used in the spectral analysis. A second-order least-square fit was then applied to the spectral components using only stations having data records over at least 11 years. It was found that in most cases a linear approximation would be sufficiently accurate.

2, Results

The "constant" term of foF2 has, of course, the largest value; it is shown (in MHz) in Figure 1 as a function of the magnetic latitude for a filtered sunspot number $R = 100$. The variation is relatively smooth and approximately symmetrical around the magnetic equator. Figure 2 shows the relative change of the amplitude for a change of sunspot numbers of 100 as a function of latitude. Surprisingly, there is very little variation, which means that worldwide this term changes uniformly by approximately 35% for a change in sunspot number of 100.

The amplitude of the semiannual component is shown in Figure 3 and shows a variation with magnetic latitude similar to that in Figure 1; the spread of the data, however, is much larger. On the other hand, the phase of the same component is quite well defined as seen in Figure 4. It is approximately constant over a wide range of latitudes, changing slightly towards the poles (the phase is given in fractions of a cycle relative to 16 December at noon). For higher frequencies the latitudinal variation of the amplitude becomes more complex and is less well defined as can be seen in Figure 5 for the 24 h period (frequency $1d^{-1}$). Again, the dependence on the magnetic latitude is similar to that in Figures 1 and 3. The relative change of the amplitude with sunspot number shown in Figure 6 is quite different from that in Figure 2. There

we had approximately the same value for all latitudes, while here the values change from positive at high and midlatitudes, to negative in the vicinity of the magnetic equator. In Figure 7, the phase of the diurnal period is plotted as a function of the dip angle. The phase values for high and low latitudes are approximately equal, and are higher than those for midlatitudes; this means that the maximum of the 24 hour period is reached earlier at midlatitudes than at high or low latitudes.

Instead of presenting the seasonal sidebands of the diurnal (24 h) period individually, we computed the modulation. This is the sum of the amplitudes of the two sidebands, which differ by $\pm 1a^{-1}$ from the exact 24 h period, divided by the amplitude of this latter. This 'modulation ratio' is shown in Figure 8 as a function of the magnetic latitude. It has maxima at midlatitudes and very low values at the magnetic equator and near the poles. There are, however, a few exceptions and there is one extremely high value for Argentine Island which is located in the South Atlantic anomaly. There is also an indication of an asymmetry between the two hemispheres (values are higher in the northern hemisphere than in the southern). The amplitude of the semidiurnal component is shown in Figure 9 as a function of the dip angle. Again it seems to be similar to the amplitude plots shown above. The phase of the semidiurnal component (frequency $2d^{-1}$) shown in Figure 10, and it shows a greater variation with latitude than the diurnal component.

3, Discussion

The examples shown are not a complete set of all the components found, but are typical of the general situation. The amplitudes shown are roughly similar in their variation with latitude, but are different in magnitude and in scatter around a mean curve. Part of the scatter, of course, is due to 'noise' caused by different effects. One factor is the quality and reliability of sounding equipment, including its calibration and the reduction of the records. During the very high sunspot maximum in 1957/1958 the noon critical frequency foF2 at some stations exceeded the upper limit of the frequency range of the ionosonde, leading to a distortion of the diurnal variation of foF2 and to errors in the spectral components. There are also geophysical reasons, for example, the high rate of occurrence of spread-F at certain hours, which results in smaller numbers of measured values and hence in less reliable monthly medians. At present, it is virtually impossible to estimate the noise level, especially since it is likely to change with season, sunspot cycle and equipment changes.

Another part of the scatter is caused by the complex structure of the Earth's magnetic field. It has been shown, for example, that the phase of the 24-hour period, and also the modulation in the 24-hour band, are closely related to the magnetic declination /Paul, 1978/.

In the world-wide picture, the amplitudes of the components used in our analysis show more variation with latitude and more spread than do their phases, seasonal modulation, and amplitude variation with sunspot number. It should be feasible to find simple functions to represent all the spectral components in their latitudinal variation and sunspot dependence. Since higher frequencies than $2d^{-1}$ were not considered, it cannot be expected that data recomputed from those spectral component functions will always agree very closely with the observed data, but the errors should be well within the day-to-day variability of foF2, with a few exceptions, e.g. in the area of the South Atlantic anomaly.

4, Conclusions

Such a model could be significantly improved by applying the analysis to the data recorded since 1972, which was the last year included in the

data base used so far. This would increase the number of stations with at least 11 years of data collection, thus providing a better resolution of the global variation. This in turn would permit a more detailed study of the dependence of the spectral components on the magnetic field vector and would yield a more accurate and more detailed model. With such a global description of the spectral components and their dependence on sunspot numbers, a representative value of the critical frequency foF2 could easily be computed for any location, any given time and any given sunspot number.

Comparing its complexity with that of the descriptive models actually used in the present IRI, ours has certainly more parameters than that of Chiu /1975/, but fewer than the official CCIR model /1974/. Of course, the quality of representation achievable with models depends on the number of coefficients used, but it depends also on the choice of the functions used. Since we tried to choose our frequencies for reasons of 'geophysical economy', we feel that our model presents some advantages. Since CCIR, for each individual month, has independent sets of a large number of coefficients, our representation is certainly more economic. We hope it may be possible to establish an easier, but nevertheless sufficiently accurate descriptive worldwide model along the lines of our approach.

In conclusion, it may be remarked that foF2 is only one of the parameters included in IRI. It can be expected that other quantities such as temperature, height of maximum etc. will show similar complex behavior if studied in detail, and this should be kept in mind in comparing observations with the International Reference Ionosphere.

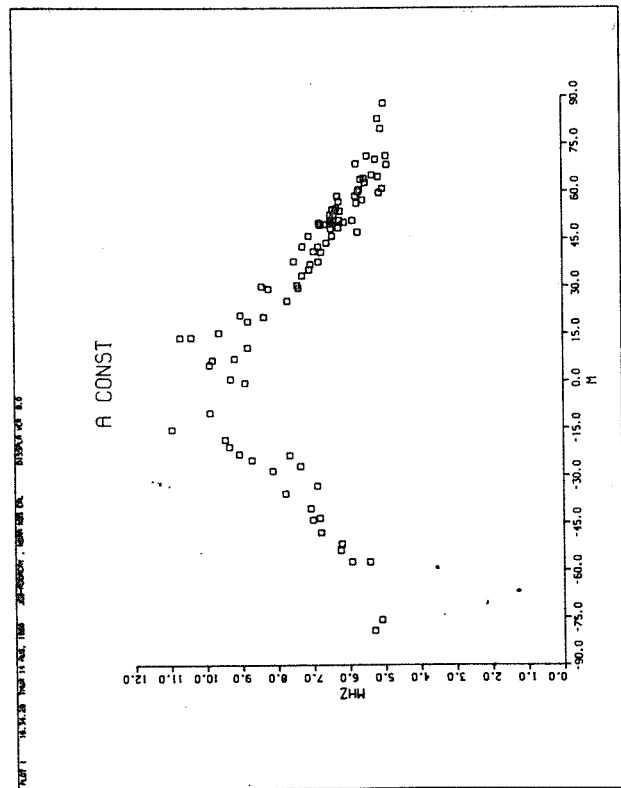


Fig. 1

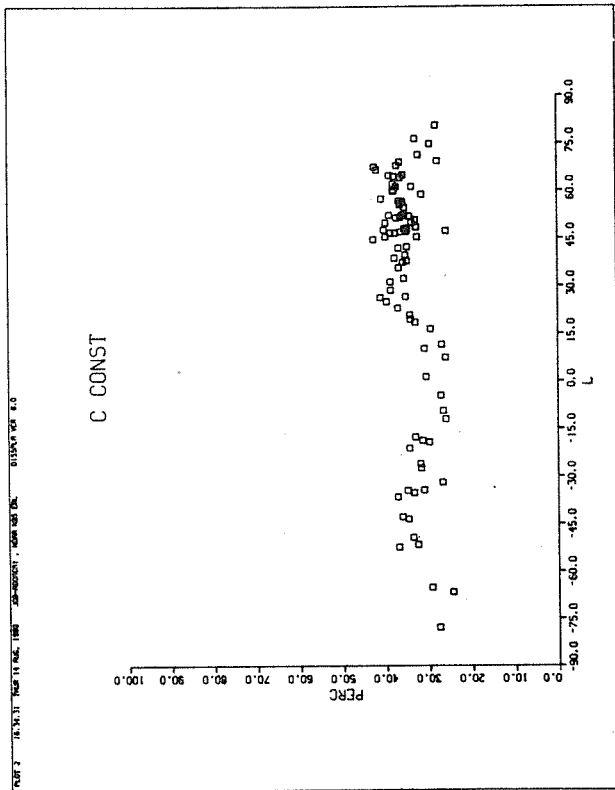


Fig. 2

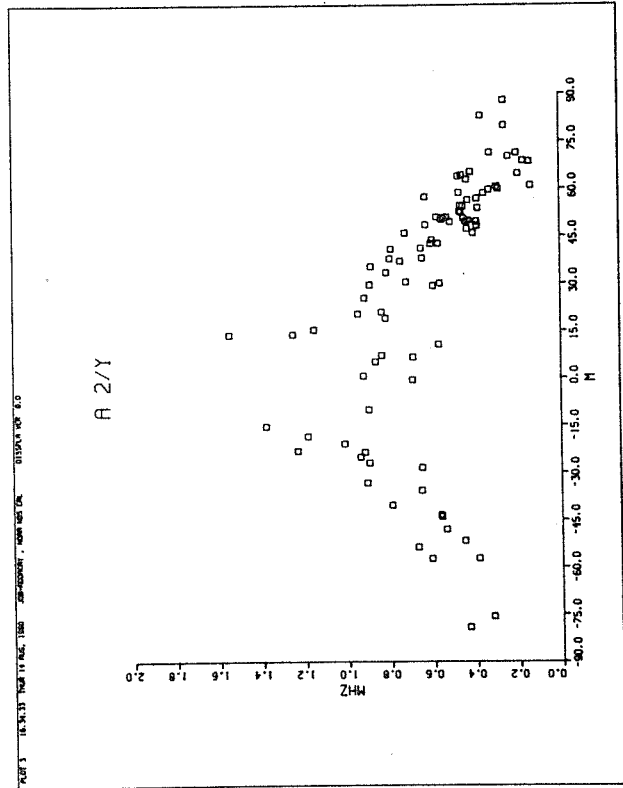


Fig. 3

Fig. 1 The average value of foF2 (constant term) as a function of magnetic latitude for a sunspot number $R = 100$.

Fig. 2 Change of the constant term for a change of R by 100.

Fig. 3 Amplitude of the semiannual period as a function of magnetic latitude.

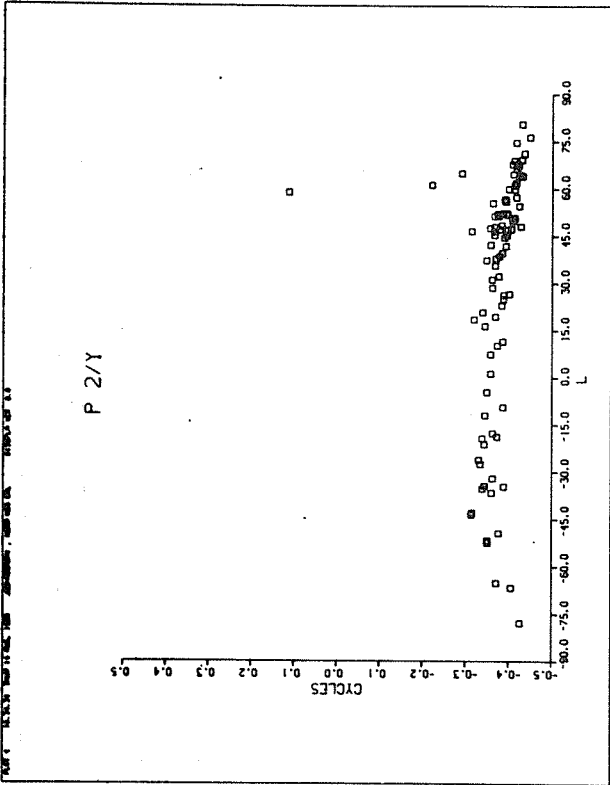


Fig. 4

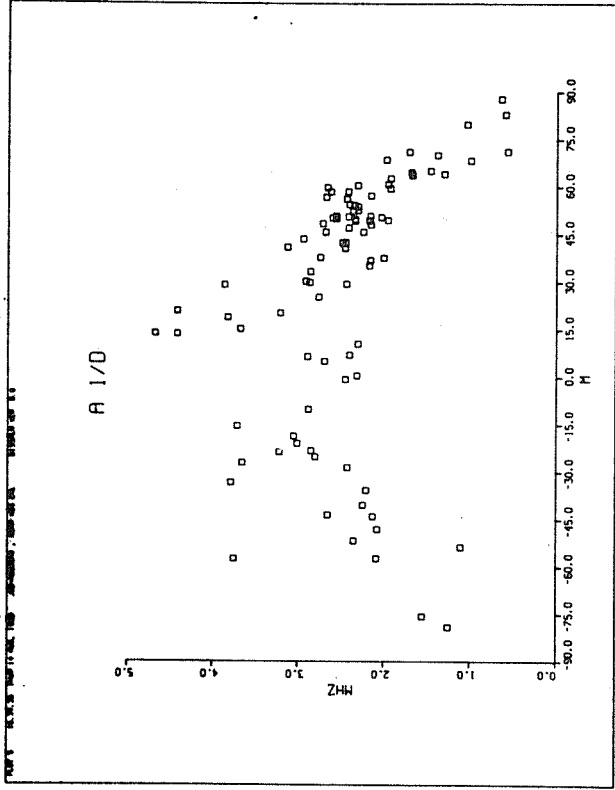


Fig. 5

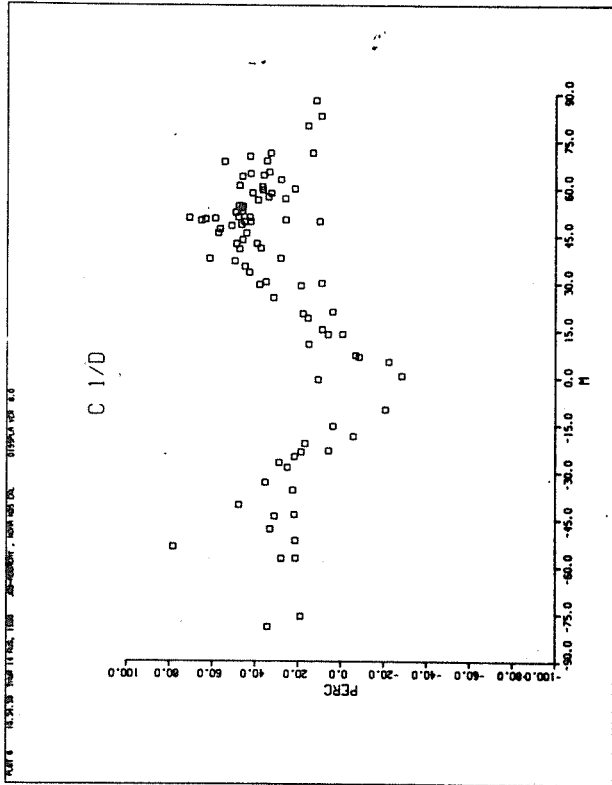


Fig. 6

Fig. 4 Phase of the semiannual period.

Fig. 5 Amplitude variation of the diurnal component with magnetic latitude.

Fig. 6 Percentage variation of the diurnal amplitude for a change of sunspot numbers by 100.

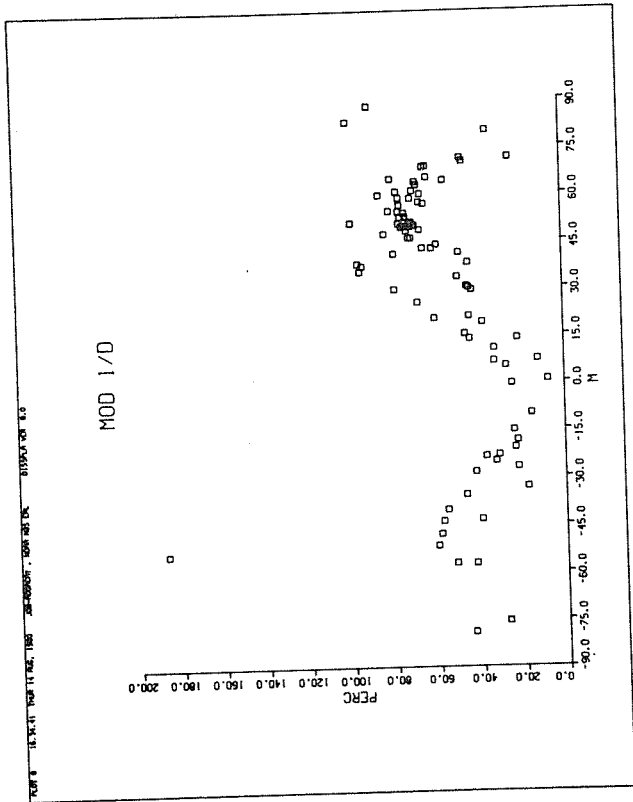


Fig. 8

Fig. 7 Phase variation of the diurnal component with dip angle.

Fig. 8 Modulation of the diurnal component as a function of magnetic latitude.

Fig. 9 Amplitude of the semi-diurnal component as a function of the dip angle.

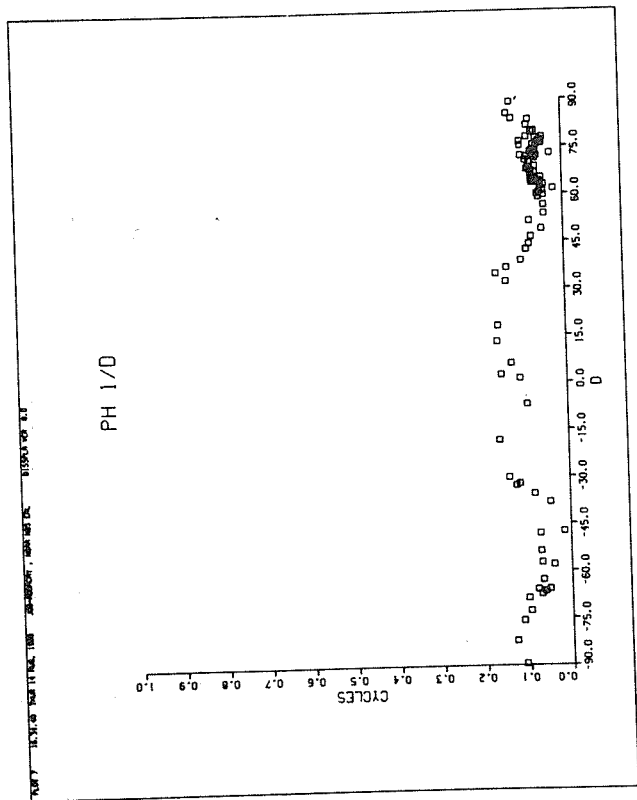


Fig. 7

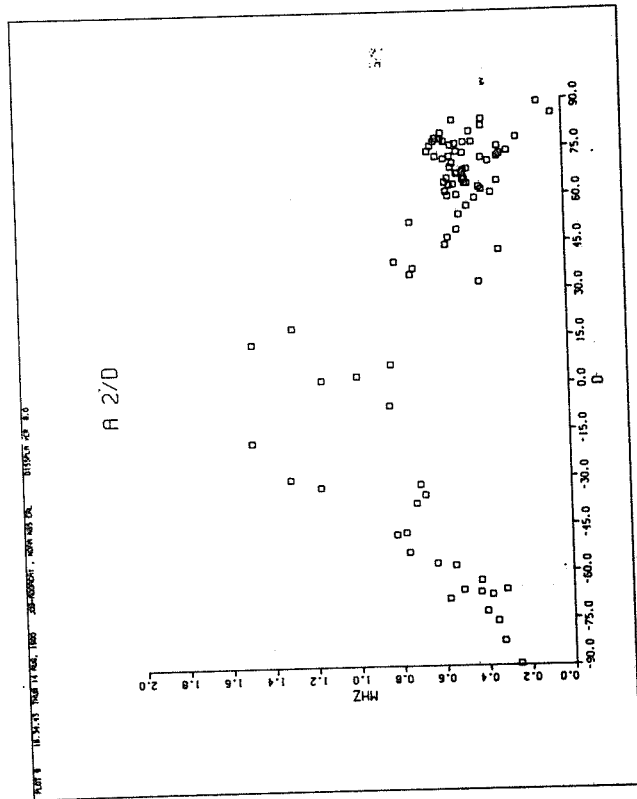


Fig. 9

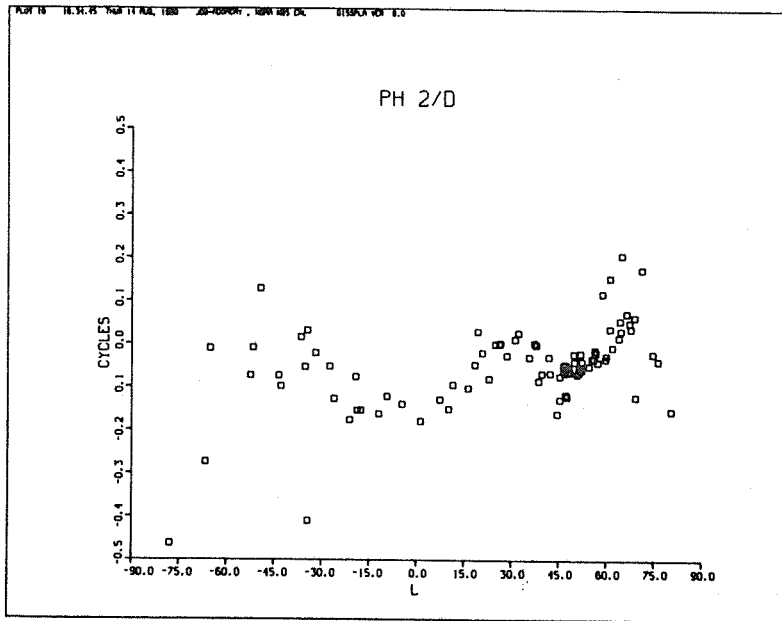


Fig. 10 Phase of the semidiurnal component as a function of latitude.

3.2.2. Comparison of the IRI Model and the Real Planetary Distribution of F2-Ionospheric Layer Charged Particles Based on Satellite Measurement Data

I.B. Balev, A.A. Goldin, E.G. Greenwald, V.A. Iavlenko,
A.I. Savin, V.L. Telrose

Polytechnical Institute, Kharkov, USSR

Abstract: In this paper the planetary distribution of electron concentration in the F2-layer, as given by the IRI model, is considered, and compared with the real distribution of the total charge concentration, at one preselected altitude, measured during the flight of Kosmos-469. The comparison shows possible differences between the real global charged particle concentration distribution and the average used in the IRI model. The measurements also disclose some new information on the ionospheric fine structure which was naturally not available during the elaboration of the IRI.

1, Introduction

Kosmos 469 was launched on 25th Dec. 1971 in a circular orbit of 65° inclination at 268 ± 8 km altitude. Because of the Earth's rotation and orbital precession on every pass, the track of the satellite was displaced in longitude by 22.7° to the West relative to the Earth's surface. For 16 orbits, covering almost 24 hours, the tracks formed a grid with a 22.7° longitude separation over a latitude range of 65° . The grid lines formed during the subsequent 16 passes were displaced to the West relative to the former ones by 3° , or 330 km at the equator. The entire Earth's surface was covered during the first 111 orbits. The 112th and 113th orbit coincided with the first and second.

The ascending branch of the orbit was fully illuminated by the Sun. The major part of the descending branch was in the Earth's shadow, with twilight conditions in the latitude range 45°S to 65°S where the solar zenith angle approached zero. Direct measurements of ion concentration were made continuously during 9 days (144 passes of the satellite) from 25th Dec. 1971 to 3th Jan. 1972, under conditions of quiet activity.

The instrument used for the concentration measurements included planar ion traps mounted on a boom 1.5 m long and a measuring unit placed inside the instrument container. The measuring unit consisted of an ion current modulator, an a.c. amplifier with automatic selection of the measurement range, and a synchronous detector. The entrance apertures of the ion traps were oriented along the incoming flow velocity vector throughout the entire experimental period.

In the zone of direct view, the data were transferred to Earth with a sampling rate of 50 Hz. Beyond this zone the information was recorded by the onboard memory with a sampling rate of 0.1 Hz.

2, Results and Comparison with IRI

The information was decoded on the ground at 30 s intervals corresponding to 240 km along the satellite orbit. The average concentration values in such intervals constituted our input data. The total error of the ion concentration measurement due to errors in measuring the ion trap collector current, and to the effects of satellite body potential

variations, and of the data recording, storing, transmission and processing, did not exceed 10% (in the density range of 10^9 to 10^{12}m^{-3}).

The experiment made it possible to obtain a continued succession of $26 \cdot 10^2$ values of ion concentration along one orbit. For comparison the IRI model was used to calculate a planetary distribution of F2-layer charged particles. The peak data (NmF2, hmF2) were determined by the Chiu-method. The results from the model and from the satellite are shown in Figures 1 to 4 as maps of the plasma density distribution over the Earth's surface.

Figure 1 shows the plasma density distribution for the daytime ionosphere as given by the IRI model. The scale that connects the local time in the pass area with the geographical latitude of the satellite is given on the right. The minimum value is in the range 1 to $3 \cdot 10^{11} \text{m}^{-3}$, see the upper and lower parts of the Figure. The maximum value varies from 1 to $3 \cdot 10^{12} \text{m}^{-3}$, see the equatorial zone. Figure 2 shows the satellite data for a series of passes covering 24 hours. In Figures 1 and 2, there is a rough coincidence of the global distribution of charged particle concentration, but the measured values are lower than those calculated from the model by approximately half an order of magnitude. The absence of fine structure along the equator in Figure 1 is quite natural since the model is based on an average latitude statistics.

Figures 3 and 4 represent the nighttime distribution as given by the model and by the satellite respectively. The nighttime ionosphere differs much more substantially from the model and is characterized by far more fine structure, and a very uneven geographical distribution. Within the long, nearly homogeneous areas, one can see more than 30 clearly separated zones with concentrations lower than those in the background by several orders of magnitude, and perhaps three less developed zones with higher concentrations which we consider as less typical.

After seven days the whole map was covered with satellite passes containing data points spaced 330 km by 240 km from each other. We drew closed contours through the points with equal concentration, and every contour contains from several to several tens of experimental points. A number of passes are shown in the Figures 2 and 4 as examples to demonstrate the 330 km shift of the nearest subsequent passes.

3, Comparison with Other Measurements

These results seemed to provide strong evidence to show that the local and very detailed inhomogeneity of the night ionosphere is geographically constant during at least nine days. Unfortunately, we had no measurements of other sources, to make a full scale comparison of the distribution for a longer period. Fortunately, we had some fragmentary measurements, made along three passes of Kosmos 125, in July 1965, which coincided with some of the passes of Kosmos 469. The circles above and below the map in Figure 4 give the numbers of passes for the two satellites. There are 12 groups of curves in Figure 5. The solid and dashed curves in each group represent passes spaced 7 days apart in the 1971 to 1972 experiments with the changes in density along each pass. One can see the remarkable coincidence of the positions of the maxima. Moreover one can see three incomplete curves for the 1965 experiment (three left-hand side plots). The curves represented by the dash-dotted lines in three cases out of four demonstrate, we believe, the coincidence with data measured 5 1/2 years later. Actually one or two peculiarities on the old curves could still leave some doubt about the degree of constancy of the geographical picture.

It seemed to be of interest to compare our data with the measurements made by Sharp, who used the U.S. Satellite 42A in Nov. 1963. Unfortunately, the space resolution of Sharp's measurements was 10 times less than

ours, because of a 100 s time constant of his amplifier, but it was good enough for Sharp to discover a large belt of reduced ion concentration around the North Polar region as shown in Figure 6. The heights of Sharp's passes and their variations (288 to 359 km) did not permit a very detailed comparison, but we found that a number of minima in Sharp's curves did coincide with what we had discovered. The curves in Figure 7 are taken from Sharp's paper. We marked obvious minima in the curves by circles (in the non-polar region), and then indicated the geographical locations of these minima with vertical lines on Figure 4, which shows our results. This comparison seems to provide evidence for the constancy of the zones of density minimum in the nighttime F2-layer both in time and space.

It is a pity that Sharp had only 4 1/2 days at his disposal for obtaining data, otherwise he might have discovered the permanent zones, even with his lower resolution. Of course, the geographical constancy is the main subject in this paper. The inhomogeneity of the ionosphere, as such, is a very well-known phenomenon, and certainly the IRI model has never pretended to describe it.

What about the lower layers of the ionosphere? Several months ago a group of Soviet researchers, when analyzing radiowave absorption measurements using the A1 method, noted that the regions with anomalously high daytime values of absorption in the D-layer coincide geographically with the local zones of anomalously reduced concentration in the nighttime ionosphere for the F2 layer discussed above. It is worth remembering that the anomalously high daytime absorption in Alma-Ata (which was not explained during the International Geophysical Year 1957/1958) exceeds the absorption in Kostov-Don, Ashkhabad, Tomsk and Irkutsk by as much as 10 to 15 dB. As can be seen in Figure 4, Alma-Ata is situated in one of the zones of anomalously reduced density of the nighttime ionosphere. To avoid any misunderstanding, we must stress that the D-layer anomaly refers to an increase in the concentration.

4, Conclusion

We feel that we have shown that there exist geographically well defined narrow local zones of reduced density in the night-time ionosphere. Therefore, we believe that the time is coming when it will be desirable not only to repeat measurements of this kind, but also to look downwards and to try to find a source, or perhaps sources, for the discovered phenomena in the lithosphere.

Acknowledgement

The authors are grateful to A.A. Nikitin, L.L. Suchatsheva for the help in IRI model computation, and to A.D. Danilov for his permanent interest in this work and participation in discussions.

Discussion remark:

The IRI model, as pointed out by K. Kawer, is applied either with peak data fed in from the CCIR numerical maps, or with the much simpler approximation due to Chiu /1975/. The authors have used the latter approach which must end up with a very much smoothed map. That of CCIR (which is recommended as first choice) also gave a complex pattern, but not so irregular as Figure 4. In particular, the "holes" appearing in the equatorial zones would not be given by the CCIR-model. It might be that the phenomenon which is observed at constant altitude, could be due to an undulation of the bottom of the F-region which is seen when cutting with a satellite orbit of fixed altitude.

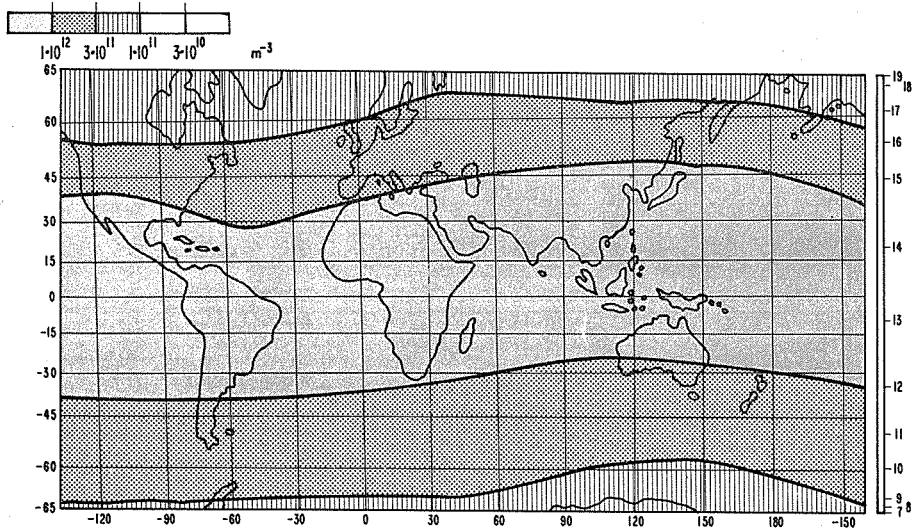


Fig. 1 Electron density distribution over the Earth's surface in daytime at 270 km altitude after IRI with Chiu peak-model.

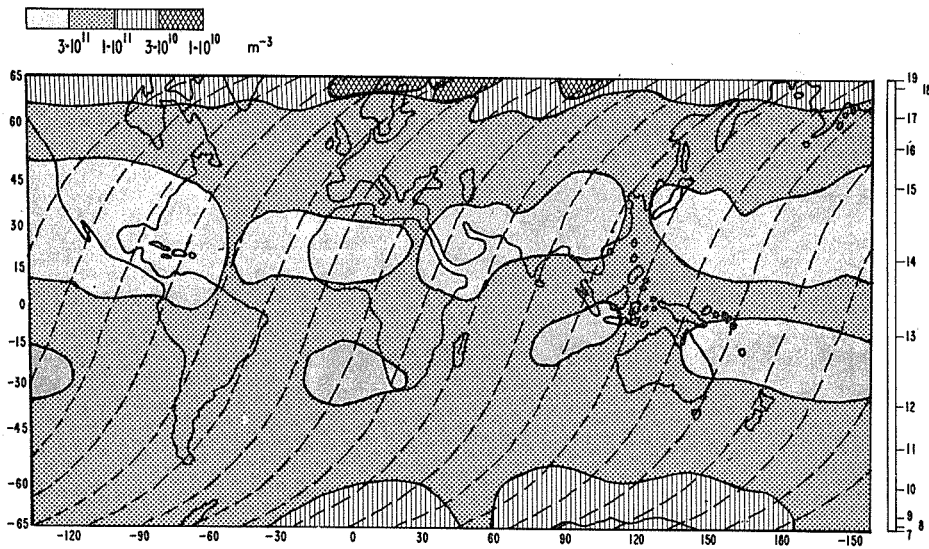


Fig. 2 Electron density distribution over the Earth's surface in daytime at 270 km altitude from satellite (Kosmos 469) measurements (25 Dec. 71 ... 3 Jan. 72).

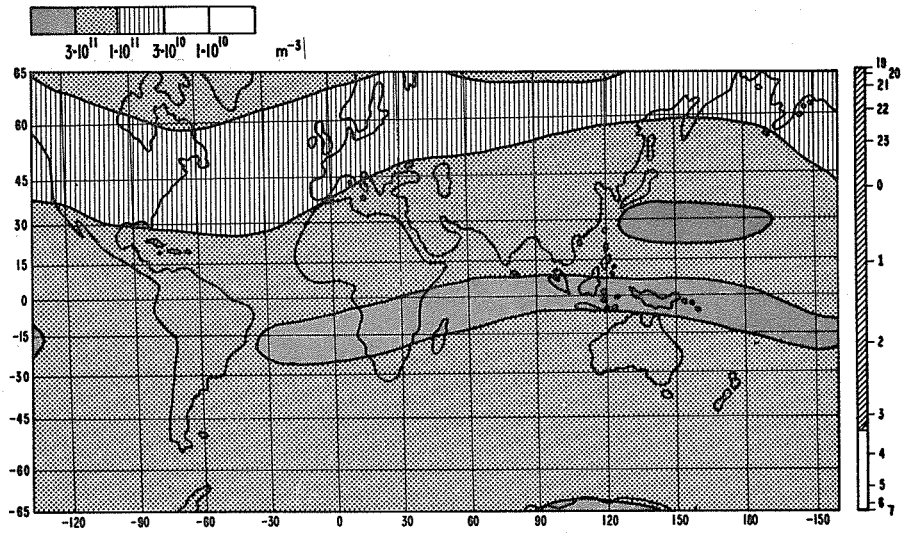


Fig. 3 Electron density distribution over the Earth's surface at night at 270 km altitude after IRI with Chiu peak-model.

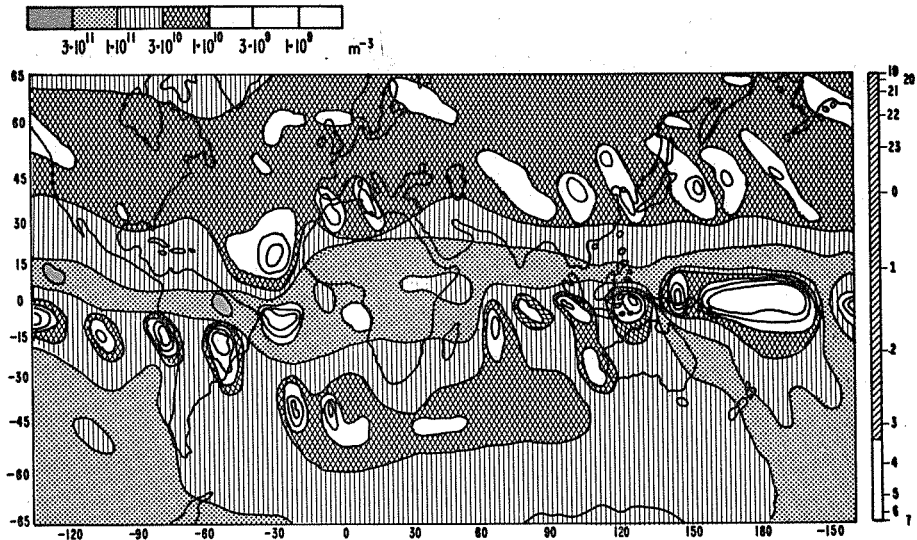


Fig. 4a Electron density distribution over the earth's surface at night at 270 km altitude from satellite (Kosmos 469) measurements (25 Dec. 71 ... 3 Jan. 72).

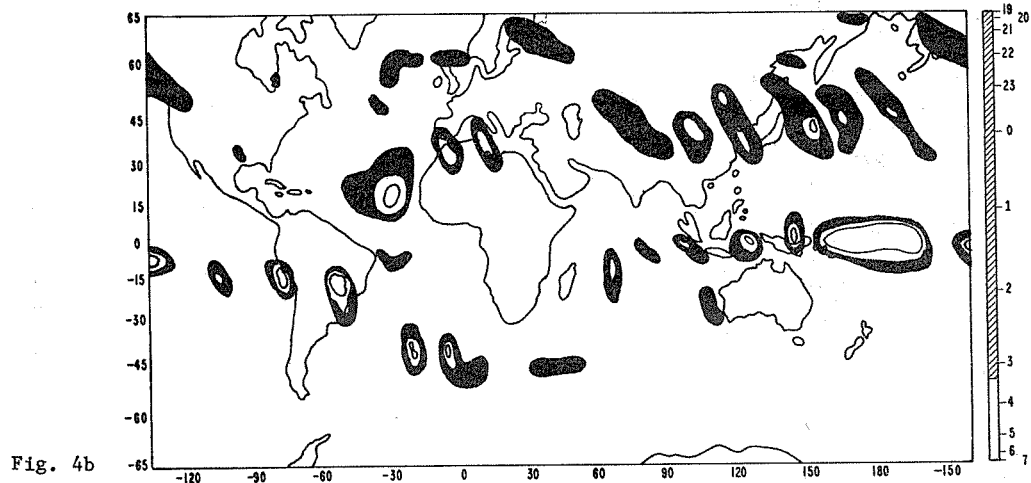


Fig. 4b

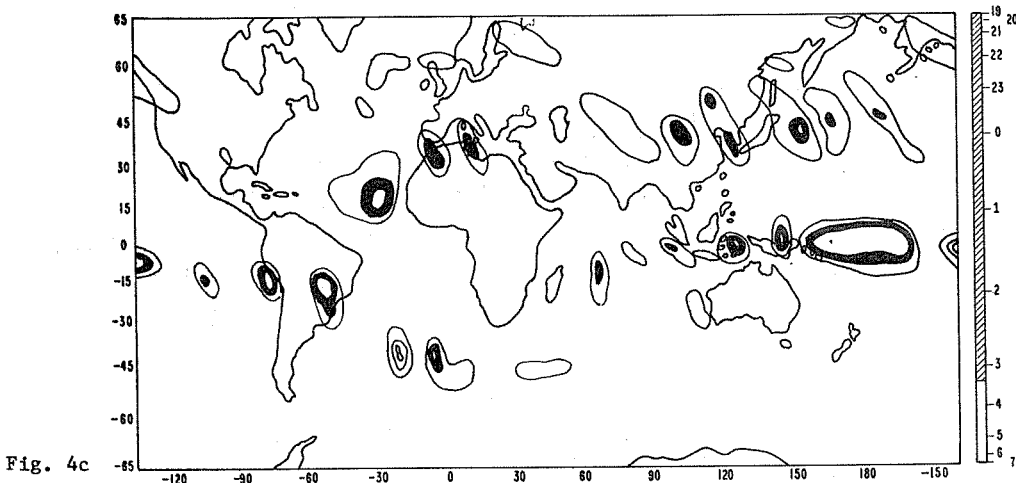


Fig. 4c

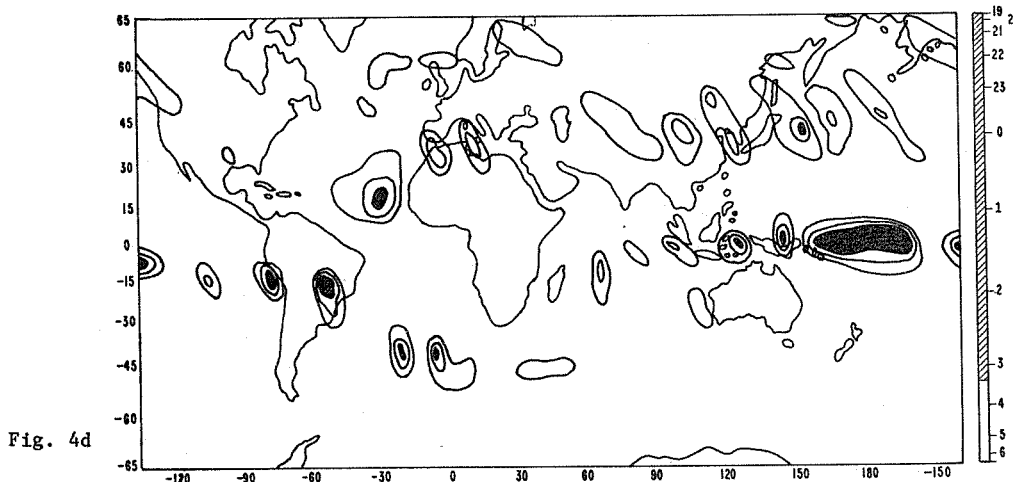


Fig. 4d

Fig. 4b,c,d "Index charts" to Fig. 4a. The solid black identifies the geographic areas covered by the lowest three contour intervals

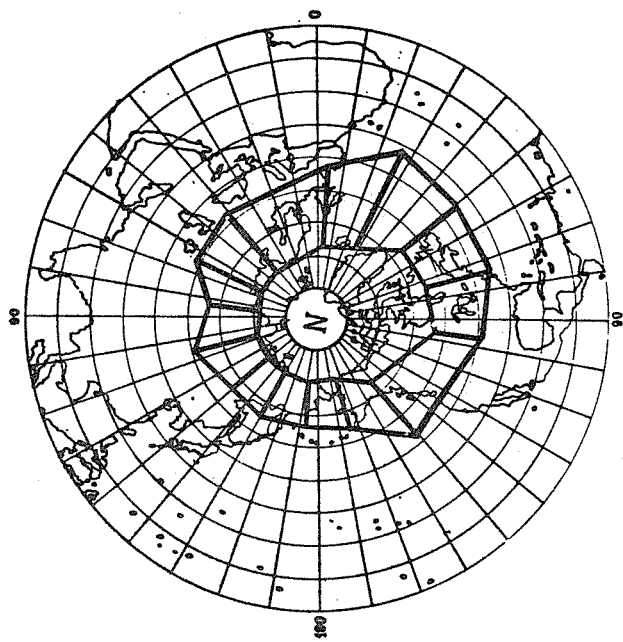


Fig. 6

Electron density variations as a function of latitude in the trough range along geographically coincident paths of two satellites: ---- and "Kosmos-469"; —, —, — "Kosmos-125".

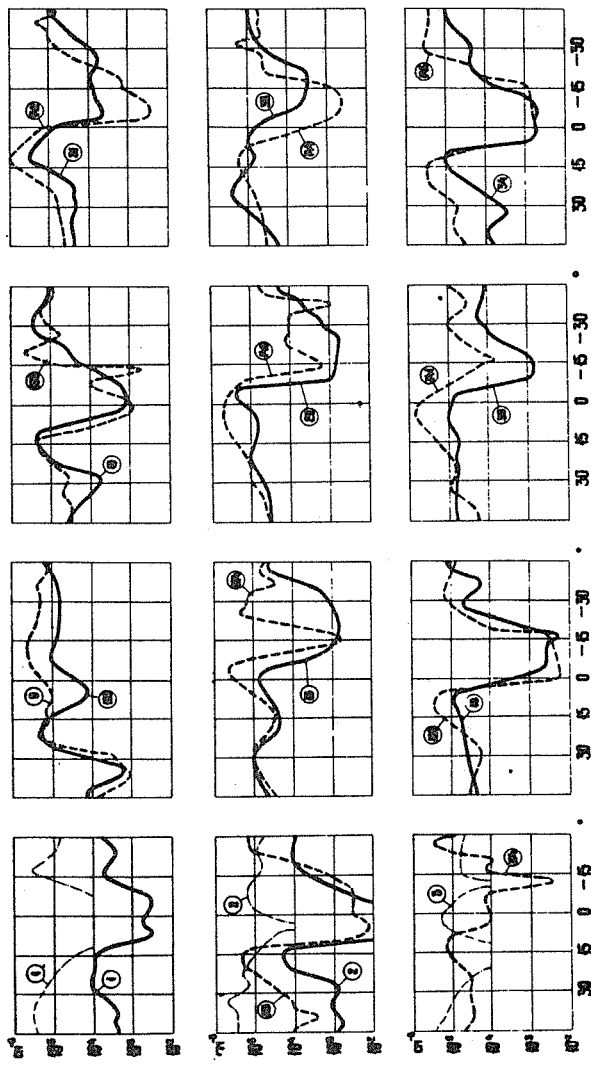


Fig. 5

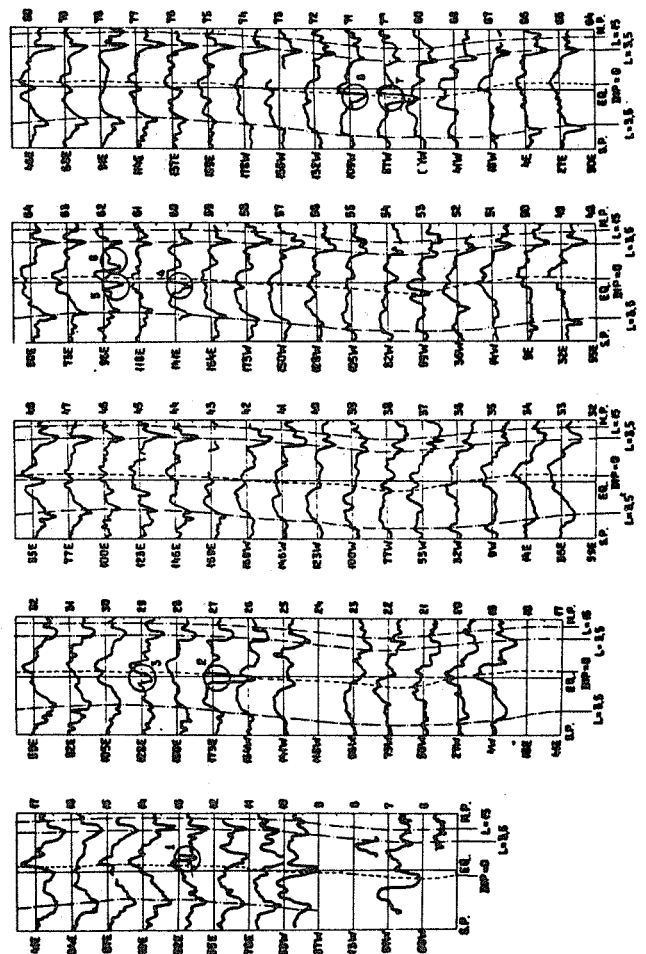


Fig. 7

Global trough in concentration observed by Sharp in a US-42A satellite experiment.

Charged particle concentration measurements summarized for 64 passes of the US-42A satellite flight.

3.2.3 Upper Atmosphere Dynamics and the International Reference Ionosphere

E.S. Kazimirovsky

Siberian Institute of Terrestrial Magnetism, Ionosphere and Radio Propagation, Siberian Department of the USSR Academy of Sciences, 664033, F/E 4, Irkutsk, USSR

Abstract: The effects of upper atmosphere dynamics have only partially been included in IRI. Yet transport processes are very significant factors in the space-time distribution of ionospheric plasma parameters. They effectively connect the magnetosphere, the ionosphere and various other regions throughout the atmosphere, and the ionospheric structure is conditioned by the dynamics. In recent years several theoretical models have been developed which consider the effects of large-scale atmospheric motions. Moreover there are many experimental data concerning ionospheric motions: rocket and satellite measurements, ground-based radio sounding, including incoherent scatter, optical methods, etc.

Thus, we may discuss the problem of elaborating a model of the ionospheric motions as an addition to IRI. In the first stage, it might contain information about the horizontal and vertical drift as a function of latitude, ionospheric layer, season and phase of the solar cycle. In the second stage, the longitudinal effect and information about wave-like processes might be included.

1, Introduction

It has now become clear that the creation of physical models of the upper atmosphere requires both a theoretical and an experimental study of the velocity parameters of the natural macroscopic motions of both neutral and ionized components of the ionospheric plasma. The CIKA-72 model provides information not only about the empirical picture of the space-time distribution of horizontal wind in the stratosphere and mesosphere, mainly from rocket measurements, but also about the general atmospheric circulation at ionospheric levels. However, these motions, especially above 130 km, have so far been calculated only theoretically, using the Navier-Stokes equation for viscous compressible fluid simultaneously with continuity equations, the equation of conservation of energy and the equation of state of a gas. The problem of the development of a fully adequate model has not yet been solved; this is due both to mathematical difficulties and to insufficient knowledge of energy sources and sinks, and also to insufficient experimental data for the formulation of boundary and initial conditions.

The description of motions of the neutral atmosphere has so far not been included in the development of the IRI /Rawer et al., 1978a/. However, it is clear that the interaction between the neutral and ionized components realized in collisions with the associated transfer of energy and momentum, ultimately determines the space-time distribution of electron density.

Ionospheric motions may be roughly divided into two classes: hydrodynamical (winds) and hydromagnetic (drifts). In the first case, the energy is concentrated in neutral particles (but the ionization effect does exist); in the second case, in electromagnetic fields, it is concentrated in the drifting charged particles, but later it is partly transferred to neutral particles. The presence of horizontal winds and drifts, and the principle of conservation of mass, require the existence of vertical motions. As is known, these may be associated with the heating and cooling essential for the ionosphere, and also with the redistribu-

bution of electron density and even ion composition.

These reasons, as well as the fact that, for the solution of many applied problems the parameters of motions in the ionosphere are not less essential than the distribution of electron density, temperature and ion composition, justify a consideration of the question of supplementing the model of the upper atmosphere and ionosphere with information on the dynamical regime. Thus, the neutral wind model could equally apply to models of both the GFA and the IRI type, but the ionospheric drift model (and perhaps the electric field model) could specifically apply only to IRI.

2. Experimental Procedures

All current methods of measuring motions in the ionosphere are based either on observing the motion of natural or artificial tracers moving with the wind (drift), or on measurements based on the effect of the medium on mechanical or electromagnetic waves propagating in it /Kent, 1970; Evans, 1972; Nagy and Cicerone, 1974; Kazimirovsky and Kokourov, 1979a/. Most experimental data on motions in the D- and E-regions have been obtained from rocket experiments (artificial clouds), meteor trail radar, spaced receivers (D1) with vertical incidence pulse soundings, partial reflections, space reception of broadcasting transmitter signals and incoherent scatter measurements.

Most experimental data on motions in the F-region have been obtained by the spaced receiver (D1) method, incoherent scatter or observation of the 630 nm Doppler shift in airglow. The optical method provides directly the velocity of the neutral wind, while radio-physical methods, at these heights, at best provide a plasma drift velocity. Anyway, global monitoring of the upper atmosphere dynamical regime can be achieved only by D1, optical and other relatively simple and inexpensive methods, while measurements using rockets, satellites and incoherent scatter radars might serve for calibrating and for occasional complex experiments.

Most appropriate for synoptic monitoring is the spaced receiver method (D1) in all its modifications. Strictly speaking, it was this method that, during the International Geophysical Year, allowed the main facts about the global distribution of horizontal ionospheric drifts to be discovered /Harnischmacher and Rawer, 1958; Shimazaki, 1959; Rawer, 1959; Rao and Rao, 1963; Kazimirovsky, 1963a,b/.

Then for many years, the question of the physical significance of this method and of the different types of data treatment were critically discussed /Harnischmacher and Rawer, 1968/. The resolutions of the International Symposium on Waves in the Upper Atmosphere (Toronto, Canada, 1970) recommended that calibration of the D1 radio method by meteor and rocket wind measurements should be carried out as a first priority, and such experiments were successfully realized.

As for the partial reflection method applied to the E- and F-regions, the agreement of the results with meteor wind measurements (Figure 1) proved to be excellent /Stubbs and Vincent, 1973; Geller et al., 1976; Wright et al., 1976a/. The spaced-receiver method, in its usual version using full reflection from the E-region, was also calibrated by meteor measurements made at the same time, at the same altitude, and with the same ionospheric volume illuminated /Pelgate, 1975/. In addition, similar experiments were carried out using the D1 method, with simultaneous tracking of artificial clouds /Kent, 1970; Andreeva et al., 1973; Pfister, 1974/. Good agreement of the results was demonstrated by a direct comparison of the plasma meridional drift velocity in the E- and F-regions, obtained by the incoherent scatter method, and by the method using the so-called "kinesonde" /Wright et al., 1976b/.

A general conclusion that can be drawn from the results of complex experiments is that radio drift measurements provide reliable information about the transfer processes, and that these may be interpreted as neutral wind measurements at heights up to 140 km, and as measurements of plasma drift as a whole above 180 km but below the main maximum. The error in the velocity determination is of the order of 20% in modulus and 30° in direction.

3. Discussion

In the last 20 to 25 years, more than 60 geophysical stations, observatories and expeditions have conducted such measurements. Observations have covered many parts of the world but, unfortunately, the stations are concentrated in the region 5° to 70° N and 5° W to 175° E. The Western and Southern hemispheres are covered worst of all. The working programs at the stations were determined by their respective economic and technical capabilities but, on the whole, they corresponded with the International Geophysical Calendar and the recommendations of the UKSI International Working Group on drifts. Coordinates of most of the drift stations are contained in the WDC B1 Geophysical Data Catalogue, WDC1, Colorado, USA, 1971 and, for the IGY, in Rawer /1965/. The enormous variability of the ionospheric plasma parameters, pointed out by Rawer et al. /1978/, is highly characteristic also of ionospheric drifts. The drift velocity, as observed, is a complex function of spatial coordinates, local time, season and solar activity, and this implies the need for averaged values of the velocity. The velocity variability from hour to hour, is also very great both in magnitude and in direction.

Nevertheless, one can perform a global synthesis of the data, and prove the presence of a well-defined system of motions at ionospheric levels; one can also ascertain the character of the space-time variations of prevailing winds and drifts, as well as of the main tidal components /Kazimirovsky et al., 1979a, b, c; Vergasova et al., 1978/. Earlier results of such an analysis for the IGY period /Kazimirovsky, 1963a/ have already been used in wind regime models /Murgatroyd, 1965; Groves, 1970/ which were then included in the CIRA-72 model.

Already one can establish some major differences between the lower and upper ionosphere; there are pronounced seasonal differences in the motion system in the lower ionosphere but not in the upper ionosphere; also in the upper ionosphere, the geomagnetic control is stronger and diurnal variations seem to be smaller. At the same time there are some common features in the regularities of the motion in the E- and F-regions: the same most probable velocities (80 to 100 m/s), similarity of diurnal variations by day at some stations, prevalence of the diurnal harmonic at high and low latitudes, prevalence and great regularity of zonal transport in contrast to meridional transport.

4. Modelling

As an example of the possibility of constructing empirical models of motions, Table 1 contains averaged characteristics of the zonal (U) and meridional (V) drift in the E-region for the period 1958 to 1970. The Table lists, for each season, the results of a harmonic analysis of the diurnal velocity variations: the prevailing velocity and the amplitudes of the diurnal and semidiurnal waves /Kazimirovsky et al., 1979b/. Figure 3 demonstrates for the same period the latitudinal distribution of the prevailing drift and the amplitude of the diurnal wave in the F-region /Kazimirovsky et al., 1979b/. Empirical regularities of motions in the D- and E-regions, as obtained by Kazimirovsky and Kokourov /1979a/, agree well with rocket data, and those in the F-region with incoherent scatter data.

On the basis of drift data, one is even able to calculate the distri-

bution of midlatitude ionospheric electric fields, the direct measurement of which gives rise to great difficulties /Kazimirovsky et al., 1979a/. These calculations of space-time field variations do not contradict the available semiempirical models /Baran, 1974/ and the direct experimental measurements /Pehnke and Hagfors, 1974/; they are, in our opinion, a valuable addition to the results of the electric field determinations based on incoherent scatter data /Carpenter and Kirchhoff, 1975; Elanc, 1976/.

Of course, the presently available sketches of empirical models of dynamics have essential limitations. First of all, one should not consider as sufficient the number of available measurements as a whole, especially in some latitude intervals; in addition, the network of stations is not uniform. It should be noted that for ion composition and some other ionospheric parameters, there is also a great shortage of data, but this did not hinder their inclusion in the IRI. The shortage of data, in particular, prevents the construction of reliable vertical profiles of drift characteristics which are especially important for the D- and E-regions. For the F-region, the drift height variations are apparently less notable, even during magnetic disturbances. This is apparent from drift measurements by the incoherent scatter method /Evans, 1972b; Kino, 1972/ shown in Figures 4 and 5. Finally, because of the scarcity of appropriate measurements, it is difficult to take into account the longitudinal effect which undoubtedly exists in the D-region /Kazimirovsky and Kokourov, 1979/, and may exist also above 100 km owing to the interaction between the upper ionosphere and the underlying atmosphere.

The physico-statistical analysis of horizontal ionospheric drift measurements by the D1 method cannot and should not be the only source of data for an empirical model. One can be optimistic about the continuous increase of information regarding three-dimensional motions being gained from incoherent scatter radars in different regions, and from satellites of the type Atmosphere Explorer /Esyr and Harris, 1979; Elanc, 1977/ and from other sources.

As a first step, the dynamics supplement to the IRI might be a series of tables containing values of the prevailing horizontal wind, and the amplitude and phase of the diurnal and semidiurnal harmonics. Such tables could be compiled for three height intervals (80 to 100 km, 100 to 140 km, 180 to 300 km) for four seasons, for maximum and minimum solar activity and for three latitude ranges: 10° to 30° , 40° to 50° , and above 60° . As data become available, these tables could be supplemented with information on vertical motions, on electric fields, on characteristic parameters of wave disturbances and ionospheric irregularities, and on longitudinal variations of the dynamical characteristics.

In conclusion it should be emphasized that there is an urgent need a) to discuss, on an international basis, the prospects of developing different methods of measuring ionospheric motions, the relative values of the data for the IRI, and the presentation of the data; and b) to recommend a special program of coordinated experiments at selected stations, designed to lead to the improvement of the International Reference Ionosphere.

Editor's remark:

Since in many method the direction of the drift vector is much better defined than its amplitude, one should preferentially use in future analysis work polar coordinates instead of cartesian ones.

Table 1

Average zonal (U) and meridional (V) drift velocities in the E-region, measured during the period 1958 to 1970

Season	Latitude interval ON	U ₀ m/s	U ₁ m/s	U ₂ m/s	V ₀ m/s	V ₁ m/s	V ₂ m/s
Winter	10	-8	37	22	-6	34	15
	20	-15	6	36	-38	8	12
	30	-7	-	9	-1	-	12
	40	-11	19	4	-13	21	17
	50	-14	19	17	-30	7	20
	60	-2	47	16	-7	11	15
Spring	10	35	16	7	-19	15	40
	20	30	-	12	28	-	13
	30	7	5	8	-2	4	9
	40	13	18	9	-3	17	10
	50	4.5	7	5	1	11	10
	60	-15	26	12	15	71	7
Summer	10	12.5	10	1	-15.5	8	2
	20	17	33	16	-26	17	10
	30	7	16	9	-4	8	6
	40	13	14	12	7	14	23
	50	9	2	2.5	2	11	4
	60	9	6	2	4	5	11
Autumn	10	1	55	19	-35	18	8
	20	-3	24	29	-35	20	27
	30	-2	12	3	-8	6	9
	40	-9	6	8	-11	13	8
	50	-5	9	11	-3	4	15
	60	-20	-	17	-4	-	4

Note(Suffixes) 0 = prevailing (steady) component; 1 = diurnal, 2 = semi-diurnal component.

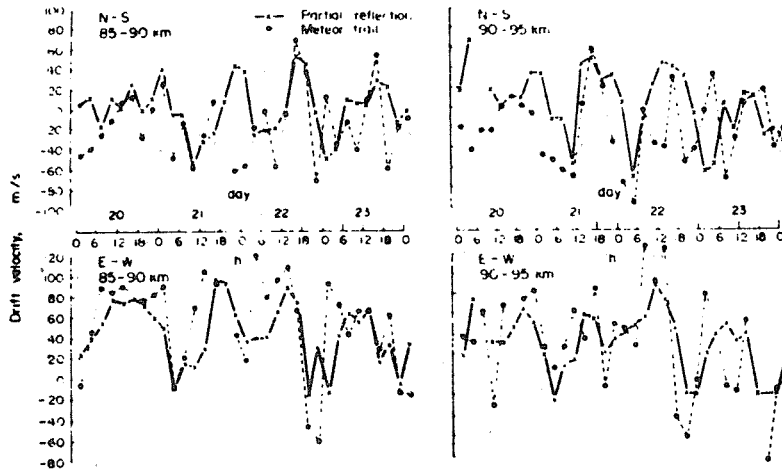


Fig. 1 The winter daily mean velocity variations measured simultaneously by the method D1 (partial reflections) - solid line, and by the meteor radar - dotted line (Stubbs and Vincent, 1973).

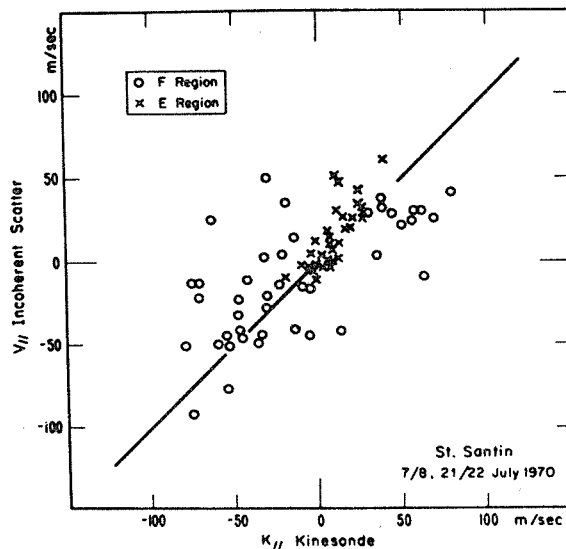


Fig. 2 The comparison between field-aligned ion drifts observed by incoherent scatter (V_{II}) and by kinesonde (K_{II}) (Wright et al., 1976).

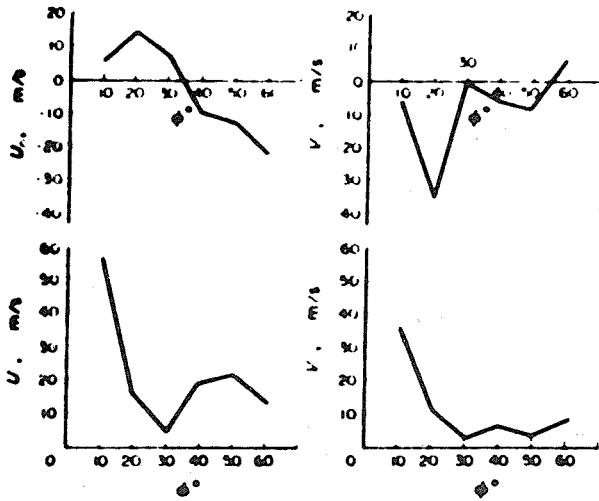


Fig. 3 The latitudinal variation of prevailing drift in the F-region and the amplitudes of the diurnal wave (Kazimirovsky et al., 1979b).

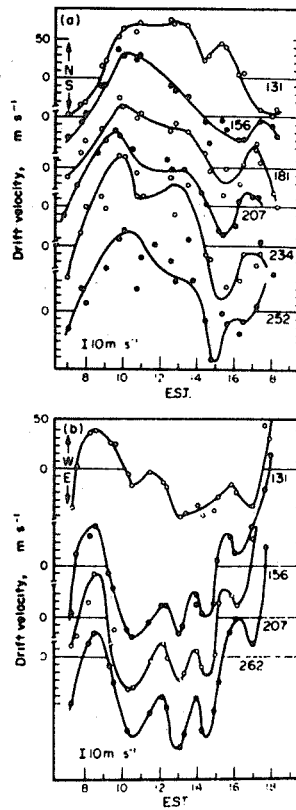


Fig. 4 Variations of the drift velocity observed by the incoherent scatter method at several heights on 17 April 1969 (Evans, 1972b). (a) N-S component, (b) E-W component.

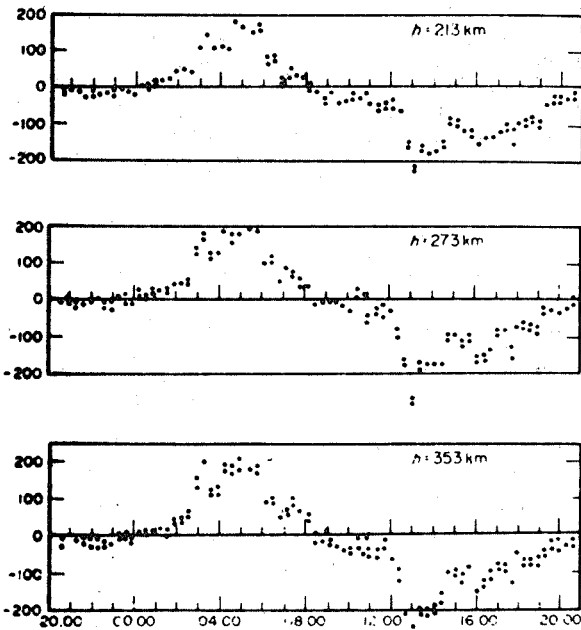


Fig. 5 Variations of the drift velocity along the radar beam at three levels during a magnetic disturbance on 9-10 August 1971. Chatanika, USA. (Rino, 1972).

Section 3.3 Present and Future IRI

3.3.1 Limitations of the IRI-78 Models

S. Ramakrishnsn, D. Bilitza, H. Thiemann

Fraunhofer-Institut for Physikalische Messtechnik,
D-7800 Freiburg, F.R.Germany

Abstract: IRI-1978 was published as a short summary of experimental evidence about the ionosphere which was readily available at that time, in a form suitable for computer use. The different sources of information cannot give a full picture so that improvement of the data base followed by improvement of the model is a task for the coming few years.

1, Plasma Density Profiles

Since we reduce the profiles to the density and height at the peak, the world-wide distribution of peak density and height is a separate one. This is dealt with by Working Group G.8 of U.R.S.I. (in particular in view of introducing satellite data into the C.C.I.R. model) while our group G.4 restricts its activity to the shape of the electron density profile. Problems appeared particularly at high and low altitudes, and with the valley. For the D-region the present model is based upon the compilation of rocket results mainly from the northern middle latitudes by Mechtly and Bilitza /1974/. We note that Taubenheim's /private communication/ effort to reproduce ground based absorption measurements with these profiles have been unsuccessful.

Our basic input for the topside ionosphere was the Bent and Llewellyn /1970/ model, which uses a composite mathematical description in four layers and is discontinuous in latitude. For IRI-78 we have replaced this model by a fully analytical description, which is continuous in both coordinates. Basically, it describes the inverse scale height (K) by a sum of two Epstein-step functions. We have compared this "harmonized Bent model" with the original one, and with a very detailed analysis of topside-sounder profiles made by Becker /1971, 1972/. In Figures 1 and 2 discrete values of K (Bent's values) corresponding to foF2 = 2, 5, 8 and 11 MHz, for 3 fixed altitudes (500, 700 and 900 km) are shown by dots. The crosses are calculated from our function, which was obtained by optimising the original discrete values of K. From these Figures it can be seen that at lower heights the original data deviate very much from the smoothed function.

This is understandable because at lower heights in the region of maximum density, the scale heights vary drastically with altitude so that our continuous function is better suited than the original one with a fixed scale height. In Figures 3, 4, 5 and 6 we have compared the normalised N(h) profiles from the three different models. (The geophysical data assumed for each of these profiles are indicated.) It can be seen from these Figures that, generally, the values from the IRI-78 N(h) profile agree better with those found experimentally by Becker /1971/. In Figures 7, 8 and 9 we compared the IRI-78 N(h) profiles with the original BENT model and with in-situ measurements of Ne obtained by the German-US aeronomy satellite AEROS-B. The results show clearly the differences between the profiles obtained from smoothed (IRI-78) and fixed (BENT) scale heights. In all comparisons with satellite data, we found that the global IRI-78 topside model agreed fairly well with the in-situ measurements.

2, Temperatures

Again input information was limited but now more sources are at hand. Incoherent scatter measurements were particularly helpful in the range below 200 km. Above that height between 250 and 800 km satellite results from AEROS-A could be used; for the electron temperature Spenner and Plugge /1978/ have given a world-wide mathematical description in terms of a Legendre development with a polynomial height dependence. To avoid the very large set of coefficients we fitted a much simpler formula with their development, neglecting the longitudinal effect which, in the monthly average, is quite small. Unfortunately, we have no clear evidence on a solar cycle dependence, the only incoherent scatter station useful in this context (Millstone Hill, USA) showing no clear evidence of an effect at all.

One of us (D.B.) has made an effort to compress 'Atmospheric Explorer' data into a mathematical presentation so that they might be incorporated into an improved presentation including greater altitudes (2.2.1). It has still to be decided what kind of coordinates are appropriate to this end. Our present description uses geomagnetic latitude, which is certainly better than geographic coordinates as Spenner and Plugge /1978/ have shown; but possibly a dip coordinate might be preferable.

3, Ion Composition

The area where basic information was particularly scarce is composition of the major ions. First of all because of very poor experimental evidence, we had to exclude heights below 100 km, where clusters and negative ions appear. The remaining heights can be subdivided at a height (around 350 km) where O^+ has almost at all times 100%. Above that level, there is a slow increase of H^+ and He^+ , with very different altitude profile by day and night. Below the range of O^+ dominance molecular ions are present, mainly as O_2^+ and NO^+ . Our data basis for the lower range is a compilation due to Danilov and Semenov /1978/, ending up with hand-drawn curves. These are based upon quite a few northern middle latitude, day-time rocket experiments. Unfortunately, there is no useful information under true night conditions and, almost none from low or southern latitudes. Our mathematical representation of the curves, as originally reproduced in IRI-78, was found to be inconsistent under certain conditions. It has since been improved (edited in a May 79 correction sheet). The individual height profiles of relative ion density were first approximated by broken straight lines, which were then represented by a continuous analytical function (an integrated set of a few EPSTEIN-steps). This is a quite flexible form of presentation which was used for O^+ and O_2^+ ions while the value for NO^+ was chosen so as to fill up to 100%.

The same kind of presentation is applied at greater altitudes with O^+ , H^+ and He^+ (the latter being always adjusted to 10% of the H^+ density, a preliminary guess). The data basis was due to a few earlier NASA determinations and, mainly, the AEROS-A satellite data. Our difficulty is that most satellite data are until now edited as absolute densities which is not very helpful for our purpose. One of us (D.B.) has meanwhile undertaken to transform data obtained with the recent Atmospheric Explorers of NASA into relative densities.

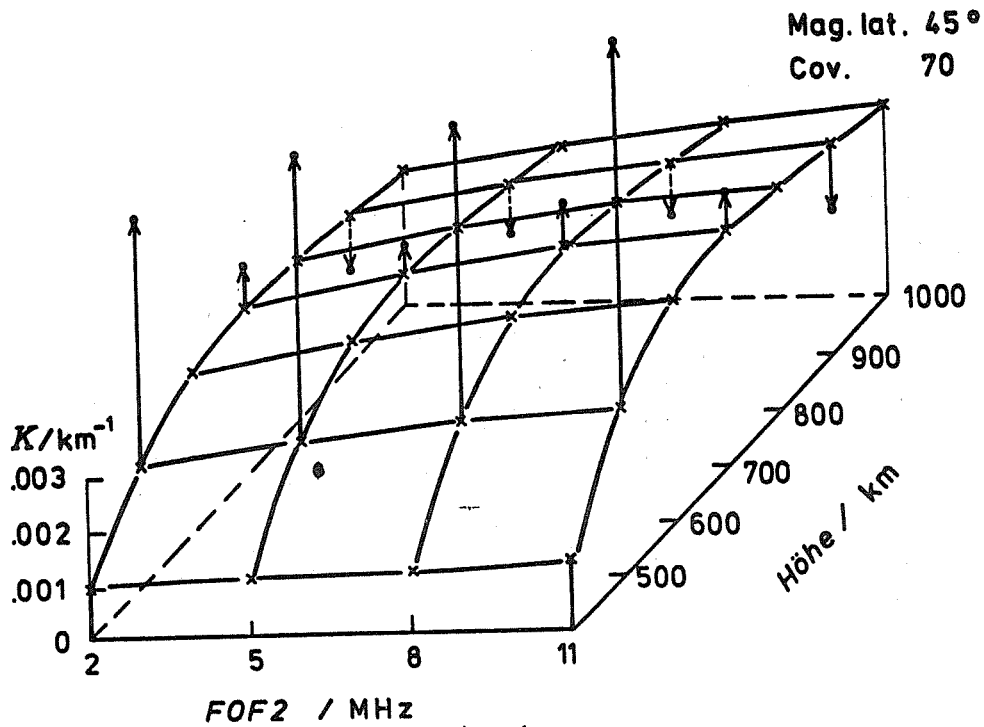


Fig. 1

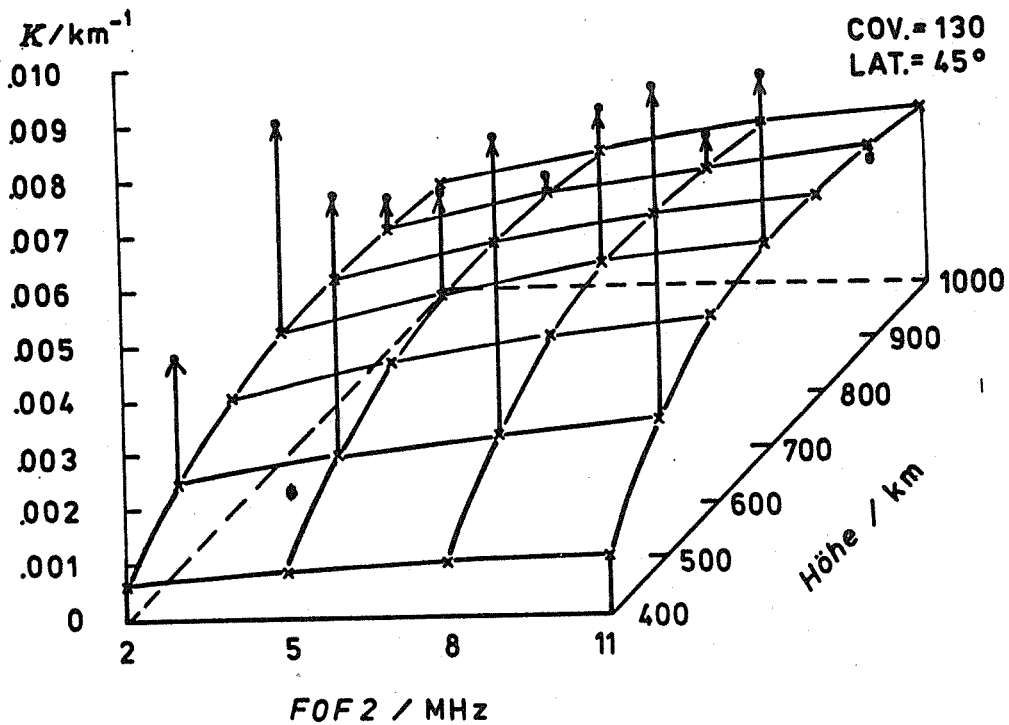


Fig. 2

Figs. 1 and 2 Inverse scale heights (K) obtained from the smoothed and optimised IRI-78 model (given by crosses) compared against the fixed values from the original Bent model.

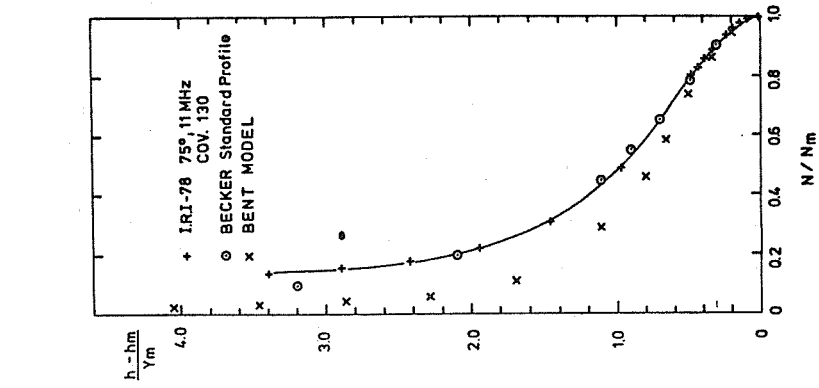


Fig. 3

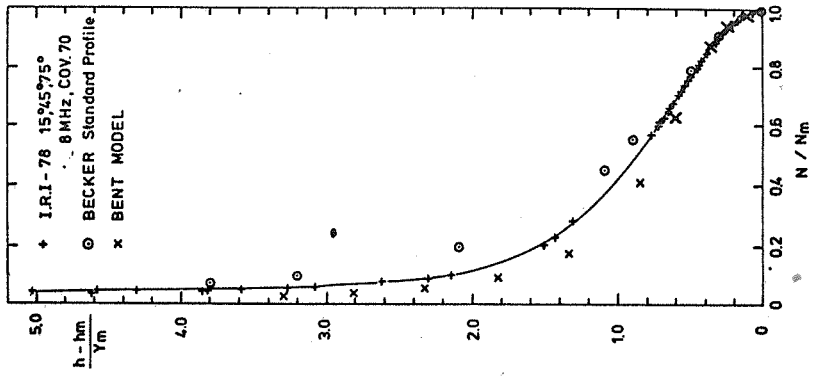


Fig. 4

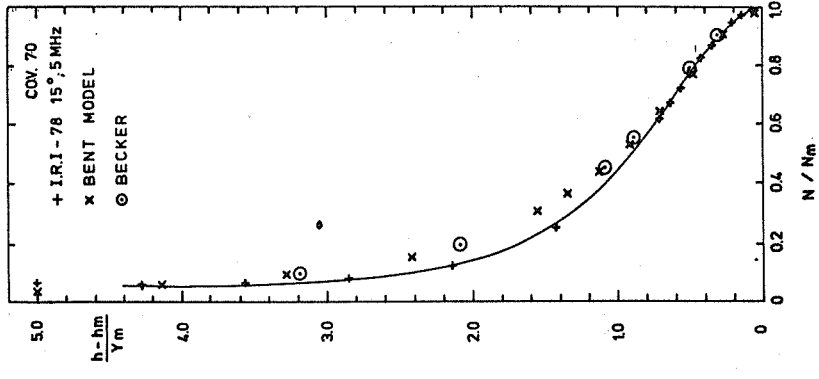


Fig. 5

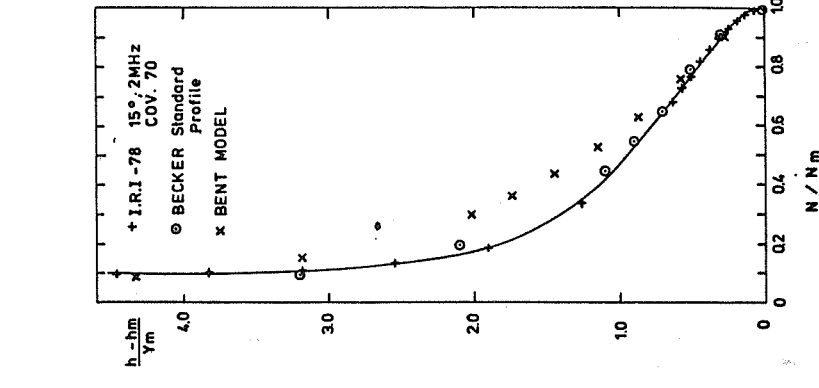


Fig. 6

Figs. 3, 4, 5 and 6 Normalised electron density profiles obtained from the global IRI-78 model compared against the discrete models of Bent and Becker.

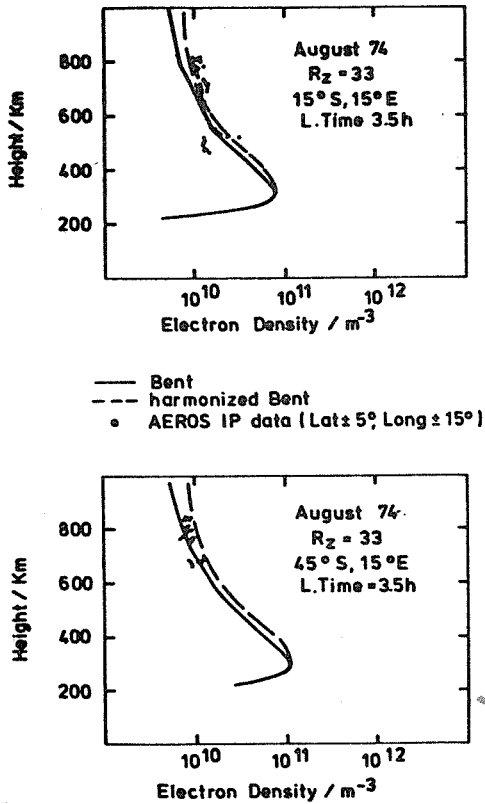


Fig. 7

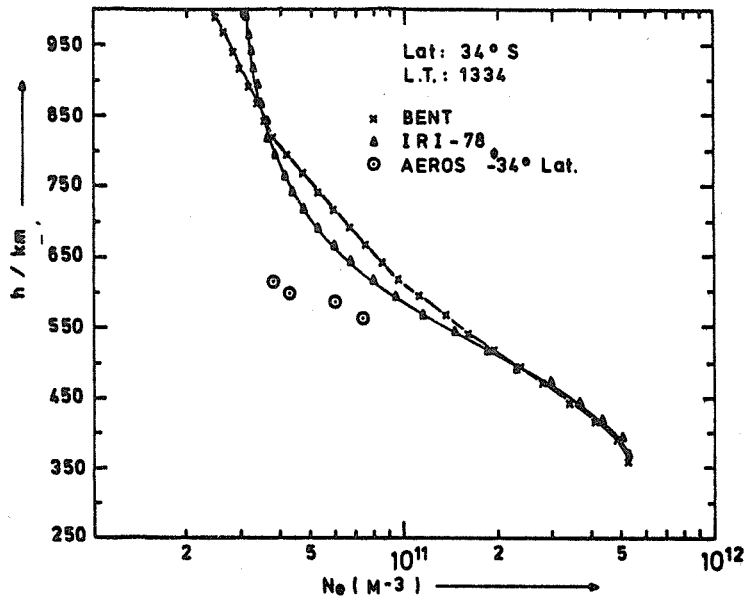


Fig. 8

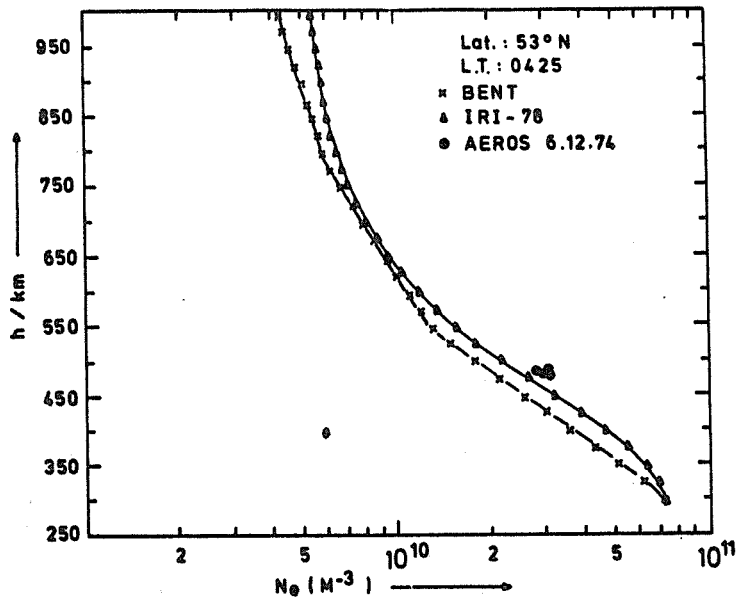
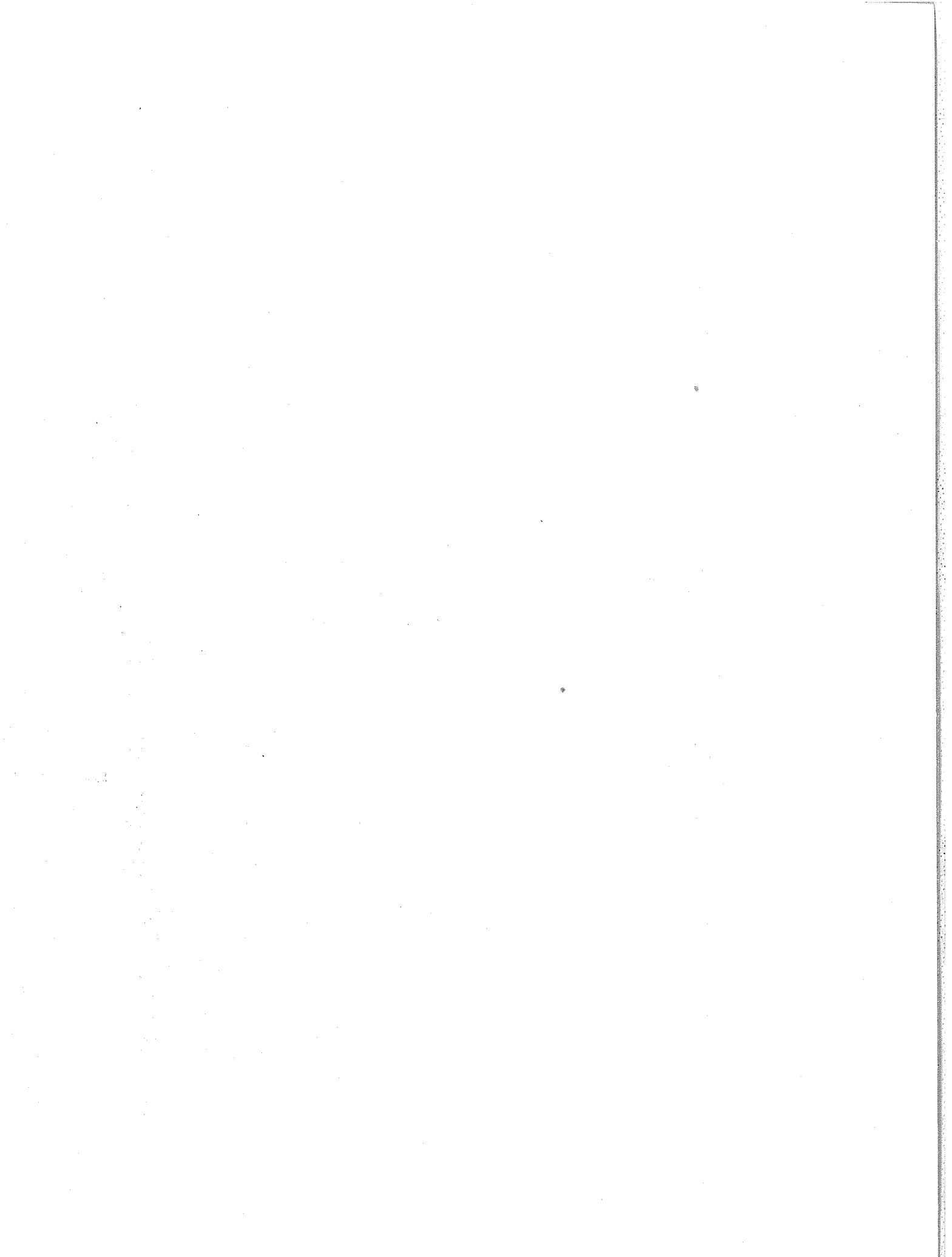


Fig. 9

Figs. 7, 8 and 9 Electron density profiles obtained from the IRI-78 and Bent models compared against the in-situ measurements from Aeros-B satellite.



3.3.2 Summary and Conclusions Concerning IRI

K. Rawer

University, D-7800 Freiburg, F.R.Germany

After going through the foregoing contributions we felt that our request for 'critical checking', expressed in IRI-78, has been widely followed in our international group (which is known in URSI as 'Working Group G.4' and in COSPAR as 'Task Group on IRI'). A large effort was made in many countries ending up with quite a few well defined proposals for improvement some of which appear to be practicable soon.

1, Electron Density Profile Ne(h)

First of all it should be stated that our main task was establishing the profile shape leaving the description of the F2-peak to Working Group G.8 in URSI, and to CCIR. We are fully aware of shortcomings of the still valid CCIR /1974/ peak description, particularly in regions which are not well served with ionospheric sounding stations. The task remains to combine the basic information used in CCIR Report 340 with now existing satellite data. As for the Chiu-model used in the simplified IRI-version, due to the small number of coefficients used, it cannot be more than a first approximation which is probably rather superficial in many regions of Earth.

Since the peak itself is outside of our official attributions let us now consider the shape around it, beginning with the topside. We did not expect so good agreement as became apparent in several contributions (2.2.3, 2.2.4). Our shape formula - it is quite near to Booker's /1977/ proposal - must probably be fitted now at greater heights to more recent satellite data which more and more are becoming available. In midlatitude winter a steeper density decrease was experimentally found (2.2.4). Larger deviations from IRI's shape are reported from low latitudes (Jicarcarca: 1.3.3, 1.3.4) where the density above and below the peak seems to decrease much quicker than after IRI, i.e. IRI gives a too large layer thickness (see, however, 1.4.2).

Unexpectedly, more critical remarks came against our bottomside F-region. I must, however, admit that the present combination of height ranges is somewhat artificial. The 'junction' between the 'intermediate region' and F1 is said to need higher density (1.2.1). Instead of a multi-layer expression we should better use an analytical formula similar to that used for the topside, perhaps along the line indicated by Mme. Gulyaeva. The E-F-valley width seems to depend on solar activity, should be twice our value for high activity (1.2.1). Still difficult is the shape of the very deep valley appearing at night (1.2.1, 1.2.3); measured data are still scarce. Whether the second maximum (1.2.3) is stable or a transient phenomenon is not yet clear.

Also the lower ionosphere profile is far from being final. IRI-78 stops at 65 km (thus no C-layer), but even at heights below 80 km the measured densities are reported to differ considerably from IRI, the latter giving too high values by day (1.2.3) but too low ones at night (1.2.4). Comparison with absorption measurements, though improved against the preliminary tables /Rawer et al., 1975/, still shows unsatisfactory solar cycle variation (1.1.1: too large by day, too small at night). Also the effect of the wave frequency upon absorption is overestimated when computing with the IRI Ne-profile (1.1.1, CIRA /1972/ for collision frequencies). The diurnal variation seems to be underestimated for winter days (1.1.1). This may largely be due to our assumption that NMD remains constant during nighttime, it should even depend

on solar activity (1.1.1). There remains the problem of reconciling this height-integrated data with the results of in-situ experiments though the interpretation of these latter is not so straightforward at very low heights.

2, Electron Temperature T_e

Four main criticisms were expressed when summarizing observed data:

(i) The diurnal variation: it is a) more specific than assumed during dawn (with an early morning peak near the equator) and dusk (2.1.1, 2.1.3, 2.2.1), and b) it decreases with increasing height (at 3000 km - above the present range - it should practically disappear: 2.1.1).

(ii) The seasonal effect is height dependent; it is probably larger below about 800 km (2.1.3, 2.2.1), smaller above 1200 km (2.1.1) than given by IRI.

(iii) The latitudinal dependence is in the actual IRI (via H_0) discontinuous at $\phi = 40^\circ$ and should be made continuous (2.1.3).

(iv) It is strongly recommended, instead of an independent T_e -formula, to reintroduce a $T_e(N_e)$ dependence, which must, however, be more involved than the direct relation used in the preliminary IRI (Rawer et al., 1975). At present $T_e(\text{IRI})$ agrees with the observations when N_e is near the average but differs considerably in other cases (2.1.1, 2.1.4).

Apart from these main concerns there is some discussion about the temperature profile at low latitudes which should (by day) potentially peak at lower height than given by IRI (2.1.2). As for the effect of solar activity it is certainly not unique but seems to work in both directions, according to the conditions (2.2.1).

3, Ion Temperature T_i

At midlatitudes T_i should be nearer T_e , thus somewhat greater than given by IRI (2.2.4).

4, Ion Composition

The O^+/H^+ transition level shows a rather complex world map with, at night, a trough near $30^\circ S$ dipole latitude where the isolines are displaced towards South (3.1.2).

It is certainly premature to give a detailed model for the different types of cluster ions (3.1.1, 3.1.5) but their total sum should be represented in a future IRI.

On behalf of the 'executive members' I like to thank all contributors to this report and hope for further fruitful cooperation in future.

CHAPTER 4. REFERENCES

- AGGARWAL, K.M., NARINDER NATH and C.S.G. SETTY 1979 Collision frequency and transport properties of electrons in the ionosphere, Plan. Space Sci., 27, 753-768.
- AGGSON, T.L., and J.P. HEPPNER 1977 J. Geophys. Res., 82, 5155.
- AIKIN, A.C., R.A. GOLDBERG, Y.V. SOMAYAJULU, and M.B. AVADHANULU 1972 Electron and positive ion altitude distributions in the equatorial D-region, J. Atm. Terr. Phys., 34, 1483-1494.
- AL'PERT, Ja.L. 1958 Russian Uspekhi Fis. Nauk (UFN), 64, 3.
- AL'PERT, Ja.L. 1960 Russian Uspekhi Fis. Nauk (UFN), 71, 369.
- AL'PERT, Ja.L. 1976 Space Sci.Rev., 18, 551.
- ANDREEVA, L.A. et al. 1971 Rocket investigations of the ionosphere at mid-latitudes, Space Res.XI, 1043-1050.
- ANDREEVA, L.A., E.S. KAZI-MIROVSKY, B.O. VUGMEISTER et al. 1973 Results of simultaneous wind measurements in the stratosphere, mesosphere and low thermosphere, Space Res.XIII, 191.
- ANDRIYAKO, V.A. et al. 1978 Kosmicheskyye issledovaniya 16, N6, 705.
- ANUFRIEVA, T.A., T.L. GULYAEVA, G.F. KADUKHIN, T.N. SOBOLEVA, and A.G. SHLIONSKY 1980 Prediction of parameters of the maximum of the vertical electron density gradient, in: Solar-Terrestrial Predictions Proceedings, Vol. IV, C-57 C-64, Boulder, Colo. U.S.A
- APPLETON, E.V. 1946 Two anomalies in the ionosphere, Nature 157, 691.
- ARNOLD, F., and D. KRANKOWSKY 1971 Negative ions in the lower ionosphere: A comparison of a model computation and a mass-spectrometer measurements, J.Atm.Terr.Phys. 33, 1693-1702.
- ARNOLD, F., and D. KRANKOWSKY 1974 Measurements of $H_2O_2^+$ in the D-region and implications for mesospheric H_2O_2 , Geophys. Res.Let. 1, 243-245.
- ARNOLD, F., and D. KRANKOWSKY 1977 Rate constants of NO^+N_2 formation at low temperatures, J.Atm.Terr.Phys., 39, 625-629.

- ARNOLD, F., and D. KRANKOWSKY 1979 Mid-latitude lower ionosphere structure and composition measurements during winter, J.Atm.Terr. Phys., 41, 1127-1140.
- AZARNIN, G.V., and A.B. ORLOV 1976 Geomagnetizm i Aeronomija, Russian 10, 754. (engl.transl.)
- AZARNIN, G.V., and A.B. ORLOV 1978 in: Problems of wave diffraction and propagation, 16, Leningrad State University, 119.
- BAILEY, G.J., R.J. MOFFETT, W.B. HANSON, and S. SANATANI 1973 Effects of interhemispheric transport on plasma temperatures at low latitudes, J.Geophys.Res., 78, 5597-5610.
- BAIN, W.C., and B.R. MAY 1967 D-region electron density distributions from propagation data, Proc.IEE, 114, 1593-1597.
- BAIN, W.C., and M.D. HARRISON 1972 Model ionosphere for D-region at summer moon during sunspot maximum, Proc.IEE, 119, 790-796.
- BALEV, I.B., A.A. GOLDIN, E.G. GREENWALD, V.A. PAVLENKO, A.I. SAVIN, M.K. SEROV, V.L. TALROSE 1980 Russian "Globalnoje issledovanie raspredeleniya kontsentratsii ionov v ionosfere."
- BANKS, P.M. 1969 Proc.IEEE, 57, 258.
- BANKS, P.M., and G. KOCKARTS 1973 Aeronomy, Acad. Press, New York and London.
- BARAN, D.E. 1974 Neutral winds and electric fields from model studies using reduced ionograms. Penn.State Univ., Ionosph. Res.Lab.Sci.Rep., 431.
- BARCLAY, L.W. 1963 Nomograms for calculating the solar zenith distance and azimuth at any latitude, The Marconi Rev., No. II, 163.
- BARRINGTON, R.E., and E.V. THRANE 1962 The determination of D-region electron densities from observations of cross modulation, J.Atmos.Terr.Phys., 24, 31-42.
- BECKER, W. 1971 German Einige Ergebnisse aus Lindauer Elektronendichteprofil-Berechnungen für die innere und äußere Ionosphäre, Kleinheubacher Berichte, 14, 145.

- BEHNKE, R.A., and S.T. HAGFORS 1974 Evidence for the existence of night-time region polarization fields at Arecibo, Radio Sci., 9, 211.
- BEHROOZI-TOOSI, A.B., and H.G. BOOKER 1980 Application of a simplified theory of ELF propagation to a simplified model of the ionosphere, preprint.
- BELII, V.V. et al. 1977 Geomagnetizm i Aeronomija, Russian 17, 663-666. (engl.transl.)
- BELINSKAYA, S.I. et al. 1976 Russian Concentration and temperature distribution of electrons and ions at the heights of E- and F-regions from direct measurement data, preprint N 7-76, SibIZMIR, Irkutsk.
- BELROSE, J.S., and B. SEGAL 1974 On the interpretation of CW propagation data for long radio waves, in: Methods of measurement and results of lower ionosphere structure, see Rawer (ed.), 1974.
- BENNETT, F.D.G., J.E. HALL, and P.H.G. DICKINSON 1972 D-region electron densities and collision frequencies from Faraday rotation and differential absorption measurements, J.Atmos.Terr.Phys., 34, 1321-1328.
- BENT, R.B., and S.K. LLEWELLYN 1970 DBA Systems, Melbourne Pa. USA (Report).
- BIBL, K. 1958 German Zur Dynamik der Ionosphäre, Zeitschr.f.Geophys., 24, 1.
- BIBL, K. 1964a The Detection of an Important Anomaly in the F-Region Ionization Above Central Europe, Annls. Géophys., 20, 447.
- BIBL, K. 1964b Large-Scale Fluctuations of the Ionosphere, AFCLR-64-900.
- BIBL, K. 1967 Seasonal Dependence of Movement and Turbulence Phenomena in Equatorial F-Layer Ionization, AGARD 95, 505.
- BIBL, K., and B.W. REINISCH 1978 A Universal Digital Ionosonde, Radio Sci., 13, 519.

- BILITZA, D., N.M. SHEIKH,
K. RAWER, and R. EYFRIG 1978 A global model of the
height of the F2-maximum
using M3000 values from
CCIR, in: URSI Internatio
nal Symposium on Radio
Waves and the Ionosphere,
(abstracts), 104, Helsin-
ki, Finland.
- BILITZA, D. 1981 Models for the Electron
and Ion Temperature, UAG
report, No. 81, World Data
Center A, Boulder/Col.,
U.S.A.
- BIRUKOV, A.V., I.A. KNORIN,
Ju.V. MUSATOV, V.A. RUDAKOV
and L.A. SHNIREVA 1972 Russian Abstracts of X Conference
on Radio Wave Propagation,
USSR, Nauka, 65.
- BJORN, L.G., F. ARNOLD,
D. KRANKOWSKY, B. GRANDAL,
O. HAGEN, and E.V. THRANE 1979 Lower ionosphere ion pro-
duction, density and compo-
sition in an auroral absorp-
tion event, J.Atmos.Terr.
Phys., 41, 1184-1194.
- BJONTEGAARD, G. 1974 J.Atmos.Terr.Phys., 36,
693.
- BLANC, M., and P.
AMAYENC 1976 Contribution of incoherent
scatter radars to the stu-
dy of middle and low lati-
tude ionospheric electric
fields, in: Atmospheric
Physics from Spacelab, 61.
- BLANC, M. 1977 Electrodynamics of the
ionosphere from incohe-
rent scatter, A review,
Invited paper at Joint
IAGA/IAMAP Assembly,
Seattle, U.S.A.
- BOOKER, H.G. 1977 Fitting of multiregion
ionospheric profiles of
electron density by a
single analytic function
of height, J.Atmos.Terr.
Phys., 39, 25-34, and
619-623.
- BOURDEAU, R.E. et al. 1966 J.Geophys.Res., 71, 727.
- BRACE, L.H., and N.W.
SPENCER 1964 First electrostatic pro-
be results from Explorer
17, J.Geophys.Res., 69,
4686-4689.
- BRACE, L.H., and B.M.
REDDY 1965 Early electrostatic pro-
be results from Explorer
22, J.Geophys.Res., 70,
5783-5792.
- BRACE, L.H., B.M. REDDY,
and H.G. MAYR 1967 Global behaviour of the
ionosphere at 1000 kilo-
meters altitude, J.Geophys.
Res., 72, 265-283.

- BRACE, L.H., H.G. MAYR,
and B.M. REDDY 1968 J.Geophys.Res., 73, 1607.
- BRACE, L.H. 1970 Global structure of ionosphere temperature, Space Res. X, North Holland Publ. Co., Amsterdam, 633-651.
- BRACE, L.H., R.F. THEIS, and
A. DALGARNO 1973 The Cylindrical electrostatic probes of Atmosphere Explorers C, D and E, Radio Sci., 8, 341-348.
- BRACE, L.H., and R.F.
THEIS 1974 The behaviour of the plasmapause at mid-latitudes, ISIS-1 Langmuir probe measurements, J.Geophys.Res., 79, 1871-1884.
- BRACE, L.H., and R.F.
THEIS 1978 An empirical model of the interrelationship of electron temperature and density in the daytime thermosphere at solar minimum, Geophys.Res.Lett., 5, 275-278.
- BRACE, L.H., and R.F.
THEIS 1980 X-document in preparation, Goddard Space Flight Center, Greenbelt, Maryland.
- BREMER, H., and W. SINGER 1977 Diurnal, Seasonal and solar cycle variations of electron densities in the ionospheric D and E-region, J.Atmos.Terr.Phys., 39, 25-34.
- BUDDEN, K.G. 1962 Radio Waves in the Ionosphere, Cambridge Univ. Press, see p. 88-145.
- CAIRO, L., C. ALTMAN,
and E. FIJALKOW 1974 Construction of D-region electron density profiles by combined use of ground based reflection and satellite based transmission coefficients, in: Methods of measurements and results of lower ionosphere structure, see Rawer (ed.) 1974.
- CARPENTER, D.L. 1966 J.Geophys.Res., 71, 693.
- CARPENTER, L.A., and V.W.
KIRCHOFF 1975 Comparison of high-latitude and mid-latitude ionospheric electric fields, J.Geophys.Res., 80, 1810.
- CARRU, H. et al. 1967
French Mesures de temperatures électroniques et ioniques par diffusion incoherente, J.Atmos.Terr.Phys., 29, 351-366.

- CAUFFMAN, D.P., and N.C. MAYNARD 1974 J.Geophys.Res., 79, 2427.
- CCIR (U.I.T., Genève) 1974 Atlas CCIR des caractéristiques ionosphériques, Rapport 340-2.
French
Spanish
- CHAKRABARTY, D.K., P. CHAKRABARTY, and G. WITT 1973 The effect of variations in temperature and nitric oxide density on ion clustering in the mesopause region during winter anomaly, J.Atmos.Terr. Phys., 40, 1147-1152.
- CHAKRABARTY, P., and D.K. CHAKRABARTY 1979 Mesopause temperature from the $\text{NO}^+ \cdot \text{H}_2\text{O} / \text{NO}^+$ ratio, J.Geophys.Res., 84, 3403-3408.
- CHAN, K.L., and L. COLIN 1979 Global electron density distributions from topside soundings, Proc. IEEE, 57, 990-1004.
- CHANIN, L.M., A.V. PHELPS, and M. BIONDI 1959 Measurement of the attachment of slow electrons in oxygen, Phys.Rev.Lett., 2, 344-346.
- CHAPKUNOV, S.K., TS.P. DACHEV, and T.N. IVANOVA 1979 Bulgarian A Device for the Measurement of Ion Structural Parameters in the Ionosphere, Patent application No 77251.
- CHASOVITIN, Yu.K. et al. 1974 Rocket measurements of electron density and electron temperature at sunset, in: COSPAR, Methods of Measurements and results of lower ionosphere structure, see Rawer (ed), 1974.
- CHASOVITIN, Yu.K., and N.M. KLYUEVA 1975 Electron temperature variation at 100-200 km from probe measurements, Space Res. XV, 369-377.
- CHASOVITIN, Yu.K. et al. 1976 Space Res., 16, 445.
- CHASOVITIN, Yu.K., and V.B. SHUSHKOVA 1978 Paper presented at International Symposium on Solar - Terrestrial physics, Innsbruck, Austria.
- CHASOVITIN, YU.K., and N.M. KLYUEVA 1978 Russian Rocket measurements of electron temperature in the polar region at 100-200 km, in: Polar ionosphere and magnetosphere-ionosphere relationships, Koisy subsidiary of AS USSR, Apatity, 142-160.

- CHASOVITIN, Yu.K., and V.B. Shushkova 1980 Russian Ionosphernye issledovania 35.
- CHIU, Y.T. 1975 An improved phenomenological model of ionosphere density, J. Atmos. Terr. Phys., 37, 1563-1570.
- CIRA 1972 1972 COSPAR International Reference Atmosphere, Akademie Verlag, Berlin.
- CLARK, W.L., J.P. McCLURE, and T.E. Van ZANDT 1976 Description and Catalog of Ionospheric F-region Data, World Data Center A, NOAA, Boulder, Col.
- COLE, A.E., and A.J. KANTOR 1978 Air Force Reference Atmospheres, AF GL-TR-78-005.
- COLE, A.E. 1979 Review of data and models of the middle atmosphere, Space Res., 19, 153-163.
- COSPAR International Reference Atmosphere 1972 Akademie-Verlag, Berlin.
- DACHEV, TS.P. 1978 Bulgarian Longitudinal variation of the equatorial ionosphere, Ph.D. Thesis.
- DACHEV, TS.P., HR.T. BRANISOV, Yu.N. MATVII-CHUK, and N.G. BANKOV 1980 An empirical model of night equatorial ionosphere on data from RPA on OGO-6 satellite, Low latitude aeronomical processes, COSPAR, Vol. 8, 127, Pergamon press.
- DALGARNO, A., M.B. McELROY, and R.J. MOFFETT 1963 Electron temperature in the ionosphere, Planet. Space Sci., 11, 463-484.
- DANILOV, A.D., and S.U. LEDOMSKAYA 1979 Russian Geomagnetizm i aeronomija 19, 961. (engl. transl.)
- DANILOV, A.D., and V.K. SEMENOV 1978 Relative ion composition model at mid-latitudes, J. Atmos. Terr. Phys., 40,
- DAVIES, K. 1970 In: AGARD Conf. Proc., 33, 463-469.
- DEEKS, K. 1966 D-region electron distributions in middle latitudes from the reflection of long radio waves, Proc. Roy. Soc. A., 291, 413-437.
- DEMINOV, M.G., V.K. KOZLOV, and Ju.S. SITNOV 1977a Russian O^+ concentrations over the geomagnetic equator, in: Inverstigations in the field of Solar-Terrestri-

- al Physics, Report IZMIRAN, Moscow, 22-30.
- DEMINOV, M.G., V.K.
KOZLOV, and Ju.S.
SITNOV 1977b
Russian Distribution of atomic ions over the geomagnetic equator, in Investigations in the field of Solar-Terrestrial Physics, Report IZMIRAN, Moscow, 31-39.
- DEMINOVA, G.F., V.V.
KULIKOV, Ju.S. SITNOV,
and L.A. JUDOVICH 1979
Russian Variations of concentrations of charged particles over the geomagnetic equator related to levels of solar activity, in Study of Ionospheric Dynamics, Report IZMIRAN, Moscow, 69-75.
- DEMYKIN, S.M. et al. 1974
Russian Radioteknika i Elektronika 19, 2060.
- DENISENKO, P.F., and
V.V. SOTSKY 1978
Russian
(engl.transl.) Possibility of establishing the existence of a valley from ionograms, Geomagnetizm i Aeronomija 18, 1045-1050.
- DONNELLY, R.F. 1968
ESSA Techn.Rep. ERL
92-SDL 6, Boulder, Col.
- DONNELLY, R.F. 1976
J. Geophys. Res., 81,
4745-4753.
- DORLING, E.G., and
W.S. RAITT 1976
Electron Temperature Models of the Thermosphere to 1100 km Based on ESRO-4 Measurements, Planet.Space Sci., 24,
739-747.
- DUNKIN, D.B., F.C.
FEHSENFELD, A.L.
SCHMELTEKOPF, and E.E.
FERGUSON 1971
Three-body association reactions of NO^+ with O_2 , N_2 and CO_2 , J.Chem. Phys., 54, 3817-3822.
- DYMEK, M.K. 1980
Photochemical model of ion composition and electron density in the ionosphere at 70-300 km, Low Latitude Aeronomical Processes, COSPAR Symposium Series, Vol. 8, 115-118.
- EVANS, J.V., and G.P.
MANTAS 1968
J.Atmos.Terr.Phys., 30,
563.
- EVANS, J.V., 1969
Millstone Hill Thomson Scatter Results for 1965, Tech.Rep., 474, Lincoln Lab., M.I.T., Lexington Mass,
- EVANS, J.V. 1970
Midlatitude ionospheric

- temperatures during three magnetic storms in 1965, J.Geophys.Res., 75, 4803-4813.
- EVANS, J.V. 1972a Ionospheric movements measured by incoherent scatter. A review. J.Atmos. Terr.Phys., 34, No.2, 175.
- EVANS, J.V. 1972b Measurements of horizontal drifts in the E- and F-regions at Millstone Hill, J.Geophys.Res., 77, No. 13, 2341.
- EVANS, J.V. 1973 Seasonal and Sunspot Cycle Variation of F-region Electron Temperatures and Protonospheric Heat Fluxes, J.Geophys. Res., 78, 2344-2349.
- EVANS, J.V. 1974 Millstone Hill Thomson Scatter Results for 1969, Tech.Rep. 513, Lincoln Lab., M.I.T., Lexington, Mass.
- EVANS, J.V., B.A. EMERY, and J.M. HOLT 1978 Millstone Hill Thomson scatter results for 1971, Tech.Rep. 528, Lincoln Lab., Lexington, Mass.
- EVANS, J.V., and J.M. HOLT 1978 Millstone Hill Thomson Scatter Results for 1972, Tech.Rep. 530, Lincoln Lab., Lexington, Mass.
- EYFRIG, R.W. 1963 The effect of the magnetic declination on the F2-layer, J.Geophys.Res., 68, 2529.
- FARLEY, D.T., and J.P. McCLURE, D.L. STERLING, and J.L. GREEN 1967 Temperature and Composition of the Equatorial Ionosphere, J.Geophys. Res., 72, 5837-5851.
- FEDYASHEV, A.B., and G.A. TUCHKOV 1972 Russian Abstracts of X Conference on Radio Wave Propagation, USSR, Nauka, 77.
- FEHSENFELD, F.C., A.L. SCHMELTEKOPF, H.I. SCHIFF, and E.E. FERGUSON 1967 Laboratory measurements of negative ion reactions of atmospheric interest, Planet.Space Sci. 15, 373-379.
- FEHSENFELD, F.C., E.E. FERGUSON, and D.K. BOHME 1969 Additional flowing afterglow measurements of negative ion reactions of D-region interest, Planet. Space Sci. 17, 1759-1762.

- FEHSENFELD, F.C.,
and E.E. FERGUSON 1969 Origin of water cluster ions in the D-region, J.Geophys.Res. 74, 2217-2222.
- FEHSENFELD, F.C., M.
MOSESMAN, and E.E. FER-
GUSON 1971 Ion - molecule reactions in $\text{NO}^+ - \text{H}_2\text{O}$ system, J.Chem.Phys., 55, 2120-2125.
- FEJER, B.G., D.T. FARLEY,
R.F. WOODMAN, and C.
CALDERON 1979 Dependence of equatorial F-region vertical drifts on season and solar cycle, J.Geophys.Res., 84, 5792-5796.
- FELGATE, D.G. 1975 Comparative studies of E-region ionospheric drifts and meteor winds, Planet.Space Sci., 23, 389.
- FERGUSON, E.E. 1974 Laboratory measurements of ionospheric ion-molecule reaction rates, Rev. of Geophys. and Space Phys. 12, 703-713.
- FERGUSON, E.E. 1969 Laboratory measurements of F-region reaction rates, Annls.Géophys., 25, 819-823.
- FINDLAY, J.A., and L.H.
BRACE 1969 Cylindrical electrostatic probes employed on Alouette II and Explorer 31 satellites, Proc.IEEE, 57, 1054-1056.
- FOLEY, G., T.B. JONES,
and B. BURGESS 1977 A comparison of the calculated and measured daytime propagation characteristics of the omega Trinidad transmissions, in: Propagation limitations of Navigation and Positioning Systems, AGARD Conf. Proc., 209, 17.1-17.9.
- FRENCH, M.A., L.P. HILLS,
and P. KEBARLE 1973 Kinetics and temperature dependence of the hydration of NO^+ in the gas phase, Can.J.Chem., 51, 456-461.
- GALYUK, Yu.P., and V.I.
IVANOV 1978 Russian in: Problems of wave diffraction and propagation, Leningrad State Univ., 16, 148.
- GAYVORONSKAYA, T.V., T.N.
SOBOLEVA, I.A. TUSHENTSOVA,
and E.E. TZEDILINA 1974 Russian Three-dimensional model of electron collision frequency distribution γ_e and diurnal variation of mid-latitudes profiles of γ_e

- in quiet ionosphere, Geomagn. And Aeronom., 14, 25-30.
- GAYVORONSKAYA, T.V.,
T.N. SOBOLEVA, I.A.
TUSHENTSOVA, E.E. TZEDILINA
1975
Russian
Moscow, Preprint IZMIRAN, 9.
- GEISLER, J.E., and S.A.
BOWHILL
1965
J.Atmos.Terr.Phys., 27, 457.
- GELLER, M.A., and G.C. HESS
1975
Simultaneous partial reflection and meteor radar wind observations at Urbana, Ill. during the winter of 1974-75, J. Atmos.Terr.Phys., 38, 3, 287.
- GIVISHVILI, G.V., M.D.
FLIGEL, L.N. LESCHENKO,
Yu.A. AFINOGENOV, and V.A. (engl.transl.)
GARBATSEBICH
1980
Russian
Planetarnoje raspredelenije pogloscheniya radiovoln v ionosfere, Geomagnetizm i Aeronomija, 2.
- GOGOSHEV, M.M., and
B.P. KOMITOV
1980
Russian
(engl.transl.)
Photodissociative excitation of twilight red oxygen emission at different levels of solar activity, to be published in: Geomagnetizm i Aeronomija.
- GOGOSHEV, M.M.
1978
Intercomparison of photometric systems of observatories in Arecibo and Stara Zagora, Comptes Rendus Acad.Bul.Sci., 31, 529.
- GOLDBERG, R.A., and L.J.
BLUMLE
1970
Positive ion composition from a rocket-borne mass spectrometer, J.Geophys. Res. 75, 133-142.
- GOLSHAN, N., and C.F.
SECHRIST
1975
Seasonal and solar cycle variation of E-region nitric oxide, Radio Sci., 10, 305-315.
- GRINGAUZ, K.I.
1958
Russian
Dokladi Akademii Nauk (DAN), 120, 1234.
- GRINGAUZ, K.I., and
V.A. RUDAKOV
1961
Russian
Iskusstvennie Sputniki Zemli, 6, 48.
- GRINGAUZ, K.I., G.L.
GDALEVICH, and V.A.
RUDAKOV
1970
Russian
Proceedings of the RIAN USSR, 1, 106.
- GRINGAUZ, K.I., G.L.
GDALEVICH, V.A. RUDAKOV,
and N.M. SHUTTE
1968
Russian
(engl.transl.)
The "Vertical" Rockets Payload, Geomagnetizm i Aeronomija 8, 224.
- GROVES, G.V.
1970
Seasonal and latitudinal models of atmospheric struc-

- ture between 30 and 120 km altitude, Space Res. X, 137.
- GULYAEVA, T.L. 1972 Russian (engl.transl.) On a non-ambiguous statement of the problem of computing the N(h) profiles of the bottomside ionosphere, Geomagnetizm i Aeronomija, 12, 551-553.
- GULYAEVA, T.L. 1974 Russian (engl.transl.) The effect of the ionisation vertical gradient on the ionogram, Geomagnetizm i Aeronomija, 14, 741-743.
- GULYAEVA, T.L. 1979 Criteria for determining the valley depth from ionograms, preprint 21, IZMIRAN, Moscow, submitted to J.Atmos.Terr. Phys.
- GULYAEVA, T.L. 1980 Use of a key point in the F-layer for N(h) analysis of ionograms, Radio Sci., in press.
- GUPTA, S.P., and S. PRAKASH 1979 Plan. of Space Sci. 27, 145.
- GUPTA, S.P. 1980 Space Res. XX, Pergamon Press, Oxford.
- GUREVICH, A.V., D.I. FISCHUK, and E.E. TZEDILINA 1972 Three-dimensional analytical model of electron concentration distribution in the quiet ionosphere, Moscow, Preprint IZMIRAN, 36.
- GUREVICH, A.V., and E.E. TZEDILINA 1979 Russian Super Long Propagation of Short Radio Waves, Moscow, Nauka.
- GUREVITCH, A.V. 1978 Nonlinear phenomena in the ionosphere, Springer-Verlag.
- HAGEN, J.B., and P.Y.S. HSU 1974 J.Geophys.Res., 79, 4269.
- HALL, J.C. 1973 Lower ionosphere electron densities from rocket measurement employing LF radio propagation and D.C. Probe techniques, Planet. Space Sci., 21, 119-131.
- HANSON, W.B. 1963 Electron temperatures in the upper ionosphere, Space Res. III, 382-402.
- HANSON, W.B., and R.J. MOFFETT 1966 Ionization transport effects in the equatorial

- F-region, J.Geophys.Res., 71, 5559-5572.
- HANSON, W.B., S. SANATANI, 1970 Plasma measurements with
D. ZUCCARO, and T.W. the retarding potential
FLOWERDAY analyzer on Ogo 6, J.
Geophys.Res., 75, 5483.
- HARNISCHMACHER, E., and K. 1958 Drift observations eva-
RAWER luated by the method of
"Similar Fades", J.Atmos.
Terr.Phys., 13, 1-16.
- HARNISCHMACHER, E., and K. 1968 Some observed phenomena
RAWER to be explained by theori-
es of ionospheric drift,
J.Atmos.Terr.Phys., 38,
871-884.
- HEDIN, A.E., C.A. REBER, 1977 A global thermospheric
G.P. NEWTON, N.W. SPENCER, model based on mass spec-
H.C. BRINTON, and H.G. MAYR trometer and incoherent
scatter data. MSIS. 2.
Composition, J.Geophys.
Res., 82, 2148-2156.
- HEELIS, R.A., G.J. BAILEY, and 1978 Ion temperature troughs
W.B. HANSON and interhemispheric
transport observed in the
equatorial ionosphere,
J.Geophys.Res., 83,
3683-3689.
- HEIMERL, J.M., and J.V. 1971 N₂ Clustering to NO⁺,
VANDERHOFF Trans.Am.Geophys.Un.,
52, 870.
- HERBERT, Th. 1967 Tables of virtual heights
for models of monoto-
nic and non monctonic
ionospheric layers,
Radio Sci., 2, 1269-
1277.
- HEROUX, L., M. COHEN, 1974 Electron densities bet-
and J.E. HIGGINS ween 110-300 km derived
from solar EUV fluxes
of August 23, J.Geo-
phys.Res., 79, 5237-
5244.
- HERRMANN, U., and C.R. 1980 The influence of meso-
PHILBRICK spheric temperature vari-
ation on the positive
ion composition during
the 1979 solar eclipse,
Trans.Am.Geophys.Un.,
61, 311.
- HEY, J.S., J.B.G. ROBERTS, 1968 Nature, London, 220,
G.N. TAYLOR, and C.D. WATKINS 865.
- HIRAO, K., and K. OYAMA 1972 Sounding rocket data in
Japan, I (1958-1972),
Department of Space Sci.,
ISAS, Univ. of Tokyo.

- HIRAO, K. 1975 The TAIYO Mission, J. Geo. mag. Geoelectr., 27, 265-270.
- HIRAO, K., and K. OYAMA 1970 An Improved Type of Electron Temperature Probe, J. Geomag. Geoelectr., 22, 393-402.
- HIRAO, K., and K. OYAMA 1972 A Critical Study on the Reliability of Electron Temperature Measurements with Langmuir Probe, J. Geomag. Geoelectr., 24, 415-427.
- HIRAO, K., and K. OYAMA 1980 Experimental Model of the Electron Temperature Profile in the Ionosphere at Middle Latitude -1 (Solar Activity Dependency), J. Geomag. Geoelectr., 32, 95-104.
- HO, M.C., and D.R. MOORCRAFT 1971 Planet. Space Sci., 19, 1441.
- HOEGY, W.R., and L.H. BRACE 1978 The importance of electron heat conduction in the energy balance of the F-region, Geophys. Res. Lett., 5, 269-272.
- HOFFMANN, J.H., W.B. HANSON, C.R. LIPPINCOTT, and E.E. FERGUSON 1973 The magnetic ion-mass spectrometer on Atmosphere Explorer, Radio Sci., 8, 315.
- HOFFMAN, J.H., W.H. DODSON, C.R. LIPPINCOTT, and H.D. HAMMACK 1974 Initial ion composition results from the ISIS 2 satellite, J. Geophys. Res., 79, 4246.
- HUFFMAN, R.E., D.E. PAULSEN, J.C. LARRABEE, and R.B. CAIRNS 1971 Decrease in D-region O₂ (¹Ag) photoionization rates resulting from CO₂ absorption. J. Geophys. Res., 76, 1028-1038.
- International Reference Ionosphere 1978 URSI, Brussels, Belgium
- IRI 1978 International Reference Ionosphere, K. Rawer, D. Bilitza and S. Ramakrishnan (eds.), URSI, Brussels.
- IVANOV-KHOLODNY, G.S., and V.V. FIRSOV 1974 The short-wave solar radiation spectrum under different activity levels, Geomagnetizm i Aeronomija, 14, 393-398.
Russian
(engl.transl.)

- IVANOV-KHOLODNY, G.S., and A.V. MIKHAILOV 1976 Russian (engl.transl.) A connection of the parameters of the ionosphere F2 region with the parameters of neutral atmosphere at a fixed height, Geomagnetizm i Aeronomija, 16, 799-802.
- JACCHIA, L.G. 1977 Thermospheric temperature, density and composition; new models, SAO Special Report 375, Smithsonian Inst. Cambridge, U.S.A.
- JESPERSEN, M., and B. MOLLER PEDERSEN 1970 J.Atmos.Terr.Phys., 32, 1859.
- JOHANNESSEN, A., and D. KRANKOWSKY 1972 Positive - ion composition measurement in the upper mesosphere and lower termosphere. J. Geophys.Res., 77, 2888-2901.
- JOHANNESSEN, A., and D. KRANKOWSKY 1974 Daytime positive ion composition measurement in the altitude range 73-137 km above Sardinia, J.Atmos.Terr.Phys., 36, 1233-1247.
- JOHNSON, R., Ch.M. HUANG, and M.A. BIONDI 1975 The formation and break-up of $NO^+ \cdot N_2$ clusters in N_2 at low temperatures, J.Chem.Phys., 63, 3374-3378.
- KADUKHIN, G.F., and T.N. SOBOLEVA 1978 Russian Latitude variation of electron concentration for studies of the propagation of radio waves, in: The Propagation of Radio Waves in the Ionosphere, Collection of IZMIRAN, Moscow, Nauka, 140-149.
- KANE, J.A. 1961 J.Atmos.Terr.Phys., 23, 338.
- KANE, J.A. 1972 Evidence for the existence of negative ions in the D- and lower E-regions at twilight, GSFC Preprint, X-615-72-18.
- KASHPAR, Yu.V. et al. 1978 Russian in: Proceedings of 12th National Conference on Radiowave Propagation, Nauka Publ. House, Moscow, Part 1, 193.
- KASHPAR, Yu.V. et al. 1979 Russian Radioteknika i Elektronika, 24, N7, 1316.

- KASHPAR, Yu.V. et al. 1978 Russian in: Proceedings of 12th National Conference on Radiowave Propagation, Nauka Publ. House, Moscow, Part 1, 189.
- KAZIMIROVSKY, E.S. 1963a Russian (engl.transl.) Wind systems in the lower ionosphere, Geomagnetizm i Aeronomija, 3, 3, 463.
- KAZIMIROVSKY, E.S. 1963b Russian (engl.transl.) The horizontal drifts of ionospheric irregularities in the upper ionosphere, Geomagnetizm i Aeronomija, 3, 5, 578.
- KAZIMIROVSKY, E.S., and V.D. KOKOUROV 1979a Russian Ionospheric Movements (Monograph), Novosibirsk 344.
- KAZIMIROVSKY, E.S., V.D. KOKOUROV, and E.I. ZHOVTY 1979b Dynamics of the quiet thermosphere (a review), J.Atmos.Terr.Phys., 41, No 7/8, 867.
- KAZIMIROVSKY, E.S., and V.D. KOKOUROV 1979c Coordinated measurements of E-layer drifts, J. Geomag.Geolectr., 31, 195.
- KEBARLE, P., S.K. SEARLES, A. ZOLLA, J. SCARBOROUGH, and M.A. ARSHADI 1967 The solvation of the hydrogen ion by water molecules in the gas phase, Heats and entropies of solvation of individual reactions: $H^+(H_2O)_{n-1} + H_2O \rightarrow H^+(H_2O)_n$, J.Am.Chem.Soc., 89, 6393-6399.
- KENT, G.S. 1970 Measurements of ionospheric movements, Rev. Geophys. and Space Phys., 8, 229.
- KHRIUKIN, V.G., and YU.K. CHASOVITIN 1976 Proceedings of the Institute of Experimental Meteorology, 5, 80.
- KLYUEVA, N.M. et al. 1973 Space Res., 13, 535.
- KLYUEVA, N.M. et al. 1977 Proceedings of the Institute of Experimental Meteorology, 6, 64.
- KLYUEVA, H.M. 1978 Russian Electron temperature variations at 110-200km from incoherent scatter data, in: Proceedings of Institute of Experimental Meteorology, 6, 74, Hydrometeoizdat, Moscow, 74-82.

- RLYUEVA, H.M. et al. 1978 Russian The dependence of electron concentration and temperature on solar zenith angle at 90-180km, in: Proceedings of the Institute of Experimental Meteorology, 6, 74, Hydrometeoizdat, Moscow, 64-73.
- KNUDSEN, W.C. 1966 Evaluation and demonstration of the use of retarding potential analyzers for measuring several ionospheric quantities, J.Geophys.Res., 71, 4669-4678.
- KNUDSEN, W.C., and G.W. SHARP 1968 J.Geophys.Res., 73, 6275.
- KOHL, H., J.W. KING, and D. COLES 1969 An explanation of the magnetic declination effect in the ionospheric F2-layer, J.Atmos. Terr.Phys., 31, 1011.
- KOPP, E., P. EBERHARDT, and U. HERRMANN 1978 Summer daytime ion composition in the D-region above Wallops Island, Space Res., 18, 245-248.
- KOPP, E., L. ANDRÉ, P. EBERHARDT and U. HERRMANN 1980 Negative ion composition of the D-region during the 1979 solar eclipse, Trans.Am.Geophys.Un., 61, 311.
- KORIAKINA, E.A., and V.B. SHUSHKOVA 1979 Proceedings of the Institute of Experimental Meteorology, 9, 45.
- KOUTIEV, I.S. 1972 Determining the equivalent delay from the regions below f_{min} upon calculating $N(h)$ profiles, Compt.Rend.Acad.Bulg.Sci., 25, 193-196.
- KRANKOWSKY, D., F. ARNOLD, H. WIEDER, and J. KISSEL 1972 The elemental and isotopic abundance of metallic ions in the lower E-region as measured by a cryogenically pumped quadrupole mass spectrometer, Int.J.Mass Spectrom. Ion Phys., 8, 379-389.
- KRASNUSHKIN, P.E., and T.A. KNYAZEVA 1970 Russian (engl.transl.) Geomagnetizm i Aeronomija, 10, 993.
- KRASNUSHKIN, P.Ye., and T.A. KNYAZEVA 1970 Russian (engl.transl.) Diurnal seasonal and 11 year variations of the electron density profile in the lower ionos-

- where, Geomagnetizm i Aeronomiya, 10, 789-796.
- KRASNUSHKIN, P.Ye., and N.L. KOLESNIKOV 1962 Russian Investigation of the lower ionosphere by means of long radio waves and low frequency probes installed in a rocket, Dokl.Akad. Nauk SSSR, 146, 596-599.
- KUMAR, S., and W.B. HANSON 1980 The morphology of metallic ions*in the upper atmosphere, J.Geophys. Res., in print.
- KUSHNEREVSKY, Ju.V., and G.V. VASILEV (ed.) 1980 Russian Devices for the study of topside ionosphere, Report IZMIRAN, Moscow.
- LABITZKE, K. et al. 1979 J.Atmos.Terr.Phys., 41, 1149.
- LÄMMERZAHN, P., and S.J. BAUER 1974 The AEROS mission, J. Geophys., 40, 5, 571-576.
- LÄMMERZAHN, P., K. RAWER, and G. SCHMIDTKE 1979a The AEROS satellites: data basis and integrated analysis, J.Geomag.Geolectr., 31, Suppl. 9.
- LÄMMERZAHN, P., K. RAWER, and M. RÖHMER 1979b German Ergebnisse des AEROS-Satelliten-programms, MPI H-1930-V3, MPI für Kernphysik, Heidelberg.
- LAKSHMI, D.R., and B.M. REDDY 1974 Indian J.Radio and Space Phys., 3, 162.
- LOBB, R.J., and J.E. TITHERIDGE 1977 The valley problem in bottomside ionogram analysis, J.Atmos.Terr.Phys., 39, 35.
- MAEDA, K. 1969 Mid-latitude electron density profiles as revealed by rocket experiments, J. Geomag.Geolectr., 21, 557-567.
- MAHAJAN, K.K. 1967 Extent of thermal non-equilibrium in the ionosphere, J.Atmos.Terr. Phys., 29, 1137-1151.
- MAHAJAN, K.K. 1977 Models of electron temperature in the ionospheric F-region using electron density height profiles, J.Atmos.Terr.Phys., 39, 637-639.
- MAHAJAN, K.K., and V.P. PANDEY 1978 Electron temperature and concentration in the plasmasphere at an altitude of 3000 km from ISIS-1 Langmuir probe measurements,

- Indian J. Radio and Space
Phys., 7, 305-310.
- MAHAJAN, K.K., and V.K. PANDEY 1979 Solar Activity Changes in the Electron Temperature at 1000 km Altitude from the Langmuir Probe Measurements on ISIS 1 and Explorer 22 Satellites, J. Geophys. Res., 84, 5885-5889.
- MAHAJAN, K.K., and V.K. PANDEY 1980 Models of electron temperature in the topside ionosphere for low and medium solar activity conditions, J. Geophys. Res., 85, 213-216.
- MANTAS, G.P. 1973 Electron Collision Processes in the Ionosphere, Aeronomy Rep. No. 54, Univ. of Illinois.
- MAYR, H.G., J. HARRIS, and N.W. SPENCER 1978 Some properties of upper atmosphere dynamics, Rev. Geophys. Space Phys., 16, 539.
- MAYR, H.G., and I. HARRIS 1979 F-region dynamics, Rev. Geophys. Space Phys., 17, 4, 492.
- McCLURE, J.P., D.T. FARLEY 1970 Ionospheric Electron Concentration Measurements above the Magnetic Equator, 1964-1966, Report, WDC-A (S.T.P.) Boulder, Col.
- McFARLAND, M., D.L. ALBRITTON, F.C. FEHSENFELD, E.E. FERGUSON, and A.L. SCHMELTEKOPF 1973 Flow-drift technique for ion mobility and ion-molecule reaction rate constant measurements. II. Positive ion reactions of N^+ , O^+ , N_2^+ with O_2 , with N_2 from thermal to 2 eV, J. Chem. Phys., 59, 6620-6628.
- McNAMARA, L.F. 1978 Ionosphere D-region data base, A collection of computer accessible experimental profiles of the D- and lower E-regions, Report UAG 67, WDC-A, NOAA Boulder, Col., U.S.A.
- MECHTLY, E.A. 1967 J. Geophys. Res., 72, 5239.
- MECHTLY, E.A., and D. BILITZA 1974 Models of D-region electron concentrations, Sci. Rep., Inst. Phys., Welt-raumforschung, IPW-WB 1.
- MECHTLY, E.A., S.A. BOWHILL, and L.G. SMITH 1972 Changes of lower ionosphere electron concentrations

- with solar activity, J. Atmos. Terr. Phys., 34, 1899-1907.
- MECHTLY, E.A., and L.G. SMITH 1968 Growth of the D-region at sunrise, J. Atmos. Terr. Phys., 30, 363-369.
- MEIRA, L. G. 1971 Rocket measurements of upper atmosphere nitric oxide and their consequences to the lower ionosphere, J. Geophys. Res., 76, 202-212.
- MITRA, A.P., and J.N. ROWE 1972 Ionospheric effects of solar flares - VI. Changes in D-region ion chemistry during solar flares, J. Atmos. Terr. Phys., 34, 795-806.
- MITRA, A.P. 1974 Ionospheric Effects of Solar Flares, D.Reidel Publ. Co., North Holland.
- MITRA, A.P., and Y.V. SOMAYAJULU 1979 A global model of D-region ionization, Space Res., 19, 269-273.
- MIYAZAKI, S. 1979 Ion transition height distribution obtained with the satellite TAIYO, J. Geomag. Geoelectr., 31, 5113-5124.
- MORGAN, M.G., and MAYNARD, N.C. 1976 J. Geophys. Res., 81, 3992.
- MORSE, F. et al. 1978 Operations plan for JAS-PIC, private communication.
- MOSS, S.J., and E. HYMAN 1968 Minimum variance technique for the analysis of ionospheric data acquired in satellite retarding potential analyzer experiments, J. Geophys. Res., 73, 4315-4323.
- MUL, P.M., and J.W. MCGOWAN 1979 Merged electron-ion beam experiments III. Temperature dependence of dissociative recombination for atmospheric ions NO^+ , O_2^+ and N_2^+ , J. Phys. B: Atom. Molec. Phys., 12, 1591-1601.
- MULDREW, D.B. 1965 J. Geophys. Res., 70, 2635.
- MURGATROYD, R.J. 1965 Winds in the mesosphere and lower thermosphere, Proc. Roy. Soc., 288, 575.
- NAGY, A.F., and R.J. CICERONE 1974 Simultaneous measurements of ion and neutral motions by radar and optical tech-

- niques, J.Atmos.Terr. Phys., 36, 1877.
- NARCISI, R.S., and A.D. BAILEY 1965 Mass spectrometric measurements of positive ions at altitudes from 64 to 112 km, J.Geophys.Res., 70, 3687-3700.
- NARCISI, R.S., A.D. BAILEY, L. DELLA LUCA, G. SHERMANN, and D.M. THOMAS 1971 Mass spectrometric measurements of negative ions in the D- and lower E-regions, J.Atmos.Terr. Phys., 33, 1147-1159.
- NARCISI, R.S., C.R. PHILBRICK, D.M. THOMAS, A.D. BAILEY, L.E. WLODYKA, D. BAKER, G. FREDERICO, R. WLODYKA, and M.E. GARDNER 1972 Positive ion composition of the D and E-regions during a PCA. Proceedings of COSPAR Symposium on Solar Particle event of Nov. 1969, APCRL-72-0474, Air Force Cambridge Res. Lab., Bedford, Mass.,
- NERTNEY, R.J. 1953 J.Atmos.Terr.Phys., 3, 92.
- NESKE, E., and R. KIST 1973 Rocket observations in the equatorial ionosphere, Space Res., 13, 485-488.
- NESKE, E., and R. KIST 1974 Impedance probe. The AEROS-B Electron Density Experiment, J.Geophys., 40, 5, 593-600.
- NESKE, E. et al. 1979 Analysis of Electron Density for TAIYO AEROS-B Encounters, J.Geomag. Geoelectr., 31, 31-35.
- NESKE, E. 1980 Analysis of a High Latitude Electron Density structure, Space Res., 20, 163-166.
- NESKE, E., K. RAWER, and C. REBSTOCK 1980 Longitudinal variation of peak electron density at low latitudes, in: Low Latitude Aeronomical Processes, COSPAR Symposium Series, 8, 107.
- NESTOROV, G., and K. SERAFIMOV 1963 German Ein neuer Parameter für Erfassung in der Ionisation Änderungen in der D-Region, Geophys.pura et appl. 56, 135.
- NILES, F.E., J.M. HEINERL, and G.E. KELLER 1972 Cluster, switch, and rearrangement reactions for positive ions in the D-region, Trans.Am.Geophys. Un., 53, 456.

- NOAA, 1979 1979 Solar Geophysical Data, Prompt Rpt, National Oceanic and Atmospheric Administration, No. 328, Part 1, June 1979 and No. 417, Part 1, May 1979.
- NOOR SHEIKH, M., E. NESKE, K. RAWER, and C. REBSTOCK 1978 Comparison of peak electron densities of the F2 layer derived from in-situ measurements with CCIR predictions, Telecomm.J., 45, 225.
- NOVIKOV, V.D., and I.N. ODINTSOVA 1976 Russian (engl.transl.) J.Geomagnetizm i Aeronomija, 16, 1013-1017.
- NOVIKOV, V.D., and I.N. ODINTSOVA 1979 J.Atmos.Terr.Phys., 41, 1015-1019.
- NOVIKOV, V.D. 1977 Russian In: Diffraction Effects of Decameter Radiowaves in the Ionosphere, Nauka, Moscow, 144-150.
- OFFERMANN, D. 1979 J.Atmos.Terr.Phys., 41, 1047.
- OGAWA, T., and T. SHIMAZAKI 1975 Diurnal variation of odd nitrogen and ionic densities in the mesosphere and lower thermosphere: simultaneous solution of photochemical-diffusive equations, J.Geophys. Res., 80, 3945-3960.
- OPPENHEIMER, M., A. DALGARNO, F.P. TREBINO, L.H. BRACE, H.C. BRINTON, and J.H. HOFFMANN 1977 Daytime chemistry of NO⁺ from atmosphere Explorer C measurements, J.Geo-phys.Res., 82, 191-194.
- OSHIO, M., R. MAEDA, and H. SAKAGAMI 1966 Height distribution of local photoionization efficiency, J.Radio Res. Lab., 13, 245-261.
- OYA, H., and T. OBAYASHI 1968 Space Res., 8, 332.
- OYA, H. et al. 1970 Rocket observations of the winter ionosphere using plasma probes, Space Res., 10, 707-711.
- OYAMA, K., and K. HIRAO 1979 Anomalous Heating of the Thermal Electrons Near the Focus of the Sq Current Vortex, J.Geo-mag.Geolectr., 31, 11-19.
- PAUL, A.K. 1966 Phase height and the ionospheric valley ambiguity, Radio Sci., 1, 441.

- PAUL, A.K. 1978 Temporal and spatial distribution of the spectral components of foF2, J. Atmos. Terr. Phys., 40, 135-144.
- PAULSEN, D.E., R.E. HUFFMAN, and J.C. LARRABEE 1972 Improved photo-ionization rates of O₂ (⁴A_g) in D-region, Radio Sci. 7, 51-55.
- PFISTER, W. 1974 Drift measurements with spectral analysis during of chemical releases into the ionosphere, in Kawer (ed.) 1974.
- PHARO, M.W. et al. 1971 An experimental study of the ion chemistry and thermal balance in the E- and F-regions above Wallops Island, Planet. Space Sci., 19, 15-25.
- PHELPS, A.V., and J.L. PACK 1959 Electron collision frequencies in nitrogen and in the lower ionosphere, Phys. Rev. Lett. 3, 340-342.
- PHILBRICK, C.R. 1974 Satellite measurements of neutral atmospheric composition in the altitude range 150 to 450 km, Space Res., 14, 151.
- PHILBRICK, C.R. 1976 Recent satellite measurements of upper atmospheric composition, Space Res., 16, 289
- PIGGOTT, W.R., M.L.V. PITTEWAY, and E.V. THRANE 1965* The numerical calculation of wavefields, reflection coefficients and polarizations for long radio waves in the lower ionosphere II, Phil. Trans. Roy. Soc. (London), 257, 243-27.
- PITTEWAY, M.L.V. 1965 The numerical calculation of wave fields, reflection coefficients and polarization for long radio waves in the lower ionosphere I, Phil. Trans. Roy. Soc. (London), 257, 219-24.
- PRAKASH, S., S.P. GUPTA, and B.H. SUBBARAYA 1970 A study of the irregularities in the nighttime equatorial E-region using a Langmuir probe and plasma noise probe, Planet. Space Sci., 18, 1307-1318.

- PRAKASH, S. et al. 1974 Methods of measurements and results of lower ionospheric structure, Rawer (ed.), Akademie Verlag, Berlin.
- PROLSS, G.W., U.V. ZAHN, and W.J. RAITT 1975 J.Geophys.Res., 80, 3715.
- PUCKET, L.J., and M.W. TEAGUE 1971 Production of $H_2O^+ \cdot nH_2O$ from NO^+ precursor in $NO-H_2O$ gas mixtures, J.Chem.Phys., 54, 2564-2572.
- RADIO SCIENCE (special edition) 1973 Atmospheric Explorer Experiments, Radio Sci., 8, 261-405.
- RAO, G.L., and B.R. RAO 1963 World-wide study of horizontal drifts and anisotropy of ionospheric irregularities in the E-region, J.Atmos.Terr.Phys., 25, 10, 553.
- RAWER, K. 1959 Drifts in the E-region, J.Atmos.Terr.Phys. 13, 1-16, 15, 141-144.
- RAWER, K. (ed.) 1965 Ionospheric Drifts, Annls. of IGY, 33.
- RAWER, K. (ed.) 1968 Wind and Turbulence in Stratosphere, Mesosphere and Ionosphere, Amsterdam: North-Holland Publ. Co. and New York:Academic Press.
- RAWER, K. (ed.) 1974 Methods of Measurements and Results of Lower Ionosphere structure, K. Rawer (ed.), Acad.Verlag, Berlin.
- RAWER, K., S. RAMAKRISHNAN, and D. BILITZA 1975 Preliminary reference profiles for electron and ion densities and temperatures proposed for the international reference ionosphere, IPW, Sci.Rep. W.B. 2.
- RAWER, K., S. RAMAKRISHNAN, and D. BILITZA 1977 Private communication.
- RAWER, K. 1977 Mid- and high latitude reference ionosphere, in: Dynamical and Chemical Coupling between the Neutral and Ionized Atmosphere, B. Grandal and J. A. Holtet (eds.), D.Reidel Publ.Co., Dordrecht, Holland, 129-143.

- RAWER, K. 1977 Report to COSPAR Panel 4B and the IRI Steering Committee, presented at the XXth COSPAR Meeting, Tel Aviv.
- RAWER, K., D. BILITZA, and S. RAMAKRISHNAN 1978 Goals and status of the International Reference Ionosphere, Rev.Geophys., 16, 177-181.
- RAWER, K., and S. RAMAKRISHNAN 1978a International Reference Ionosphere, URSI, Brussels, Belgium.
- RAWER, K. 1979 Corrections to IRI 1978, Freiburg, F.R.G.
- RAWER, K., S. RAMAKRISHNAN, and D. BILITZA 1981 International Reference Ionosphere, 1980, UAG-Report 81, World Data Center-A (S.T.P.), Boulder Col., U.S.A.
- REES, D. et al. 1976 Space Res., 16, 407.
- REID, G.C. 1977 The production of water-cluster positive ions in the quiet daytime D-region, Planet.Space Sci., 25, 275-290.
- REID, G.C. 1975 Ice clouds at the summer polar mesopause, J.Atmos. Sci., 32, 523-535.
- RICH, F.J., R.C. SAGALYN, and P.J.L. WILDMAN 1979 Electron temperature profiles measured up to 8000 km by S3-3 in the late afternoon, J.Geophys. Res., 84, 1328-1332.
- RINNERT, K. 1973 Radio Sci., 8, 829.
- RINO, C.L. 1972 Radar measurements of ionosphere motion in the presence of current induced spectral asymmetries, Radio Sci., 7, 1049.
- RISHBETH, H., T.E. van ZANDT, and W.B. HANSON 1977 Ion temperature through in the equatorial topside ionosphere, Planet.Space Sci., 25, 629.
- ROBLE, R.G. et al. 1978 The calculated and observed ionospheric properties during Atmospheric Explorer-C satellite crossings over Millstone Hill, J.Atmos.Terr.Phys., 40, 21-33.
- ROWE, J.N., A.P. MITRA, A.J. FERRARO, and H.S. LEE 1974 An experimental and theoretical study of the D-re-

- gion II. A semi-empirical model for mid-latitude D-region, J.Atmos.Terr.Phys., 36, 755-785.
- SCARABUCCI, R.R. 1969 Analytical and numerical treatment of wave propagation in the lower ionosphere, Technical Report No. 3412-11, Radio Sci. Lab., Electronics Lab., Stanford Univ., Stanford, Cal., U.S.A.
- SCMIDTKE, G., K. RAWER, H. BOTZEK, D. NORBERT, K. HOLZER 1977 Solar EUV photon fluxes measured aboard Aeros-A, J.Geophys.Res., 82, 2423-2427.
- SCHUNK, R.W., and A.F. NAGY 1978 Electron temperatures in the F-region of the ionosphere: theory and observations, Rev.Geophys. and Space Phys., 16, 355-399.
- SCHUNK, R.W., W.J. RAITT, and P.M. BANKS 1975 Effects of electric fields on the daytime high latitude E and F-regions, J. Geophys.Res., 80, 3121.
- SECHRIST, C.F. 1974 Radio Sci., 2, 137.
- SEDDON, J.C. 1953 J.Geophys.Res., 58, 3, 323.
- SEN, H.K., and A.A. WYLLER 1960 On the generalization of the Appleton-Hartree magneto-ionic formulas, J. Geophys.Res., 65, 3931-3950.
- SERAFIMOV, K., M. GOGOSHEV, and Ts. GOGOSHEVA 1977 Russian (engl.transl.) Geomagnetizm i Aeronomija, 17, 1044.
- SERAFIMOV, K.B., S.K. CHAPKUNOV, M.Ch. PETRUNOVA, and T.N. IVANIVA 1977 Vertical distribution of Ion Concentration Measured on Board the Vertical 3 Rocket, Space Res., 17, 453.
- SERAFIMOV, K.B. et al. 1979 Dynamical Behaviour of Daytime Topside Ionosphere Inferred from Vertical-6 Rocket Data, Space Res., 19, 291.
- SERAFIMOV, K.B. 1977 Bulgarian Model for Profile of Topside Ionosphere, Compt. Rend.Acad.Bulg.Sci., 30, 539.
- SERAFIMOV, K.B. 1979 Bulgarian Adaptibility of N(h) - Profile by Model IRI to Measurements of Coherent

- Frequencies, Compt. rend. Acad. Bulg. Sci., 12, 1651.
- SERAFIMOV, K.B., and I. KUTLEV 1979 Bulgarian Approximations for Electron Temperature Distribution by English Vertical Rockets Data, Compt. Rend. Bulg. Acad. Sci., 32, 31.
- SERAFIMOV, K.B., Ts.P. DACHEV, I.S. KUTIEV, and L.G. BANKOV 1980 Ionospheric peculiarities in the South Atlantic magnetic anomaly and its longitudinally adjacent regions, J. Atmos. Terr. Phys., in print.
- SINEL'NIKOV, V.M., G.P. L'VOVA, T.L. GULYAEVA, S.V. PAKHOMOV, and A.P. GLOTOV 1980 Russian The Phase Doppler method for rocket measurements of the electron density profile in the bottom-side ionosphere, in: Study of Structure and Wave Features of Space Plasma, Nauka, Moscow, 56.
- SINGER, W. 1976 Zeitschr. für Meteorologie, 26, 230.
- SINGER, W., J. TAUBENHEIM, and J. BREMER 1980 A test of IRI lower ionosphere models by comparison with radio propagation data, J. Atmos. Terr. Phys., 42, 241-248.
- SHARP, G.W. 1966 J. Geophys. Res., 71, 1345.
- SHAW, R.R., and D.A. GURNETT 1975 J. Geophys. Res., 80, 4259.
- SHELLMAN, C.H. 1970 Electron density distributions in the lower ionosphere with associated error bars derived from VLF and LF sounder data, Radio Sci., 5, 1127-1135.
- SHELLMAN, C.H. 1973 Determination of D-region electron density distributions from radio propagation data, Naval Electronics Laboratory Centre, San Diego, Cal., Res. Rep., NBLC/TR-1856.
- SHIMAZAKI, T. 1959 World-wide measurements of horizontal ionospheric drifts, Rep. Ionosphere Japan, 13, 1, 21.
- SHIMAZAKI, T., and A.R. LAIRD 1972 Seasonal effects on distributions of minor neutral constituents in the mesosphere and lower thermosphere, Radio Sci., 7, 23-43.
- SHINN, D.H., and H.A. WHALE 1952 Group velocities and group

- heights from the magneto-ionic theory, J.Atmos. Terr. Phys., 2, 85.
- SMITH, L.G. 1970 J.Atmos.Terr.Phys., 32, 7. 1247.
- SMITH, L.G. 1977 Space Res., 17, 427.
- SMITH, D., N.G. ADAMS, and D. GRIEF 1977 Implications of some laboratory determinations of NO⁺ reaction rates to cluster ion formation in the D-region, J.Atmos.Terr. Phys., 39, 513-521.
- SMITH, L.G., E.K. WALTON, and E.A. MECHTLY 1978 Vertical incidence absorption calculated using electron density profiles from rocket experiments and comparison with observations during winter anomaly, J.Atmos.Terr. Phys., 40, 1185-1197.
- SOBOLEVA, T.N. 1972a Russian The global model of integral transverse conductivity of the ionosphere, Moscow, Dep. VINIII, No 3504-71.
- SOBOLEVA, T.N. 1972b Russian The model profiles of diurnal distribution of electron concentration of the quiet ionosphere at mid-latitudes, Moscow, Preprint IZMIRAN No. 20.
- SOBOLEVA, T.N. 1973 Russian The latitudinal model of electron concentration distribution of the quiet ionosphere, Moscow, Preprint IZMIRAN, No. 16.
- SPENNER, K., and A. DUMBS 1974 The retarding potential analyzer on AEROS-B, J. Geophys., 40, 585.
- SPENNER, K.A., A. DUMBS, W. LOTZE, and H. WOLF 1974 Correlation between daytime electron temperature and density variation at low latitudes, Space Res., 14, 259-263.
- SPENNER, K., and H. WOLF 1975 Comparison between electron density and temperature during daytime, Space Res., 15, 321-325.
- SPENNER, K., and R. PLUGGE 1978 Electron Temperature Model derived from AEROS-A, Space Res., 18, 241-244.
- SPENNER, K., H. WOLF, K. HIRAO, and P. LAEMMERZAHN 1979 Intercomparison of F-region Electron Temperature Measured by the Satel-

- lites AEROS-B and TAIYO, J.Geomag.Geolectr., 31, Suppl. 21-31.
- SPENNER, K, and R. PLUGGE 1979 Empirical Model of Global Electron Temperature Distribution between 300 and 700 km Based on Data from AEROS-A, J.Geophys., 46, 43-56.
- STUBBS, T.J., and R.A. VINCENT 1973 Studies of D-region drifts during the winters of 1970-1972, Aust.J.Phys., 26, 645.
- SWARTS, E., and J.S. NISBET 1972 Revised calculations of F-region ambient electron heating by photoelectrons, J.Geophys.Res., 77, 6259-6261.
- SWIDER, W., and R.S. NARCISI 1974 Ion composition in an IBC class II aurora, 2, Model, J.Geophys.Res., 79, 2849-2852.
- SWIDER, W., and R.S. NARCISI 1975 A study of nighttime D-region during a PCA event, J.Geophys.Res., 80, 655-664.
- SWIDER, W. 1977 Aeronomic aspects of the polar D-region, Space Sci. Rev., 20, 69-114.
- SWIDER, W. 1978 Daytime nitric oxide at the base of the thermosphere, J.Geophys.Res., 83, 4407-4410.
- TARAN, V.I. 1976 Russian Incoherent scatter measuring complex of the Khar'kov polytechnic institute, Radiotechn.i electron, 21, 1-10.
- TAYLOR, G.N., and G.L. WRENN 1970 Comparisons of simultaneous satellite and ground based measurements of ionospheric parameters, Planet.Space Sci., 18, 1663.
- THOMAS, L., and M.R. BOWMAN 1972 The diurnal variation of hydrogen and oxygen constituents in the mesosphere and lower thermosphere, J.Atmos.Terr.Phys., 34, 1843-1858.
- THOMAS, L., and M.D. HARRISON 1970 The electron density distributions in the D-region during night and pre-sunrise period, J.Atmos.Terr.Phys., 32, 1-1.

- THOMAS, L. 1976 Mesospheric temperatures and the formation of water cluster ions in the D-region, J.Atmos.Terr. Phys., 38, 1345-1350.
- THOME, G.D., and L.S. WAGNER 1971 J.Geophys.Res., 76, 6883-6895.
- THRANE, E.V. 1968 Collision frequency in the high latitude D-region, in: K. Folkestad (ed.), Ionospheric Radio Communication, Plenum Press, New York.
- TITHERIDGE, J.E. 1976 Ion transition heights from topside electron density profiles, Planet. Space Sci., 24, 229-245.
- TOHMATSU, T., and N. IWAGAMI 1975 Measurement of nitric oxide distribution in the upper atmosphere, Space Res., 15, 241-245.
- TORKAR, K.M. 1977 German Die untere Ionosphäre und ihre Bedeutung im Energiehaushalt der hohen Atmosphäre unter Berücksichtigung der Messung von Elektronendichten und Stoßzahlen mit Raketen, Ph.D. Thesis, Techn.Univ.Graz.
- TORKAR, K.M., M. FRIEDRICH, W. WALLNER, G. ROSE, and H.U. WIDDEL 1978 Preliminary results of absorption measurements of a central European A3 path, Kleinheubacher Ber., 21, 155-161.
- TORKAR, K.M., and M. FRIEDRICH 1980 Ion production and loss in the D- and E-regions, Report, INW 8004, Techn. Univ. Graz.
- TORR, D.G., and M.R. TORR 1979 Chemistry of the thermosphere and ionosphere, J. Atmos.Terr.Phys., 41, 797-839.
- TURCO, R.P. 1977 On the formation and destruction of chlorine negative ions in the D-region, J.Geophys.Res., 82, 3583-3592.
- TURNER, D.L., and D.C. CONWAY 1976 Stability of the NO^+N_2 ion cluster, J.Chem.Phys., 65, 3944-3947.
- TUSHENTSOVA, I.A., and D.I. FISCHUK 1975 Russian Corrected coefficients for the three-dimensional analytical model of the ionosphere, The Investiga-

- tion of Superlong Propagation of Short Radio-waves, Collection of IZMIRAN reports, Moscow, 143-150.
- TZEDILINA, E.E. 1980
Russian
(engl.transl.) The discrete structure of round the world signals, Geomagnetizm i Aeronomija, 20, 148-151.
- VERGASOVA, G.V., E.I.ZHOVTY, 1978
and E.S. KAZIMIROVSKY Empirical model for general circulation of the atmosphere at ionospheric levels above 100 km, Planet.Space Sci., 26, 387.
- WAIT, J.R. 1961 A diffraction theory for LF skywave propagation, J.Geophys.Res., 66, 1713-1724.
- WATT, A.D. 1967 VLF Radio Engineering, Pergamon Press, Oxford, p. 177, 178, 31-338.
- WALDTEUFEL, P. 1971 Annls.Géophys., 27, 167.
- WALLS, F.L., and G.H. DUNN 1974 Measurement of total cross sections for electron recombination with NO⁺ and O₂ using ion storage techniques, J.Geophys.Res., 79, 1911-1915.
- WATANABE, Y., and T. 1977
OBAYASHI Japanese The transition height of the ion composition observed by the impedance probe, in: Bull.Inst. Space and Aeronaut.Sci., Univ. Tokyo, 13, 979-987.
- WHALEN, J.A. 1970 Auroral oval plotter and nomograph for determining corrected geomagnetic local time, latitude, and longitude for high latitudes in the northern hemisphere, AFCRL-70-0422, Environmental Res.Papers, 327, AFCRL, Bedford, Mass., USA.
- WOODMAN, R.F. 1970 Vertical drift velocities and east-west electric fields at the magnetic equator, J.Geophys.Res., 75, 6249-6259.
- WRIGHT, J.W., A.K. PAUL, 1975
and E.A. MECHTLY Electron density profiles from ionograms: underlying ionisation corrections and their comparison with rocket results, Radio Sci., 10, 255-270.

- WRIGHT, J.W., M. GLASS,
and A. SPIZZICHINO 1976a The interpretation of ionospheric radio drift measurements. VIII. Direct comparisons of meteor radar winds and kitesonde measurements: mean and random motions, J.Atmos.Terr. Phys., 38, 7, 713.
- WRIGHT, J.W. 1976b The interpretation of ionospheric radio drift measurements. IX. Direct comparison between field-aligned ion drifts by incoherent scatter and kitesonde measurements, J.Atmos.Terr. Phys., 38, 7, 731.
- ZBINDEN, P.A., M.A. HIDALGO,
P. EBERHARDT, and J. GEISS 1975 Mass spectrometer measurements of the positive ion composition in the D- and E-regions of the ionosphere, Planet.Space Sci., 23, 1621-1642.
- ZELENOVA, T.I. et al. 1976 Russian in: Physics and the empirical modelling of the ionosphere, Nauka Publ. House, Moscow, p. 40, p. 71.
- 1973 Physical and chemical characteristic of the Earth atmosphere, Handbook Defense Nuclear Agency USA, 3467H.

5 Index of Authors

Afonin, V.V.	2.2.3, 2.3.1	Mendov, I.	2.3.2
Apa'thy, I.	2.2.3	Migulin, V.V.	2.3.1
Balev, I.B.	3.2.2	Mikhailov, A.V.	1.3.3
Bankov, L.	3.1.3	Moraitis, G.	2.3.2
Bankov, N.	3.1.3	Morgan, M.J.	1.3.4
Bencze, P.	2.2.3	Neske, E.	1.3.1, 1.3.2
Bezrukikh, V.V.	1.3.4	Nikitin, A.A.	1.2.3
Bibl, K.	1.4.1	Novikov, V.D.	1.4.2
Bilitza, D.	2.2.1, 3.3.1	Okintsova, I.N.	1.4.2
Brace, L.H.	2.1.1	Pakhomov, S.V.	1.2.2
Bremer, J.	1.1.1	Pandey, V.K.	2.1.4
Chasavitin, Yu.K.	1.2.3, 2.1.3	Pashova, Ts.	2.3.2
Dachev, Ts.	2.2.2, 3.1.3	Paul, A.K.	3.2.1
Danilov, A.D.	1.2.3	Pavlenko, V.A.	3.2.2
Deminova, G.F.	1.3.5	Philbrick, C.R.	1.3.2, 3.1.4
Dymek, Maria	3.1.5	Ramakrishnan, S.	1.3.1, 3.3.1
Fligel, M.D.	2.3.1	Ramanamurty, Y.V.	1.1.2
Friedrich, M.	1.1.3	Rawer, K.	3.3.2
Glotov, A.P.	1.2.2	Rebstock, C.	1.3.1
Gluyaeva, T.L.	1.2.1	Rogozhkin, E.V.	2.2.4
Gogoshev, M.M.	2.3.1, 2.3.2	Rycroft, M.J.	1.3.4
Gogosheva, Ts.	2.3.2	Savin, A.I.	3.2.2
Goldin, A.A.	3.2.2	Serafimov, K.B.	2.1.5, 2.3.1, 3.1.2, 3.1.3
Gulyaeva, T.L.	1.2.2, 1.2.3, 1.2.4	Shushkova, V.B	1.2.3
Gupta, S.P.	1.2.5	Shutte, N.	2.2.3
Heelis, K.	3.1.2	Similauer, J.	2.3.1
Hirao, K.	2.1.2	Singel'nikov, V.M.	1.2.2
Israetel, A.G.	1.2.4	Singer, W.	1.1.1
Ivanov, V.I.	1.2.3	Smilauer, J.	2.3.1
Karadimov, M.	3.1.2	Smith, A.J.	1.3.4
Kazimirovsky, E.S.	3.2.3	Soboleva, T.N.	1.2.4
Kemykin, S.M.	1.2.3	Spasov, S.	2.3.2
Khriukin, V.G.	1.2.3	Sukhacheva, L.L.	1.2.3
Kiraga, A.	2.3.1	Szemerey, I.	2.2.3
Kirov, B.	3.1.3	Talrose, V.L.	3.2.2
Klos, Z.	2.3.1	Taneva-Mendava, B.	2.3.2
Klyueva, N.M.	2.1.3	Taran, V.I.	2.2.4
Komitov, B.	2.3.2	Taubenheim, J.	1.1.1
Kopp, E.	3.1.1	Teodosiev, D.	3.1.3
Kovacs, K.	2.2.3	Theis, R.F.	2.1.1
Kubat, K.	2.3.1	Thiemann, H.	3.3.1
Kunev, K.	2.3.2	Thomas, T.W.	1.3.4
Kushnerevsky, Yu.V.	2.3.1	Tikhomirov, S.P.	1.2.3
Kutiev, I.	3.1.2, 3.1.3	Torkar, K.M.	1.1.3
L'vova, G.P.	1.2.2	Trendafilov, N.S.	2.2.2
Laemmerzähl, P.	1.3.2	Triska, P.	2.3.1
Leshchinskaya, T.Yu.	1.2.4, 1.3.3	Tzedilina, E.E.	1.2.4
Mahajan, K.K.	2.1.4	Williams, D.V.	1.3.4
Markova, T.	2.3.2	Yudovich, L.A.	1.3.5
Maynard, N.C.	1.3.4		

UAG SERIES OF REPORTS

Fewer than four UAG Reports are published at irregular intervals each year. Copies of these publications may be purchased through the NATIONAL GEOPHYSICAL DATA CENTER, Solar-Terrestrial Physics Division (E/GC2), 325 Broadway, Boulder, Colorado 80303, USA. A \$4.00 handling charge per order will be added to the single-copy price, if any, listed below. Please note, too, that some reports are available on microfiche only. Orders must include check or money order payable in U.S. currency to the Department of Commerce, NOAA/NGDC.

- UAG- 1 IQSY NIGHT AIRGLOW DATA, by L.L. Smith, F.E. Roach, and J.M. McKennan, ESSA Aeronomy Laboratory, Boulder, CO, July 1968, 305 pp, \$1.75.
- UAG- 2 A REEVALUATION OF SOLAR FLARES, 1964-1966, by Helen W. Dodson and E. Ruth Hedeman, McMath-Hulbert Observatory, University of Michigan, Pontiac, MI, August 1968, 28 pp.
- UAG- 3 OBSERVATIONS OF JUPITER'S SPORADIC RADIO EMISSION IN THE RANGE 7.6-41 MHZ, 6 JULY 1966 THROUGH 8 SEPTEMBER 1968, by James W. Warwick and George A. Dulk, University of Colorado, Boulder, CO, October 1968, 35 pp.
- UAG- 4 ABBREVIATED CALENDAR RECORD 1966-1967, by J. Virginia Lincoln, Hope I. Leighton and Dorothy K. Kropp, ESSA now NOAA, Aeronomy and Space Data Center, Boulder, CO, January 1969, 170 pp, \$1.25.
- UAG- 5 DATA ON SOLAR EVENT OF MAY 23, 1967, AND ITS GEOPHYSICAL EFFECTS, compiled by J. Virginia Lincoln, World Data Center A, Upper Atmosphere Geophysics, ESSA now NOAA, Boulder, CO, February 1969, 120 pp.
- UAG- 6 INTERNATIONAL GEOPHYSICAL CALENDARS 1957-1969, by A.H. Shapley and J. Virginia Lincoln, ESSA Research Laboratories, now NOAA, Boulder, CO, March 1969, 25 pp.
- UAG- 7 OBSERVATIONS OF THE SOLAR ELECTRON CORONA: FEBRUARY 1964 - JANUARY 1968, by Richard T. Hansen, High Altitude Observatory, NCAR, Boulder, CO, and Kamuela, HI, October 1969, 12 pp.
- UAG- 8 DATA ON SOLAR-GEOPHYSICAL ACTIVITY OCTOBER 24 - NOVEMBER 6, 1968, Parts 1 and 2, compiled by J. Virginia Lincoln, World Data Center A, Upper Atmosphere Geophysics, ESSA now NOAA, Boulder, CO, March 1970, 312 pp, \$1.75 (includes Parts 1 and 2).
- UAG- 9 DATA ON COSMIC RAY EVENT OF NOVEMBER 18, 1968, AND ASSOCIATED PHENOMENA, compiled by J. Virginia Lincoln, World Data Center A, Upper Atmosphere Geophysics, ESSA now NOAA, Boulder, CO, April 1970, 109 pp.
- UAG-10 ATLAS OF IONOGRAMS, edited by A.H. Shapley, ESSA Research Laboratories now NOAA, Boulder, CO, May 1970, 243 pp, \$1.50.
- UAG-12 SOLAR-GEOPHYSICAL ACTIVITY ASSOCIATED WITH THE MAJOR GEOMAGNETIC STORM OF MARCH 8, 1970, Parts 1, 2 and 3, compiled by J. Virginia Lincoln and Dale B. Bucknam, World Data Center A, Upper Atmosphere Geophysics, ESSA now NOAA, Boulder, CO, April 1971, 466 pp, \$3.00 (includes Parts 1-3).
- UAG-13 DATA ON THE SOLAR PROTON EVENT OF NOVEMBER 2, 1969, THROUGH THE GEOMAGNETIC STORM OF NOVEMBER 8-10, 1969, compiled by Dale B. Bucknam and J. Virginia Lincoln, World Data Center A, Upper Atmosphere Geophysics, ESSA now NOAA, Boulder, CO, May 1971, 76 pp.
- UAG-14 AN EXPERIMENTAL, COMPREHENSIVE FLARE INDEX AND ITS DERIVATION FOR 'MAJOR' FLARES, 1955-1969, by Helen W. Dodson and E. Ruth Hedeman, McMath-Hulbert Observatory, University of Michigan, Pontiac, MI, July 1971, 25 pp.
- UAG-16 TEMPORAL DEVELOPMENT OF THE GEOPHYSICAL DISTRIBUTION OF AURORAL ABSORPTION FOR 30 SUBSTORM EVENTS IN EACH OF IQSY (1964-65) AND IASY (1960), by F.T. Berkey, University of Alaska, Fairbanks, AK; V.M. Driatskiy, Arctic and Antarctic Research Institute, Leningrad, USSR; K. Henriksen, Auroral Observatory, Tromson, Norway; D.H. Jelly, Communications Research Center, Ottawa, Canada; T.I. Shchuka, Arctic and Antarctic Research Institute, Leningrad, USSR; A. Theander, Kiruna Geophysical Observatory, Kiruna, Sweden; and J. Yliniemi, University of Oulu, Oulu, Finland, September 1971, 131 pp, \$1.50 (microfiche only).
- UAG-17 IONOSPHERIC DRIFT VELOCITY MEASUREMENTS AT JICAMARCA, PERU (JULY 1967 - MARCH 1970), by Ben B. Balsley, NOAA Aeronomy Laboratory, Boulder, CO, and Ronald F. Woodman, Jicamarca Radar Observatory, Instituto Geofisico del Peru, Lima, Peru, October 1971, 45 pp, \$1.50 (microfiche only).
- UAG-18 A STUDY OF POLAR CAP AND AURORAL ZONE MAGNETIC VARIATIONS, by K. Kawasaki and S.-I. Aka-sofu, University of Alaska, Fairbanks, AK, June 1972, 21 pp.

UAG SERIES OF REPORTS (Continued)

- UAG-19 REEVALUATION OF SOLAR FLARES 1967, by Helen W. Dodson and E. Ruth Hedeman, McMath-Hulbert Observatory, University of Michigan, Pontiac, MI, and Marta Rovira de Miceli, San Miguel Observatory, Argentina, June 1972, 15 pp.
- UAG-21 PRELIMINARY COMPILATION OF DATA FOR RETROSPECTIVE WORLD INTERVAL JULY 26 - AUGUST 14, 1972, by J. Virginia Lincoln and Hope I. Leighton, World Data Center A for Solar-Terrestrial Physics, NOAA, Boulder, CO, November 1972, 128 pp.
- UAG-22 AURORAL ELECTROJET MAGNETIC ACTIVITY INDICES (AE) FOR 1970, by Joe Haskell Allen, National Geophysical and Solar-Terrestrial Data Center, Boulder, CO, November 1972, 146 pp.
- UAG-23 U.R.S.I. HANDBOOK OF IONOGRAM INTERPRETATION AND REDUCTION, Second Edition, November 1972, edited by W.R. Piggott, Radio and Space Research Station, Slough, UK, and K. Rawer, Arbeitsgruppe fur Physikalische Weltraumforschung, Freiburg, GFR, November 1972, 324 pp, \$1.75.
- UAG-23A U.R.S.I. HANDBOOK OF IONOGRAM INTERPRETATION AND REDUCTION, Second Edition, Revision of Chapters 1-4, edited by W.R. Piggott, Radio and Space Research Station, Slough, UK, and K. Rawer, Arbeitsgruppe fur Physikalische Weltraumforschung, Freiburg, GFR, November 1972, 135 pp, \$2.14.
- UAG-24 DATA ON SOLAR-GEOPHYSICAL ACTIVITY ASSOCIATED WITH THE MAJOR GROUND LEVEL COSMIC RAY EVENTS OF 24 JANUARY AND 1 SEPTEMBER 1971, Parts 1 and 2, compiled by Helen E. Coffey and J. Virginia Lincoln, World Data Center A for Solar-Terrestrial Physics, NOAA, Boulder, CO, December 1972, 462 pp, \$2.00 (includes Parts 1 and 2).
- UAG-25 OBSERVATIONS OF JUPITER'S SPORADIC RADIO EMISSION IN THE RANGE 7.6-41 MHZ, 9 SEPTEMBER 1968 THROUGH 9 DECEMBER 1971, by James W. Warwick, George A. Dulk and David G. Swann, University of Colorado, Boulder, CO, February 1973, 35 pp.
- UAG-26 DATA COMPILATION FOR THE MAGNETOSPHERICALLY QUIET PERIODS FEBRUARY 19-23 AND NOVEMBER 29 - DECEMBER 3, 1970, compiled by Helen E. Coffey and J. Virginia Lincoln, World Data Center A for Solar-Terrestrial Physics, NOAA, Boulder, CO, May 1973, 129 pp.
- UAG-27 HIGH SPEED STREAMS IN THE SOLAR WIND, by D.S. Intriligator, University of Southern California, Los Angeles, CA, June 1973, 16 pp.
- UAG-28 COLLECTED DATA REPORTS ON AUGUST 1972 SOLAR-TERRESTRIAL EVENTS, Parts 1, 2 and 3, edited by Helen E. Coffey, World Data Center A for Solar-Terrestrial Physics, NOAA, Boulder, CO, July 1973, 932 pp, \$4.50.
- UAG-29 AURORAL ELECTROJET MAGNETIC ACTIVITY INDICES AE(11) FOR 1968, by Joe Haskell Allen, Carl C. Abston and Leslie D. Morris, National Geophysical and Solar-Terrestrial Data Center, Boulder, CO, October 1973, 148 pp.
- UAG-30 CATALOGUE OF DATA ON SOLAR-TERRESTRIAL PHYSICS, prepared by NOAA Environmental Data Service, Boulder, CO, October 1973, 317 pp, \$1.75. Supersedes catalogs UAG-11, 15 and 20.
- UAG-31 AURORAL ELECTROJET MAGNETIC ACTIVITY INDICES AE(11) FOR 1969, by Joe Haskell Allen, Carl C. Abston and Leslie D. Morris, National Geophysical and Solar-Terrestrial Data Center, Boulder, CO, February 1974, 142 pp.
- UAG-32 SYNOPTIC RADIO MAPS OF THE SUN AT 3.3 MM FOR THE YEARS 1967-1969, by Earle B. Mayfield, Kennon P. White III, and Fred I. Shimabukuro, Aerospace Corp., El Segundo, CA, April 1974, 26 pp.
- UAG-33 AURORAL ELECTROJET MAGNETIC ACTIVITY INDICES AE(10) FOR 1967, by Joe Haskell Allen, Carl C. Abston and Leslie D. Morris, National Geophysical and Solar-Terrestrial Data Center, Boulder, CO, May 1974, 142 pp.
- UAG-34 ABSORPTION DATA FOR THE IGY/IGC AND IQSY, compiled and edited by A.H. Shapley, National Geophysical and Solar-Terrestrial Data Center, Boulder, CO; W.R. Piggott, Appleton Laboratory, Slough, UK; and K. Rawer, Arbeitsgruppe fur Physikalische Weltraumforschung, Freiburg, GFR, June 1974, 381 pp, \$2.00.
- UAG-36 AN ATLAS OF EXTREME ULTRAVIOLET FLASHES OF SOLAR FLARES OBSERVED VIA SUDDEN FREQUENCY DEVIATIONS DURING THE ATM-SKYLAB MISSIONS, by R.F. Donnelly and E.L. Berger, NOAA Space Environment Laboratory; Lt. J.D. Busman, NOAA Commissioned Corps; B. Henson, NASA Marshall Space Flight Center; T.B. Jones, University of Leicester, UK; G.M. Lerfald, NOAA Wave Propagation Laboratory; K. Najita, University of Hawaii; W.M. Retalack, NOAA Space Environment Laboratory and W.J. Wagner, Sacramento Peak Observatory, October 1974, 95 pp.

UAG SERIES OF REPORTS (Continued)

- UAG-37 AURORAL ELECTROJET MAGNETIC ACTIVITY INDICES AE(10) FOR 1966, by Joe Haskell Allen, Carl C. Abston and Leslie D. Morris, National Geophysical and Solar-Terrestrial Data Center, Boulder, CO, December 1974, 142 pp.
- UAG-38 MASTER STATION LIST FOR SOLAR-TERRESTRIAL PHYSICS DATA AT WDC-A FOR SOLAR-TERRESTRIAL PHYSICS, by R.W. Buhmann, World Data Center A for Solar-Terrestrial Physics, Boulder, CO; Juan D. Roederer, University of Denver, Denver, CO; and M.A. Shea and D.F. Smart, Air Force Cambridge Research Laboratories, Hanscom AFB, MA, December 1974, 110 pp, \$1.60.
- UAG-39 AURORAL ELECTROJET MAGNETIC ACTIVITY INDICES AE(11) FOR 1971, by Joe Haskell Allen, Carl C. Abston and Leslie D. Morris, National Geophysical and Solar-Terrestrial Data Center, Boulder, CO, February 1975, 144 pp, \$2.05.
- UAG-40 H-ALPHA SYNOPTIC CHARTS OF SOLAR ACTIVITY FOR THE PERIOD OF SKYLAB OBSERVATIONS, MAY 1973 - MARCH 1974, by Patrick S. McIntosh, NOAA Space Environment Laboratory, Boulder, CO, February 1975, 32 pp.
- UAG-41 H-ALPHA SYNOPTIC CHARTS OF SOLAR ACTIVITY DURING THE FIRST YEAR OF SOLAR CYCLE 20 OCTOBER 1964 - AUGUST 1965, by Patrick S. McIntosh, NOAA Space Environment Laboratory, Boulder, CO and Jerome T. Nolte, American Science and Engineering, Inc., Cambridge, MA, March 1975, 25 pp.
- UAG-42 OBSERVATIONS OF JUPITER'S SPORADIC RADIO EMISSION IN THE RANGE 7.6-80 MHZ, 10 DECEMBER 1971 THROUGH 21 MARCH 1975, by James W. Warwick, George A. Dulk and Anthony C. Riddle, University of Colorado, Boulder, CO, April 1975, 49 pp.
- UAG-43 CATALOG OF OBSERVATION TIMES OF GROUND-BASED SKYLAB-COORDINATED SOLAR OBSERVING PROGRAMS, compiled by Helen E. Coffey, World Data Center A for Solar-Terrestrial Physics, NOAA, Boulder, CO, May 1975, 159 pp, \$3.00.
- UAG-44 SYNOPTIC MAPS OF SOLAR 9.1 CM MICROWAVE EMISSION FROM JUNE 1962 TO AUGUST 1973, by Werner Graf and Ronald N. Bracewell, Stanford University, Stanford, CA, May 1975, 183 pp, \$2.55.
- UAG-45 AURORAL ELECTROJET MAGNETIC ACTIVITY INDICES AE(11) FOR 1972, by Joe Haskell Allen, Carl C. Abston and Leslie D. Morris, National Geophysical and Solar-Terrestrial Data Center, Boulder, CO, May 1975, 144 pp, \$1.50 (microfiche only).
- UAG-46 INTERPLANETARY MAGNETIC FIELD DATA 1963-1964, by Joseph H. King, National Space Science Data Center, NASA Goddard Space Flight Center, Greenbelt, MD, June 1975, 382 pp, \$1.95.
- UAG-47 AURORAL ELECTROJET MAGNETIC ACTIVITY INDICES AE(11) FOR 1973, by Joe Haskell Allen, Carl C. Abston and Leslie D. Morris, National Geophysical and Solar-Terrestrial Data Center, Boulder, CO, June 1975, 144 pp, \$1.50 (microfiche only).
- UAG-48A SYNOPTIC OBSERVATIONS OF THE SOLAR CORONA DURING CARRINGTON ROTATIONS 1580-1596 (11 OCTOBER 1971 - 15 JANUARY 1973), [Reissue of UAG-48 with quality images], by R.A. Howard, M.J. Koomen, D.J. Michels, R. Tousey, C.R. Detwiler, D.E. Roberts, R.T. Seal, and J.D. Whitney, U.S. Naval Research Laboratory, Washington, DC, and R.T. Hansen and S.F. Hansen, C.J. Garcia and E. Yasukawa, High Altitude Observatory, NCAR, Boulder, CO, February 1976, 200 pp, \$4.27. Supersedes UAG-48.
- UAG-50 HIGH-LATITUDE SUPPLEMENT TO THE URSI HANDBOOK ON IONOGRAM INTERPRETATION AND REDUCTION, edited by W.R. Piggott, British Antarctic Survey, c/o Appleton Laboratory, Slough, UK, October 1975, 294 pp, \$4.00.
- UAG-51 SYNOPTIC MAPS OF SOLAR CORONAL HOLE BOUNDARIES DERIVED FROM HE 11 304A SPECTROHELIOGRAMS FROM THE MANNED SKYLAB MISSIONS, by J.D. Bohlin and D.M. Rubenstein, U.S. Naval Research Laboratory, Washington, DC, November 1975, 30 pp.
- UAG-52 EXPERIMENTAL COMPREHENSIVE SOLAR FLARE INDICES FOR CERTAIN FLARES, 1970-1974, by Helen W. Dodson and E. Ruth Hedeman, McMath-Hulbert Observatory, University of Michigan Pontiac, MI, November 1975, 27 pp.
- UAG-53 DESCRIPTION AND CATALOG OF IONOSPHERIC F-REGION DATA, JICAMARCA RADIO OBSERVATORY (NOVEMBER 1966 - APRIL 1969), by W.L. Clark and T.E. Van Zandt, NOAA Aeronomy Laboratory, Boulder, CO, and J.P. McClure, University of Texas at Dallas, Dallas, TX, April 1976, 10 pp.
- UAG-55 EQUIVALENT IONOSPHERIC CURRENT REPRESENTATIONS BY A NEW METHOD, ILLUSTRATED FOR 8-9 NOVEMBER 1969 MAGNETIC DISTURBANCES, by Y. Kamide, Cooperative Institute for Research in Environmental Sciences, University of Colorado, Boulder, CO; H.W. Kroehl, Data Studies Division, National Geophysical and Solar-Terrestrial Data Center, Boulder, CO; M. Kanamitsu, Advanced Study Program, National Center for Atmospheric Research, Boulder, CO; Joe Haskell Allen, Data Studies Division, National Geophysical and Solar-Terrestrial Data Center, Boulder, CO; and S.-I. Akasofu, Geophysical Institute, University of Alaska, Fairbanks, AK, April 1976, 91 pp, \$1.50 (microfiche only).

UAG SERIES OF REPORTS (Continued)

- UAG-56 ISO-INTENSITY CONTOURS OF GROUND MAGNETIC H PERTURBATIONS FOR THE DECEMBER 16-18, 1971, GEOMAGNETIC STORM, Y. Kamide, Cooperative Institute for Research in Environmental Sciences, University of Colorado, Boulder, CO, April 1976, 37 pp, \$1.39.
- UAG-57 MANUAL ON IONOSPHERIC ABSORPTION MEASUREMENTS, edited by K. Rawer, Institut fur Physikalische Weltraumforschung, Freiburg, GFR, June 1976, 302 pp, \$4.27.
- UAG-58 ATS6 RADIO BEACON ELECTRON CONTENT MEASUREMENTS AT BOULDER, JULY 1974 - MAY 1975, by R.B. Fritz, NOAA Space Environment Laboratory, Boulder, CO, September 1976, 61 pp.
- UAG-59 AURORAL ELECTROJET MAGNETIC ACTIVITY INDICES AE(11) FOR 1974, by Joe Haskell Allen, Carl C. Abston and Leslie D. Morris, National Geophysical and Solar-Terrestrial Data Center, Boulder, CO, December 1976, 144 pp, \$2.16.
- UAG-60 GEOMAGNETIC DATA FOR JANUARY 1976 [AE(7) INDICES AND STACKED MAGNETOGRAMS], by Joe Haskell Allen, Carl C. Abston and Leslie D. Morris, National Geophysical and Solar-Terrestrial Data Center, Boulder, CO, July 1977, 57 pp.
- UAG-61 COLLECTED DATA REPORTS FOR STIP INTERVAL 11 20 MARCH - 5 MAY 1976, edited by Helen E. Coffey and John A. McKinnon, World Data Center A for Solar-Terrestrial Physics, Boulder, CO, August 1977, 313 pp, \$2.95.
- UAG-62 GEOMAGNETIC DATA FOR FEBRUARY 1976 [AE(7) INDICES AND STACKED MAGNETOGRAMS], by Joe Haskell Allen, Carl C. Abston and Leslie D. Morris, National Geophysical and Solar-Terrestrial Data Center, Boulder, CO, September 1977, 55 pp.
- UAG-63 GEOMAGNETIC DATA FOR MARCH 1976 [AE(7) INDICES AND STACKED MAGNETOGRAMS], by Joe Haskell Allen, Carl C. Abston and Leslie D. Morris, National Geophysical and Solar-Terrestrial Data Center, Boulder, CO, September 1977, 57 pp.
- UAG-64 GEOMAGNETIC DATA FOR APRIL 1976 [AE(8) INDICES AND STACKED MAGNETOGRAMS], by Joe Haskell Allen, Carl C. Abston and Leslie D. Morris, National Geophysical and Solar-Terrestrial Data Center, Boulder, CO, February 1978, 55 pp.
- UAG-65 THE INFORMATION EXPLOSION AND ITS CONSEQUENCES FOR DATA ACQUISITION, DOCUMENTATION, PROCESSING, by G.K. Hartmann, Max-Planck-Institut fur Aeronomie, Lindau, GFR, May 1978, 36 pp.
- UAG-66 SYNOPTIC RADIO MAPS OF THE SUN AT 3.3 MM 1970-1973, by Earle B. Mayfield and Fred I. Shimabukuro, Aerospace Corp., El Segundo, CA, May 1978, 30 pp.
- UAG-67 IONOSPHERIC D-REGION PROFILE DATA BASE, A COLLECTION OF COMPUTER-ACCESSIBLE EXPERIMENTAL PROFILES OF THE D AND LOWER E REGIONS, by L.F. McNamara, Ionospheric Prediction Service, Sydney, Australia, August 1978, 30 pp, \$1.50 (microfiche only).
- UAG-68 A COMPARATIVE STUDY OF METHODS OF ELECTRON DENSITY PROFILE ANALYSIS, by L.F. McNamara, Ionospheric Prediction Service, Sydney, Australia, August 1978, 30 pp, \$1.50 (microfiche only).
- UAG-69 SELECTED DISTURBED D-REGION ELECTRON DENSITY PROFILES. THEIR RELATION TO THE UNDISTURBED D REGION, by L.F. McNamara, Ionospheric Prediction Service, Sydney, Australia, October 1978, 50 pp, \$1.50 (microfiche only).
- UAG-70 ANNOTATED ATLAS OF H-ALPHA SYNOPTIC CHARTS FOR SOLAR CYCLE 20 (1964-1974) CARRINGTON SOLAR ROTATIONS 1487-1616, by Patrick S. McIntosh, NOAA Space Environment Laboratory, Boulder, CO, February 1979, 327 pp, \$3.50.
- UAG-71 MAGNETIC POTENTIAL PLOTS OVER THE NORTHERN HEMISPHERE FOR 26-28 MARCH 1976, A.D. Richmond, NOAA Space Environment Laboratory, Boulder, CO; H.W. Kroehl, National Geophysical and Solar-Terrestrial Data Center, Boulder, CO; M.A. Henning, Lockheed Missils and Space Co., Aurora, CO; and Y. Kamide, Kyoto Sangyo University, Kyoto, Japan, April 1979, 118 pp, \$1.50.
- UAG-72 ENERGY RELEASE IN SOLAR FLARES, PROCEEDINGS OF THE WORKSHOP ON ENERGY RELEASE IN FLARES, 26 FEBRUARY - 1 MARCH 1979, CAMBRIDGE, MASSACHUSETTS, U.S.A., edited by David M. Rust, American Science and Engineering, Inc., Cambridge, MA, and A. Gordon Emslie, Harvard-Smithsonian Center for Astrophysics, Cambridge, MA, July 1979, 68 pp, \$1.50 (microfiche only).
- UAG-73 AURORAL ELECTROJET MAGNETIC ACTIVITY INDICES AE(11-12) FOR JANUARY - JUNE 1975, by Joe Haskell Allen, Carl C. Abston, J.E. Salazar and J.A. McKinnon, National Geophysical and Solar-Terrestrial Data Center, NOAA, Boulder, CO, August 1979, 114 pp, \$1.75.

UAG SERIES OF REPORTS (Continued)

- UAG-74 ATS-6 RADIO BEACON ELECTRON CONTENT MEASUREMENTS AT OOTACAMUND, INDIA, OCTOBER - JULY 1976, by S.D. Bouwer, K. Davies, R.F. Donnelly, R.N. Grubb, J.E. Jones and J.H. Taylor, NOAA Space Environment Laboratory, Boulder, CO, and R.G. Rastogi, M.R. Deshpande, H. Chandra and G. Sethia, Physical Research Laboratory, Ahmedabad, India, March 1980, 58 pp, \$2.50.
- UAG-75 THE ALASKA IMS MERIDIAN CHAIN: MAGNETIC VARIATIONS FOR 9 MARCH - 27 APRIL 1978, by H.W. Kroehl and G.P. Kosinski, National Geophysical and Solar-Terrestrial Data Center, Boulder, CO; S.-I. Akasofu, G.J. Romick, C.E. Campbell and G.K. Corrick, University of Alaska, Fairbanks, AK; and C.E. Hornback and A.M. Gray, NOAA Space Environment Laboratory, Boulder, CO, June 1980, 107 pp, \$3.00.
- UAG-76 AURORAL ELECTROJET MAGNETIC ACTIVITY INDICES AE(12) FOR JULY - DECEMBER 1975, by Joe Haskell Allen, Carl C. Abston, J.E. Salazar and J.A. McKinnon, National Geophysical and Solar-Terrestrial Data Center, NOAA, Boulder, CO, August 1980, 116 pp, \$2.50.
- UAG-77 SYNOPTIC SOLAR MAGNETIC FIELD MAPS FOR THE INTERVAL INCLUDING CARRINGTON ROTATIONS 1601-1680, MAY 5, 1973 - APRIL 26, 1979, by J. Harvey, B. Gillespie, P. Miedaner and C. Slaughter, Kitt Peak National Observatory, Tucson, AZ, August 1980, 66 pp, \$2.50.
- UAG-78 THE EQUATORIAL LATITUDE OF AURORAL ACTIVITY DURING 1972-1977, by N.R. Sheeley, Jr. and R.A. Howard, E.O. Hulbert Center for Space Research, U.S. Naval Research Laboratory, Washington, DC and B.S. Dandekar, Air Force Geophysics Laboratory, Hanscom AFB, MA, October 1980, 61 pp, \$3.00.
- UAG-79 SOLAR OBSERVATIONS DURING SKYLAB, APRIL 1973 - FEBRUARY 1974, I. CORONAL X-RAY STRUCTURE, II. SOLAR FLARE ACTIVITY, by J.M. Hanson, University of Michigan, Ann Arbor, MI; and E.C. Roelof and R.E. Gold, The Johns Hopkins University, Laurel, MD, December 1980, 43 pp, \$2.50.
- UAG-80 EXPERIMENTAL COMPREHENSIVE SOLAR FLARE INDICES FOR 'MAJOR' AND CERTAIN LESSER FLARES, 1975-1979, compiled by Helen W. Dodson and E. Ruth Hedeman, The Johns Hopkins University, Laurel, MD, July 1981, 33 pp, \$2.00.
- UAG-81 EVOLUTIONARY CHARTS OF SOLAR ACTIVITY (CALCIUM PLAGES) AS FUNCTIONS OF HELIOGRAPHIC LONGITUDE AND TIME, 1964-1979, by E. Ruth Hedeman, Helen W. Dodson and Edmond C. Roelof, The Johns Hopkins University, Laurel, MD 20707, August 1981, 103 pp, \$4.00.
- UAG-82 INTERNATIONAL REFERENCE IONOSPHERE - IRI 79, edited by J. Virginia Lincoln and Raymond O. Conkright, National Geophysical and Solar-Terrestrial Data Center, NOAA, Boulder, CO, November 1981, 243 pp, \$4.50.
- UAG-83 SOLAR-GEOPHYSICAL ACTIVITY REPORTS FOR SEPTEMBER 7-24, 1977 AND NOVEMBER 22, 1977, Parts 1 and 2, compiled by John A. McKinnon and J. Virginia Lincoln, World Data Center A for Solar-Terrestrial Physics, NOAA, Boulder, CO, February 1982, 553 pp, \$10.00.
- UAG-84 CATALOG OF AURORAL RADIO ABSORPTION DURING 1976-1979 AT ABISKO, SWEDEN, by J.K. Hargreaves, C.M. Taylor and J.M. Penman, Environmental Sciences Department, University of Lancaster, Lancaster, UK, July 1982, 69 pp, \$3.00.
- UAG-85 CATALOG OF IONOSPHERE VERTICAL SOUNDINGS DATA, edited by Raymond O. Conkright and H. Irene Brophy, National Geophysical Data Center, NOAA, Boulder, CO, July 1982, 107 pp, \$3.50. Supersedes UAG-54.
- UAG-86 INTERNATIONAL CATALOG OF GEOMAGNETIC DATA, compiled by J.H. Allen and C.C. Abston, National Geophysical Data Center, NOAA, Boulder, CO; E.P. Kharin and N.E. Papitashvili, Academy of Sciences of the USSR, World Data Center B2, Moscow, USSR; and V.O. Papitashvili, IZMIRAN, Moscow Region, USSR, November 1982, 191 pp, \$4.00. Supersedes UAG-35 and 49.
- UAG-87 CHANGES IN THE GLOBAL ELECTRIC FIELDS AND CURRENTS FOR MARCH 17-19, 1978, FROM SIX IMS MERIDIAN CHAINS OF MAGNETOMETERS, by Y. Kamide, Kyoto Sangyo University, Kyoto, Japan; H.W. Kroehl, National Geophysical Data Center, NOAA, Boulder, CO; and A.D. Richmond, NOAA Space Environment Laboratory, Boulder, CO, November 1982, 102 pp, \$3.50.
- UAG-88 NUMERICAL MODELING OF IONOSPHERIC PARAMETERS FROM GLOBAL IMS MAGNETOMETER DATA FOR THE CDAW-6 INTERVALS, by Y. Kamide, Kyoto Sangyo University, Kyoto, Japan; H.W. Kroehl, National Geophysical Data Center, NOAA, Boulder, CO; and B.A. Hausman, National Geophysical Data Center, NOAA, Boulder, CO, November 1983, 197 pp, \$4.00.
- UAG-89 ATMOSPHERIC HANDBOOK: ATMOSPHERIC DATA TABLES AVAILABLE ON COMPUTER TAPE, by V.E. Derr, NOAA Environmental Research Laboratories, Boulder, CO, May 1984, 56 pp.
- UAG-90 EXPERIENCE WITH PROPOSED IMPROVEMENTS OF THE INTERNATIONAL REFERENCE IONOSPHERE (IRI): CONTRIBUTED PAPERS, MAINLY FROM THE URSI-COSPAR WORKSHOP HELD IN BUDAPEST IN 1980, edited by K. Rawer, University of Freiburg, Federal Republic of Germany, and C.M. Minnis, former Secretary General of URSI, Brussels, Belgium, May 1984, 233 pp, \$6.00.